

1993

Multibond Graph Method For Flexible Multibody System Dynamics

Simon Xun-nan He

Follow this and additional works at: <https://ir.lib.uwo.ca/digitizedtheses>

Recommended Citation

He, Simon Xun-nan, "Multibond Graph Method For Flexible Multibody System Dynamics" (1993). *Digitized Theses*. 2209.
<https://ir.lib.uwo.ca/digitizedtheses/2209>

This Dissertation is brought to you for free and open access by the Digitized Special Collections at Scholarship@Western. It has been accepted for inclusion in Digitized Theses by an authorized administrator of Scholarship@Western. For more information, please contact tadam@uwo.ca, wlsadmin@uwo.ca.

TABLE OF CONTENTS

	Page
CERTIFICATE OF EXAMINATION	ii
ABSTRACT	iii
ACKNOWLEDGEMENTS	v
TABLE OF CONTENTS	vi
LIST OF FIGURES	ix
LIST OF TABLES	xi
NOMENCLATURE	xii
- Chapter 1 -	
Introduction	1
1.1 Introduction to Flexible Multibody System Dynamics	1
1.2 Introduction to Bond Graph Method	3
1.3 Objectives of this Thesis	5
- Chapter 2 -	
Concepts from Multibond Graph for the Dynamics of a Single Rigid Body	7
2.1 Introduction	7
2.2 Mathematical Preliminaries	7
2.2.1 Frames and Cartesian Coordinates	7
2.2.2 Vectors, Dyadics and their Matrix Representations	9
2.3 The Frames, Position Vectors and Orientation Definitions for a Body	11
2.4 Kinematics of a Rigid Body	15
2.5 Dynamics of a Rigid Body	17
2.5.1 Mass Geometry of a Rigid Body	17
2.5.2 Momentum	19
2.5.3 Dynamics of a Rigid Body	20
2.6 Multibond Graph Modelling of a Single Rigid Body	22
- Chapter 3 -	
The Vibration Behavior of a Flexible Body in Multibody Systems	30
3.1 Introduction	30
3.2 Transverse Vibration of a Beam Under Axial Forces	31
3.3 In-Plane Transverse Vibrations of Rotating Bars	42
- Chapter 4 -	
Equations of Motion of a Free Moving Flexible Body	47
4.1 Introduction	47
4.2 Kinematics of a Flexible Body	48

MULTIBOND GRAPH METHOD FOR FLEXIBLE MULTIBODY SYSTEM DYNAMICS

by

Simon Xun-Nan He

Department of Mechanical Engineering
Faculty of Engineering Science

Submitted in partial fulfillment
of the requirements for the degree of
Doctor of Philosophy

Faculty of Graduate Studies
The University of Western Ontario
London, Ontario
October 1992

© Simon Xun-Nan He 1992



National Library
of Canada

Acquisitions and
Bibliographic Services Branch

395 Wellington Street
Ottawa, Ontario
K1A 0N4

Bibliothèque nationale
du Canada

Direction des acquisitions et
des services bibliographiques

395, rue Wellington
Ottawa (Ontario)
K1A 0N4

Your file *Votre référence*

Our file *Notre référence*

The author has granted an irrevocable non-exclusive licence allowing the National Library of Canada to reproduce, loan, distribute or sell copies of his/her thesis by any means and in any form or format, making this thesis available to interested persons.

L'auteur a accordé une licence irrévocable et non exclusive permettant à la Bibliothèque nationale du Canada de reproduire, prêter, distribuer ou vendre des copies de sa thèse de quelque manière et sous quelque forme que ce soit pour mettre des exemplaires de cette thèse à la disposition des personnes intéressées.

The author retains ownership of the copyright in his/her thesis. Neither the thesis nor substantial extracts from it may be printed or otherwise reproduced without his/her permission.

L'auteur conserve la propriété du droit d'auteur qui protège sa thèse. Ni la thèse ni des extraits substantiels de celle-ci ne doivent être imprimés ou autrement reproduits sans son autorisation.

ISBN 0-315-81290-7

Canada

- Chapter 8 -	
Derivation of Equations from Multibond Graphs and Numerical Algorithms for Simulation	104
8.1 Introduction	104
8.2 Causality Consideration	104
8.3 The Equations of Motion of Multibody Systems and Numerical Algorithms in Other Computer-Aided Modelling Methods	113
8.4 The Equations of Motion Generated from Causal Multibond Graphs	i20
- Chapter 9 -	
Applications	132
9.1 Introduction	132
9.2 Computer Program MULBOND	132
9.3 A Rotating beam	136
9.4 A Crank-Rocker Mechanism with Flexible Coupler	144
9.5 A Flexible Robotic Manipulator System	152
- Chapter 10 -	
Summary and Conclusions	168
References	170
Vita	178

Figure 8-4 Multibond graphs of links and joints of a two flexible link system with zero flow constraints	110
Figure 8-5 Multibond graphs of links and joints of a two flexible link system with constraint elements	111
Figure 9-1 Environment of MULBOND for multibond graph construction	133
Figure 9-2 "add element" panel	134
Figure 9-3 "add bond" panel	134
Figure 9-4 "delete" panel	134
Figure 9-5 "move" panel	134
Figure 9-6 "inquiry" panel	134
Figure 9-7 "process" panel	135
Figure 9-8 "Save" frame	135
Figure 9-9 "load" frame	135
Figure 9-10 "Quit" frame	136
Figure 9-11 Rotating beam example	136
Figure 9-12 2-D Euler beam	137
Figure 9-13 Multibond graph of the rotating beam in MULBOND environment	139
Figure 9-14 The first two eigenvalues of the rotating beam	142
Figure 9-15 Tip deflections of the rotating beam in the rotation plane	143
Figure 9-16 Crank-rocker mechanism example	145
Figure 9-17 Multibond graph of the crank-rocker mechanism	146
Figure 9-18 Transient response during start-up of a crank-rocker mechanism	147
Figure 9-19 Transient response during start-up of crank-rocker mechanism	150
Figure 9-20 Flexible manipulator system example	154
Figure 9-21 Multibond graph of the flexible manipulator system	155
Figure 9-22 Ideal tip trajectory and joint angular velocity and displacement	158
Figure 9-23 Payload tip deviation v.s. rigid body case and joint torques of the 2-D motion of the manipulator	160
Figure 9-24 Positions of the manipulator during the maneuver	162
Figure 9-25 Tip deviations v.s. rigid body case and joint torques of the 3-D motion of the manipulator	164
Figure 9-26 Positions of the flexible manipulator during the maneuver	167

of contemporary interest in flexible multibody system dynamics. They include a rotating beam which shows the stiffening effect on the vibration of the beam in the rotation plane, a four bar mechanism which indicates the softening effect, and a four body manipulator system with two flexible links which investigates the influence of the flexibility on 2-D and 3-D maneuvers. The significant advantages of the method developed in this thesis are the ease of modelling, particularly evident in the case of mixed energy domains. It has been revealed from the solutions of these example problems, that the geometric stiffening and softening of flexible beams under large dynamic axial forces have significant effects on the prediction of dynamic behavior and digital simulation of the flexible systems. It has also been shown that the inverse dynamic control of a flexible multibody system without consideration of the flexibility of the system would cause unacceptable errors in position control. These examples demonstrate the validity of this multibond graph approach.

ACKNOWLEDGEMENTS

The author acknowledges Professor W. H. ElMaraghy for his support for this research project, and for his assistance throughout the project.

For his assistance in computer programming and the use of commercial software in our computer network, Mr. Dan Corrin is specially thanked. I am also grateful to my colleagues in the Design Automation and Manufacturing Research Laboratory (DA&MR) for the exciting academic and friendly atmosphere they provided during the course of this work.

This research was carried out under the financial support from Professor W. H. ElMaraghy, through his grants from NSERC (Natural Science and Engineering Research Council), The Federal Centre of Research Excellence in Robotics, IRIS (Institute for Robotics and Intelligent Systems), the Ontario Centre for Research Excellence MRCO (Manufacturing Research Corporation of Ontario), and The University of Western Ontario through teaching assistantships.

I also thank Jing for her encouragement and patience.

TABLE OF CONTENTS

	Page
CERTIFICATE OF EXAMINATION	ii
ABSTRACT	iii
ACKNOWLEDGEMENTS	v
TABLE OF CONTENTS	vi
LIST OF FIGURES	ix
LIST OF TABLES	xi
NOMENCLATURE	xii
 - Chapter 1 -	
Introduction	1
1.1 Introduction to Flexible Multibody System Dynamics	1
1.2 Introduction to Bond Graph Method	3
1.3 Objectives of this Thesis	5
 - Chapter 2 -	
Concepts from Multibond Graph for the Dynamics of a Single Rigid Body	7
2.1 Introduction	7
2.2 Mathematical Preliminaries	7
2.2.1 Frames and Cartesian Coordinates	7
2.2.2 Vectors, Dyadics and their Matrix Representations	9
2.3 The Frames, Position Vectors and Orientation Definitions for a Body	11
2.4 Kinematics of a Rigid Body	15
2.5 Dynamics of a Rigid Body	17
2.5.1 Mass Geometry of a Rigid Body	17
2.5.2 Momentum	19
2.5.3 Dynamics of a Rigid Body	20
2.6 Multibond Graph Modelling of a Single Rigid Body	22
 - Chapter 3 -	
The Vibration Behavior of a Flexible Body in Multibody Systems	30
3.1 Introduction	30
3.2 Transverse Vibration of a Beam Under Axial Forces	31
3.3 In-Plane Transverse Vibrations of Rotating Bars	42
 - Chapter 4 -	
Equations of Motion of a Free Moving Flexible Body	47
4.1 Introduction	47
4.2 Kinematics of a Flexible Body	48

4.3 Dynamics of a Free-Moving Flexible Body	52
4.3.1 Variational Principle and Non-Linear Strain	52
4.3.2 Equations of Motion of a Flexible Body	56
4.3.3 Equations of Motion of a Flexible Body in Matrix form	61
4.4 Form of Equations of Motion of a Flexible Body for Multibond Graph Representation	65
 - Chapter 5 -	
The Application of Floating Frames	69
5.1 Introduction	69
5.2 Floating Frames for Flexible Bodies	70
5.2.1 Body-Fixed Frame	70
5.2.2 Principal-axis Frame	73
5.2.3 The Buckens Frame	73
5.2.4 The Tesserand Frame	76
 - Chapter 6 -	
Multibond Graphs of a Flexible Body	79
6.1 Introduction	79
6.2 Multibond Graph Representation of a Flexible Body	79
6.3 Multibond Graphs of a Flexible Body under Floating Frames	84
6.3.1 The Mass Center Located Body Fixed Frame	84
6.3.2 The Buckens Frame	86
6.3.3 The Tisserand Frame	86
 - Chapter 7 -	
Multibond Graphs of Mechanical Constraints and Whole Flexible Multibody Systems	89
7.1 Introduction	89
7.2 The Multibond Graph Structure of Mechanical Constraints	89
7.2.1 Spherical Joints	90
7.2.2 Pin Joints	92
7.2.3 Cylindrical Joints	93
7.2.4 Translational Joints	95
7.2.5 Screw Joint	96
7.2.6 Planar Joint	98
7.2.7 Universal Joint	99
7.3 Lagrange Multipliers and Artificial Constraint Element	101
7.4 Multibond Graph of Flexible Multibody Systems	103

- Chapter 8 -	
Derivation of Equations from Multibond Graphs and Numerical Algorithms for Simulation	104
8.1 Introduction	104
8.2 Causality Consideration	104
8.3 The Equations of Motion of Multibody Systems and Numerical Algorithms in Other Computer-Aided Modelling Methods	113
8.4 The Equations of Motion Generated from Causal Multibond Graphs	i20
- Chapter 9 -	
Applications	132
9.1 Introduction	132
9.2 Computer Program MULBOND	132
9.3 A Rotating beam	136
9.4 A Crank-Rocker Mechanism with Flexible Coupler	144
9.5 A Flexible Robotic Manipulator System	152
- Chapter 10 -	
Summary and Conclusions	168
References	170
Vita	178

LIST OF FIGURES

	Page
Figure 2-1 Frame, Cartesian coordinates and position vector	8
Figure 2-2 Coordinate systems and position vectors for a rigid body	12
Figure 2-3 (a) 1-junctions for velocity variables	27
Figure 2-3 (b) Multibond graph of kinematics of a rigid body with one joint	28
Figure 2-3 (c) Multibond graph of dynamics of a rigid body with one joint	29
Figure 3-1 Frame and Cartesian coordinates of a beam	32
Figure 3-2 Forces on an element of the beam	33
Figure 3-3 Rotating bar example	43
Figure 4-1 Coordinate System and Position Vectors	49
Figure 6-1 Multibond graph of kinematics of a flexible body with one joint	80
Figure 6-2 Multibond graph for the dynamics of a flexible body with one joint	83
Figure 6-3 Multibond graph of dynamics of a flexible body with one joint under mass center located body fixed reference frame and free-free modes	85
Figure 6-4 Multibond graph of constraint condition on generalized coordinates	87
Figure 6-5 Multibond graph of dynamics of a flexible body with one joint under the Tisserand reference frame and free-free modes	88
Figure 7-1 Sketch of a spherical joint between two bodies	90
Figure 7-2 Multibond graph of a spherical joint	92
Figure 7-3 Sketch of a pin joint	93
Figure 7-4 Multibond graph of a pin joint	93
Figure 7-5 Sketch of a cylindrical joint	94
Figure 7-6 Multibond graph of a cylindrical joint	94
Figure 7-7 Sketch of a translational joint	95
Figure 7-8 Multibond graph of a translational joint	96
Figure 7-9 Sketch of a screw joint	97
Figure 7-10 Multibond graph of a screw joint	97
Figure 7-11 Sketch of a planar joint	98
Figure 7-12 Multibond graph of a planar joint	99
Figure 7-13 Sketch of a universal joint	100
Figure 7-14 Multibond graph of a universal joint	100
Figure 7-15 Multibond graph of a joint with Lagrange Multiplier	102
Figure 7-16 The structure of multibond graph of multibond systems	103
Figure 8-1 Multibond graph of a flexible body with integral causality	106
Figure 8-2 A flexible manipulator system	107
Figure 8-3 Multibond graphs of links and joints of a two flexible link system	108

Figure 8-4 Multibond graphs of links and joints of a two flexible link system with zero flow constraints	110
Figure 8-5 Multibond graphs of links and joints of a two flexible link system with constraint elements	111
Figure 9-1 Environment of MULBOND for multibond graph construction	133
Figure 9-2 "add element" panel	134
Figure 9-3 "add bond" panel	134
Figure 9-4 "delete" panel	134
Figure 9-5 "move" panel	134
Figure 9-6 "inquiry" panel	134
Figure 9-7 "process" panel	135
Figure 9-8 "Save" frame	135
Figure 9-9 "load" frame	135
Figure 9-10 "Quit" frame	136
Figure 9-11 Rotating beam example	136
Figure 9-12 2-D Euler beam	137
Figure 9-13 Multibond graph of the rotating beam in MULBOND environment	139
Figure 9-14 The first two eigenvalues of the rotating beam	142
Figure 9-15 Tip deflections of the rotating beam in the rotation plane	143
Figure 9-16 Crank-rocker mechanism example	145
Figure 9-17 Multibond graph of the crank-rocker mechanism	146
Figure 9-18 Transient response during start-up of a crank-rocker mechanism	147
Figure 9-19 Transient response during start-up of crank-rocker mechanism	150
Figure 9-20 Flexible manipulator system example	154
Figure 9-21 Multibond graph of the flexible manipulator system	155
Figure 9-22 Ideal tip trajectory and joint angular velocity and displacement	158
Figure 9-23 Payload tip deviation v.s. rigid body case and joint torques of the 2-D motion of the manipulator	160
Figure 9-24 Positions of the manipulator during the maneuver	162
Figure 9-25 Tip deviations v.s. rigid body case and joint torques of the 3-D motion of the manipulator	164
Figure 9-26 Positions of the flexible manipulator during the maneuver	167

LIST OF TABLES

	Page
Table 2-1 Vector, dyadic terms in geometric and matrix forms	11
Table 2-2 Multibond graph terminology	25
Table 9-1 Geometric data of the flexible manipulator system	153

NOMENCLATURE

Roman Symbols

$[A^{0i}]$	transformation matrix between the inertial frame and the i th body reference frame; page 14
$[B^1]$ to $[B^6]$	coefficient matrices for strain; page 56
CM	symbol of the center of mass of a body; Figure 2-2
D	a joint; Figure 7-1 on page 90
$\{D\}$	defined in Equation (3.35)
$\{\vec{D}\}$	vector array related to the assumed modes; Equation (4.48)
$\{\vec{D}_c\}$	vector array related to the assumed modes; Equation (4.84)
$\{\hat{e}\}$	vector array of bases of a frame; page 8
$\hat{e}_x \hat{e}_y \hat{e}_z$	three perpendicular bases of a frame; page 8
$\{\hat{e}^o\}$	vector array of bases of the inertial frame; page 9
$\{\hat{e}^i\}$	vector array of bases of the i th body reference frame; page 9
$\{e^d\}$	vector array of bases of a joint frame; Figure 7-1 on page 90
$[E]$	elastic matrix; page 56, or unit matrix
\hat{E}	unit dyadic; page 10
\vec{F}	the resultant force on a body; page 20
F_d	resultant force on the joint of a body; page 82
\vec{F}_o	the resultant force of the surface traction on the origin of the body reference frame; page 58
\vec{F}_s	the resultant surface traction; page 20
$\{F_s\}$	coordinates of \vec{F}_s ; page 20
$[G(\vec{\Omega})]$	damping matrix due to the gyroscopic effect; Equation (4.55)
$[G_c(\vec{\Omega})]$	damping matrix due to the gyroscopic effect; Equation (4.55)
\hat{g}	gravity acceleration; page 20
$\{g(q, \dot{q})\}$	constraint conditions; page 114

\vec{H}_0	angular momentum of a body about a fixed point in the inertial frame; page 19
\vec{H}	angular momentum of a body about the origin of the body reference frame; page 19
\vec{H}_c	angular momentum of a body about the center of mass; page 19
$[H^0]$ to $[H^6]$	Boolean matrices; page 55
$[H]$	Jacobian matrix of the constraint condition; page 101 and page 114
$[H^*]$	Jacobian matrix of the constraint condition; page 118
$\{h\}$	compact form of all velocities; Equation (4.73)
\hat{J}	dyadic of moment of inertia of a body with respect to the origin of the body reference frame; Equation (2.30)
$[J]$	the inertia matrix of a body with respect to the origin of the body reference frame; Equation (2.31)
\hat{J}_c	dyadic of moment of inertia of a body with respect to the center of mass; Equation (2.32)
$[J_c]$	the inertia matrix of a body with respect to the center of mass; Equation (2.33)
\hat{J}^*	dyadic defined in Equation (4.47) on page 59
\hat{J}_c^*	dyadic defined in Equation (4.83)
$[K]$	stiffness matrix; Equation (3.29)
$[K_g]$	dynamic geometric stiffness matrix; Equation (3.30)
$[K_n(\vec{\Omega})]$	stiffness matrix due to the centrifugal acceleration; Equation (4.54)
$[K_{nc}(\vec{\Omega})]$	stiffness matrix due to the centrifugal acceleration; Equation (4.93)
$[K_{eq}]$	equivalent stiffness matrix; Equation (4.67)
$[K_{eqc}]$	equivalent stiffness matrix; Equation (4.97)
$[L_d], [L_i]$	matrices defined in Equation (8.50) and Equation (8.51)
$[L]^*$	matrix defined in Equation (8.55)
m	mass of a body; Equation (2.29)
M	bending moment on a beam; Figure 3-2 on page 33

$[M]$	generalized mass matrix; Equation (3.33)
$[M_c]$	generalized mass matrix; Equation (4.91)
$[M_\xi]$	generalized mass matrix; Equation (6.5)
$[N]$	a 9 by n matrix; Equation (4.21)
\vec{P}	position vector of a point of a body; page 9
\vec{P}_c	position vector of the center of mass of a body in the inertial frame; page 12
$\{P\}$	coordinates of position vector \vec{P} in the inertial frame; page 10
P	axial force on a beam; Figure 3-2 on page 33
p	distributed load on a 2-D beam; Figure 3-2 on page 33
Q	shear force on a beam; Figure 3-2 on page 33
$\{Q\}$	generalized force; Equation (3.38)
$\{Q(q, \dot{q})\}$	generalized forces caused by displacement and velocities; page 114
\vec{q}	position vector of a point in a flexible body; on page 33 and Figure 4-1 on page 49
\vec{q}_c	position vector of the center of mass in a flexible body; Figure 4-1 on page 49
$\{q\}$	variables to describe the position, orientation and vibrational deformation of the each body in a multibody system; page 114
\vec{R}	position vector of the origin of the body reference frame; page 12
$[R]$	orthogonal complement of Jacobian matrix of constraint condition; page 116
\vec{r}	position vector of a point of a body in the body reference frame; page 12
\vec{r}_c	position vector of the center of mass of a body in the body reference frame; page 12
$\{S\}$	defined in Equation (3.34)
$\{\vec{S}\}$	defined in Equation (4.6)
$[S]$	coordinate matrix of $\{\vec{S}\}$; Equation (4.65)
\vec{T}	the torque about the origin of the body reference frame due to the

	surface traction; page 21
T_d	resultant torque on the joint of a body; page 82
\vec{T}_o	the torque about the origin of the body reference frame due to the surface traction in 3-D problem; page 58
$\{T\}$	coordinates of \vec{T} ; page 22
T	kinetic energy of a beam; Equation (3.5)
U	potential energy of a beam; Equation (3.9)
U_b	strain energy; Equation (3.6)
U_a	potential energy due to the axial force; Equation (3.8)
\hat{u}	elastic deformation of a flexible body; Figure 4-1 on page 49
u, v and w	deformations of the flexible body in x, y and z axes of the body reference frame; page 54
\bar{u}, \bar{v}	the longitudinal and transverse vibrational deformations of the neutral axis of a 2-D beam; page 137
W	work done by external force; Equation (3.10)
X_i	energy variables at the storage elements with integral causal signs; page 121
X_d	energy variables at the storage elements with derivative signs; page 121
$y(x, t)$	transverse deflection of a 2-D beam; Figure 3-2 on page 33

Greek Symbols

$\Phi_j(x)$	assumed mode shape for a beam; Equation (3.26)
$\vec{\Phi}_j(\dot{r})$	assumed mode shape vector for a 3-D flexible body; Equation (4.3)
$\{\vec{\Phi}(\dot{r})\}, \{\vec{\Phi}\}$	mode shape array for a 3-D flexible body; Equation (4.3)
η_j	j th generalized coordinate; Equation (3.26)
$\{\eta\}$	generalized coordinates
$\vec{\Omega}$	the absolute angular velocity of the body reference frame; page 16

Ω	angular velocity of a body in 2-D motion; Equation (3.3)
ρ	mass density of a body; page 18
$\vec{\nabla}$	curl operator; Equation (4.12)
$\hat{\pi}$	angular displacement due to the vibrational deformation of a flexible body; Equation (4.13)
$\{\delta\}$	defined in Equation (4.19)
$\{\dot{\xi}\}$	compact form of rotational and vibrational velocities; Equation (6.4)
$\{\epsilon\}$	strains in a flexible body
$\{\sigma\}$	stress in a flexible body
$\{\lambda\}$	Lagrange multipliers; page 101
$\{\Upsilon\}$	defined in Equation (8.7)
$\{\Upsilon^\circ\}$	defined in Equation (8.10)
Δt	time step; page 119

Symbols in Multibond Graphs

C:	compliance element; Table 2-2 on page 25
C_0	zero compliance; page 102
CN	Constraintor; page 103
{e}	efforts of a multibond; Table 2-2 on page 25
EJS:	Euler junction; Figure 2-3 (c) on page 29
{f}	flow of a multibond; Table 2-2 on page 25
I:	inertia element; Table 2-2 on page 25
MGY:	modulated gyrator element; Table 2-2 on page 25
TF: (MTF:)	(modulated) transform element; Table 2-2 on page 25
R :	resistant element; Table 2-2 on page 25
R_∞	infinite resistor; page 102
$S_e:$	effort source element; Table 2-2 on page 25

S_f :	flow source element; Table 2-2 on page 25
SUM:	summation element; Table 2-2 on page 25
1	“1” junction; Table 2-2 on page 25
0	“0” junction; Table 2-2 on page 25

Special Symbols

\tilde{V}	tilde matrix of a vector V , defined in Equation (4.64)
$\delta ()$	variation of a variable

The author of this thesis has granted The University of Western Ontario a non-exclusive license to reproduce and distribute copies of this thesis to users of Western Libraries. Copyright remains with the author.

Electronic theses and dissertations available in The University of Western Ontario's institutional repository (Scholarship@Western) are solely for the purpose of private study and research. They may not be copied or reproduced, except as permitted by copyright laws, without written authority of the copyright owner. Any commercial use or publication is strictly prohibited.

The original copyright license attesting to these terms and signed by the author of this thesis may be found in the original print version of the thesis, held by Western Libraries.

The thesis approval page signed by the examining committee may also be found in the original print version of the thesis held in Western Libraries.

Please contact Western Libraries for further information:

E-mail: libadmin@uwo.ca

Telephone: (519) 661-2111 Ext. 84796

Web site: <http://www.lib.uwo.ca/>

- Chapter 1 -

Introduction

1.1 Introduction to Flexible Multibody System Dynamics

The dynamic models of multibody systems with flexible members are being increasingly considered in the simulation of dynamics and control of mechanical systems because of the trend towards higher operating speeds, heavier pay loads and lighter weights used in the design of mechanical systems such as satellites, aircraft, trains, mechanisms and robots. This interest is due to the fact that the dynamic loads at the interconnections of the systems and the position accuracy of the bodies can be influenced significantly by the vibrational deformation of the flexible members in the system.

Flexible multibody systems are characterized by rigid and flexible bodies with inertia and springs, dampers, servomotors, interconnected by rigid or flexible joints. For multibody systems with all rigid bodies, the governing equations of this kind of system are highly non-linear equations of motion. Many methods can be used to derive these governing equations, such as the Newton-Euler method [Gupta 1974], Lagrange's equation [Paul 1975], Lagrange's multipliers [Nikravesh 1984], Kane's equations [Kane 1968], and Wittenburg's approach [Wittenburg 1977]. For multibody systems with flexible members, vibrational deformation of these flexible members must be considered in the dynamic analysis.

During the last two decades, many investigators have been pursuing research in the area of dynamics of multibody systems containing flexible bodies. One approach to model this problem was to employ finite elements with large displacement coordinates. Likins [1972] developed this method to formulate flexible appendages on

satellites. Similar work was done by Cavin and Dusto [1977]. In this method, to model a flexible member many elements would be required. This made the number of coordinates, and degrees of freedom to be included, extremely large. An approach which eliminated many of these coordinates was presented by Dubowsky, et al. [1977]. In this approach, component mode synthesis was used to reduce the number of coordinates by doing a modal reduction on the internal degrees of freedom. Modal coordinates for the lower frequencies were used to represent the deformation of the flexible bodies. Similar approaches were proposed using component modes by Shabana [1982], Turcic [1984], and Wu and Haug [1989]. These methods used different approaches to formulate the overall equations and solution methods.

Another approach to formulate the vibrational deformation of flexible members is to attach a local reference frame to an assumed rigid body to the flexible body and employ component normal modes defined relative to this reference frame [Ho 1977, Huston 1988, Wielenga 1984, Singh 1985, Book 1984]. The differences between the approaches used by these authors lie in the different principles used to derive the governing equations. This method in fact is the same as the simplified finite element method using component modes to reduce the number of coordinates. It is an issue that this method does not adequately consider the phenomenon called dynamic stiffening and softening, also called motion induced stiffness of flexible members [Banerjee and Dickens 1990]. It was first pointed out by Kane [1987] and further investigated by Amirouche [1989] and Banerjee [1990] that the non-linear geometric stiffness due to the axial force of beams and mid-surface force of plate has considerable effect on the prediction of the dynamical behavior of these flexible members in a multibody system. The typical examples are beams and plates subject to high speed overall motion [Kane 1987, Banerjee 1989].

The mechanics of spin-stiffening of beams has long been known, for example, Bisplinghoff et al. [1955], and Meirovitch [1967]. For a more general rotating structure, Likins [1974] was one of the earliest to suggest the use of geometric stiffness to augment the structure stiffness and hence correctly represent the dynamic response.

This geometric stiffness method was further developed by many other researchers using different assumptions and approaches [Levinson and Kane 1976, Turcic and Midha 1984, Wu and Haug 1988, Ider and Amirouche 1989, Banerjee et al. 1990, 1991]. Among them, the way to extract geometric stiffness by including non-linear strain-stress relationship [Ider and Amirouche 1989] is the most interesting for multibond graph modelling.

1.2 Introduction to Bond Graph Method

The bond graph is a unified approach to the modelling of dynamics of multidisciplinary physical systems. It was introduced by Paynter [1961] and developed by Karnopp and Rosenberg [1968, 1975], and Thoma [1975]. The bond graph is an energy based graphical representation of physical systems. In a bond graph, every kind of lumped physical system can be modelled by a bond graph element, such as storage, dissipation or transformation of energy. All elements are interconnected through energy conserving bonds or junction structures to perform energy exchange between these elements. A complete bond graph represents a physical system, gives insight into its physical structure and keeps all physical quantities or states of the physical system. Another important aspect of bond graph is its computation structure. Explicit or implicit governing equations of the system, and their form for numerical solution, can be conveniently extracted from the bond graph by a systematic procedure. There have been programs for the system simulation that use bond graph as media, such as ENPORT [Rosenberg 1974], CAMP [Grand 1982], TUTSIM [Meerman 1981], SYSBOND [McInnis and ElMaraghy 1989], CAMAS [Broenink 1990], and BONDYN [Felez 1990].

The application of bond graph techniques into particle dynamics was initiated from the beginning of development of the bond graph technique [Karnopp and Rosenberg 1968, Rosenberg 1972, Brown 1972]. However, the real application of the

bond graph technique in multibody system dynamics was pioneered by Karnopp [1976] and improved by Bos [1986]. Karnopp proposed a non-linear bond graph structure called Modulated GYrator array (MGY) to model the rotation property of a rigid body in spatial motion. This structure was given a specific name Euler Junction Structure (EJS) [Karnopp 1978] and was accepted by most investigators [Breedveld 1985, Bos 1985, Tiernego 1985]. However, as the number of bodies in a multibody system increases, it becomes more and more cumbersome to use the conventional bond graph. Just as matrix algebra makes algebra much simpler in notation and digital computation, the multibond graph was developed to reduce the complexity of a bond graph in complex physical systems [Bonderson 1975, Breedveld 1982, 1984, 1985]. Bos applied this multibond notation into multibody system dynamics and discussed many issues in this application [Bos 1986]. Recently, a program developed by Felez [Felez 1991] for modelling and simulation of multibody systems was identical in theory to Bos' thesis [1986].

Until now, bond graphs were mostly used to model lumped parameter systems. The application of bond graphs into flexible multibody system dynamics started with Margolis's work [Margolis 1978], in which he used normal modes of flexible structures to turn distributed systems into lumped systems which can then be represented by bond graphs for vibration analysis. This idea was developed in his late work [Margolis 1980] and further extended into flexible multibody system dynamics [Margolis and Karnopp 1979]. They developed a bond graph to model a free-moving beam undergoing planar overall translation and rotation with in plane vibrations. Although they did not explicitly state it in their paper, they used free-free normal modes and a mean-axis local reference frame to decouple the coupling between rotation and vibrations. However, it has been shown [Wielenga 1984] that this kind of choice results in a significant error for a flexible link under boundary conditions such as fixed-free (cantilever), fixed-hinged, and fixed-fixed. Yoshimura [1989] and others proposed a multibond graph representation for flexible multibody systems. In their work, however, only elasticity of the flexible members is considered using compliance elements, while

the dynamic forces caused by the vibration of the flexible bodies are ignored. Samanta [1990] presented a bond graph method for flexible multibody system dynamics. In his paper, the same bond graph as Margolis' [1979] for a planar moving flexible body with in-plane vibrations was used, which is subject to the same restrictions in application. The common problem of all bond graphs for flexible multibody system dynamics mentioned above is that they cannot deal with three dimensional problems. Three dimensional problem involves coupling of accelerations between translational, rotational and flexible vibration modes. A multibond graph representation for a 3-D moving flexible body was developed by Yazman [1989]. However, many simplifications have been assumed in the multibond graph representation and this may cause problems in high speed motion.

1.3 Objectives of this Thesis

This thesis is intended to provide a general computer-aided modelling approach and simulation of dynamics of a three dimensional flexible multibody system including mixed energy domains. With consideration given to the state of the art in flexible multibody system dynamics and multibond graph with its application into multibody dynamics, the following objectives were formed.

- To investigate the vibration behavior of a flexible body in a multibody system which is subject to high speed rotation and large axial forces. This will give a better understanding of the effect of non-linear geometric stiffness on the vibration of the flexible body in a multibody system.

- To derive the equations of motion of a flexible body undergoing 3-D overall motion with consideration of geometric stiffness, in the form easy for multibond graph representation which also lends itself to convenient computer-aided modelling.

- To discuss the simplification of equations of motion by using different types of body reference frames.

- To develop a general form of multibond graph, and other forms of multibond graphs in terms of different types of body reference frames, and a general procedure for modelling a flexible body.

- To develop multibond graphs for mechanical joints and a procedure for modelling of flexible multibody systems.

- To discuss the derivation of equations of motion from multibond graph and the algorithm for their numerical solution.

- To develop a computer-aided modelling and simulation software for the implementation of construction of multibond graphs and derivation of equations of motion.

- To use the developed techniques and computer software to study some problems in flexible multibody system dynamics.

- Chapter 2 -

Concepts from Multibond Graph for the Dynamics of a Single Rigid Body

2.1 Introduction

A flexible multibody system usually consists of flexible members (beams, plates, membranes, etc.) as well as rigid members. The rigid multibody dynamics has been well developed in the literature for a long time. The bond graph technique has also been applied to rigid body dynamics for more than a decade. One of the reasons that this chapter is included is to provide a review of principles and equations of rigid body dynamics from which the basic principle and many terms in the flexible body dynamics will be more easily recognized. It also provides a review of multibond graph representation of rigid body kinematics and dynamics from which some of the strategies used in the multibond graph representation of a single rigid body can be carried over to a flexible body. In addition the notations of vectors, tensors as well as matrices are defined for coordinate systems, generalized displacement, velocities as well as generalized forces which will be used throughout the thesis.

2.2 Mathematical Preliminaries

2.2.1 Frames and Cartesian Coordinates

In classical mechanics, to describe geometrical and mechanical relations it is required to define a frame of axes spanning the space. It is common practice to use the

Cartesian frame which is characterized by the location of its origin o and by the orientation of three perpendicular axes, represented by three unit vectors \hat{e}_x , \hat{e}_y , \hat{e}_z , ordered in a right-handed system. These three unit vectors are called the base of the frame and the base is identified in a compact form $\{\hat{e}\}$ which is defined as

$$\{\hat{e}\} = \{\hat{e}_x \ \hat{e}_y \ \hat{e}_z\}^T \quad (2.1)$$

In this thesis a frame will be referenced by its base with a specified number as superscript.

Having established a frame, the location of an arbitrary point P is specified with respect to this frame by its Cartesian Coordinates p_x p_y p_z shown in Figure 2-1.

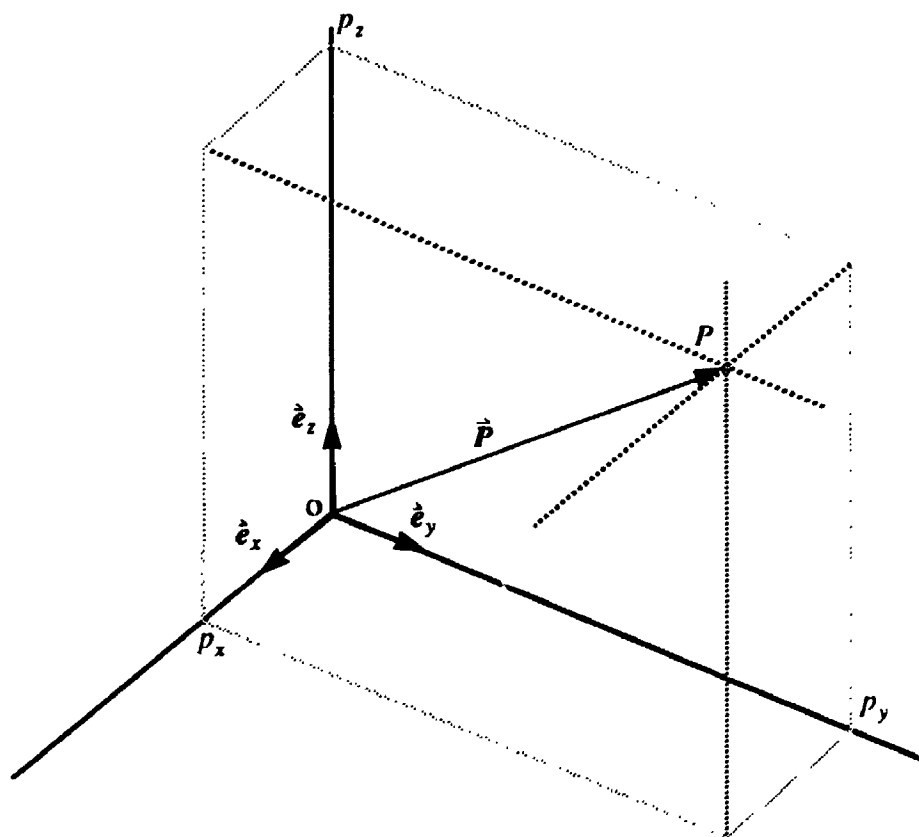


Figure 2-1 Frame, Cartesian coordinates and position vector

In multibody system dynamics, more than one frame is necessary. Usually each body has a frame attached to it and there is a global one for the whole system. The motion of the system and the relative motion between the bodies can be represented by the motion of these frames. In this thesis, the frame for the whole multibody system will be denoted as $\{\dot{e}^o\}$. The motion of frame $\{\dot{e}^i\}$ with respect to frame $\{\dot{e}^o\}$ can be regarded as being composed of two simple motions called translation and rotation. The translation can be determined by the coordinates of the origin of frame $\{\dot{e}^i\}$ in frame $\{\dot{e}^o\}$. The rotation can be represented in different ways such as Euler angles, Braynt angles or Euler parameters [Wittenburg 1977].

2.2.2 Vectors, Dyadics and their Matrix Representations

Vectors are commonly used in classical mechanics, visualized as directed line segments having a specified length and direction. These kinds of vectors can be called geometric vectors and will be graphically identified by an arrow and symbolically by an identifier with an arrow on top. Geometry of motion is at the heart of both the kinematics and dynamics of mechanical systems. Vector analysis is the time-honored tool for classical mechanics. In its geometric form, however, vector algebra is not well suited for computer implementation. In all computer aided kinematic and dynamic analysis, a systematic matrix formulation of vector algebra, referred to as algebraic vector representation, is commonly used. This section gives the elementary properties of matrix and algebraic vectors.

A vector can be used to represent position of a point in space and be measured with respect to different frames. For example, the position of point P in Figure 2-1 can be represented by vector \vec{P} .

When measured in frame $\{\dot{e}\}$, the vector \vec{P} can be represented by a linear combination of three unit base vectors

$$\vec{P} = p_x \dot{e}_x + p_y \dot{e}_y + p_z \dot{e}_z = \{P\}^T \{\dot{e}\} = \{\dot{e}\}^T \{P\} \quad (2.2)$$

where column matrix $\{P\}$ is the coordinate component of vector \vec{P} in base $\{\hat{e}\}$. In this thesis, $\{P\}$ will be called the algebraic vector of \vec{P} . The original vector will be distinguished as a geometric vector. These two forms of a vector will be simply called vectors, while the difference can be distinguished by the symbol.

An often used skew-symmetric matrix associated with a algebraic vector $\{P\}$ is defined as

$$[\tilde{P}] = \begin{bmatrix} 0 & -p_z & p_y \\ p_z & 0 & -p_x \\ -p_y & p_x & 0 \end{bmatrix} \quad (2.3)$$

where the tilde placed over the vector indicates that the components of the vector are used to generate the skew-symmetric matrix. This operation is used to represent cross multiplication of vectors in a matrix form.

A dyadic is a mathematical notation which is defined as

$$\hat{Q} = \hat{a}\hat{b} + \hat{c}\hat{d} + \dots \quad (2.4)$$

where $\hat{a} \dots$ are arbitrary vectors. The dyadic is used in vector algebra, in which dot multiplication (pre- or post-) of a dyadic with a vector produces a vector. Applying the algebraic form of a vector to the right hand side of the dyadic with respect to the same base, the algebraic form of a dyadic can be obtained as

$$\hat{Q} = \{\hat{e}\}^T (\{a\}^T \{b\} + \{c\}^T \{d\} + \dots) \{\hat{e}\} = \{\hat{e}\}^T [Q] \{\hat{e}\} \quad (2.5)$$

where matrix $[Q]$ is made of the coordinates of the dyadic and is symmetric.

A special dyadic in rigid body dynamics is unit dyadic which is defined as

$$\hat{E} = \hat{e}_x \hat{e}_x + \hat{e}_y \hat{e}_y + \hat{e}_z \hat{e}_z = \underbrace{\{\hat{e}\}^T}_{\text{row}} [E] \underbrace{\{\hat{e}\}}_{\text{column}} \quad (2.6)$$

where $[E]$ is a unit matrix. The dot multiplication of a unit dyadic with a vector gives the vector itself.

The application of a dyadic in rigid body dynamics is the simplification of double cross multiplication of vectors. Recalling that a double cross multiplication of three vectors can be simplified as two vectors, and using the properties of dyadic and unit dyadic introduced above, a double cross multiplication of three vectors can be written as a dot multiplication of a dyadic and a vector

$$\begin{aligned}\hat{a} \times (\hat{b} \times \hat{c}) &= (\hat{a} \cdot \hat{c}) \hat{b} - \hat{c} (\hat{a} \cdot \hat{b}) \\ &= [(\hat{a} \cdot \hat{c}) \hat{E} - \hat{c} \hat{a}] \cdot \hat{b}\end{aligned}\tag{2.7}$$

The basic relations between the vector, dyadic operation and their algebraic forms are listed in Table 2-1. The verification of this relation can be found in textbooks [Wittenberg 1977, Roberson 1988].

Table 2-1 Vector, dyadic terms in geometric and matrix forms

Geometric	Matrix
\hat{a}	$\{a\}$
$\hat{a} + \hat{b}$	$\{a\} + \{b\}$
$\beta \hat{a}$	$\beta \{a\}$
$\hat{a} \cdot \hat{b}$	$\{a\}^T \{b\}$
$\hat{a} \times \hat{b}$	$[\tilde{a}] \{b\}$
$\hat{Q} \cdot \hat{a}$	$[Q] \{a\}$
$\hat{a} \times (\hat{b} \times \hat{c})$	$(\{a\}^T \{c\} [E] - \{c\} \{a\}^T) \{b\}$

2.3 The Frames, Position Vectors and Orientation Definitions for a Body

In order to locate a body in space, an inertial frame fixed on the earth or moving

relative to the earth at constant velocity and a body reference frame attached on the body are usually used, which is shown in Figure 2-2. The unit vector array $\{\hat{e}^o\}$ forms a Cartesian coordinate system of the inertial frame, and the unit vector array $\{\hat{e}^i\}$ forms another Cartesian coordinate system of the body reference frame for the body, which are

$$\{\hat{e}^o\} = \{\hat{e}_x^o, \hat{e}_y^o, \hat{e}_z^o\}^T \quad (2.8)$$

$$\{\hat{e}^i\} = \{\hat{e}_x^i, \hat{e}_y^i, \hat{e}_z^i\}^T \quad (2.9)$$

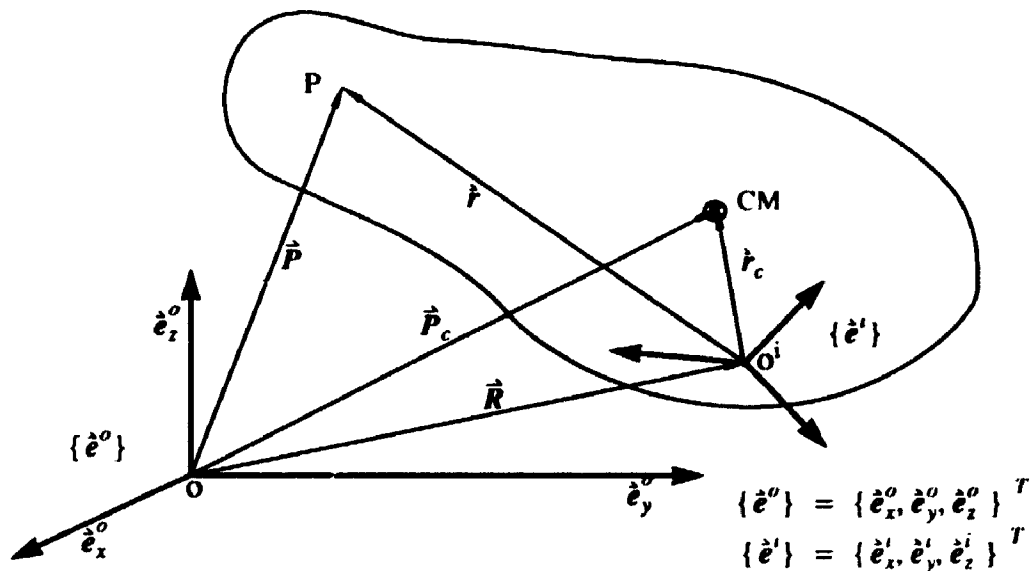


Figure 2-2 Coordinate systems and position vectors for a rigid body

Vector \vec{R} locates the origin of the body reference frame in the inertial frame, which determines the position of the body in space. Vector \vec{r} shows the position of an arbitrary point P in the body reference frame. Vector \vec{r}_c is the position vector of the mass center of the body in the body reference frame. The instantaneous position of the point P and the mass center of the body in the inertial frame is \vec{P} and \vec{P}_c . It is obvious that

$$\vec{P} = \vec{R} + \vec{r} \quad (2.10)$$

$$\vec{P}_c = \vec{R} + \vec{r}_c \quad (2.11)$$

The orientation of the body in space can be described by the orientation of the body reference frame relative to the inertial frame. There are several coordinate systems for the description of this orientation.

In Euler's theorem [Wittenberg 1977] it is stated that two arbitrarily oriented bases with coinciding origins can be made to coincide with each other by rotating one of them through a certain angle about an axis. So the orientation of a coordinate system with respect to the other can be defined by a rotation angle and an axis of rotation. Euler parameters are derived from this idea. In practice, orientations are also described in Bryant angles or Euler angles. Both Euler angles and Bryant angles use sets of three successive rotation angles as coordinates. Euler angles use so called 3-1-3 sequence, or precessing, nutation and spin angles; Bryant angles use 1-2-3 sequence, or roll, pitch and yaw. The advantages of these two coordinates are that it is easy for physical implementation of these angles by three angular drivers corresponding to each angle. Another advantage of Bryant angles lies in that the transformation matrix can be linearized when the angles are small. However, both Euler angles and Bryant angles share two disadvantages

1. All terms in the transformation matrix are trigonometric functions which are inefficient in computer simulation.

2. Both angles have a critical situation in which two angles can not be identified uniquely. For Euler angles, when the nutation angle approaches $n\pi$, $n = 0, 1, \dots$, precessing angle and spin angle can not be determined uniquely. For Bryant angles, when the pitch angle approaches to $\frac{\pi}{2} + n\pi$, roll and yaw angles become indeterminate.

Euler parameters avoid these two disadvantages. The transformation matrix is simply a quadratic function of parameters. And its parameters can always be determined uniquely. However, this coordinate system has four parameters and a constraint condition is attached to them. Another disadvantage of Euler parameters is

that they are not as convenient as both Euler angles and Bryant angles to implement rotation displacement on general rotation of a body. Due to their advantages and difficulties, the question of which rotation coordinate system should be used in this thesis will be answered by the practical problems.

A vector can be described in different frames and the relation between these different descriptions is represented by a transformation matrix. For the two frames described in this section, the relation is

$$\{\dot{e}^0\} = [A^{0i}] \{\dot{e}^i\} \quad \text{or} \quad \{\dot{e}^i\} = [A^{i0}] \{\dot{e}^0\} \quad (2.12)$$

where $[A^{0i}]$ is the transformation matrix between these two frames. It is an orthogonal matrix which has a property of

$$[A^{0i}]^{-1} = [A^{0i}]^T = [A^{i0}] \quad (2.13)$$

For vector \vec{V} , for which column matrices $\{V^0\}$ and $\{V^i\}$ are its coordinates in frame $\{\dot{e}^0\}$ and frame $\{\dot{e}^i\}$, the following relation holds in terms of equation (2.12)

$$\{V^0\} = [A^{0i}] \{V^i\} \quad (2.14)$$

In Figure 2-2, if vector \vec{P} is described in inertia frame $\{\dot{e}^0\}$ and others are described in body reference frame $\{\dot{e}^i\}$, the algebraic vector form of equation (2.10) can be also written as

$$\{P\} = [A^{0i}] (\{R\} + \{r\}) \quad (2.15)$$

In different rotation coordinates, the transformation matrix is different. Let ψ, θ, ϕ represent precessing, nutation and spin angles in Euler angles, ϕ_1, ϕ_2, ϕ_3 as roll, pitch and yaw in Bryant angles and $\{p\} = \{p_0 \ p_1 \ p_2 \ p_3\}^T$ as Euler parameters. The transformation matrices in these rotation coordinates are as follows [Roberson 1988]:

Euler angle

$$[A^{i0}] = \begin{bmatrix} c\psi c\varphi - s\psi c\theta s\varphi & c\psi s\varphi + s\psi c\theta c\varphi & s\psi s\theta \\ -s\psi c\varphi - c\psi c\theta s\varphi & -s\psi s\varphi + c\psi c\theta c\varphi & c\psi s\theta \\ s\theta s\varphi & -s\theta c\varphi & c\theta \end{bmatrix} \quad (2.16)$$

where $s(\) = \sin(\)$ and $c(\) = \cos(\)$.

Bryant angles

$$[A^{i0}] = \begin{bmatrix} c\phi_2 c\phi_3 & c\phi_1 s\phi_3 + s\phi_1 s\phi_2 c\phi_3 & s\phi_2 s\phi_2 - c\phi_1 s\phi_2 c\phi_3 \\ -c\phi_2 s\phi_3 & c\phi_1 c\phi_3 - s\phi_1 s\phi_2 s\phi_3 & s\phi_1 c\phi_3 + c\phi_1 s\phi_2 s\phi_3 \\ s\phi_2 & -s\phi_1 c\phi_2 & c\phi_1 c\phi_2 \end{bmatrix} \quad (2.17)$$

Euler parameters

$$[A^{i0}] = 2 \begin{bmatrix} p_0^2 + p_1^2 - \frac{1}{2} & p_1 p_2 + p_0 p_3 & p_1 p_3 - p_0 p_2 \\ p_1 p_2 - p_0 p_3 & p_0^2 + p_2^2 - \frac{1}{2} & p_2 p_3 + p_0 p_1 \\ p_1 p_3 + p_0 p_2 & p_2 p_3 - p_0 p_1 & p_0^2 + p_3^2 - \frac{1}{2} \end{bmatrix} \quad (2.18)$$

2.4 Kinematics of a Rigid Body

Velocities are the time derivatives of position vectors with respect to different frames. Velocities with respect to the inertial frame are called absolute velocities and otherwise are relative velocities. In this thesis, velocities are denoted by a dot on the top of the position vectors.

The velocity of the point P and the center of mass P_c of the rigid body can be

obtained by taking the derivative of its position vector, which is

$$\dot{\vec{P}} = \dot{\vec{R}} + \vec{\Omega} \times \vec{r} \quad (2.19)$$

$$\dot{\vec{P}}_c = \dot{\vec{R}} + \vec{\Omega} \times \vec{r}_c \quad (2.20)$$

where $\dot{\vec{P}}$ is the absolute velocity of the mass point P, $\dot{\vec{R}}$ is the absolute translational velocity of the body reference frame $\{\hat{e}^i\}$ and $\vec{\Omega}$ is the absolute angular velocity of the body reference frame. The acceleration of the point P is the second derivative of the position vectors, which is

$$\ddot{\vec{P}} = \ddot{\vec{R}} + \dot{\vec{\Omega}} \times \vec{r} + \vec{\Omega} \times (\vec{\Omega} \times \vec{r}) \quad (2.21)$$

If vectors \vec{P} and \vec{P}_c are described in the inertial frame $\{\hat{e}^o\}$ and others are described in the body reference frame $\{\hat{e}^i\}$, the algebraic vector form of equations (2.19), (2.20) and (2.21) can be written as

$$\{\dot{\vec{P}}\} = [A^{0i}] (\{\dot{\vec{R}}\} - [\vec{r}] \{\Omega\}) \quad (2.22)$$

$$\{\dot{\vec{P}}_c\} = [A^{0i}] (\{\dot{\vec{R}}\} - [\vec{r}_c] \{\Omega\}) \quad (2.23)$$

$$\{\ddot{\vec{P}}\} = \{\ddot{\vec{R}}\} - [\vec{r}] \{\dot{\Omega}\} + \vec{\Omega} \times (\vec{\Omega} \times \vec{r}) \quad (2.24)$$

The position of the point P in time can be obtained by integration of $\{\dot{\vec{P}}\}$. However, this integration is meaningless until the angular velocity is expressed in terms of rotation coordinates because the finite rotation is not a vector. The angular velocities in terms of different rotation coordinate systems are as follows [Roberson 1988]:

Euler angles

$$\{\Omega\} = \begin{bmatrix} s\theta s\varphi & c\varphi & 0 \\ s\theta c\varphi & -s\varphi & 0 \\ c\theta & 0 & 1 \end{bmatrix} \begin{Bmatrix} \dot{\Psi} \\ \dot{\theta} \\ \dot{\varphi} \end{Bmatrix} \quad (2.25)$$

Bryant angles

$$\{\Omega\} = \begin{bmatrix} c\phi_1 c\phi_3 & s\phi_3 & 0 \\ -c\phi_2 s\phi_3 & c\phi_3 & 0 \\ s\phi_2 & 0 & 1 \end{bmatrix} \begin{Bmatrix} \dot{\phi}_1 \\ \dot{\phi}_2 \\ \dot{\phi}_3 \end{Bmatrix} \quad (2.26)$$

Euler parameters

$$\{\Omega\} = 2 \begin{bmatrix} -p_1 & p_0 & p_3 & p_2 \\ -p_2 & -p_3 & p_0 & p_1 \\ -p_3 & p_2 & -p_1 & p_0 \end{bmatrix} \{\dot{p}\} \quad (2.27)$$

The inverse of these three relations can also be used to obtain the rotation coordinates of the body reference frame in the inertial frame.

2.5 Dynamics of a Rigid Body**2.5.1 Mass Geometry of a Rigid Body**

The motion of a rigid body depends not only on the forces and torques acting on it, but also on the mass geometry of the body. For the dynamics of a rigid body, it is not necessary to know in detail how mass is distributed throughout the body. All one needs to know is the location of the mass center, as well as six quantities called moments of inertia and products of inertia.

The mass center of a body is a unique and special point CM that meets the following relation (referring to Figure 2-2)

$$\mathbf{r}_c = \frac{1}{m} \int_v \mathbf{r} \rho dv \quad (2.28)$$

where ρ is mass density of the body, v the volume of the body and m the mass of the body which is

$$m = \int_v \rho dv \quad (2.29)$$

When the reference point o^i is located at the mass center, \mathbf{r}_c will be zero.

To define moments of inertia and products of inertia of a body, an inertia dyadic should be first introduced. Referring to Figure 2-2, the inertia dyadic of the body relative to reference point o^i is defined as

$$\hat{J} = \int_v ((\mathbf{r} \cdot \mathbf{r}) \hat{E} - \mathbf{r} \mathbf{r}) \rho dv \quad (2.30)$$

Assuming that the dyadic and vector are measured in the body reference frame $\{\hat{e}^i\}$, the matrix form of this inertia dyadic can be written as

$$\begin{aligned} \hat{J} &= \{\hat{e}^i\}^T \int_v ((\{r\}^T \cdot \{r\}) [\hat{E}] - \{r\} \{r\}^T) \rho dv \{\hat{e}^i\} \\ &= \{\hat{e}^i\}^T [J] \{\hat{e}^i\} \end{aligned} \quad (2.31)$$

where matrix $[J]$ is called the inertia matrix. It is a symmetric matrix and therefore only six of its elements are independent. The three diagonal elements are called moments of inertia and the three off diagonal elements are called products of inertia.

It should be noted that the inertia dyadic defined above is about reference point o^i , the origin of the body reference frame. If the reference point changes, the inertia dyadic will also change. It is very useful to find the relation between these inertia dyadics about different reference points. The Huygens-Steiner rule meets this requirement [Wittenburg 1977]. It states that if \hat{J} and \hat{J}_c are inertia dyadics about reference point o^i and mass center CM respectively, the following relation holds

$$\hat{\mathbf{J}} = \hat{\mathbf{J}}_c + m(\{\hat{\mathbf{r}}_c \cdot \hat{\mathbf{r}}_c\} \hat{\mathbf{E}} - \hat{\mathbf{r}}_c \hat{\mathbf{r}}_c) \quad (2.32)$$

or in matrix form

$$[\mathbf{J}] = [\mathbf{J}_c] + m((\{\mathbf{r}_c\}^T \cdot \{\mathbf{r}_c\}) [\mathbf{E}] - \{\mathbf{r}_c\} \{\mathbf{r}_c\}^T) \quad (2.33)$$

2.5.2 Momentum

Linear momentum of a mass element in the rigid body is defined as $\{\dot{\mathbf{P}}\} \rho dv$. The definition of angular momentum \vec{H}_0 of a rigid body about a fixed point in an inertial frame, say o , is

$$\vec{H}_0 = \int_v \hat{\mathbf{P}} \times \dot{\hat{\mathbf{P}}} \rho dv \quad (2.34)$$

Substituting equations (2.10) and (2.19) for $\hat{\mathbf{P}}$, $\dot{\hat{\mathbf{P}}}$ and using equation (2.20), the angular momentum becomes

$$\vec{H}_0 = m\vec{R} \times \dot{\hat{\mathbf{P}}}_c + m\hat{\mathbf{r}}_c \times \dot{\vec{R}} + \hat{\mathbf{J}} \cdot \vec{\Omega} \quad (2.35)$$

If the origin of the body reference frame coincides with the origin of the inertial frame, the angular momentum changes to about point o' , which is

$$\vec{H} = m\hat{\mathbf{r}}_c \times \dot{\vec{R}} + \hat{\mathbf{J}} \cdot \vec{\Omega} \quad (2.36)$$

Further, if the origin of body reference frame o' coincides with mass center CM, the angular momentum becomes

$$\vec{H}_c = \hat{\mathbf{J}}_c \cdot \vec{\Omega} \quad (2.37)$$

2.5.3 Dynamics of a Rigid Body

The motion of a single rigid body can be described completely in Cartesian coordinates, such as $\{\hat{e}^i\}$ and $\{\hat{e}^o\}$. In these coordinate systems, Newton-Euler laws are the best method to describe the motion of the rigid body.

Newton's second law describes the relation between the resultant force on the body and the translational acceleration of the body as

$$m\ddot{\hat{P}}_c = \vec{F} \quad (2.38)$$

where vector \vec{F} is the resultant force which is resulted from volume force and surface traction on the body, which can be defined as

$$\begin{aligned} \vec{F} &= \int_v \hat{g} \rho dv + \int_s d\vec{F}_s \\ &= m\hat{g} + \vec{F}_s \end{aligned} \quad (2.39)$$

where \hat{g} is gravity, \vec{F}_s is resultant surface traction and s is the surface of the body.

The matrix form of this equation can be obtained by referring to the earlier section. Assuming that \hat{P}_c and \hat{g} are represented in the inertial frame $\{\hat{e}^o\}$ and \vec{F} is given in the body reference frame, the matrix form of the equation is

$$\frac{d}{dt}(m\hat{P}_c) = m\{g\} + [A^{0i}] \{F_s\} \quad (2.40)$$

Euler's law states that the time derivative of the angular momentum of the body equals the resultant torque on the body, both being about the fixed point in the inertial frame, say o ,

$$\frac{d\vec{H}_0}{dt} = \vec{T}_o \quad (2.41)$$

where

$$\begin{aligned} \vec{T}_o &= \int_V \vec{P} \times \dot{\vec{g}} \rho dv + \int_S \vec{P} \times d\vec{F}_s \\ &= \vec{P}_c \times m\dot{\vec{g}} + \vec{R} \times \vec{F}_s + \int_S \vec{r} \times d\vec{F}_s \\ &= \vec{R} \times (m\dot{\vec{g}} + \vec{F}_s) + \vec{r}_c \times m\dot{\vec{g}} + \vec{T} \end{aligned} \quad (2.42)$$

The term \vec{T} above is the torque about the origin of the body reference frame due to the surface traction represented by \vec{T} , which is

$$\vec{T} = \int_S \vec{r} \times d\vec{F}_s \quad (2.43)$$

According to equation (2.35), the time derivative of the angular momentum can be written as

$$\frac{d\vec{H}_0}{dt} = m\vec{R} \times \ddot{\vec{P}}_c + m\vec{r}_c \times \ddot{\vec{R}} + \dot{\vec{J}} \cdot \dot{\vec{\Omega}} + \vec{\Omega} \times (\dot{\vec{J}} \cdot \vec{\Omega}) \quad (2.44)$$

When this expression and equation (2.42) are substituted into equation (2.41), the Euler equation for a rigid body is obtained as

$$m\vec{r}_c \times \ddot{\vec{R}} + \dot{\vec{J}} \cdot \dot{\vec{\Omega}} + \vec{\Omega} \times (\dot{\vec{J}} \cdot \vec{\Omega}) = \vec{T} + \vec{r}_c \times m\dot{\vec{g}} \quad (2.45)$$

Equations (2.38) and (2.45) are the most general equations of motion for a rigid body. When the origin of the body reference frame coincides with the mass center of the body the equation (2.45) will have simpler form which is

$$\dot{\vec{J}}_c \cdot \dot{\vec{\Omega}} + \vec{\Omega} \times (\dot{\vec{J}}_c \cdot \vec{\Omega}) = \vec{T} \quad (2.46)$$

Equation (2.45) is not suitable for multibond graph representation. The reason for this will be discussed in next section. Here, the Huygens-Steiner rule is used to change the inertia dyadic about the origin of the body reference frame to the inertia dyadic about the mass center. When equation (2.32) is substituted in equation (2.45), the equation becomes

$$m\dot{\vec{r}}_c \times (\ddot{\vec{R}} + \dot{\vec{\Omega}} \times \dot{\vec{r}}_c + \vec{\Omega} \times (\vec{\Omega} \times \dot{\vec{r}}_c)) + m + \mathbf{J}_c \cdot \dot{\vec{\Omega}} + \vec{\Omega} \times (\mathbf{J}_c \cdot \vec{\Omega}) = \vec{T} + \dot{\vec{r}}_c \times m\vec{g} \quad (2.47)$$

Noting that the terms in the large bracket forms the acceleration of the mass center, the equation can be written as

$$m\dot{\vec{r}}_c \times \ddot{\vec{P}}_c + \mathbf{J}_c \cdot \dot{\vec{\Omega}} + \vec{\Omega} \times (\mathbf{J}_c \cdot \vec{\Omega}) = \vec{T} + \dot{\vec{r}}_c \times m\vec{g} \quad (2.48)$$

The matrix form of equations (2.46) and (2.48) are, respectively

$$[\mathbf{J}_c] \cdot \{\dot{\vec{\Omega}}\} - [\tilde{H}_c] \{\vec{\Omega}\} = \{T\} \quad (2.49)$$

$$[\mathbf{J}_c] \cdot \{\dot{\vec{\Omega}}\} + [\tilde{r}_c] [A^{0i}] \frac{d}{dt}(m\dot{\vec{P}}_c) - [\tilde{H}_c] \{\vec{\Omega}\} = \{T\} + m[\tilde{r}_c] \{g\} \quad (2.50)$$

2.6 Multibond Graph Modelling of a Single Rigid Body

The bond graph is a symbolic representation of physical systems. In this thesis, it is assumed that the reader is familiar with the concepts of bond graphs. A detailed discussion can be found in textbooks written by Karnopp and Rosenberg [1975, 1983]. For mechanical systems, especially multibody systems, a more concise multibond notation has been used [Breeveld 1985, Bos, etc. 1985, 1986]. The notation of

multibond graphs which are used in this thesis is given in Table 2-2. The multibond is denoted by an arrow with a double lined tail. A number in between the two lines means the dimension of the bond. Multiport elements are denoted by bold capital characters. The matrices on the right side of or under the capital characters are the constitutive relations of the elements.

From Table 2-2, it can be seen that the constitutive laws of multiport elements are based on matrix operations. This gives the fundamentals of multibond graph modelling for the motion of a rigid body. The multibond graph modelling of a rigid body has been extensively discussed by Bos [1986]. This section lists the multibond graphs for kinematics and dynamics of a single rigid body based on Bos' results.

Assuming that Figure 2-2 represents a freely moving rigid body having its mass center at point CM and a joint at point P, two coordinate systems have been set up. Frame $\{\hat{e}^o\}$ is the inertial frame fixed on the ground and frame $\{\hat{e}^i\}$ the body reference frame attached to the body at an arbitrarily chosen reference point. The procedure to establish multibond graphs for kinematics and dynamics of the rigid body is as follows:

1. To set up 1-junctions

In bond graphs, 1-junction represents flow which is velocity in mechanical systems. The multibond graph for a rigid body should include all important velocity variables in kinematics and dynamics of a rigid body. Referring to the last several sections, these velocities should appear in the bond graph as: absolute velocity of the reference point $\dot{\vec{R}}$, angular velocity of the body reference frame $\vec{\Omega}$, absolute velocity of the mass center $\dot{\vec{P}}_c$, and absolute velocity of the joint $\dot{\vec{P}}$.

For the convenience of bond graph representation, all velocities are measured in the body reference frame except the absolute velocity of the mass center, which is measured in both frames. Therefore, there is a 1-junction array for each velocity component vector except the absolute velocity of the mass center which has two 1-junction arrays, one is the component vector in body reference frame and the other in the inertial frame. These 1-junctions are plotted in Figure 2-3 (a).

2. To set up multibond graph for kinematics

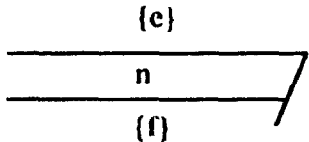
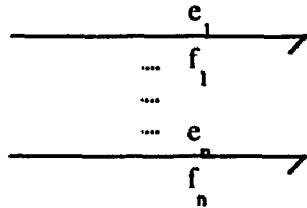
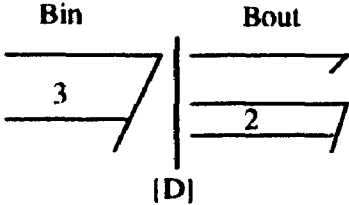
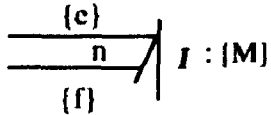

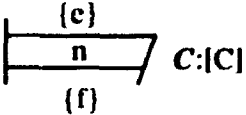

This step sets up the relations between the velocity variables through adding 3-dimensional multibond, 0-junction arrays and modulated transformations. The relations are based on the kinematic equations (2.22) and (2.23). From equation (2.23), the component vector in the inertial frame of the absolute velocity of the center of mass is the superposition of absolute velocity of the reference point and the velocity due to the rotation of the body, and then the transformation from the body reference frame to the inertial frame. The velocity due to rotation is directly proportional to the angular velocity of the body which is represented by a transformation element. The superposition is represented by a 0-junction and the coordinate transformation is represented by a modulated transformation element because the transformation matrix is a function of the orientation of the body. The velocity of the joint can be obtained in the same procedure except the coordinate transformation if the velocity is measured in the body reference frame. These two multibond graph structures form the multibond graph for kinematics of a rigid body, which is drawn in Figure 2-3 (b).

3. To add dynamic properties

The multibond graph for dynamics of a rigid body can be obtained by adding multiport elements which represent elementary dynamic properties of the body. These elements are the translational and rotational inertia, effort source representing gravity force and surface traction, and an Euler Junction Structure. The basic equations are equations (2.40) and (2.50). The equation (2.40) can be represented in the multibond graph by adding an effort source of gravity and an inertia array with unit constitutive matrix multiplying the mass of the body at the 1-junction of velocity component in inertial frame and adding an effort source of the resultant surface traction at the 1-junction of translational velocity of the reference point. The equation (2.50) can be represented in the multibond graph by adding a multiport inertia element of the component matrix of the inertia dyadic, a Euler junction structure and a torque due to

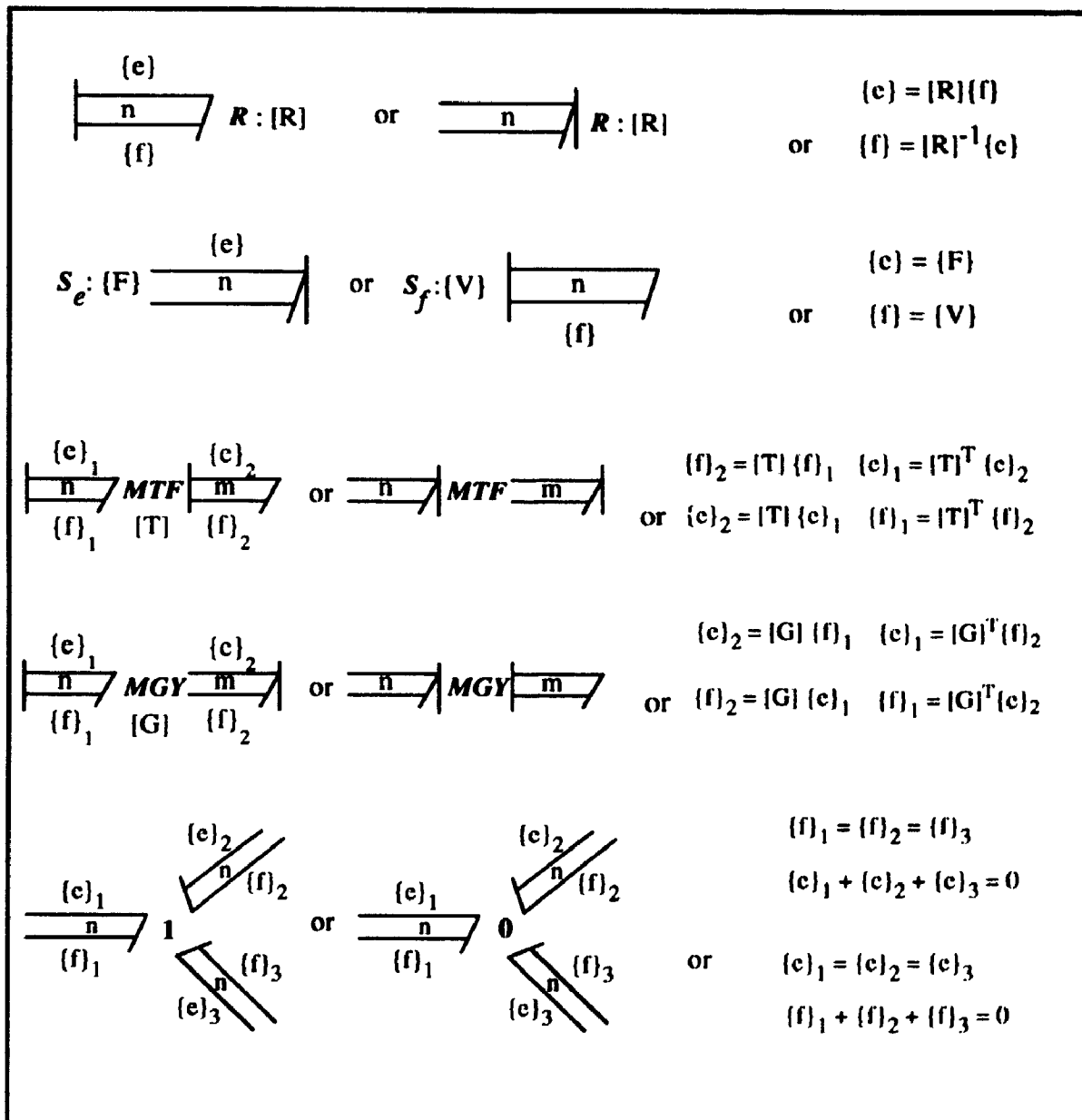
the surface traction at the angular velocity of the body. This is shown in Figure 2-3 (c).

Table 2-2 Multibond graph terminology

Multibond	
Multibond	Single Bond Equivalence
	
$\{e\} = \{e_1 \dots e_n\}$ $\{f\} = \{f_1 \dots f_n\}$	
Multiport Elements and Element Arrays	
Multibond Graphs	Constitutive laws
<p>SUM: [D]</p> 	$D = \begin{bmatrix} 0 & 1 & 0 \\ 0 & 0 & 1 \\ 1 & 0 & 0 \end{bmatrix}$ $\{Bout\} = D^T \{Bin\}$
	$\{f\} = [M]^{-1} \int \{e\} dt$
	$\text{or } \{e\} = [M] d\{f\}/dt$
	$\{e\} = [C]^{-1} \int \{f\} dt$
	$\text{or } \{f\} = [C] d\{e\}/dt$

(Table 2-2 continued on next page)

Table 2-2 (Cont'd)



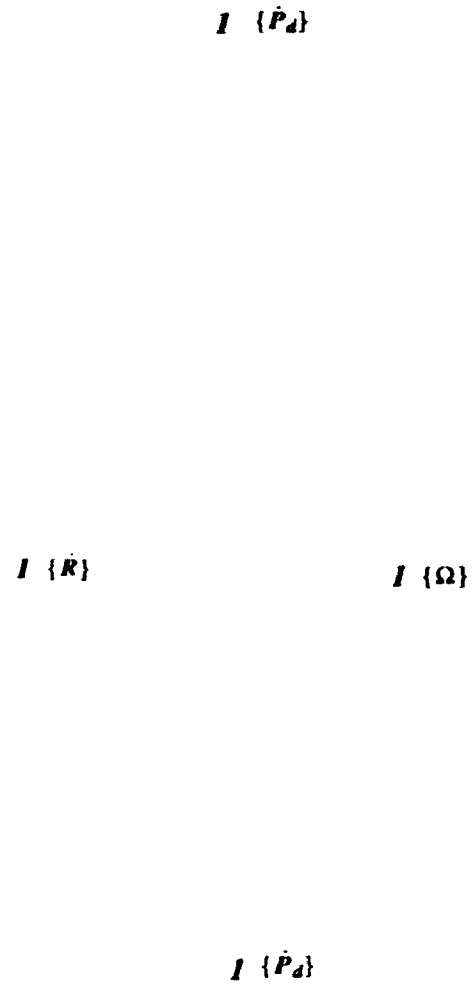


Figure 2-3 (a) 1-junctions for velocity variables

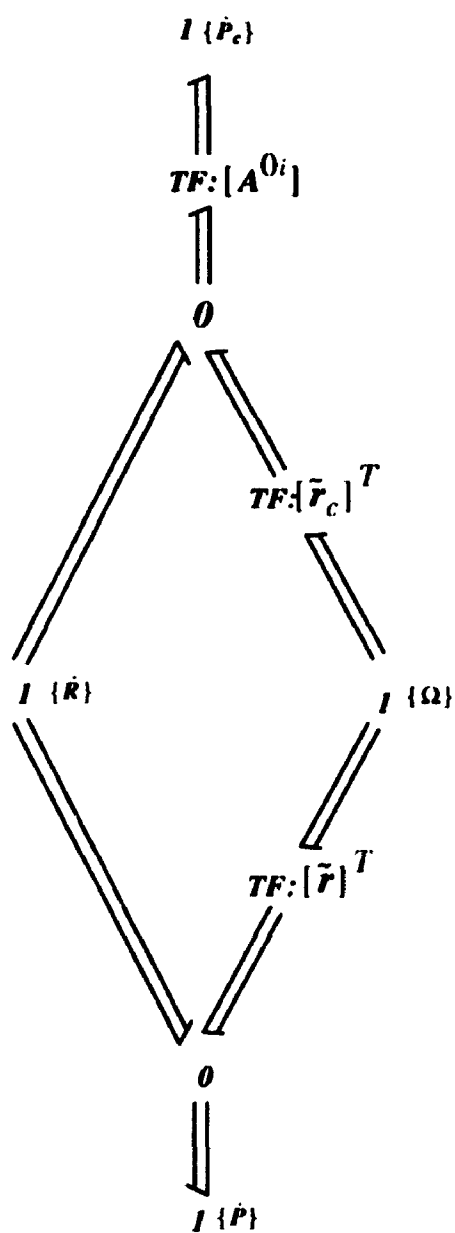


Figure 2-3 (b) Multibond graph of kinematics of a rigid body with one joint

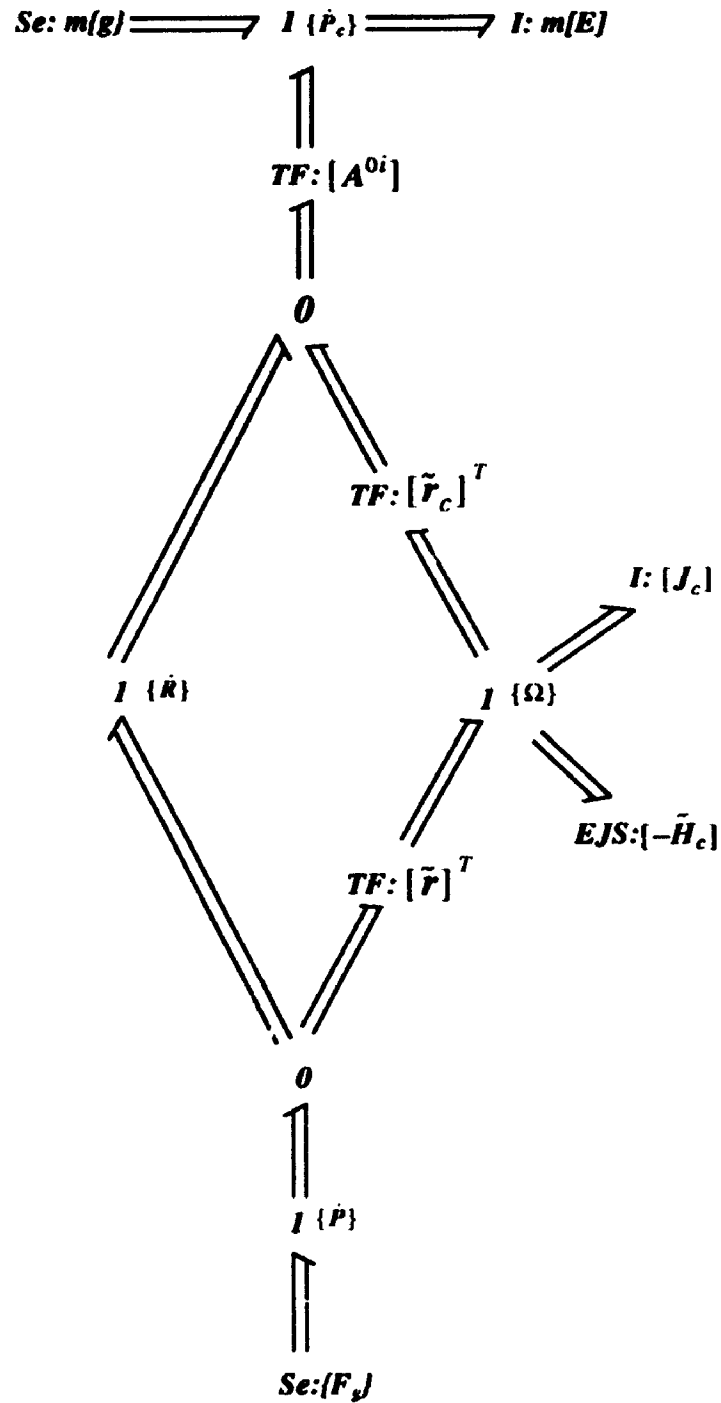


Figure 2-3 (c) Multibond graph of dynamics of a rigid body with one joint

- Chapter 3 -

The Vibration Behavior of a Flexible Body in Multibody Systems

3.1 Introduction

The motion of a flexible body in a multibody system has been considered as the combination of a overall motion of the attached body reference frame and vibration of the flexible body itself about the reference frame. At the beginning of the investigation of this problem, the overall motion and the vibration were analyzed separately by several researchers. The flexible body was treated as a rigid body first. The motion of the rigid multibody system was obtained through available techniques. Then the inertial forces due to the rigid body motion were imposed on flexible bodies to analyze the vibration of these bodies [Erdman etc. 1971, Winfrey 1972]. The coupling between the overall motion and the vibrations of the flexible body was ignored. This method gives an approximation of the motion of the flexible multibody system. Later, the overall motion and vibrations of the flexible bodies were considered together in the derivation of the equations of motion of multibody systems, in which linear vibration theory was adopted to account for the vibrational deformation of the flexible bodies [Likins 1972, Book 1982, 1984, Ho 1977, 1985, Huston, 1981]. This concept was believed valid until Kane [1987] pointed out that there is a problem in this approach. Kane investigated the motion of a cantilever beam attached to a rotating base and found that the vibrational deformation based on the approach was unbounded. Then, he took into consideration the coupling effect between transverse deformation and axial deformation and used non-linear vibration theory and obtained more reliable results. Later, Ider and Amirouche [1989], Wu and Haug [1988] investigated the same problem

in different ways and concluded that the coupling of the transverse deformation and axial deformation can not be ignored in flexible multibody system dynamics when angular velocity is high. However, the consideration of this coupling makes the analysis very complicated. Banerjee and Dickens [1989] proposed a method in which only the axial deformation caused by inertial force due to rigid body motion was considered, which simplified the derivation of the equations of motion and gave results which agree with Kane's results.

In this chapter, this phenomenon is investigated from the point of view of vibrations of a continuous system. The vibrations of continuous beams and plates have been extensively investigated for many years. This can give a better understanding of the vibration behavior of a flexible body in a multibody system and leads to a modelling method for this problem.

3.2 Transverse Vibration of a Beam Under Axial Forces

Transverse vibrations of bars under static axial forces has been discussed by Meirovitch [1967]. In the vibration of a flexible beam in a multibody system, the axial deformation is caused by axial forces. The axial forces can be either the inertial forces of the flexible body itself or the constraint forces acting on the joints of the body. These axial forces will affect the transverse or bending vibration behavior of the beam. The terms due to this effect can be seen in the partial differential equations for the vibration of the beam.

Consider a beam connected to a multibody system through the joints at the ends of the beam, which is shown in Figure 3-1. A body reference frame is attached at one joint of the beam in such a way that x axis is along the centroid axis of the beam and the other two axes are along the two principal axes of the cross section of the beam. The beam could vibrate in $x-y$ plane and $x-z$ plane. The cross section is assumed symmetric about the principal axes. Therefore the vibrations in these two planes are

decoupled and can be analyzed separately. Since the vibrations are described relative to the body reference frame, the forces acting on the body are the inertial forces of the body due to the motion of the body reference frame and the reaction forces at the joints of the body. The components of the forces perpendicular to the centroid axis of the beam form the excitation of the transverse vibration and the components of the forces along the centroid axis of the beam form the axial force. To investigate the effect of the axial force on the transverse vibration of the beam, plane problems are discussed in this section. Spatial vibration problems will be discussed later, in the next chapter, together with the dynamics of a flexible body.

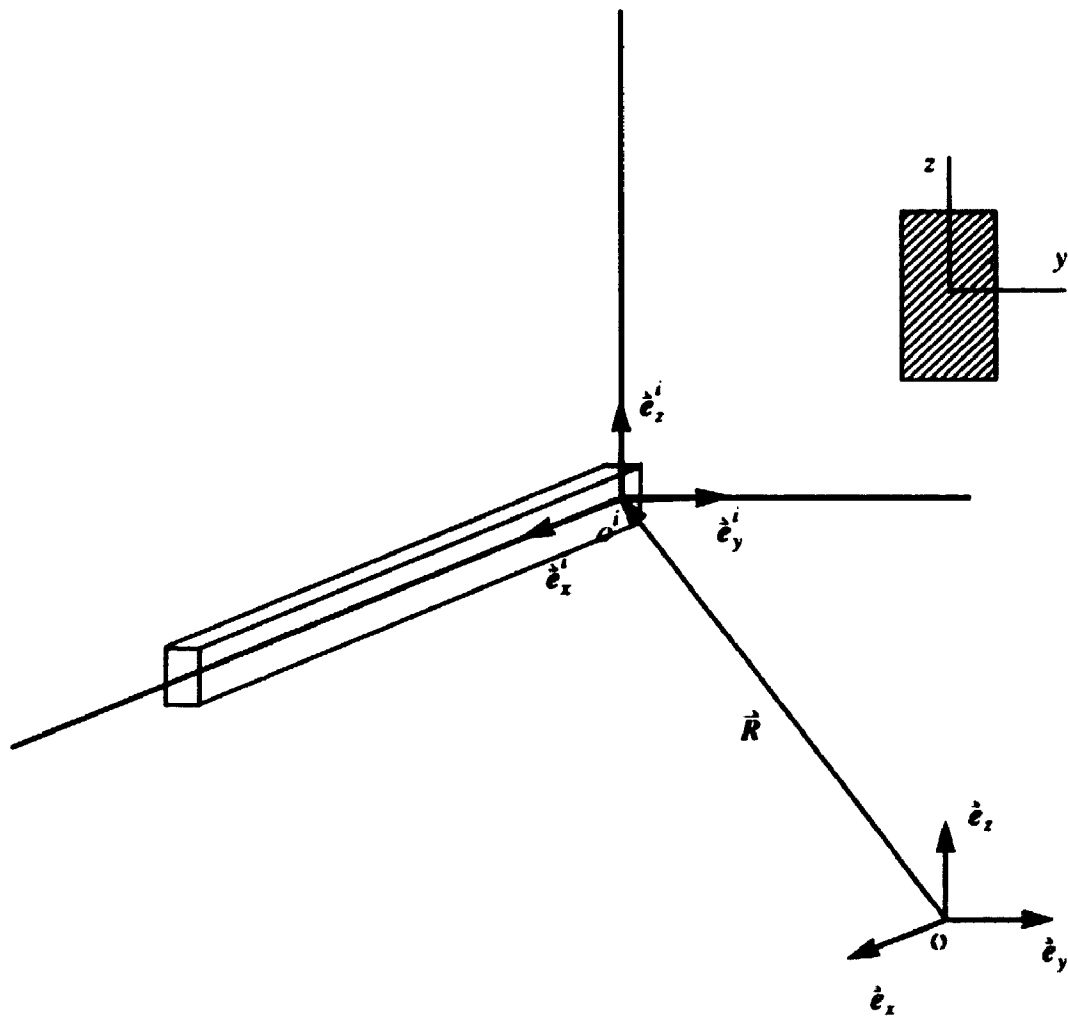


Figure 3-1 Frame and Cartesian coordinates of a beam

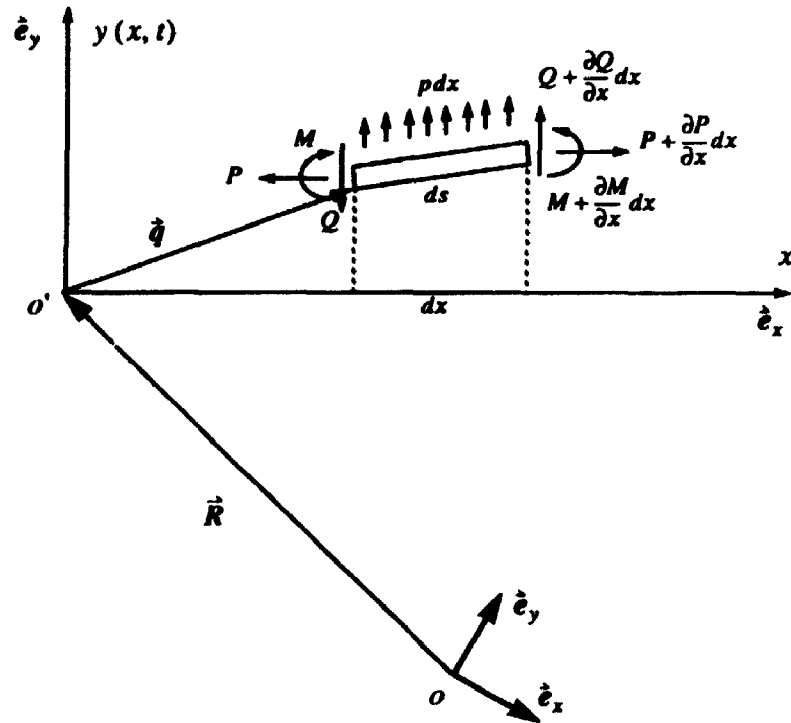


Figure 3-2 Forces on an element of the beam

Let us take a look at the schematic model of a beam segment in Figure 3-2. In the figure, x is the coordinate of any cross section of the beam and $y(x, t)$ is the transverse deflection field of the beam in $x - y$ plane. M , Q and P are bending moment, shear force and axial force, respectively. The letter p represents the distributed excitation. Vectors \vec{R} and \vec{q} are the position of the origin of the body reference frame in inertial frame and the position of the beam segment in the body reference frame respectively. The body reference frame is moving in the plane and the beam is vibrating about the body reference frame in the plane. The position of the beam segment in the inertial frame can be defined as

$$\begin{aligned}\dot{\vec{P}} &= \dot{\vec{R}} + \dot{\vec{q}} \\ &= \dot{\vec{R}} + x\dot{\vec{e}}_x + y(x, t)\dot{\vec{e}}_y\end{aligned}\quad (3.1)$$

The Bernoulli-Euler beam theory is used, which assumes that rotary inertia and shear deformation effects can be neglected. This is true for slender beams.

The vibration equation of the beam can be obtained by Hamilton's principle or Lagrange's equation. For both it is needed to evaluate the kinetic energy, potential energy, and work function. The absolute velocity of the beam element is

$$\begin{aligned}\vec{V} &= \frac{d\vec{P}}{dt} = \dot{\vec{R}} + \vec{\Omega} \times \vec{q} + \dot{\vec{q}} \\ &= \dot{\vec{R}} + \vec{\Omega} \times (x\dot{\vec{e}}_x + y(x, t)\dot{\vec{e}}_y) + \frac{\partial y}{\partial t}\dot{\vec{e}}_y\end{aligned}\quad (3.2)$$

where $\vec{\Omega}$ is the angular velocity of the body reference frame which is

$$\vec{\Omega} = \Omega\dot{\vec{e}}_z \quad (3.3)$$

The dot multiplication of the velocity is needed in the kinetic energy expression, which is

$$\vec{V} \cdot \vec{V} = \dot{R}^2 + \Omega^2(x^2 + y^2) + \left(\frac{\partial y}{\partial t}\right)^2 + 2\Omega(\dot{R}_y x - \dot{R}_x y) + 2\dot{R}_y \frac{\partial y}{\partial t} + 2x\Omega \frac{\partial y}{\partial t} \quad (3.4)$$

where \dot{R} is the magnitude of the velocity $\dot{\vec{R}}$, \dot{R}_x and \dot{R}_y are its components in the body reference frame.

With this expression, the kinetic energy of the beam can be written as

$$\begin{aligned}T &= \frac{1}{2} \int_0^L \rho (\vec{V} \cdot \vec{V}) dx \\ &= \frac{1}{2} \int_0^L \rho (\dot{R}^2 + \Omega^2(x^2 + y^2) + \left(\frac{\partial y}{\partial t}\right)^2 + 2\Omega(\dot{R}_y x - \dot{R}_x y) + 2(\dot{R}_y + x\Omega) \frac{\partial y}{\partial t}) dx\end{aligned}\quad (3.5)$$

The potential energy should include the effect of the bending moment and the axial force. The potential energy due to the bending moment is

$$U_b = \frac{1}{2} \int_0^L EI(x) \left(\frac{\partial^2 y}{\partial x^2} \right)^2 dx \quad (3.6)$$

To evaluate the potential energy due to the axial force, the change in the projection on the x axis of a beam segment dx needs to be calculated, this is

$$ds - dx = \sqrt{(dx)^2 + \left(\frac{\partial y}{\partial x} \right)^2 (dx)^2} - dx \approx \frac{1}{2} \left(\frac{\partial y}{\partial x} \right)^2 dx \quad (3.7)$$

Here the assumption has been made that the transverse deformation is small enough that, in the binomial expansion, the higher order can be neglected. Also based on this assumption, the axial force and transverse load are considered as unchanged during the deformation. Then the potential energy due to the axial force P is

$$U_a = P(ds - dx) = \frac{1}{2} \int_0^L P \left(\frac{\partial y}{\partial x} \right)^2 dx \quad (3.8)$$

The total potential energy is

$$U = U_b + U_a \quad (3.9)$$

The work done by the external transverse load p is

$$W = \int_0^L p(x, t) y(x, t) dx \quad (3.10)$$

Hamilton's principle is used in this section to derive the partial differential

equation of this continuous system, which states

$$\int_{t_1}^{t_2} (\delta T - \delta U + \delta W) dt = 0 \quad (3.11)$$

In this problem the variation in kinetic energy due to the vibrational deformation and the vibrational velocity is

$$\begin{aligned} \delta T &= \int_0^L \rho \left[\left(\frac{\partial y}{\partial t} + \dot{R}_y + x\Omega \right) \delta \left(\frac{\partial y}{\partial t} \right) + (\Omega^2 y - \Omega \dot{R}_x) \delta y \right] dx \\ &= \int_0^L \rho \left[\left(\frac{\partial y}{\partial t} + \dot{R}_y + x\Omega \right) \frac{\partial}{\partial t} (\delta y) + (\Omega^2 y - \Omega \dot{R}_x) \delta y \right] dx \end{aligned} \quad (3.12)$$

Therefore, since by definition, $\delta y(x, t)$ is zero at t_1 and t_2 ,

$$\begin{aligned} \int_{t_1}^{t_2} (\delta T) dt &= \int_0^L \rho \left\{ \int_{t_1}^{t_2} \left[\left(\frac{\partial y}{\partial t} + \dot{R}_y + x\Omega \right) \frac{\partial}{\partial t} (\delta y) + (\Omega^2 y - \Omega \dot{R}_x) \delta y \right] dt \right\} dx \\ &= \int_0^L \rho \left\{ \left(\frac{\partial y}{\partial t} + \dot{R}_y + x\Omega \right) \delta y \Big|_{t_1}^{t_2} - \int_{t_1}^{t_2} \left[\frac{\partial}{\partial t} \left(\frac{\partial y}{\partial t} + \dot{R}_y + x\Omega \right) \delta y - (\Omega^2 y - \Omega \dot{R}_x) \delta y \right] dt \right\} dx \\ &= - \int_{t_1}^{t_2} \int_0^L \rho \left[\left(\frac{\partial^2 y}{\partial t^2} + \ddot{R}_y + x\dot{\Omega} \right) \delta y - (\Omega^2 y - \Omega \dot{R}_x) \delta y \right] dx dt \end{aligned} \quad (3.13)$$

The variations of the potential energy and work function can be written as

$$\begin{aligned} \delta U &= \delta U_b + \delta U_a \\ &= \int_0^L \left[\frac{\partial^2}{\partial x^2} \left(EI \frac{\partial^2 y}{\partial x^2} \right) - \frac{\partial}{\partial x} \left(P \frac{\partial y}{\partial x} \right) \right] \delta y dx \\ &\quad - EI \frac{\partial^2 y}{\partial x^2} \delta \left(\frac{\partial y}{\partial x} \right) \Big|_0^L + \left[\frac{\partial}{\partial x} \left(EI \frac{\partial^2 y}{\partial x^2} \right) - P \frac{\partial y}{\partial x} \right] \delta y \Big|_0^L \end{aligned} \quad (3.14)$$

$$\delta W = \int_0^L p(x, t) \delta y dx \quad (3.15)$$

By substitution of equations (3.13), (3.14) and (3.15) into Hamilton's principle, equation (3.11) becomes

$$\begin{aligned} & - \int_{t_1}^{t_2} \left\{ \int_0^L \left[\rho \left(\frac{\partial^2 y}{\partial t^2} + \ddot{R}_y + x \dot{\Omega} \right) - \rho (\Omega^2 y - \Omega \dot{R}_x) + \frac{\partial^2}{\partial x^2} \left(EI \frac{\partial^2 y}{\partial x^2} \right) - \frac{\partial}{\partial x} \left(P \frac{\partial y}{\partial x} \right) - p \right] dx \delta y - \right. \\ & \left. - EI \frac{\partial^2 y}{\partial x^2} \delta \left(\frac{\partial y}{\partial x} \right) \Big|_0^L + \left[\frac{\partial}{\partial x} \left(EI \frac{\partial^2 y}{\partial x^2} \right) - P \frac{\partial y}{\partial x} \right] \delta y \Big|_0^L \right\} dt = 0 \end{aligned} \quad (3.16)$$

The integral must vanish for any arbitrary values of δy and $\delta \left(\frac{\partial y}{\partial x} \right)$, so these two variations can be set equal to zero at $x = 0$ and $x = L$, and different from zero, in between, throughout the domain. Therefore, the following is obtained

$$\rho \left(\frac{\partial^2 y}{\partial t^2} + \ddot{R}_y + x \dot{\Omega} \right) - \rho (\Omega^2 y - \Omega \dot{R}_x) + \frac{\partial^2}{\partial x^2} \left(EI \frac{\partial^2 y}{\partial x^2} \right) - \frac{\partial}{\partial x} \left(P \frac{\partial y}{\partial x} \right) = p \quad (3.17)$$

$$EI \frac{\partial^2 y}{\partial x^2} \delta \left(\frac{\partial y}{\partial x} \right) \Big|_0^L = 0 \quad (3.18)$$

$$\left[\frac{\partial}{\partial x} \left(EI \frac{\partial^2 y}{\partial x^2} \right) - P \frac{\partial y}{\partial x} \right] \delta y \Big|_0^L = 0 \quad (3.19)$$

Equation (3.17) is the partial differential equation for the transverse vibration of the beam. Equations (3.18), and (3.19) indicate the natural and geometric boundary conditions, which take into account the possibility that either

$$EI \frac{\partial^2 y}{\partial x^2} = 0 \quad \text{or} \quad \frac{\partial y}{\partial x} = 0 \quad \text{at } x = 0 \text{ and } x = L \quad (3.20)$$

and that

$$\frac{\partial}{\partial x} \left(EI \frac{\partial^2 y}{\partial x^2} \right) - P \frac{\partial y}{\partial x} = 0 \quad \text{or} \quad y = 0 \quad \text{at} \quad x = 0 \quad \text{and} \quad x = L \quad (3.21)$$

The first of these two equations represents the vanishing of the bending moment and the vertical forces, and the second implies the vanishing of the deflection and its slope. These expressions cover the clamped, pinned, and free end conditions. It has been pointed out, earlier, that the axial force in equation (3.17) is caused by the constraint forces at the joints and the inertial force of the beam itself due to the motion of the body reference frame. The axial force can be expressed in terms of these factors.

In Figure 3-2, applying Newton's second law to the beam segment in the x direction, the following is obtained

$$(\ddot{R}_x - x\Omega^2) \rho dx = \frac{\partial P}{\partial x} dx \quad (3.22)$$

It can be integrated over the whole beam into

$$P(x) = \rho \left(x\ddot{R}_x - \frac{x^2}{2} \Omega^2 \right) - P(0) \quad (3.23)$$

where $P(0)$ is the axial force at the origin of body reference frame which is determined by constraint forces.

Substituting equation (3.23) into equation (3.17), the partial differential equation becomes

$$\begin{aligned} \rho \left(\frac{\partial^2 y}{\partial t^2} \right) + \frac{\partial^2}{\partial x^2} \left(EI \frac{\partial^2 y}{\partial x^2} \right) - \frac{\partial}{\partial x} \left[\left(\rho \left(x\ddot{R}_x - \frac{x^2}{2} \Omega^2 \right) - P(0) \right) \frac{\partial y}{\partial x} \right] - \rho \Omega^2 y \\ = \rho - \rho (\Omega \dot{R}_x + \ddot{R}_y + x\dot{\Omega}) \end{aligned} \quad (3.24)$$

The partial differential equation of transverse vibration for a no-overall-motion beam can be obtained from equation (3.17) by eliminating the terms related to the motion of the body reference frame \ddot{R}_y , $\dot{\Omega}$, Ω and \dot{R}_x , as well as the axial force P , that

is

$$\rho \left(\frac{\partial^3 y}{\partial t^3} \right) + \frac{\partial^2}{\partial x^2} \left(EI \frac{\partial^2 y}{\partial x^2} \right) = p \quad (3.25)$$

which is the well-known Bernoulli-Euler equation for bending vibration of a slender beam.

From equations (3.24) and (3.25), the differences between transverse vibrations of a beam in a multibody system and a beam in a fixed configuration can be found. Firstly, the overall motion creates transverse loads on the beam which appear at the right side of equation (3.24). Secondly, the Coriolis acceleration, due to the coupling between rotation and vibration, and the axial force due to the end constraints and inertial force along the centroid axis, affect the property of the partial differential equation of the transverse vibration of the beam. It can be seen that the effect of this on the transverse stiffness of the beam should be considered.

In practice, it is not easy to solve the partial differential equations, with the geometric and natural boundary conditions, in closed form. Instead, approximation methods are usually used to solve the eigenvalue problem and the dynamic response, numerically. The assumed modes method is commonly used for such solutions and simulation.

Assume a solution in the form of a series

$$y(x, t) = \sum_{j=1}^n \eta_j(t) \phi_j(x) = \{ \Phi(x) \}^T \{ \eta(t) \} \quad (3.26)$$

where $\Phi_j(x)$ are the assumed modes and η_j are the generalized coordinates.

Based on this series the kinetic energy in equation (3.5) can be expressed as

$$T = \frac{1}{2} \int_0^L \rho [\dot{R}^2 + \Omega^2 (x^2 + \{ \eta \}^T \{ \Phi \} \{ \Phi \}^T \{ \eta \}) + \{ \dot{\eta} \}^T \{ \Phi \} \{ \Phi \}^T \{ \dot{\eta} \} + 2\Omega (\dot{R}_y x - \dot{R}_x \{ \eta \}^T \{ \Phi \}) + 2 (\dot{R}_y + x\Omega) \{ \dot{\eta} \}^T \{ \Phi \}] dx \quad (3.27)$$

The potential energy due to the work done by the internal forces is

$$\begin{aligned}
 U &= \frac{1}{2} \left[\int_0^L EI \left(\frac{\partial^2 y}{\partial x^2} \right)^2 dx + \int_0^L P \left(\frac{\partial y}{\partial x} \right)^2 dx \right] \\
 &= \frac{1}{2} \{ \eta \}^T \left(\int_0^L EI \{ \Phi'' \} \{ \Phi'' \}^T dx + \int_0^L P \{ \Phi' \} \{ \Phi' \}^T dx \right) \{ \eta \} \\
 &= \frac{1}{2} \{ \eta \}^T ([K] + [K_g]) \{ \eta \}
 \end{aligned} \tag{3.28}$$

where

$$[K] = \int_0^L EI \{ \Phi'' \} \{ \Phi'' \}^T dx \tag{3.29}$$

$$\begin{aligned}
 [K_g] &= \int_0^L P \{ \Phi' \} \{ \Phi' \}^T dx \\
 &= \int_0^L \left(\rho (x \ddot{R}_x - \frac{1}{2} x^2 \Omega^2) - P(0) \right) \{ \Phi' \} \{ \Phi' \}^T dx \\
 &= \ddot{R}_x \int_0^L \rho x \{ \Phi' \} \{ \Phi' \}^T dx - \frac{1}{2} \Omega^2 \int_0^L \rho x^2 \{ \Phi' \} \{ \Phi' \}^T dx - P(0) \int_0^L \{ \Phi' \} \{ \Phi' \}^T dx \\
 &= \ddot{R}_x [K_{g1}] - \frac{1}{2} \Omega^2 [K_{g2}] - P(0) [K_{g0}]
 \end{aligned} \tag{3.30}$$

Matrix $[K]$ is known as the bending stiffness of the beam. Matrix $[K_g]$ is the effect, on the bending stiffness, of the axial forces which are caused by the overall motion of the beam and the constraint forces. Some references call this matrix the "geometric stiffness matrix" based on the fact that it depends only on the geometry of the beam. In this problem, however, matrix $[K_g]$ not only depends on the geometry of the beam, but also on the overall motion of the beam. Therefore, it is suggested to call matrix $[K_g]$ the "dynamic geometric stiffness matrix".

Given the kinetic energy and potential energy, Lagrange's equation can then be

used to obtain the equation of motion, which is

$$\frac{d}{dt} \left(\frac{\partial T}{\partial \{\dot{\eta}\}} \right) - \frac{\partial T}{\partial \{\eta\}} + \frac{\partial U}{\partial \{\eta\}} = \{Q\} \quad (3.31)$$

Based on the kinetic energy in equation (3.27), the first term in Lagrange's equation is

$$\begin{aligned} \frac{d}{dt} \left(\frac{\partial T}{\partial \{\dot{\eta}\}} \right) &= \frac{d}{dt} \left\{ \int_0^L \rho \{ \Phi \} \{ \Phi \}^T \{\dot{\eta}\} + (\dot{R}_y + x\Omega) \{ \Phi \} \right\} dx \\ &= \left(\int_0^L \rho \{ \Phi \} \{ \Phi \}^T dx \right) \{\ddot{\eta}\} + \ddot{R}_y \int_0^L \rho \{ \Phi \} dx + \dot{\Omega} \int_0^L \rho x \{ \Phi \} dx \\ &= [M] \{\ddot{\eta}\} + m\ddot{R}_y \{S\} + m\dot{\Omega} \{D\} \end{aligned} \quad (3.32)$$

where m is the mass of the beam and

$$[M] = \int_0^L \rho \{ \Phi \} \{ \Phi \}^T dx \quad (3.33)$$

$$\{S\} = \frac{1}{m} \int_0^L \rho \{ \Phi \} dx \quad (3.34)$$

$$\{D\} = \frac{1}{m} \int_0^L \rho x \{ \Phi \} dx \quad (3.35)$$

The other terms in Lagrange's equation are

$$\begin{aligned} \frac{\partial T}{\partial \{\eta\}} &= \Omega^2 \left(\int_0^L \rho \{ \Phi \} \{ \Phi \}^T dx \right) \{\eta\} - \Omega \dot{R}_x \int_0^L \rho \{ \Phi \} dx \\ &= \Omega^2 [M] \{\eta\} - m\Omega \dot{R}_x \{S\} \end{aligned} \quad (3.36)$$

$$\frac{\partial U}{\partial \{\eta\}} = ([K] + [K_g]) \{\eta\} \quad (3.37)$$

$$\{Q\} = \int_0^L p(x, t) \{\Phi\} dx \quad (3.38)$$

Substituting all these terms into Lagrange's equation, the equation of the transverse vibration is obtained

$$[M] \{\ddot{\eta}\} + ([K] + [K_g] - \Omega^2 [M]) \{\eta\} = \{Q\} + (\Omega \dot{R}_x - \ddot{R}_y) m \{S\} - \Omega \dot{m} \{D\} \quad (3.39)$$

To verify the partial differential equation and the vibration equation, based on the assumed mode method, derived in this section, and to investigate the characteristics of the transverse vibration of a beam under general motion, a special case of transverse vibrations of rotating bars is discussed in the following sections

3.3 In-Plane Transverse Vibrations of Rotating Bars

A slender beam built into a rigid shaft is shown in Figure 3-3. The shaft is driven and rotates about the z -axis at the angular velocity Ω and the beam vibrates in the x - y plane (in the plane of rotation). The initial position of the x axis coincides with the undeformed bar. This rotating bar model is applicable to helicopter blades, turbine blades, spacecraft antennae and flexible robot arms. In such applications, the dynamic stiffening effects due to the presence of axial centrifugal forces have significant influence on the prediction of transverse vibrations of the beam.

The partial differential equation of the rotating bar can be obtained from equation (3.24) by eliminating terms related to the translational motion of the body reference frame. Because there is no translational motion for the body reference frame, the terms \ddot{R}_y and \dot{R}_x are eliminated from equations (3.24) and (3.23). The axial force at the origin of the body reference frame can be easily found as

$$P(0) = -\int_0^L \rho \Omega^2 \xi d\xi = -\frac{1}{2} \rho \Omega^2 L^2 \quad (3.40)$$

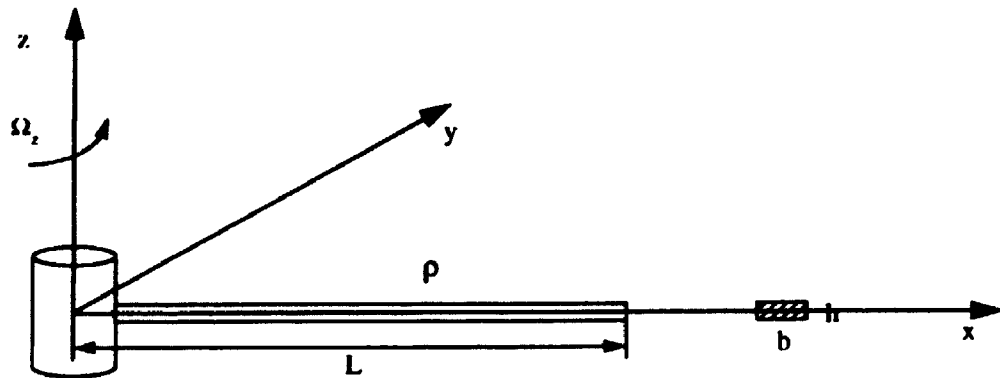


Figure 3-3 Rotating bar example

Therefore, the partial differential equation for the transverse vibration of the rotating bar is

$$\rho \left(\frac{\partial^2 y}{\partial t^2} \right) + \frac{\partial^2}{\partial x^2} \left(EI \frac{\partial^2 y}{\partial x^2} \right) - \frac{1}{2} \rho \frac{\partial}{\partial x} \left[\Omega^2 (L^2 - x^2) \frac{\partial y}{\partial x} \right] - \rho \Omega^2 y = -\rho x \ddot{\Omega} \quad (3.41)$$

The boundary conditions for this problem are

$$y = \frac{\partial y}{\partial x} = 0 \quad \text{at} \quad x = 0 \quad (3.42)$$

$$EI \frac{\partial^2 y}{\partial x^2} = \frac{\partial}{\partial x} \left(EI \frac{\partial^2 y}{\partial x^2} \right) = 0 \quad \text{at} \quad x = L \quad (3.43)$$

This is a forced vibration problem even though there is no external excitation. The angular acceleration will excite the transverse vibration. To investigate the

vibration characteristics of the rotating bar, the eigenvalue problem of the corresponding free vibration system is of interest. The corresponding free vibration system can be obtained by assuming a constant angular velocity, in which the partial differential equation becomes

$$\rho \left(\frac{\partial^2 y}{\partial t^2} \right) + \frac{\partial^2}{\partial x^2} \left(EI \frac{\partial^2 y}{\partial x^2} \right) - \frac{1}{2} \rho \Omega^2 \frac{\partial}{\partial x} \left[(L^2 - x^2) \frac{\partial y}{\partial x} \right] - \rho \Omega^2 y = 0 \quad (3.44)$$

Using the separation of variable method and assuming

$$y(x, t) = Y(x) \sin(\omega t) \quad (3.45)$$

the following characteristic equation and boundary conditions can be obtained from equation (3.41) and the boundary conditions given by equations (3.42) and (3.43)

$$EI \frac{d^4 Y}{dx^4} - \frac{1}{2} \rho \Omega^2 \frac{d}{dx} \left[(L^2 - x^2) \frac{dY}{dx} \right] - \rho \Omega^2 Y = \omega^2 \rho Y \quad (3.46)$$

$$Y = \frac{dY}{dx} = 0 \quad \text{at } x = 0 \quad (3.47)$$

$$\frac{d^2 Y}{dx^2} = \frac{d^3 Y}{dx^3} = 0 \quad \text{at } x = L \quad (3.48)$$

To solve above the eigenvalue problem, an approximation method, the Raleigh-Ritz method is used. To this end a solution is assumed in the form of a series

$$Y(x) = \sum_{j=1}^n a_j \phi_j(x) = \{\Phi(x)\}^T \{a\} \quad (3.49)$$

where a_j are coefficients to be determined and ϕ_j are comparison functions which satisfy all geometric and natural boundary conditions.

Substituting this expression into equation (3.46), then premultiplying $\{\Phi(x)\}$ to the equation, and taking the integration of the equation over the whole beam, the following discrete eigenvalue problem is obtained

$$[[K] + \Omega^2 ([K_g] - [M])] \{a\} = \omega^2 [M] \{a\} \quad (3.50)$$

where the elements of matrices $[K]$, $[K_g]$ and $[M]$ are obtained as the follows

$$\begin{aligned} k_{ij} = k_{ji} &= \int_0^L EI \phi_i \frac{d^4 \phi_j}{dx^4} dx \\ &= EI \phi_i \frac{d^3 \phi_j}{dx^3} \Big|_0^L - EI \frac{d\phi_i}{dx} \frac{d^2 \phi_j}{dx^2} \Big|_0^L + \int_0^L EI \frac{d^2 \phi_i}{dx^2} \frac{d^2 \phi_j}{dx^2} dx \\ &= \int_0^L EI \frac{d^2 \phi_i}{dx^2} \frac{d^2 \phi_j}{dx^2} dx \end{aligned} \quad (3.51)$$

$$\begin{aligned} k_{gij} = k_{gji} &= - \int_0^L \frac{1}{2} \rho \phi_i \frac{d}{dx} \left[(L^2 - x^2) \frac{d\phi_j}{dx} \right] dx \\ &= - \frac{1}{2} \rho \phi_i \left[(L^2 - x^2) \frac{d\phi_j}{dx} \right] \Big|_0^L + \frac{1}{2} \int_0^L \rho (L^2 - x^2) \frac{d\phi_j}{dx} \frac{d\phi_i}{dx} dx \\ &= \frac{1}{2} \int_0^L \rho (L^2 - x^2) \frac{d\phi_j}{dx} \frac{d\phi_i}{dx} dx \end{aligned} \quad (3.52)$$

$$m_{ij} = m_{ji} = \int_0^L \rho \phi_i \phi_j dx \quad (3.53)$$

Note that the boundary conditions (equations (3.47) and (3.48)) are used in the derivation.

The eigenvalue problem for a beam without the overall motion can be obtained from equation (3.46) by eliminating the terms related to the motion of the body reference frame, $\dot{\Omega}$ and Ω , as well as the axial force P , that is

$$[K] \{a\} = \omega^2 [M] \{a\} \quad (3.54)$$

Comparing with equation (3.50), it can be found that the term $[K_g] \Omega^2$ increases the stiffness of the system and the term $[M] \Omega^2$ decreases the stiffness of the system. Recalling from the derivation of the equations, the term $[K_g] \Omega^2$ is due to the work done by the axial force caused by transverse deformation, and the term $[M] \Omega^2$ is due to the centrifugal acceleration caused by the overall rotation of the beam shaft system. The combination of these two terms will stiffen the transverse stiffness of the beam.

In some former research in dynamics of multibody systems with flexible members [Likins 1972, Book 1982, 1984, Ho 1977, 1985, Huston, 1981], the effect of the axial forces was not included in the equations of motion for flexible members. With those models unbounded transverse deformation for this rotating beam were obtained when angular velocity exceeded a certain value. This can be seen very clearly here. If the effect of the axial force is neglected, the transverse stiffness of the rotating bar becomes

$$[K] - \Omega^2 [M] \quad (3.55)$$

Since matrix $[K]$ is constant, the combined transverse stiffness of the system will become negative when rotation speed Ω exceeds a certain number. This turns the vibration system unstable and the deformation will be unbounded if there is an excitation. This will be shown in Chapter 9.

- Chapter 4 -

Equations of Motion of a Free Moving Flexible Body

4.1 Introduction

Correct prediction of the behavior of a flexible body in a multibody system is the foundation of flexible multibody system dynamics. To formulate the motion of a flexible body undergoing translation and rotation, a number of investigators have used different methods and various assumptions about flexibility to derive the equations of motion. One of these models is to idealize a flexible member as a collection of small rigid bodies interconnected by massless springs and then to set up the equations of motion using rigid body dynamics [Huang and Lee 1988]. Another model suggests the use of the finite element method [Likins 1972, Shabana and Wehage 1983, Wu et al 1989]. In this approach the finite element method is used to calculate the deformation of the flexible members, then the results are included with Lagrange's equations or variational analysis to obtain the equations of motion of the system, the condensed mass technique and modal deduction being used. In the third approach the superposition of the mode shapes for a flexible body is used to represent the vibrational deformation, and then Lagrange's equations or Hamilton's principle are used to obtain the equations of motion [Wielenga 1984, Kane et al 1987, Low 1987].

Recently, it has been shown [Kane 1987, Ider and Amirouche 1988, and Banerjee and Dickens 1990] that the geometric stiffness or dynamic stiffness of beams and plates arising from the axial and mid-surface inertial force has considerable effect on the prediction of the dynamical behavior of beams and plates in a high-speed system. This phenomenon can be understood by studying the transverse vibrations of a beam undergoing axial forces as discussed in Chapter 3. The mode shapes and natural

frequencies of the beam with the axial force are different from those of the beam without axial force. So is the response to external excitation as the constraint forces and inertial forces, due to the translation and rotation, will form axial forces or mid-surface forces in the flexible members. In flexible multibody systems, flexible members are most likely beam or plate type members, which are connected to other members and undergo large scale translation and rotation, this effect should be considered in the formulation of motion of a flexible member, especially for high speed systems.

4.2 Kinematics of a Flexible Body

To determine the motion of a flexible body, a body reference frame and an inertial frame are necessary. The geometry and the deformation of the flexible body are represented in the body reference frame and the global position and orientation of the body are given in the inertial frame. Consider a free-moving flexible body and these two frames, as shown in Figure 4-1. In this figure, the vector array $\{\hat{e}^o\}$ is a Cartesian coordinate system of the inertial frame, $\{\hat{e}^i\}$ is a Cartesian coordinate system of the body reference frame for the body. Vector \vec{R} locates the origin of the body reference frame in the inertial frame. Vector \vec{q} shows the position of an arbitrary point P of the body, in the body reference frame, after deformation occurs. The vector \vec{q} can be resolved into \vec{r} and \vec{u} . Vector \vec{r} represents the position of the point before the body deforms and the vector \vec{u} is the displacement of the point due to elastic deformation of the body. Vector \vec{q}_c is the position vector of the mass center of the body in the body reference frame. The instantaneous position of point P in the inertial frame can be represented by vector \vec{P} , which is the sum of \vec{R} and \vec{q} . These relations can be represented as follows:

$$\vec{q} = \vec{r} + \vec{u} \quad (4.1)$$

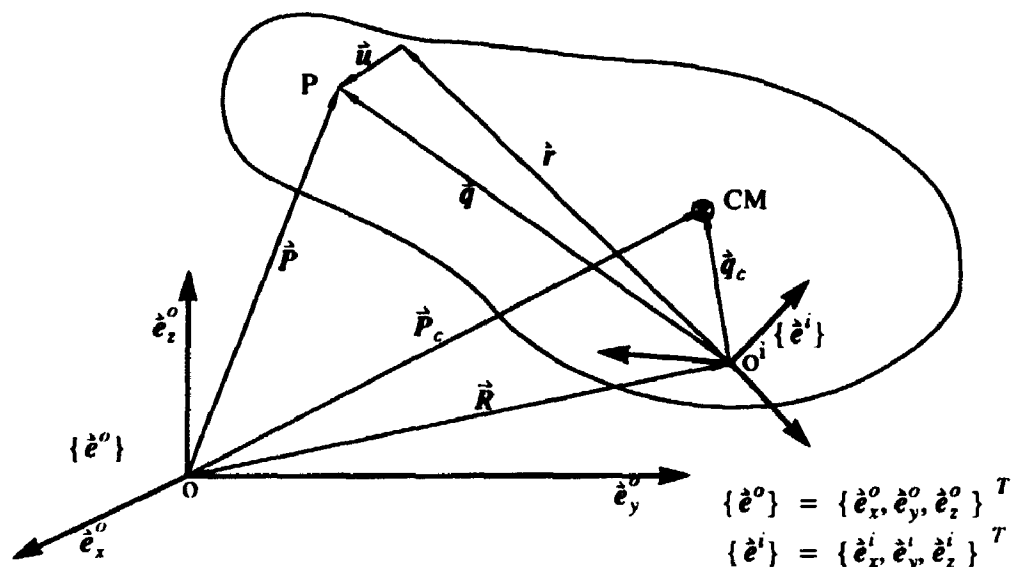


Figure 4-1 Coordinate System and Position Vectors

$$\vec{P} = \vec{R} + \vec{q} \quad (4.2)$$

To reduce the coordinates needed to determine the vibrational deformation, the assumed modes method [Meirovitch 1967] is employed. By assuming a set of deformation modes of the body, the deformation \vec{u} can be written as

$$\vec{u} = \sum_j \vec{\Phi}_j(\vec{r}) \eta_j(t) = \{\eta\}^T \{\vec{\Phi}(\vec{r})\} = \{\vec{\Phi}(\vec{r})\}^T \{\eta\} \quad (4.3)$$

$$\vec{\Phi}_j(\vec{r}) = \{\phi_x \ \phi_y \ \phi_z\} \{e^i\} \quad (4.4)$$

where the $\eta_j(t)$'s are generalized coordinates and $\vec{\Phi}_j(\vec{r})$'s are assumed mode shape vectors defined in body reference frame $\{e^i\}$. The assumed mode shapes are admissible functions which satisfy the geometric boundary conditions of the body. For the sake of simplification, $\{\vec{\Phi}(\vec{r})\}$ will be written as $\{\vec{\Phi}\}$ later in the thesis.

By definition, the position vector of the mass center of a body \vec{q}_c can be expressed

in terms of mode shapes

$$\dot{\vec{q}}_c = \frac{1}{m} \int_V \dot{\vec{q}} \rho dv = \frac{1}{m} \int_V (\dot{\vec{r}} + \{\eta\}^T \{\vec{\Phi}\}) \rho dv = \dot{\vec{r}}_c + \{\eta\}^T \{\dot{\vec{S}}\} \quad (4.5)$$

where m and V are mass and volume of the body, ρ the density of the material, $\dot{\vec{r}}_c$ the position of the mass center of the body before deformation occurs, and vector array $\{\dot{\vec{S}}\}$ is a constant vector array defined as

$$\{\dot{\vec{S}}\} = \frac{1}{m} \int_V \{\vec{\Phi}\} \rho dv \quad (4.6)$$

which indicates the displacement of the mass center due to the deformation of the flexible body.

Finally, the position vector of the mass center of the deformed body in the inertial frame is

$$\vec{P}_c = \vec{R} + \vec{q}_c \quad (4.7)$$

The absolute velocity of point P of the body is the first order derivative of \vec{P} with respect to time in the inertial frame, which is

$$\dot{\vec{P}} = \dot{\vec{R}} + \vec{\Omega} \times \vec{q} + \dot{\vec{q}} \quad (4.8)$$

where $\dot{\vec{q}}$ is the relative velocity of point P to the body reference frame, $\dot{\vec{R}}$ and $\dot{\vec{\Omega}}$ are absolute linear velocity and angular velocity of the body reference frame relative to the inertial frame.

The absolute acceleration of point P is the second order derivative of \vec{P} with respect to time in the inertial frame, which is

$$\ddot{\vec{P}} = \ddot{\vec{R}} + \ddot{\vec{q}} + \dot{\vec{\Omega}} \times \vec{q} + \vec{\Omega} \times (\vec{\Omega} \times \vec{q}) + 2\dot{\vec{\Omega}} \times \dot{\vec{q}} \quad (4.9)$$

where term $2\vec{\Omega} \times \dot{\vec{q}}$ is the Coriolis acceleration, and $\vec{\Omega} \times (\vec{\Omega} \times \vec{q})$ is the centripetal acceleration.

The velocity and acceleration of the mass center can be obtained in the same way

$$\dot{\vec{P}}_c = \dot{\vec{R}} + \vec{\Omega} \times \vec{q}_c + \dot{\vec{q}}_c \quad (4.10)$$

$$\ddot{\vec{P}}_c = \ddot{\vec{R}} + \ddot{\vec{q}}_c + \dot{\vec{\Omega}} \times \vec{q}_c + \vec{\Omega} \times (\dot{\vec{\Omega}} \times \vec{q}_c) + 2\vec{\Omega} \times \dot{\vec{q}}_c \quad (4.11)$$

For a rigid body, the angular velocity of a small mass element at point P is exactly the same as that of the body reference frame fixed on the body. For a flexible body, this is no longer true. The deformation of the body will cause an additional angular displacement to the mass element. Using the elastic theory [Boresi and Chong 1987], the small additional angular displacement, due to the deformation, can be treated as a vector which is

$$\dot{\vec{\pi}} = \frac{1}{2} \vec{\nabla} \times \dot{\vec{u}} = \frac{1}{2} \begin{vmatrix} \dot{e}'_x & \dot{e}'_y & \dot{e}'_z \\ \frac{\partial}{\partial x} & \frac{\partial}{\partial y} & \frac{\partial}{\partial z} \\ u_x & u_y & u_z \end{vmatrix} = \frac{1}{2} \vec{\nabla} \times \{\vec{\Phi}\}^T \{\eta\} \quad (4.12)$$

where $\vec{\nabla}$ is the curl operator.

The angular velocity at any point in the flexible body due to the vibrational deformation is the first order derivative of the angular displacement $\dot{\vec{\pi}}$ with respect to time in the body reference frame, which is

$$\dot{\vec{\pi}} = \frac{1}{2} \vec{\nabla} \times \dot{\vec{u}} = \frac{1}{2} \vec{\nabla} \times \{\vec{\Phi}\}^T \{\eta\} \quad (4.13)$$

The absolute angular velocity of point P, therefore, can be written as

$$\vec{\Omega}_p = \vec{\Omega} + \dot{\vec{\pi}}_p \quad (4.14)$$

where $\dot{\tilde{\pi}}_p$ is the relative angular velocity of point P due to the vibrational deformation.

To use the variational principle for derivation of the governing equations, the virtual displacement of any point P in the flexible body is given here. The virtual displacement is a possible displacement which is compatible with all constraints of the body. According to equations (4.2) and (4.12), the virtual displacement for point P in a free-moving flexible body is

$$\begin{aligned}\delta\dot{\vec{P}} &= \delta\dot{\vec{R}} + \delta\dot{\vec{\phi}} \times \dot{\vec{q}} + \delta\dot{\vec{q}} \\ &= \delta\dot{\vec{R}} + \delta\dot{\vec{\phi}} \times \dot{\vec{q}} + \delta\{\eta\}^T \{\dot{\vec{\Phi}}\}\end{aligned}\quad (4.15)$$

where $\delta\dot{\vec{\phi}}$ is the virtual infinitesimal rotation of the body reference frame, $\delta\dot{\vec{R}}$ the virtual linear displacement of frame $\{\dot{\vec{e}}'\}$ and $\delta\dot{\vec{q}}$ the variation of position of any point of the body in frame $\{\dot{\vec{e}}'\}$ due to the deformation.

4.3 Dynamics of a Free-Moving Flexible Body

4.3.1 Variational Principle and Non-Linear Strain

The dynamic equations of motion of the flexible body can be derived by Hamilton's principle, the Euler-Lagrange equations, Kane's equations, as well as the variational principle. In this chapter, the variational principle is used to derive the equations in the form which can be represented by multibond graphs.

The vectorial form of the variational principle for a deformable body can be written as [Shames and Dym 1985]

$$\int_V (\delta\dot{\vec{P}} \cdot (d\ddot{\vec{F}} - \ddot{\vec{P}}\rho dv)) = \int_V \delta\{\epsilon\}^T \{\sigma\} dv \quad (4.16)$$

where $\dot{\vec{P}}$, ρ , $\delta\dot{\vec{P}}$ and $\ddot{\vec{P}}$ have been defined before. The vector $d\ddot{\vec{F}}$ represents the

infinitesimal element of body force and surface traction acting on the point P. $\{\epsilon\}$ and $\{\sigma\}$ are strain and stress column matrices of the deformed body. The integral is taken over the total body volume.

The right side of the equation is the virtual work done by stress. It has been shown that the geometric stiffness or dynamic stiffness of the flexible body due to the high speed overall translation and rotation can be dealt with by considering the nonlinear strain-displacement relations [Modi and Ibrahim 1988, Banerjee and Dickens 1990]. Modi and Ibrahim [1988] considered fully the nonlinear strain displacement relations for general flexible bodies, and this seems to be computationally intensive. Banerjee and Dickens [1990] considered the inertial forces due to the overall translation and rotation of the undeformed flexible body as existing loads on the body. They then included the work done by these forces on the nonlinear part of the strain displacement relations to obtain the geometric stiffness matrix. This method requires the calculation of the stress in the body due to the inertial forces, which is not convenient for bond graph representation. In this thesis, a method similar to that of Modi and Ibrahim [1988] is used. A further simplification is adopted by ignoring higher order displacement terms, in the virtual work, based on the nonlinear strain displacement relations.

The nonlinear strain displacement relations (Green-Lagrange strain) are defined as [Boresi and Chong 1987]

$$\epsilon_x = u_x + \frac{1}{2} (u_x^2 + v_x^2 + w_x^2) \quad (4.17a)$$

$$\epsilon_y = v_y + \frac{1}{2} (u_y^2 + v_y^2 + w_y^2) \quad (4.17b)$$

$$\epsilon_z = w_z + \frac{1}{2} (u_z^2 + v_z^2 + w_z^2) \quad (4.17c)$$

$$\Upsilon_{xy} = u_y + v_x + (u_x u_y + v_y v_x + w_x w_y) \quad (4.17d)$$

$$\Upsilon_{yz} = v_{,z} + w_{,y} + (u_x u_{,y} + v_y v_{,z} + w_z w_{,y}) \quad (4.17e)$$

$$\Upsilon_{zx} = u_{,z} + w_{,x} + (u_x u_{,z} + v_z v_{,x} + w_x w_{,z}) \quad (4.17f)$$

where u, v and w are deformations of the flexible body in x, y and z axes of the body reference frame, and the variable in the subscript preceded by a comma indicates differentiation with respect to that variable.

Let

$$\{\epsilon\}^T = \{\epsilon_x \ \epsilon_y \ \epsilon_z \ \Upsilon_{xy} \ \Upsilon_{yz} \ \Upsilon_{zx}\} \quad (4.18)$$

$$\{\delta\} = (u_x \ u_y \ u_z \ v_x \ v_y \ v_z \ w_x \ w_y \ w_z)^T \quad (4.19)$$

By the assumed modes method, $\{\delta\}$ can be expressed as a linear function of n generalized coordinates $\{\eta\}$, which is

$$\{\delta\} = [N] \{\eta\} \quad (4.20)$$

Here $[N]$ is a 9 by n matrix which is

$$[N] = \begin{bmatrix} \frac{\partial}{\partial x} & \frac{\partial}{\partial y} & \frac{\partial}{\partial z} & 0 & 0 & 0 & 0 & 0 & 0 \\ 0 & 0 & 0 & \frac{\partial}{\partial x} & \frac{\partial}{\partial y} & \frac{\partial}{\partial z} & 0 & 0 & 0 \\ 0 & 0 & 0 & 0 & 0 & 0 & \frac{\partial}{\partial x} & \frac{\partial}{\partial y} & \frac{\partial}{\partial z} \end{bmatrix}^T \left[\{\Phi\}_1 \ \dots \ \{\Phi\}_n \right] \quad (4.21)$$

where the assumed modes are

$$\{\Phi\}_i = \begin{Bmatrix} \Phi_x \\ \Phi_y \\ \Phi_z \end{Bmatrix}_i \quad (4.22)$$

With these definitions, the nonlinear strain displacement relations can be written into matrix form

$$\{\epsilon\} = [H^0] \{\delta\} + \begin{Bmatrix} \{\delta\}^T [H^1] \{\delta\} \\ \dots \\ \{\delta\}^T [H^6] \{\delta\} \end{Bmatrix} \quad (4.23)$$

where $[H^0]$ to $[H^6]$ are Boolean matrices, which are

$$[H^0] = \begin{bmatrix} 1 & 0 & 0 & 0 & 0 & 0 \\ 0 & 0 & 0 & 1 & 0 & 0 \\ 0 & 0 & 0 & 0 & 0 & 1 \\ 0 & 1 & 0 & 1 & 0 & 0 \\ 0 & 0 & 0 & 0 & 1 & 0 \\ 0 & 0 & 1 & 0 & 0 & 1 \end{bmatrix} \quad (4.24a)$$

$$[H^1] = \frac{1}{2} \begin{bmatrix} [U^1] & [0] & [0] \\ & [U^1] & [0] \\ sym & & [U^1] \end{bmatrix} \quad [U^1] = \begin{bmatrix} 1 & 0 & 0 \\ 0 & 0 & 0 \\ 0 & 0 & 0 \end{bmatrix} \quad (4.24b)$$

$$[H^2] = \frac{1}{2} \begin{bmatrix} [U^2] & [0] & [0] \\ & [U^2] & [0] \\ sym & & [U^2] \end{bmatrix} \quad [U^2] = \begin{bmatrix} 0 & 0 & 0 \\ 0 & 1 & 0 \\ 0 & 0 & 0 \end{bmatrix} \quad (4.24c)$$

$$[H^3] = \frac{1}{2} \begin{bmatrix} [U^3] & [0] & [0] \\ & [U^3] & [0] \\ sym & & [U^3] \end{bmatrix} \quad [U^3] = \begin{bmatrix} 0 & 0 & 0 \\ 0 & 0 & 0 \\ 0 & 0 & 1 \end{bmatrix} \quad (4.24d)$$

$$[H^4] = \frac{1}{2} \begin{bmatrix} [U^4] & [0] & [0] \\ & [U^4] & [0] \\ sym & & [U^4] \end{bmatrix} \quad [U^4] = \begin{bmatrix} 0 & 1 & 0 \\ 1 & 0 & 0 \\ 0 & 0 & 0 \end{bmatrix} \quad (4.24e)$$

$$[H^5] = \frac{1}{2} \begin{bmatrix} [U^5] & [0] & [0] \\ & [U^5] & [0] \\ sym & & [U^5] \end{bmatrix} \quad [U^5] = \begin{bmatrix} 0 & 0 & 0 \\ 0 & 0 & 1 \\ 0 & 1 & 0 \end{bmatrix} \quad (4.24f)$$

$$[H^6] = \frac{1}{2} \begin{bmatrix} [U^6] & [0] & [0] \\ & [U^6] & [0] \\ \text{sym} & & [U^6] \end{bmatrix} \quad [U^6] = \begin{bmatrix} 0 & 0 & 1 \\ 0 & 0 & 0 \\ 1 & 0 & 0 \end{bmatrix} \quad (4.24g)$$

Note that $[H^1]$ to $[H^6]$ are symmetric.

Substituting equation (4.20) into equation (4.23), the relation between strain and generalized coordinates is obtained

$$\{\varepsilon\} = [B^0] \{\eta\} + \begin{Bmatrix} \{\eta\}^T [B^1] \{\eta\} \\ \dots \\ \{\eta\}^T [B^6] \{\eta\} \end{Bmatrix} \quad (4.25)$$

where

$$[B^0] = [H^0] [N] \quad (4.26)$$

$$[B^j] = [N]^T [H^j] [N] \quad j = 1 \dots 6 \quad (4.27)$$

Note that matrices $[B^1]$ to $[B^6]$ are symmetric.

4.3.2 Equations of Motion of a Flexible Body

In this section, both left and right sides of equation (4.16) are derived to obtain the equations of motion of a flexible body.

By Hooke's law, the stress can be written in terms of the strain, which is

$$\{\sigma\} = [E] \{\varepsilon\} \quad (4.28)$$

where $[E]$ is elasticity matrix.

Substituting equations (4.25) and (4.28) into the right side of equation (4.16), and ignoring 4th order terms of $\{\eta\}$, the following is obtained

$$\int_V \delta \{\epsilon\}^T \{\sigma\} dv = \delta \{\eta\}^T ([K] + [K_g(\eta)]) \{\eta\} \quad (4.29)$$

where stiffness matrices are

$$[K] = \int_V [B^0]^T [E] [B^0] dv \quad (4.30)$$

$$[K_g] = \int_V \left(2 \left[\dots [B^i] \{\eta\} \dots \right] [E] [B^0] + [B^0]^T [E] \left\{ \begin{array}{c} \{\eta\}^T [B^1] \\ \dots \\ \{\eta\}^T [B^6] \end{array} \right\} \right) dv \quad (4.31)$$

Substituting equations (4.15) and (4.29) into equation (4.16), and grouping terms with respect to different virtual displacements, the following is obtained:

$$\left[\delta \dot{R} \cdot \delta \dot{\pi} \cdot \delta \{\eta\}^T \right] \left[\begin{array}{c} \int_V (d\vec{F} - \ddot{P}\rho dv) \\ \int_V \dot{q} \times (d\vec{F} - \ddot{P}\rho dv) \\ \left[\int_V (\{\Phi\} \cdot (d\vec{F} - \ddot{P}\rho dv)) - ([K] + [K_g]) \{\eta\} \right] \end{array} \right] = 0 \quad (4.32)$$

Since the variations are arbitrary for a free moving flexible body, this equation can be written into three independent equations which are

$$\int_V (d\vec{F} - \ddot{P}\rho dv) = 0 \quad (4.33)$$

$$\int_V \dot{q} \times (d\vec{F} - \ddot{P}\rho dv) = 0 \quad (4.34)$$

$$\int_V (\{\Phi\} \cdot (d\vec{F} - \ddot{P}\rho dv)) - ([K] + [K_g]) \{\eta\} = \{0\} \quad (4.35)$$

The force terms in the above equations can be integrated as

$$\int_V d\vec{F} = \vec{F}_o + m\vec{g} \quad (4.36)$$

$$\int_V \vec{q} \times d\vec{F} = \vec{T}_o + \vec{q}_c \times m\vec{g} \quad (4.37)$$

$$\int_V (\{\Phi\} \cdot (d\vec{F})) = \{Q\} + \{\dot{S}\} \cdot m\vec{g} \quad (4.38)$$

where \vec{F}_o and \vec{T}_o are resultant force and torque due to surface tractions acting at the origin of the body reference frame, and $\{Q\}$ is the generalized force column matrix due to surface tractions which will excite vibrations of the flexible body.

Substituting equation (4.9) for the acceleration into equation (4.33), noting equations (4.5), (4.11) and that

$$\int_V \dot{\vec{q}} \rho dv = m\dot{\vec{q}}_c = m\{\dot{S}\}^T \{\dot{\eta}\} \quad (4.39)$$

$$\int_V \ddot{\vec{q}} \rho dv = m\ddot{\vec{q}}_c = m\{\ddot{S}\}^T \{\ddot{\eta}\} \quad (4.40)$$

equation (4.33) becomes

$$m(\ddot{\vec{R}} + \ddot{\vec{q}}_c + \dot{\vec{\Omega}} \times \vec{q}_c + \vec{\Omega} \times (\vec{\Omega} \times \vec{q}_c) + 2\vec{\Omega} \times \dot{\vec{q}}_c) = \vec{F}_o + m\vec{g} \quad (4.41)$$

or

$$\begin{aligned} m(\ddot{\vec{R}} + \{\ddot{S}\}^T \{\ddot{\eta}\} + (\dot{\vec{\Omega}} \times \{\dot{S}\}^T + \vec{\Omega} \times (\vec{\Omega} \times \{\dot{S}\}^T)) \{\eta\} + 2\vec{\Omega} \times \{\dot{S}\}^T \{\dot{\eta}\}) \\ = \vec{F}_o + m\vec{g} \end{aligned} \quad (4.42)$$

Substituting equations (4.9) and (4.36) into equation (4.34), completing all integrations over the whole body and rearranging, equation (4.34) can be written as

$$\begin{aligned} \int_V \vec{q} \times \ddot{\vec{P}} \rho dv &= \int_V \vec{q} \times \ddot{\vec{R}} \rho dv + \int_V \vec{q} \times (\dot{\vec{\Omega}} \times \vec{q}) \rho dv + \int_V \vec{q} \times (\vec{\Omega} \times (\vec{\Omega} \times \vec{q})) \rho dv \\ &\quad + \int_V 2\vec{q} \times (\vec{\Omega} \times \dot{\vec{q}}) \rho dv + \int_V \vec{q} \times \ddot{\vec{q}} \rho dv \\ &= \vec{T}_o + \vec{q}_c \times m\vec{g} \end{aligned} \quad (4.43)$$

Each term in the equation can be integrated as

$$\int_V \dot{\mathbf{q}} \times \ddot{\mathbf{R}} \rho dv = \int_V \dot{\mathbf{q}} \rho dv \times \ddot{\mathbf{R}} = m \dot{\mathbf{q}}_c \times \ddot{\mathbf{R}} \quad (4.44)$$

$$\int_V \dot{\mathbf{q}} \times (\ddot{\boldsymbol{\Omega}} \times \dot{\mathbf{q}}) \rho dv = \int_V ((\dot{\mathbf{q}} \cdot \dot{\mathbf{q}}) \dot{\mathbf{E}} - \dot{\mathbf{q}} \dot{\mathbf{q}}) \rho dv \cdot \ddot{\boldsymbol{\Omega}} = \mathbf{J} \cdot \ddot{\boldsymbol{\Omega}} \quad (4.45)$$

$$\begin{aligned} \int_V \dot{\mathbf{q}} \times (\ddot{\boldsymbol{\Omega}} \times (\ddot{\boldsymbol{\Omega}} \times \dot{\mathbf{q}})) \rho dv &= \ddot{\boldsymbol{\Omega}} \times \left[\int_V \dot{\mathbf{q}} \times (\ddot{\boldsymbol{\Omega}} \times \dot{\mathbf{q}}) \rho dv \right] \\ &= \ddot{\boldsymbol{\Omega}} \times (\mathbf{J} \cdot \ddot{\boldsymbol{\Omega}}) = -\dot{\mathbf{H}} \times \ddot{\boldsymbol{\Omega}} \end{aligned} \quad (4.46)$$

$$\int_V 2\dot{\mathbf{q}} \times (\ddot{\boldsymbol{\Omega}} \times \dot{\mathbf{q}}) \rho dv = 2 \int_V ((\dot{\mathbf{q}} \cdot \dot{\mathbf{q}}) \dot{\mathbf{E}} - \dot{\mathbf{q}} \dot{\mathbf{q}}) \rho dv \cdot \ddot{\boldsymbol{\Omega}} = \mathbf{J}^* \cdot \ddot{\boldsymbol{\Omega}} \quad (4.47)$$

$$\begin{aligned} \int_V \dot{\mathbf{q}} \times \ddot{\mathbf{q}} \rho dv &= \left(\int_V \dot{\mathbf{q}} \times \{\dot{\Phi}\}^T \rho dv \right) \{\ddot{\eta}\} \\ &= \left(\int_V (\dot{\mathbf{r}} + \{\eta\}^T \{\dot{\Phi}\}) \times \{\dot{\Phi}\}^T \rho dv \right) \{\ddot{\eta}\} = \{\dot{\mathbf{D}}\}^T \{\ddot{\eta}\} \end{aligned} \quad (4.48)$$

where $\dot{\mathbf{E}}$ is a unit dyadic, \mathbf{J} is the dyadic of moment of inertia of the flexible body about the origin of the body reference frame, $\dot{\mathbf{H}}$ is the angular momentum of the body about the same reference point, and $\{\dot{\mathbf{D}}\}$ is a vector array related to the assumed modes.

With expressions (4.44) to (4.48), equation (4.34) becomes

$$m \dot{\mathbf{q}}_c \times \ddot{\mathbf{R}} + \mathbf{J} \cdot \ddot{\boldsymbol{\Omega}} - \dot{\mathbf{H}} \times \ddot{\boldsymbol{\Omega}} + \mathbf{J}^* \cdot \ddot{\boldsymbol{\Omega}} + \{\dot{\mathbf{D}}\}^T \{\ddot{\eta}\} = \dot{\mathbf{T}}_o + \dot{\mathbf{q}}_c \times m \dot{\mathbf{g}} \quad (4.49)$$

For equation (4.35), substituting equation (4.9) for acceleration yields

$$\begin{aligned} \int_V (\{\dot{\Phi}\} \cdot \ddot{\mathbf{P}}) \rho dv &= \int_V (\{\dot{\Phi}\} \cdot \ddot{\mathbf{R}}) \rho dv + \int_V (\{\dot{\Phi}\} \cdot \ddot{\mathbf{q}}) \rho dv + 2 \int_V (\{\dot{\Phi}\} \cdot (\ddot{\boldsymbol{\Omega}} \times \dot{\mathbf{q}})) \rho dv \\ &\quad + \int_V (\{\dot{\Phi}\} \cdot (\ddot{\boldsymbol{\Omega}} \times (\ddot{\boldsymbol{\Omega}} \times \dot{\mathbf{q}}))) \rho dv + \int_V (\{\dot{\Phi}\} \cdot (\ddot{\boldsymbol{\Omega}} \times \dot{\mathbf{q}})) \rho dv \end{aligned} \quad (4.50)$$

By the definition of equation (4.6), the first integral at the right side of the equation

above is

$$\int_V [\{\bar{\Phi}\} \cdot \ddot{\bar{R}}] \rho dv = m \{\bar{S}\} \cdot \ddot{\bar{R}} \quad (4.51)$$

And the other terms are integrated as follows:

$$\int_V (\{\bar{\Phi}\} \cdot \ddot{\bar{q}}) \rho dv = \left[\int_V (\{\bar{\Phi}\} \cdot \{\bar{\Phi}\}^T) \rho dv \right] \{\ddot{\eta}\} = [M] \{\ddot{\eta}\} \quad (4.52)$$

$$\int_V (\{\bar{\Phi}\} \cdot (\dot{\bar{\Omega}} \times \bar{q})) \rho dv = \int_V \bar{q} \times \{\bar{\Phi}\} \rho dv \cdot \dot{\bar{\Omega}} = \{\bar{D}(\{\eta\})\} \cdot \dot{\bar{\Omega}} \quad (4.53)$$

$$\begin{aligned} \int_V (\{\bar{\Phi}\} \cdot (\bar{\Omega} \times (\bar{\Omega} \times \bar{q}))) \rho dv &= \left(\int_V (\{\bar{\Phi}\} \cdot (\bar{\Omega} \times (\bar{\Omega} \times \{\bar{\Phi}\}^T))) \rho dv \right) \{\eta\} \\ &= [K_n(\bar{\Omega})] \{\eta\} \end{aligned} \quad (4.54)$$

$$\begin{aligned} 2 \int_V (\{\bar{\Phi}\} \cdot (\bar{\Omega} \times \dot{\bar{q}})) \rho dv &= 2 \left(\int_V (\{\bar{\Phi}\} \cdot (\bar{\Omega} \times \{\bar{\Phi}\}^T)) \rho dv \right) \{\dot{\eta}\} \\ &= [G(\bar{\Omega})] \{\dot{\eta}\} \end{aligned} \quad (4.55)$$

where $[M]$ is a generalized mass matrix which is constant, $[K_n(\bar{\Omega})]$ is a stiffness matrix due to the centrifugal acceleration, and $[G(\bar{\Omega})]$ is a damping matrix due to the gyroscopic effect.

With these integrated terms in equations (4.51) to (4.55), equation (4.50) becomes

$$\int_V (\{\bar{\Phi}\} \cdot \ddot{\bar{P}}) \rho dv = m \{\bar{S}\} \cdot \ddot{\bar{R}} + [M] \{\ddot{\eta}\} + \{\bar{D}\} \cdot \dot{\bar{\Omega}} + [K_n] \{\eta\} + [G] \{\dot{\eta}\} \quad (4.56)$$

Substituting equations (4.56) and (4.38) into equation (4.35), the equation becomes

$$\begin{aligned} m \{\bar{S}\} \cdot \ddot{\bar{R}} + [M] \{\ddot{\eta}\} + \{\bar{D}\} \cdot \dot{\bar{\Omega}} + [G] \{\dot{\eta}\} + ([K] + [K_r] + [K_n]) \{\eta\} \\ = \{Q\} + \{\bar{S}\} \cdot m \dot{\bar{g}} \end{aligned} \quad (4.57)$$

Equations (4.57), (4.49) and (4.41) are the equations of motion of a free-moving flexible body in vectorial form. For convenience, they are listed together here,

$$\begin{aligned} m(\ddot{\vec{R}} + \{\dot{\vec{S}}\}^T \{\ddot{\eta}\} + (\vec{\Omega} \times \{\dot{\vec{S}}\}^T + \vec{\Omega} \times (\vec{\Omega} \times \{\dot{\vec{S}}\}^T)) \{\eta\} + 2\vec{\Omega} \times \{\dot{\vec{S}}\}^T \{\dot{\eta}\}) \\ = \vec{F}_o + m\vec{g} \end{aligned} \quad (4.58)$$

$$m\dot{\vec{q}}_c \times \ddot{\vec{R}} + \dot{\vec{J}} \cdot \dot{\vec{\Omega}} - \vec{H} \times \dot{\vec{\Omega}} + \dot{\vec{J}}^* \cdot \dot{\vec{\Omega}} + \{\dot{\vec{D}}\}^T \{\ddot{\eta}\} = \vec{T}_o + \dot{\vec{q}}_c \times m\vec{g} \quad (4.59)$$

$$\begin{aligned} m\{\dot{\vec{S}}\} \cdot \ddot{\vec{R}} + [M] \{\ddot{\eta}\} + \{\dot{\vec{D}}\} \cdot \dot{\vec{\Omega}} + [G] \{\dot{\eta}\} + ([K] + [K_g] + [K_n]) \{\eta\} \\ = \{Q\} + \{\dot{\vec{S}}\} \cdot m\vec{g} \end{aligned} \quad (4.60)$$

It can be seen that these three equations are coupled for all displacement, velocity and acceleration terms and are highly nonlinear.

4.3.3 Equations of Motion of a Flexible Body in Matrix form

The mathematical relations in multibond graphs are based on matrix operations. To be represented by multibond graphs, the vectorial form of the equations of motion in the last section should be first changed to matrix form.

A vector in a 3-D space can be represented in different frames, or different coordinate systems, resulting in different components in its matrix form. In this thesis, angular velocity $\dot{\vec{\Omega}}$ of a body reference frame and the velocity $\dot{\vec{q}}$ of the deformed body relative to the body reference frame are given in the body reference frame. The assumed mode shapes and the resultant external forces due to the surface tractions are also given in the body reference frame. The gravity acceleration \vec{g} and the absolute velocity of the center of mass of the body $\dot{\vec{P}}_c$ are measured in the inertial frame because in this frame \vec{g} has fixed direction.

The rotation transformation between the inertial frame $\{\vec{e}^0\}$ and the body

reference frame $\{\hat{e}^i\}$ can be defined as

$$\{\hat{e}^0\} = [A^{0i}] \{\hat{e}^i\} \quad \text{or} \quad \{\hat{e}^i\} = [A^{i0}] \{\hat{e}^0\} \quad (4.61)$$

where $[A^{0i}]$ is the transform matrix from body reference frame to inertial frame. Matrix $[A^{0i}]$ is an orthogonal matrix which has the property

$$[A^{0i}]^{-1} = [A^{0i}]^T = [A^{i0}] \quad (4.62)$$

For any vector \vec{V} , for which column matrices $\{V^j\}$ and $\{V^i\}$ are its coordinates in frame $\{\hat{e}^0\}$ and frame $\{\hat{e}^i\}$, the following relation holds in terms of equation (4.61)

$$\{V^0\} = [A^{0i}] \{V^i\} \quad (4.63)$$

The matrix form of dot multiplication of two vectors \vec{V} and \vec{W} , in the same frame, is $\{V\}^T \{W\}$, and the matrix form of cross multiplication of two vectors \vec{V} and \vec{W} , in the same frame, is $[\tilde{V}] \{W\}$, where the tilde matrix is formed as

$$[\tilde{V}] = \begin{bmatrix} 0 & -v_z & v_y \\ v_z & 0 & -v_x \\ -v_y & v_x & 0 \end{bmatrix} \quad (4.64)$$

For any vector array, say $\{\hat{S}\}$, its matrix form in frame $\{\hat{e}^i\}$ can be represented as $[S]$, which means

$$\{\hat{S}\} = [S] \{\hat{e}^i\} \quad (4.65)$$

For any dyadic, say \hat{J} , its matrix form in frame $\{\hat{e}^i\}$ can be represented as $[J]$ which means

$$\hat{J} = \{\dot{\hat{e}}^i\}^T [J] \{\hat{e}^i\} \quad (4.66)$$

The matrix form of the multiplication of \hat{J} and a vector $\vec{\Omega}$ measured in the same frame is $[J] \{\Omega\}$.

In terms of these relations, the kinematic equations (4.8) and (4.14) can be written as

$$\begin{aligned} \{\dot{P}\} &= (\{\dot{R}\} - [\tilde{q}] \{\Omega\} + \{\dot{q}\}) \\ &= (\{\dot{R}\} - [\tilde{q}] \{\Omega\} + [\Phi]^T \{\dot{\eta}\}) \end{aligned} \quad (4.67)$$

$$\{\Omega_p\} = \{\Omega\} + \frac{1}{2} [\tilde{V}] [\Phi_p]^T \{\dot{\eta}\} \quad (4.68)$$

Note that these vectors are all represented in the frame $\{\hat{e}^i\}$.

Assuming that all vectors in the equations of motion are represented in body reference frame $\{\hat{e}^i\}$ except \hat{g} which is always given in the inertial frame for convenience, the matrix form of equation (4.58), (4.49) and (4.57) can be expressed as

$$\begin{aligned} m(\{\ddot{R}\} + [S]^T \{\ddot{\eta}\} - [\tilde{q}_c] \{\dot{\Omega}\} + [\tilde{\Omega}] [\tilde{\Omega}] [S]^T \{\eta\} + 2[\tilde{\Omega}] [S]^T \{\dot{\eta}\}) \\ = \{F_o\} + m[A^{i0}] \{g\} \end{aligned} \quad (4.69)$$

$$\begin{aligned} m[\tilde{q}_c] \{\ddot{R}\} + [J] \{\dot{\Omega}\} - [\tilde{H}] \{\Omega\} + [J^*] \{\Omega\} + [D]^T \{\ddot{\eta}\} \\ = \{T_o\} + m[\tilde{q}_c] [A^{i0}] \{g\} \end{aligned} \quad (4.70)$$

$$\begin{aligned} m[S] \{\ddot{R}\} + [M] \{\ddot{\eta}\} + [D] \{\dot{\Omega}\} + [G] \{\dot{\eta}\} + [K_{eq}] \{\eta\} \\ = \{Q\} + m[S] [A^{i0}] \{g\} \end{aligned} \quad (4.71)$$

where the equivalent stiffness matrix $[K_{eq}]$ is

$$[K_{eq}] = [K] + [K_g] + [K_n] \quad (6.72)$$

Matrices $[D]$ and $[S]$ are n by 3 matrices. $[J]$, $[J^*]$ and $[M]$ are symmetric, $[\dot{H}]$ and $[G]$ are skew-symmetric. By definition, matrices $[J]$ and $[M]$, are not singular.

In the discussion of numerical solution, later in Chapter 8, a compact form of these equations is given. Letting

$$\{h\} = \begin{Bmatrix} \{\dot{R}\} \\ \{\Omega\} \\ \{\dot{\eta}\} \end{Bmatrix} \quad (4.73)$$

these three equations of motion can be further written into a compact form as

$$[M^*] \{\dot{h}\} = \{W(h, \eta)\} + \{F\} \quad (4.74)$$

where $[M^*]$ is the matrix of generalized mass of the flexible body which is

$$[M^*] = \begin{bmatrix} m[I] & m[\tilde{q}_c]^T & m[S]^T \\ m[\tilde{q}_c] & [J] & [D]^T \\ m[S] & [D] & [M] \end{bmatrix} \quad (4.75)$$

$\{W(h, \eta)\}$ consists of all other terms consisting of velocity and displacement of coordinates, which is

$$\{W(h, \eta)\} = \begin{Bmatrix} -[\tilde{\Omega}] [\tilde{\Omega}] [S]^T \{\eta\} - 2[\tilde{\Omega}] [S]^T \{\dot{\eta}\} \\ -[J^*] \{\Omega\} \\ -([G] \{\dot{\eta}\} + [K_{eq}] \{\eta\}) \end{Bmatrix} \quad (4.76)$$

$\{F\}$ consists of all external forces which is

$$\{F\} = \begin{Bmatrix} \{F_o\} + m[A^{i0}] \{g\} \\ \{T_o\} + m[\tilde{q}_c] [A^{i0}] \{g\} \\ \{Q\} + m[S] [A^{i0}] \{g\} \end{Bmatrix} \quad (4.77)$$

4.4 Form of Equations of Motion of a Flexible Body for Multibond Graph Representation

In multibond graph of rigid body dynamics, the translation and angular velocities are represented by separated multibonds [Tiernego and Bos 1985; Bos 1986]. This is more convenient when dealing with constraints and excitation. To keep the same multibond graph methodology, in the multibond graph of flexible body dynamics, the translation, angular and vibrational velocities will be considered to be represented by three separated multibonds. This makes it easy to represent multibody systems with both rigid and flexible bodies. However, the equations of motion generated above are not suitable for multibond graph representation because they are coupled in the acceleration terms. A slight modification to the form of these equations makes it possible for the equations to be represented by multibond graphs.

First examine equation (4.41). The acceleration terms in the bracket are actually the acceleration of the center of mass of the flexible body, which is expressed in equation (4.11). So equation (4.41) can also be written as

$$m\ddot{\mathbf{P}}_c = \ddot{\mathbf{F}}_o + m\ddot{\mathbf{g}} \quad (4.78)$$

Assuming that the velocity of the center of mass of the flexible body is represented in the inertial frame, the matrix form of equation (4.78) will be

$$m \frac{d}{dt} \{\dot{\mathbf{P}}_c\} = [A^{vi}] \{F_o\} + m \{g\} \quad (4.79)$$

where

$$\{\dot{P}_c\} = [A^{0i}] (\{\dot{R}\} - [\tilde{q}_c] \{\Omega\} + [S]^T \{\dot{\eta}\}) \quad (4.80)$$

Secondly, terms referring to the origin of the body reference frame in the left side of equation (4.49) are changed to refer to the center of mass of the flexible body. To do so, the Huygens-Steiner rule [Wittenburg, 1977] is used, which states

$$\mathbf{J} = \mathbf{J}_c + m [(\dot{\tilde{q}}_c \cdot \dot{\tilde{q}}_c) \hat{E} - \dot{\tilde{q}}_c \dot{\tilde{q}}_c] \quad (4.81)$$

where \mathbf{J}_c is the dyadic of moment of inertia of the flexible body about its center of mass.

Substituting this relation into equation (4.49), \vec{H} becomes

$$\vec{H} = \vec{H}_c + m [(\dot{\tilde{q}}_c \cdot \dot{\tilde{q}}_c) \hat{E} - \dot{\tilde{q}}_c \dot{\tilde{q}}_c] \cdot \vec{\Omega} \quad (4.82)$$

\hat{J}^* becomes

$$\hat{J}^* = \hat{J}_c^* + 2m [(\dot{\tilde{q}}_c \cdot \dot{\tilde{q}}_c) \hat{E} - \dot{\tilde{q}}_c \dot{\tilde{q}}_c] \quad (4.83)$$

and $\{\vec{D}\}^T$ can also be changed to

$$\begin{aligned} \{\vec{D}\}^T \{\ddot{\eta}\} &= \left(\int_V (\tilde{q} - \tilde{q}_c) \times \{\vec{\Phi}\}^T \rho dv + \int_V \tilde{q}_c \times \{\vec{\Phi}\}^T \rho dv \right) \{\ddot{\eta}\} \\ &= \{\vec{D}_c\}^T \{\ddot{\eta}\} + m \tilde{q}_c \times \{\vec{S}\}^T \{\ddot{\eta}\} \\ &= \{\vec{D}_c\}^T \{\ddot{\eta}\} + m \tilde{q}_c \times \ddot{\tilde{q}}_c \end{aligned} \quad (4.84)$$

Substituting equations (4.81) to (4.84) into equation (4.49) and noting equation (4.11) and

$$[(\dot{\mathbf{q}}_c \cdot \dot{\mathbf{q}}_c) \dot{\mathbf{E}} - \dot{\mathbf{q}}_c \dot{\mathbf{q}}_c] \cdot \ddot{\mathbf{\Omega}} = \dot{\mathbf{q}}_c \times (\ddot{\mathbf{\Omega}} \times \dot{\mathbf{q}}_c) \quad (4.85)$$

$$[(\dot{\mathbf{q}}_c \cdot \dot{\mathbf{q}}_c) \dot{\mathbf{E}} - \dot{\mathbf{q}}_c \dot{\mathbf{q}}_c] \cdot \ddot{\mathbf{\Omega}} = \dot{\mathbf{q}}_c \times (\ddot{\mathbf{\Omega}} \times \dot{\mathbf{q}}_c) \quad (4.86)$$

equation (4.49) can be written into the form as

$$\begin{aligned} \mathbf{J}_c \cdot \ddot{\mathbf{\Omega}} - \tilde{\mathbf{H}}_c \times \ddot{\mathbf{\Omega}} + \mathbf{J}_c^* \cdot \ddot{\mathbf{\Omega}} + \{\mathbf{D}_c\}^T \{\ddot{\eta}\} &= \dot{\mathbf{T}}_o + \dot{\mathbf{q}}_c \times m(\ddot{\mathbf{g}} - \ddot{\mathbf{P}}_c) \\ &= \dot{\mathbf{T}}_o - \dot{\mathbf{q}}_c \times \dot{\mathbf{F}}_o \end{aligned} \quad (4.87)$$

where equation (4.78) is used.

The matrix form of this equation can be written as

$$[\mathbf{J}_c] \{\ddot{\mathbf{\Omega}}\} + ([\mathbf{J}_c] - [\tilde{\mathbf{H}}_c]) \{\mathbf{\Omega}\} + [\mathbf{D}_c]^T \{\ddot{\eta}\} = \{\mathbf{T}_o\} - [\tilde{\mathbf{q}}_c] \{\mathbf{F}_o\} \quad (4.88)$$

Thirdly, repeating integration (4.50) with $\dot{\mathbf{q}}$, $\ddot{\mathbf{q}}$ and $\ddot{\mathbf{q}}$ replaced by $(\dot{\mathbf{q}} - \dot{\mathbf{q}}_c) + \dot{\mathbf{q}}_c$, $(\ddot{\mathbf{q}} - \ddot{\mathbf{q}}_c) + \ddot{\mathbf{q}}_c$ and $(\ddot{\mathbf{q}} - \ddot{\mathbf{q}}_c) + \ddot{\mathbf{q}}_c$ yields

$$\begin{aligned} \int_V (\{\Phi\} \cdot \ddot{\mathbf{P}}) \rho dv &= \int_V (\{\Phi\} \cdot (\ddot{\mathbf{R}} + \ddot{\mathbf{q}}_c + \ddot{\mathbf{\Omega}} \times \dot{\mathbf{q}}_c + \ddot{\mathbf{\Omega}} \times (\ddot{\mathbf{\Omega}} \times \dot{\mathbf{q}}_c) + 2\ddot{\mathbf{\Omega}} \times \dot{\mathbf{q}}_c)) \rho dv \\ &+ \int_V (\{\Phi\} \cdot (\ddot{\mathbf{q}} - \ddot{\mathbf{q}}_c)) \rho dv + \int_V (\{\Phi\} \cdot (\ddot{\mathbf{\Omega}} \times (\ddot{\mathbf{\Omega}} \times (\dot{\mathbf{q}} - \dot{\mathbf{q}}_c)))) \rho dv \\ &+ \int_V (\{\Phi\} \cdot (\ddot{\mathbf{\Omega}} \times (\dot{\mathbf{q}} - \dot{\mathbf{q}}_c))) \rho dv + 2 \int_V (\{\Phi\} \cdot (\ddot{\mathbf{\Omega}} \times (\dot{\mathbf{q}} - \dot{\mathbf{q}}_c))) \rho dv \end{aligned} \quad (4.89)$$

With equations (4.6) and (4.9), the first integral at the right side of the equation above is

$$\int_V \left[\{\Phi\} \cdot (\ddot{\mathbf{R}} + \ddot{\mathbf{q}}_c + \ddot{\mathbf{\Omega}} \times \dot{\mathbf{q}}_c + \ddot{\mathbf{\Omega}} \times (\ddot{\mathbf{\Omega}} \times \dot{\mathbf{q}}_c) + 2\ddot{\mathbf{\Omega}} \times \dot{\mathbf{q}}_c) \right] \rho dv = m \{\dot{\mathbf{S}}\} \cdot \ddot{\mathbf{P}}_c \quad (4.90)$$

And the other terms are integrated as follows:

$$\int_V (\{\Phi\} \cdot (\ddot{\mathbf{q}} - \ddot{\mathbf{q}}_c)) \rho dv = [\mathbf{M}_c] \{\ddot{\eta}\} \quad (4.91)$$

$$\int_V (\{\vec{\Phi}\} \cdot (\vec{\Omega} \times (\dot{\vec{q}} - \dot{\vec{q}}_c))) \rho dv = \int_V (\dot{\vec{q}} - \dot{\vec{q}}_c) \times \{\vec{\Phi}\} \rho dv \cdot \vec{\Omega} = \{\vec{D}_c(\{\eta\})\} \cdot \vec{\Omega} \quad (4.92)$$

$$\int_V (\{\vec{\Phi}\} \cdot (\vec{\Omega} \times (\vec{\Omega} \times (\dot{\vec{q}} - \dot{\vec{q}}_c)))) \rho dv = [K_{nc}(\vec{\Omega})] \{\eta\} \quad (4.93)$$

$$2 \int_V (\{\vec{\Phi}\} \cdot (\vec{\Omega} \times (\dot{\vec{q}} - \dot{\vec{q}}_c))) \rho dv = [G_c(\vec{\Omega})] \{\dot{\eta}\} \quad (4.94)$$

With these integrated terms, equation (4.57) becomes

$$\begin{aligned} & [M_c] \{\ddot{\eta}\} + \{\vec{D}_c\} \cdot \vec{\Omega} + [G_c] \{\dot{\eta}\} + ([K] + [K_g] + [K_{nc}]) \{\eta\} \\ & = \{Q\} + \{\vec{S}\} \cdot m(\dot{\vec{g}} - \dot{\vec{P}}_c) = \{Q\} - (\{\vec{S}\} \cdot \vec{F}_o) \end{aligned} \quad (4.95)$$

Its matrix form is

$$[M_c] \{\ddot{\eta}\} + [D_c] \{\dot{\Omega}\} + [G_c] \{\dot{\eta}\} + [K_{eqc}] \{\eta\} = \{Q\} - [S] \{F_o\} \quad (4.96)$$

where

$$[K_{eqc}] = [K] + [K_g] + [K_{nc}] \quad (4.97)$$

For convenience, the dynamic equations of motion, in their multibond graph representation form are listed together

$$m \frac{d}{dt} \{\dot{P}_c\} = [A^{0i}] \{F_o\} + m \{g\} \quad (4.98)$$

$$[J_c] \{\dot{\Omega}\} + ([J^*_c] - [\tilde{H}_c]) \{\Omega\} + [D_c]^T \{\ddot{\eta}\} = \{T_o\} - [\tilde{q}_c] \{F_o\} \quad (4.99)$$

$$[M_c] \{\ddot{\eta}\} + [D_c] \{\dot{\Omega}\} + [G_c] \{\dot{\eta}\} + [K_{eqc}] \{\eta\} = \{Q\} - [S] \{F_o\} \quad (4.100)$$

- Chapter 5 -

The Application of Floating Frames

5.1 Introduction

The equations of motion and the multibond graphs of a flexible body described in the previous chapters are for the general case. They are coupled in translation, rotation and vibrations and are therefore fairly complicated. Even though there have been many powerful numerical integration methods, to solve different kinds of differential equations that have been developed, the numerical solution of flexible multibody systems is still difficult and challenging for numerical integration. In addition to the development of more powerful numerical integration algorithms, another way to reduce this difficulty is to simplify the equations of motion themselves.

In the derivation of these equations of motion, the body reference frames are chosen arbitrarily. In rigid body dynamics, the local reference frame attached at the center of mass of the body can simplify the equations of motion significantly. This is also true for flexible body dynamics. The kinds of reference frames which simplify the expression of the equations of motion of a flexible body are called floating reference frames [Canavin and Likins 1977].

Floating reference frames have long been used in spacecraft dynamics. With the development of analysis techniques for spacecraft dynamics, several types of floating frames were developed. This chapter will first review these floating frames and then discuss the application of a major type of floating reference frame, the Buckens frame, into flexible body dynamics and its multibond graph representations.

5.2 Floating Frames for Flexible Bodies

The motion of a flexible body in an inertial frame can be determined by the position and the orientation of a body reference frame which moves with the body and the vibrational deformation of the body relative to this body reference frame. The way the body reference frame moves with the body is featured by the position and orientation of the body reference frame related to the body. Different approaches form different floating frames and possess different characteristics and ability to simplify the equations of motion. Four types of floating frames are discussed in this section.

5.2.1 Body-Fixed Frame

This type of body reference frame is rigidly attached at a point of the flexible body. It implies that the displacement and rotation of this point of the body due to the deformation of the body measured relative to the frame are equal to zero. This condition can be mathematically written as

$$[\Phi] = [0] \quad \text{at} \quad x, y, z = 0 \quad (5.1)$$

$$\tilde{\nabla}[\Phi] = [0] \quad \text{at} \quad x, y, z = 0 \quad (5.2)$$

This condition can be satisfied in selection of assumed modes and no more constraint equations need to be included. Therefore, it is widely used [Shabana, 1982]. However, this type of reference frame yields no simplification for the equations of motion of a flexible body when it is not located at the center of mass and gives limited simplification when it is located at the center of mass.

When the origin of the body reference frame is located at the center of mass, the position vector \hat{q}_c is equal to zero. This means that a constraint condition about the location of the body reference frame is forced which is

$$\dot{\mathbf{q}}_c = \int_V \dot{\mathbf{q}} dv = \int_V \dot{\mathbf{r}} dv + \left(\int_V \{\mathbf{\Phi}\}^T dv \right) \{\eta\} = \{\dot{\mathbf{S}}\}^T \{\eta\} = 0 \quad (5.3)$$

Note that the integral $\int_V \dot{\mathbf{r}} dv$ is equal to zero when the body reference frame is located at the center of mass of the flexible body before deformation occurs. $\{\dot{\mathbf{S}}\}^T \{\eta\} = 0$ implies that the generalized coordinates are not independent if

$$\{\dot{\mathbf{S}}\}^T \neq \{0\}^T \quad (5.4)$$

With equation (5.3) the velocity and acceleration of the center of mass are simplified from equations (4.10) and (4.11) to

$$\dot{\mathbf{P}}_c = \dot{\mathbf{R}} \quad (5.5)$$

$$\dot{\mathbf{P}}_c = \dot{\mathbf{R}} \quad (5.6)$$

and so the equations of motion (4.58), (4.49) and (4.57) in chapter 4 are simplified to

$$m\ddot{\mathbf{R}} = \vec{\mathbf{F}}_o + m\dot{\mathbf{g}} \quad (5.7)$$

$$\mathbf{J} \cdot \dot{\vec{\Omega}} - \vec{\mathbf{H}} \times \vec{\Omega} + \mathbf{J}^* \cdot \vec{\Omega} + \{\mathbf{D}\}^T \{\ddot{\eta}\} = \vec{\mathbf{T}}_o \quad (5.8)$$

$$[M] \{\ddot{\eta}\} + \{\mathbf{D}\} \cdot \dot{\vec{\Omega}} + [G] \{\dot{\eta}\} + [K_{eq}] \{\eta\} = \{Q\} + \{\dot{\mathbf{S}}\} \cdot m(\dot{\mathbf{g}} - \ddot{\mathbf{R}}) \quad (5.9)$$

It should be noted that the equations of motion of an unconstrained flexible body under the body fixed frame are not only the above three equations. They include a holonomic constraint equation about the generalized coordinates of equation (5.3) if equation (5.4) holds. This means that the mass center fixed body reference frame has limited benefits because it simplifies the differential equations of the motion but adds algebraic equations and lets the equations become differential-algebraic equations.

The real advantage of applying a mass center located body fixed frame lies in the fact that when the left side of equation (5.4) is equal to zero the constraint on the generalized coordinates of equation (5.3) can be always satisfied. This can be done by choosing appropriate assumed modes and letting

$$\int_V \{\bar{\Phi}\}^T dv = \{\bar{S}\}^T = \{0\}^T \quad (5.10)$$

At least one set of modes which satisfies this condition can be found: free-free elastic normal modes of an unconstrained flexible body [Canavin and Likins 1977]. It has been proved that free-free elastic normal modes of an unconstrained flexible body satisfy the following two conditions [Canavin and Likins 1977]

$$\int_V \{\bar{\Phi}\} dv = \{\bar{S}\} = \{0\} \quad (5.11)$$

$$\int_V (\dot{r} \times \{\bar{\Phi}\}) dv = \{0\} \quad (5.12)$$

With the first condition, the constraint conditions for the generalized coordinates can be always satisfied and the equation of motion (5.9) can be further simplified as

$$[M] \{\ddot{\eta}\} + \{\bar{D}\} \cdot \dot{\Omega} + [G] \{\dot{\eta}\} + [K_{eq}] \{\eta\} = \{Q\} \quad (5.13)$$

The second condition is not necessary for this body-fixed frame. It will be seen that it is useful in the Buckens frame and the Tisserand frame for further simplification.

However, when free-free elastic normal modes of an unconstrained flexible body are used as the assumed modes, for a constrained flexible body in multibody systems, the geometric boundary conditions of the body are not guaranteed to be satisfied. This will incorrectly predict the vibrations of the flexible bodies and the misprediction is dependent on how serious the violation of the boundary conditions is. Therefore, it can be concluded that only when the elastic normal modes of a flexible body in multibody

systems can be well approximated by the free-free elastic normal modes of the body or by other assumed modes which meet equation (5.10), does the application of this mass center located body fixed frame work well.

5.2.2 Principal-axis Frame

The principal-axis frame is so defined that the origin of the body reference frame is located at the center of mass and the orientation of the coordinate axes coincides with the principal axes of the moment of inertia of the flexible body. This condition can be expressed as

$$J_{xy} = J_{yx} = -\int_V q_x q_y \rho dv = 0 \quad (5.14a)$$

$$J_{xz} = J_{zx} = -\int_V q_x q_z \rho dv = 0 \quad (5.14b)$$

$$J_{yz} = J_{zy} = -\int_V q_y q_z \rho dv = 0 \quad (5.14c)$$

Compared with the body-fixed frame located at the center of mass, this type of body reference frame only makes the inertia matrix of the flexible body diagonal. However, it also adds three constraint conditions for the generalized coordinates, which makes the generalized coordinates for the vibrational deformation dependent. This type of body reference frame has no significance in terms of simplification of the equations of motion.

5.2.3 The Buckens Frame

The Buckens frame is derived from the idea that the vibrational deformation of the flexible body over the whole volume should be minimized through the appropriate adjustment of the body reference frame. This idea can be formulated as the following expression

$$\text{minimize } \frac{1}{2} \int_V (\dot{\mathbf{u}} \cdot \dot{\mathbf{u}}) \rho dv \quad (5.15)$$

The position and the orientation of the body reference frame which satisfies this condition can be obtained through the perturbation of the position and the orientation of the body reference frame. This leads to

$$\delta \frac{1}{2} \int_V (\dot{\mathbf{u}} \cdot \dot{\mathbf{u}}) \rho dv = \int_V (\dot{\mathbf{u}} \cdot \delta \dot{\mathbf{u}}) \rho dv = 0 \quad (5.16)$$

Since the position of an arbitrary point of the flexible body in the inertia frame does not change when the body reference frame is perturbed, the variation of the position vector should be zero

$$\begin{aligned} \delta \vec{P} &= \delta \vec{R} + \delta \vec{\phi} \times \vec{q} + \delta \dot{\vec{q}} \\ &= \delta \vec{R} + \delta \vec{\phi} \times \dot{\vec{q}} + \delta \dot{\mathbf{u}} \\ &= 0 \end{aligned} \quad (5.17)$$

Solving this equation for $\delta \dot{\mathbf{u}}$ and substituting into equation (5.17), equation (5.17) becomes

$$\int_V \dot{\mathbf{u}} \rho dv \cdot \delta \vec{R} + \int_V (\dot{\vec{q}} \times \dot{\mathbf{u}}) \rho dv \cdot \delta \vec{\phi} = 0 \quad (5.18)$$

Since the variations $\delta \vec{R}$ and $\delta \vec{\phi}$ are arbitrary and independent, equation (5.18) can be written as two constraint equations for the location and the orientation of the body reference frame

$$\int_V \dot{\mathbf{u}} \rho dv = 0 \quad (5.19)$$

$$\begin{aligned} \int_V (\dot{\vec{q}} \times \dot{\mathbf{u}}) \rho dv &= \int_V (\dot{\vec{r}} \times \dot{\mathbf{u}}) \rho dv + \int_V (\dot{\mathbf{u}} \times \dot{\mathbf{u}}) \rho dv \\ &= \int_V (\dot{\vec{r}} \times \dot{\mathbf{u}}) \rho dv = 0 \end{aligned} \quad (5.20)$$

For the first constraint condition, note that

$$\int_V \dot{\vec{q}} \rho dv = \int_V (\dot{\vec{r}} + \dot{\vec{u}}) \rho dv = 0 \quad (5.21)$$

when the origin of the body reference frame is located at the center of mass of the flexible body. This means that locating the body reference frame at the center of mass is one way to satisfy this constraint. Recalling equation (4.3), in Chapter 4, the expression of equation (5.19) in terms of the assumed modes puts a constraint on the generalized coordinates, which is

$$\int_V \dot{\vec{u}} \rho dv = \left(\int_V \{\vec{\Phi}\}^T \rho dv \right) \{\eta\} = m \{\dot{\vec{S}}\}^T \{\eta\} = 0 \quad (5.22)$$

The second constraint equation can be further expressed in terms of the assumed modes

$$\int_V (\dot{\vec{r}} \times \dot{\vec{u}}) \rho dv = \left(\int_V (\dot{\vec{r}} \times \{\vec{\Phi}\}^T) \rho dv \right) \{\eta\} = 0 \quad (5.23)$$

These two constraints imply that the generalized coordinates η 's for the vibrations of the flexible body are not independent if

$$\{\dot{\vec{S}}\}^T \neq \{0\}^T \quad (5.24)$$

and

$$\int_V (\dot{\vec{r}} \times \{\vec{\Phi}\}^T) dv \neq \{0\}^T \quad (5.25)$$

This gives rise to the same problem as for the mass center located body-fixed frame, i.e. that the differential equations of motion are changed to differential-algebraic equations. This does not give significant simplification to the equations of motion unless the free-free elastic modes of an unconstrained flexible body are adopted.

If the free-free elastic modes of an unconstrained flexible body are adopted, the left side of equations (5.24) and (5.25) are equal to zero and the equations of motion

of a flexible body can be simplified to the same form as equations (5.7), (5.8) and (5.9) with simplified matrix $\{\bar{D}\}$ in equations (5.8) and (5.9), which is

$$\begin{aligned} \{\bar{D}\}^T &= \int_V (\dot{\bar{q}} \times \{\bar{\Phi}\}^T) \rho dv \\ &= \int_V (\dot{r} \times \{\bar{\Phi}\}^T) \rho dv + \{\eta\}^T \int_V \{\bar{\Phi}\} \times \{\bar{\Phi}\}^T \rho dv \\ &= \{0\} + \{\eta\}^T [\bar{G}] \end{aligned} \quad (5.26)$$

5.2.4 The Tisserand Frame

The Tisserand frame, also known as mean axes frame [Ashley 1967, Likins 1967], is defined such that the linear and angular momentum of the flexible body, due to the vibrational deformation relative to the body reference frame, are equal to zero. These conditions are derived from minimizing the component of kinetic energy caused by the vibrations through adjusting the location and orientation of the body reference frame.

To minimize the kinetic energy caused by the vibrations of the flexible body through adjusting the location and orientation of the body reference frame, the body reference frame is perturbed and the following will hold

$$\delta \left(\frac{1}{2} \int_V (\dot{\bar{q}} \cdot \dot{\bar{q}}) \rho dv \right) = \int_V (\dot{\bar{q}} \cdot \delta \dot{\bar{q}}) \rho dv = 0 \quad (5.27)$$

The absolute velocity of any point in the flexible body is given by equation (4.8). Since the perturbations of the position and the orientation of the body reference frame does not affect the absolute velocity, there is

$$\delta \dot{\bar{P}} = \delta \dot{\bar{R}} + \delta \vec{\Omega} \times \dot{\bar{q}} + \delta \dot{\bar{q}} = 0 \quad (5.28)$$

Solving this equation for $\delta \dot{\bar{q}}$, equation (5.27) becomes

$$\int_V \dot{\mathbf{q}} \rho dv \cdot \delta \dot{\mathbf{R}} + \int_V (\dot{\mathbf{q}} \times \dot{\mathbf{q}}) \rho dv \cdot \delta \dot{\boldsymbol{\Omega}} = 0 \quad (5.29)$$

Since $\delta \dot{\boldsymbol{\Omega}}$ and $\delta \dot{\mathbf{R}}$ are arbitrary and independent, equation (5.29) leads to the constraint conditions for the Tisserand frame

$$\int_V \dot{\mathbf{q}} \rho dv = 0 \quad (5.30)$$

$$\int_V \dot{\mathbf{q}} \times \dot{\mathbf{q}} \rho dv = \int_V \dot{\mathbf{q}} \times \dot{\mathbf{u}} \rho dv = \int_V (\dot{\mathbf{r}} \times \dot{\mathbf{u}} + \dot{\mathbf{u}} \times \dot{\mathbf{u}}) \rho dv = 0 \quad (5.31)$$

Note that the left side of the first constraint condition is the linear momentum of the flexible body due to the vibrational motion relative to the body reference frame. It can be further integrated against time to

$$\int_V \dot{\mathbf{q}} \rho dv = 0 \quad (5.32)$$

This means that the origin of the body reference frame is located at the center of the mass of the body. Once the body reference frame is located at the center of mass, this constraint is always satisfied.

The left side of the second constraint condition is the angular momentum of the flexible body due to the vibrational motion relative to the origin of the body reference frame. It can be further expressed in terms of the generalized coordinates for the vibrational deformation. Using the assumed modes, equation (5.31) can be written as

$$\int_V (\dot{\mathbf{r}} \times \dot{\mathbf{u}} + \dot{\mathbf{u}} \times \dot{\mathbf{u}}) \rho dv = \left(\int_V (\dot{\mathbf{r}} \times \{\bar{\Phi}\} + \{\eta\}' \{\bar{\Phi}\} \times \{\bar{\Phi}\}) \rho dv \right) \{\dot{\eta}\} = 0 \quad (5.33)$$

If the assumed modes satisfy the condition (5.12), i.e. free-free elastic modes, the first part of the integral equals to zero and the integral becomes

$$\int_V \dot{\mathbf{q}} \rho dv \cdot \delta \dot{\mathbf{R}} + \int_V (\dot{\mathbf{q}} \times \dot{\mathbf{q}}) \rho dv \cdot \delta \dot{\boldsymbol{\Omega}} = 0 \quad (5.29)$$

Since $\delta \dot{\boldsymbol{\Omega}}$ and $\delta \dot{\mathbf{R}}$ are arbitrary and independent, equation (5.29) leads to the constraint conditions for the Tisserand frame

$$\int_V \dot{\mathbf{q}} \rho dv = 0 \quad (5.30)$$

$$\int_V \dot{\mathbf{q}} \times \dot{\mathbf{q}} \rho dv = \int_V \dot{\mathbf{q}} \times \dot{\mathbf{u}} \rho dv = \int_V (\dot{\mathbf{r}} \times \dot{\mathbf{u}} + \dot{\mathbf{u}} \times \dot{\mathbf{u}}) \rho dv = 0 \quad (5.31)$$

Note that the left side of the first constraint condition is the linear momentum of the flexible body due to the vibrational motion relative to the body reference frame. It can be further integrated against time to

$$\int_V \dot{\mathbf{q}} \rho dv = 0 \quad (5.32)$$

This means that the origin of the body reference frame is located at the center of the mass of the body. Once the body reference frame is located at the center of mass, this constraint is always satisfied.

The left side of the second constraint condition is the angular momentum of the flexible body due to the vibrational motion relative to the origin of the body reference frame. It can be further expressed in terms of the generalized coordinates for the vibrational deformation. Using the assumed modes, equation (5.31) can be written as

$$\int_V (\dot{\mathbf{r}} \times \dot{\mathbf{u}} + \dot{\mathbf{u}} \times \dot{\mathbf{u}}) \rho dv = \left(\int_V (\dot{\mathbf{r}} \times \{\Phi\} + \{\eta\}^T \{\Phi\} \times \{\Phi\}) \rho dv \right) \{\dot{\eta}\} = 0 \quad (5.33)$$

If the assumed modes satisfy the condition (5.12), i.e. free-free elastic modes, the first part of the integral equals to zero and the integral becomes

$$\int_V (\dot{\vec{r}} \times \dot{\vec{u}} + \dot{\vec{u}} \times \dot{\vec{u}}) \rho dv = (\{\eta\}^T \int_V (\{\vec{\Phi}\} \times \{\vec{\Phi}\}) \rho dv) \{\dot{\eta}\}$$

$$= \{\eta\}^T [G] \{\dot{\eta}\} = 0 \quad (5.34)$$

This constraint equation about the generalized coordinates does not have an integrated form and is therefore a nonholonomic constraint condition.

With the Tisserand frame and free-free elastic modes, the equations of motion of a flexible body can be further simplified as the following differential equations and the algebraic equation (5.34)

$$m\ddot{\vec{R}} = \vec{F}_o + m\vec{g} \quad (5.35)$$

$$\dot{\vec{J}} \cdot \dot{\vec{\Omega}} - \vec{H} \times \dot{\vec{\Omega}} + \dot{\vec{J}}^* \cdot \dot{\vec{\Omega}} = \vec{T}_o \quad (5.36)$$

$$[M] \{\ddot{\eta}\} + [G] \{\dot{\eta}\} + [K_{eq}] \{\eta\} = \{Q\} \quad (5.37)$$

In some cases the integral $\int_V (\{\vec{\Phi}\} \times \{\vec{\Phi}\}) dv$ will be zero due to the nature of the flexible body, for example, the planar transverse vibration of beams and plates, but it is not generally true. If it is true, the constraint equation (5.34) is met always and the equations of motion with Tisserand frame can be further simplified as equations (5.7), (5.8) and

$$[M] \{\ddot{\eta}\} + ([K] + [K_g] + [K_n]) \{\eta\} = \{Q\} \quad (5.38)$$

This is the simplest form of the equations of motion of a free-moving flexible body.

- Chapter 6 -

Multibond Graphs of a Flexible Body

6.1 Introduction

The bond graph is a modelling technique used to represent physical systems graphically. It has the added advantage of using a unified approach and a systematic procedure which are very suitable for computer implementation. Multibond graphs were introduced as a shorthand notation for systems which can be represented by regular, repetitive single bond structures of which multibody system dynamics is a case [Breedveld 1982, 1984; Tierneho and Bos 1985]. There are significant advantages in representation of multibody systems using multibond graphs over using single bond graphs [Tierneho and Bos 1985; Bos 1986]. In this thesis, multibond graphs are employed to represent the 3-D motion of flexible multibody systems.

6.2 Multibond Graph Representation of a Flexible Body

It has been pointed out that the kinematic and dynamic equations of a flexible body are all nonlinear equations. The bond graph was initially developed to represent linear systems. Only when modulated multiport elements [Rosenberg and Karnopp, 1975] and block bond graph [Thoma, 1985] were introduced into bond graphs, did the bond graph method become used to represent nonlinear systems. Therefore, the multibond graphs for modelling dynamics of an arbitrary flexible body developed in this thesis adopt modulated multiport elements.

In terms of equations (4.67), (4.68) and (4.80) in Chapter 4, the kinematics of a

flexible body with one joint can be represented by the multibond graph in Figure 6-1, assuming that the origin of the body reference frame is not located at the joint. In the figure, three "1" junctions represent translation and rotation velocities of the body reference frame and the velocities of generalized coordinates for vibrational deformation. The upper "0" junction gives the linear velocity of the mass center of the body in the body reference frame. Passing over a transform element of coordinate transformation, it becomes the absolute linear velocity of the mass center of the body measured in the inertial frame. The lower two "0" junctions give the linear and angular velocities of the joint of the body measured in the body reference frame. If the origin of the body reference frame is fixed at the joint, then the lower two "0" junctions will merge in "1" junctions of $\{\dot{R}\}$ and $\{\dot{\Omega}\}$. The subscript d in the figure refers to the joint.

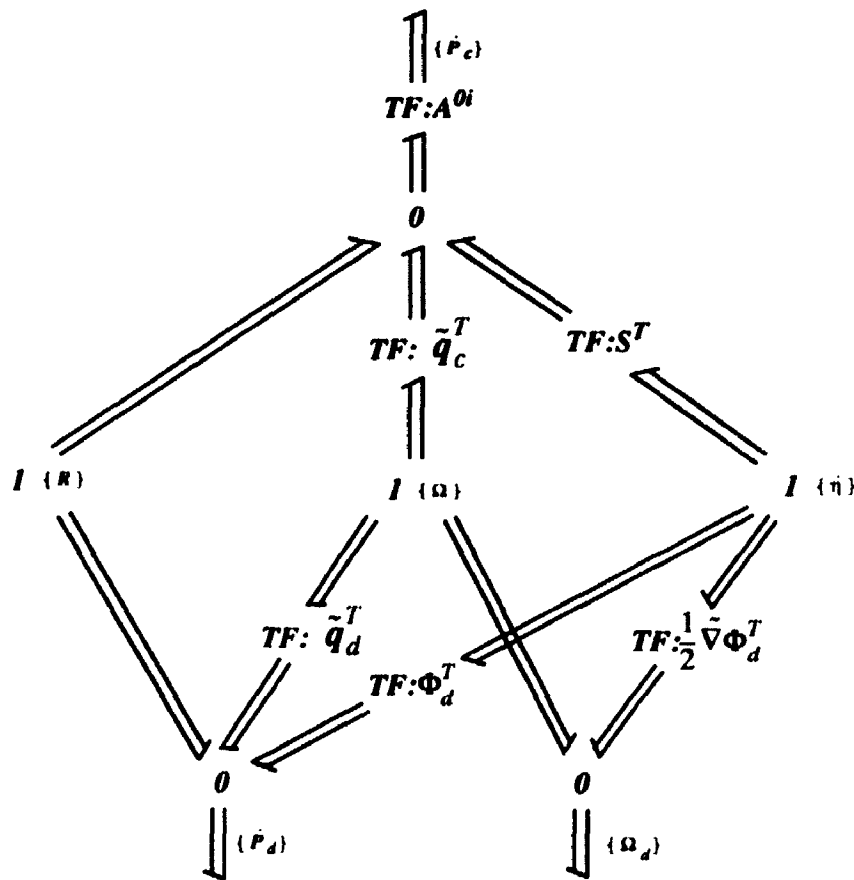


Figure 6-1 Multibond graph of kinematics of a flexible body with one joint

To confirm that this multibond graph actually represents the kinematics of a flexible body, the velocity outputs of this bond graph structure were written in terms of the constitutive laws of multibond graphs. At the upper side, the velocity output $\{\dot{P}_c\}$ is the sum of three velocities

$$\{\dot{P}_c\} = [A^{0i}] (\{\dot{R}\} + [S]^T \{\dot{\eta}\} - [\tilde{q}_c] \{\Omega\}) \quad (6.1)$$

which is exactly the same as equation (4.80). At the lower side, velocity outputs are

$$\{\dot{P}_d\} = \{\dot{R}\} + [\Phi_d]^T \{\dot{\eta}\} - [\tilde{q}_d] \{\Omega\} \quad (6.2)$$

$$\{\Omega_d\} = \{\Omega\} + \frac{1}{2} [\tilde{V}] [\Phi_d]^T \{\dot{\eta}\} \quad (6.3)$$

These equations do give the same results as equations (4.67) and (4.68).

Based on equations (4.98), (4.99) and (4.100) in Chapter 4, the dynamics of a flexible body with a joint can be represented by the multibond graph in Figure 6-2.

Note that since the equations (4.99) and (4.100) are coupled in acceleration terms, a summation element of multibond graphs is employed to form a new velocity column matrix $\{\dot{\xi}\}$ which is defined as

$$\{\dot{\xi}\} = \begin{Bmatrix} \{\Omega\} \\ \{\dot{\eta}\} \end{Bmatrix} \quad (6.4)$$

And an inertia multiport element $[M_\xi]$ is formed as

$$[M_\xi] = \begin{bmatrix} [J_c] & [D_c]^T \\ [D_c] & [M_c] \end{bmatrix} \quad (6.5)$$

which is symmetric.

Also note that the multibond graph has concentrated the surface tractions at the joint into a resultant force F_d and a torque T_d . The relations between these resultant forces and the generalized forces are

$$\{F_0\} = \{F_d\} \quad (6.6)$$

$$\{T_0\} = \{T_d\} + [\tilde{q}_d] \{F_d\} \quad (6.7)$$

$$\{Q\} = [\Phi_d] \{F_d\} + \frac{1}{2} ([\tilde{V}] [\Phi_d]^T)^T \{T_d\} \quad (6.8)$$

It is easy to confirm that this bond graph actually represents the dynamics of a flexible body by summing up the efforts at all "1" junctions. For example, the effort sum at the upper "1" junction is

$$m \frac{d}{dt} \{\dot{P}_c\} = [A^{0i}] \{F_d\} + m \{g\} \quad (6.9)$$

The effort sums at two right middle "1" junctions (e.g. the velocities $\{\Omega\}$ and $\{\dot{\eta}\}$) are

$$[J_c] \{\dot{\Omega}\} + ([J^*]_c - [\tilde{H}_c]) \{\Omega\} + [D_c]^T \{\dot{\eta}\} - [\tilde{q}_c] \{F_d\} - \{T_o\} = \{0\} \quad (6.10)$$

$$[M_c] \{\dot{\eta}\} + [D_c] \{\dot{\Omega}\} + [G_c] \{\dot{\eta}\} + [K_{eq}] \{\eta\} - [S] \{F_d\} - \{Q\} = \{0\} \quad (6.11)$$

These two equations are exactly same as equations (4.99) and (4.100).

The multibond graph in Figure 6-2 is the multibond graph of a free moving flexible body in the general case. The procedure to set up the multibond graph can be summed as following:

Step 1: set up three "1" multiport junctions for velocities variables $\{\dot{R}\}$, $\{\Omega\}$, $\{\dot{\eta}\}$ and a "1" junction for the velocity of the center of mass $\{\dot{P}_c\}$, as well as corresponding "0" junctions for the velocities of the joints of the body which

will cause energy exchange with the environment.

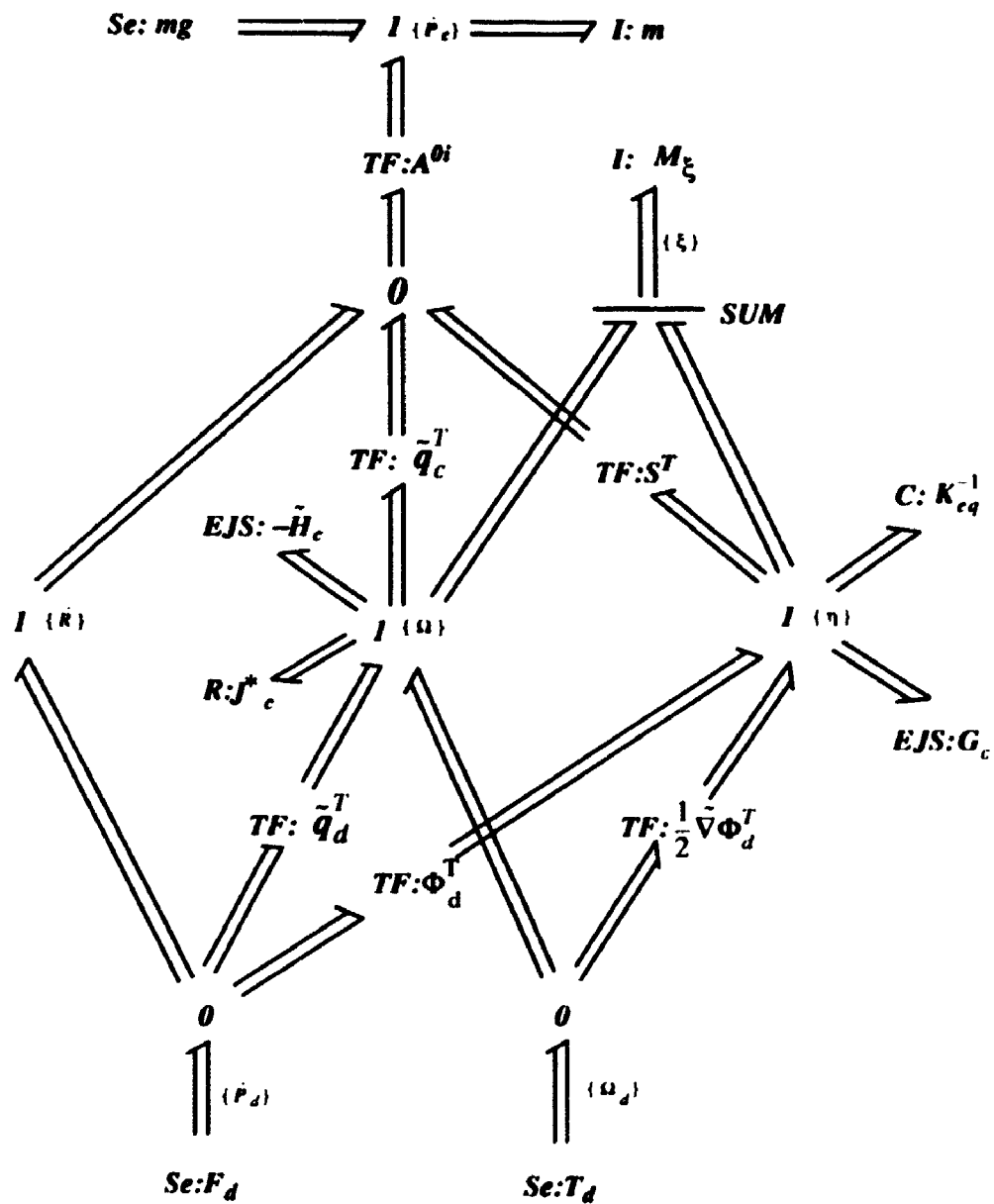


Figure 6-2 Multibond graph for the dynamics of a flexible body with one joint

Step 2: Connect these junctions through multibond and multiport transform elements based on the kinematic relationship of equations (4.67), (4.68) and (4.80). Note the directions of each multibond which point away from these three "1"

velocity variables.

Step 3: Add a summation element and a “1” junction to form a new velocity variable $\{\dot{\xi}\}$ from $\{\Omega\}$, $\{\dot{\eta}\}$ and attach dynamic terms to the relative “1” junctions following Figure 6-2.

The multibond graph in Figure 6-2 is for the general case. Once a floating frame is applied as the body reference frame, the multibond graphs will change. The following sections discuss these kinds of multibond graphs.

6.3 Multibond Graphs of a Flexible Body under Floating Frames

In Chapter 5, the equations of motion of a flexible body have been simplified through the introduction of the floating frames. The multibond graphs corresponding to these simplified equations can also be obtained.

6.3.1 The Mass Center Located Body Fixed Frame

It has been discussed in Chapter 5 that if the body fixed frame is not located at the center of mass of the flexible body, the frame does not simplify the equations. Therefore only “the mass center located body fixed frame” is discussed in this section.

In Chapter 5, equation (5.5) indicates that, with the mass center located body reference frame, the velocity of the mass center of the flexible body is the velocity of the body reference frame itself. Once the free-free normal modes of the flexible body are adopted, the translation of the flexible body is decoupled from rotation and vibrations. In this case, the equations of motion in vectorial form are equations (5.7), (5.8) and (5.9). The multibond graph of a flexible body under this kind of body reference frame can be obtained by modifying the multibond graph in Figure 6-2. Since the velocity of the body reference frame is the only contribution to the velocity of the mass center of the flexible body, two transform elements of \tilde{q}_c^T and S^T can be

eliminated. The mass center body fixed frame does not decouple the coupling between rotation and vibrations, so the multibond graph about rotation and vibrations in Figure 6-2 is unchanged. Carrying out these changes in Figure 6-2, the multibond graph of a flexible body under mass center located body fixed frame with free-free normal modes can be illustrated as in Figure 6-3. In this multibond graph, the translation of the flexible body is separated from rotation and vibrations, and is driven by the constraint force at the joint.

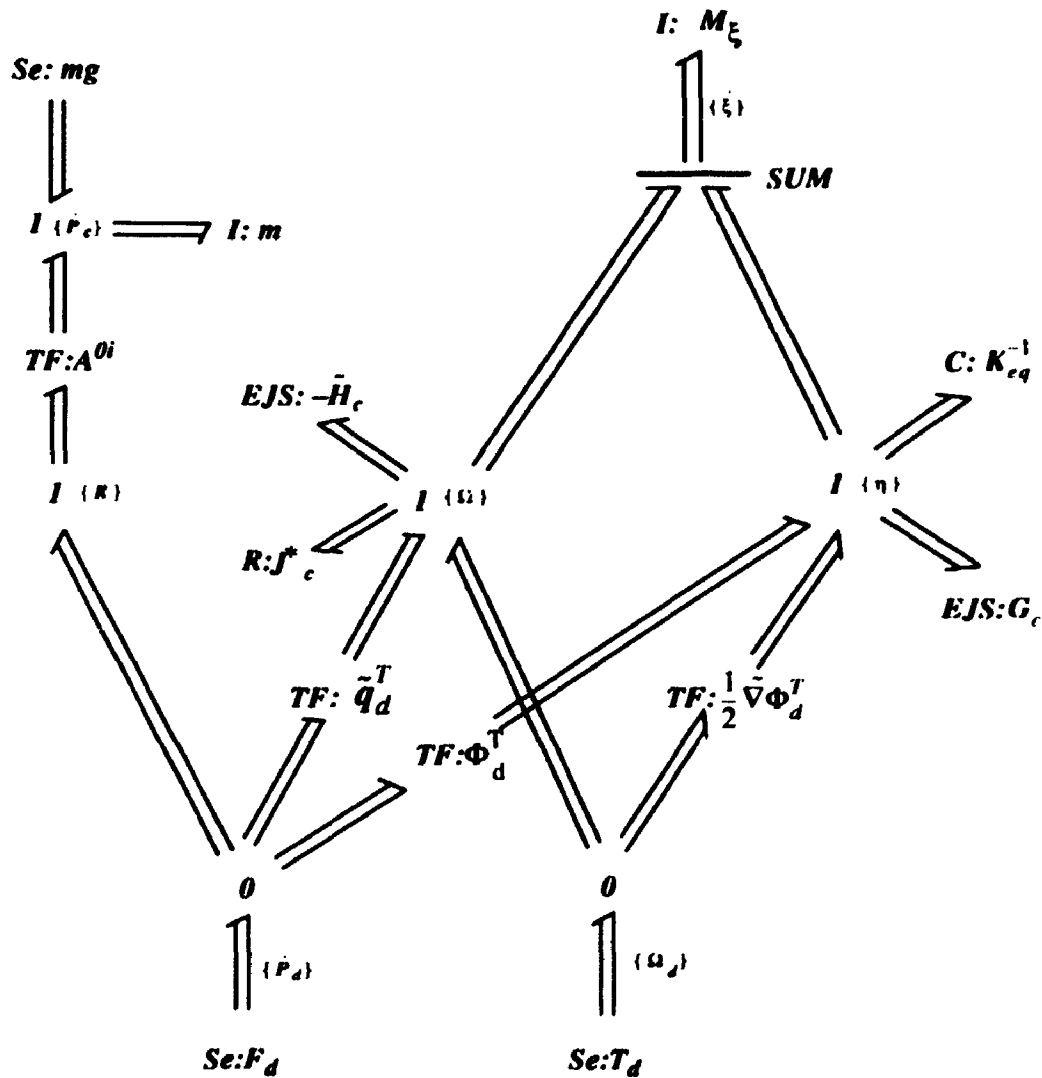


Figure 6-3 Multibond graph of dynamics of a flexible body with one joint under mass center located body fixed reference frame and free-free modes

6.3.2 The Buckens Frame

In section 5.2.3, it has been shown that the Buckens frame with free-free modes not only keeps all simplification of equations of motion of a flexible body in the mass center located body fixed frame, but also weakens the acceleration coupling between the rotation and vibrations. The weakened coupling between rotation and vibrations is indicated by the simplified matrix $\{\tilde{D}\}$ in equation (5.26). As the matrix $\{\tilde{D}\}$ is combined into matrix $[M_{\xi}]$ which is represented by a multiport inertia element in Figure 6-2, the multibond graph of a flexible body under the Buckens frame with free-free modes remains in the same form as in Figure 6-3 except the simplified inertia element $[M_{\xi}]$.

6.3.3 The Tisserand Frame

In section 5.2.4, it has been shown that with the free-free modes of the flexible body, the Tisserand frame decouples the rotations and vibration accelerations and hence leads to the simplest form of differential equations of motion of a flexible body. Therefore, the combined velocity $\{\dot{\xi}\}$ and the inertia element $[M_{\xi}]$ in the multibond graph of a flexible body are not needed. However, the added cost of simplification is the adding of a nonholonomic constraint condition, equation (5.34), in generalized coordinates for vibrational deformation. Although not generally true, in some cases the matrix $[G]$ will be zero due to the nature of the flexible body, for example, for planar transverse vibrations of beams and plates. This constraint condition about the generalized coordinates can be represented by a zero multiple flow source acting on the "1" junction of the velocities of the generalized coordinates through a multiport transform element modulated by the generalized coordinates. This is shown in Figure 6-4. With this multibond graph expression, the multibond graph of a flexible body in the Tisserand frame with free-free modes can be drawn as in the Figure 6-5, in which

the acceleration coupling between translation, rotation and vibrations has been decoupled.

$$\begin{array}{c}
 I(\ddot{\eta}) \\
 \Downarrow \\
 TF: \eta^T G \\
 \Downarrow \\
 0 \\
 \Uparrow \\
 S_f: 0
 \end{array}$$

Figure 6-4 Multibond graph of constraint condition on generalized coordinates

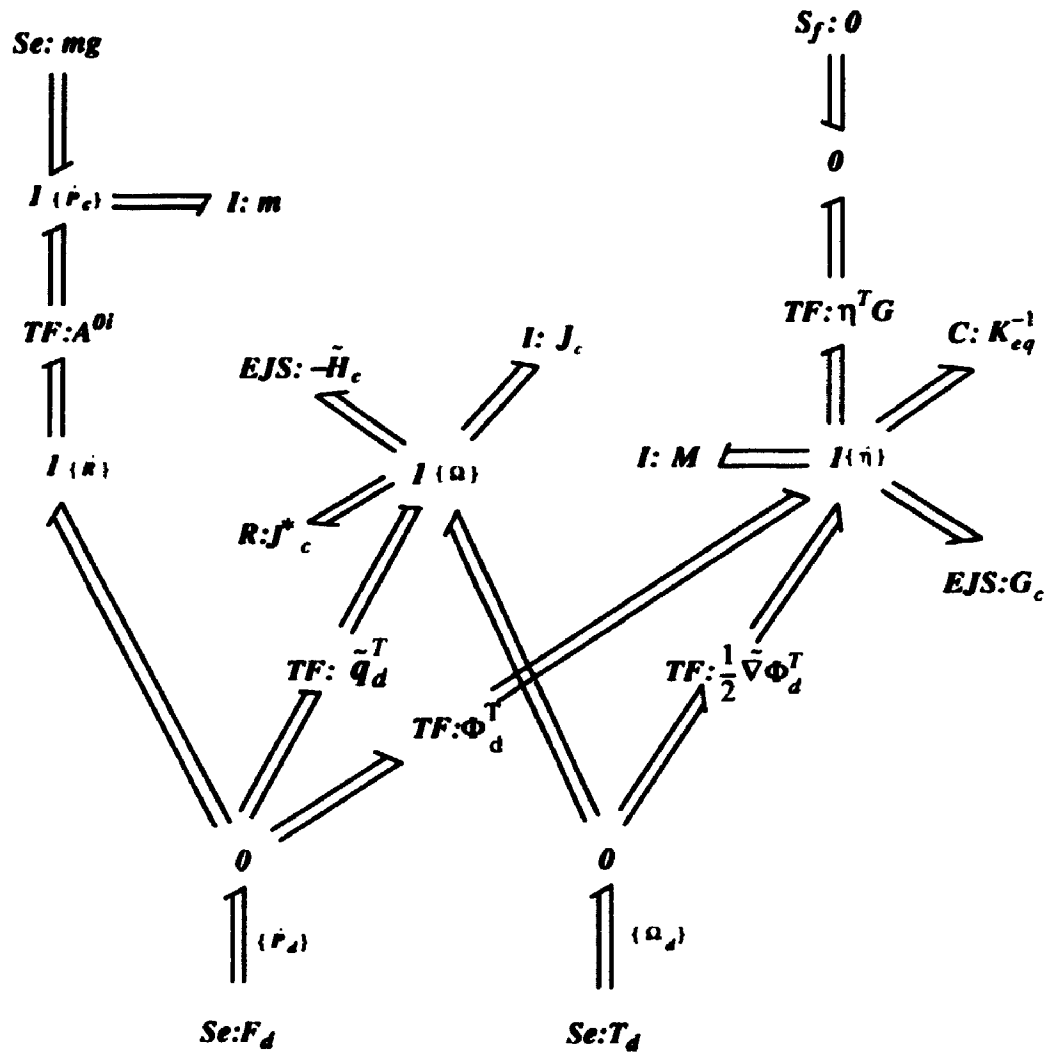


Figure 6-5 Multibond graph of dynamics of a flexible body with one joint under the Tisserand reference frame and free-free modes

- Chapter 7 -

Multibond Graphs of Mechanical Constraints and Whole Flexible Multibody Systems

7.1 Introduction

The equations of motion and the multibond graph of a free moving flexible body have been developed above. This multibond graph is also valid for a single body in a multibody system if the external resultant force and torque include constraint forces and torques at the joints. The multibond graph of the whole flexible multibody system can be obtained by connecting these multibond graphs of single flexible bodies together through multibond graphs of constraints between these bodies. Constraints on a body in a multibody system result either from direct physical contact of the body and other bodies or ground, or from an interconnection of the body with other bodies or ground by means of a kinematic constraint mechanism. Constraints restrict the translation and rotation motion of the body, thus reducing the degrees of freedom of the body. They also influence the vibrations of a flexible body. For bond graph modeling of multibody system dynamics, these constraints can be modelled by restrictions on the relative velocities between connected bodies at the joints. This chapter discusses the multibond graphs of mechanical constraints and the procedure of setting up the multibond graphs for whole flexible multibody systems.

7.2 The Multibond Graph Structure of Mechanical Constraints

Mechanical constraints result from direct physical contact between connected

bodies. Different configurations of the contact lead to different types of joints and different constraints. This section discusses some commonly used joints in mechanical systems and their multibond graph representations.

7.2.1 Spherical Joints

The general idea in modelling mechanical constraints by bond graph is the relative velocity restriction. To describe this idea, consider a spherical joint, described by D , between two flexible bodies as shown in Figure 7-1.

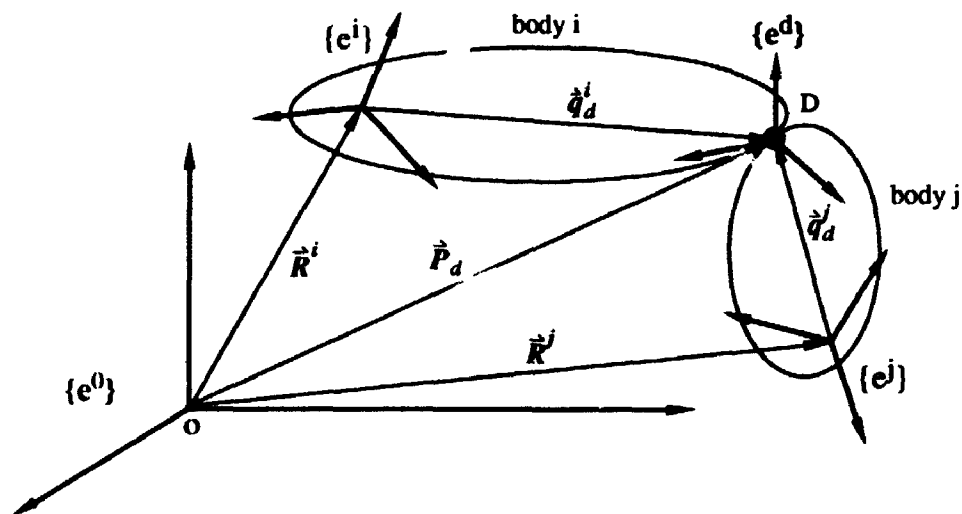


Figure 7-1 Sketch of a spherical joint between two bodies

The position vector of the spherical joint D represented in two different body reference frames attached at the connected bodies are, respectively

$$\vec{P}_d^i = \vec{R}^i + \vec{q}_d^i \quad \vec{P}_d^j = \vec{R}^j + \vec{q}_d^j \quad (7.1)$$

The absolute velocity of the joint D represented in two body reference frames is:

$$\dot{\vec{P}}_d^i = \dot{\vec{R}}^i + \dot{\vec{q}}_d^i + \vec{\Omega}^i \times \vec{q}_d^i \quad (7.2)$$

$$\dot{\vec{P}}_d^j = \dot{\vec{R}}^j + \dot{\vec{q}}_d^j + \vec{\Omega}^j \times \vec{q}_d^j \quad (7.3)$$

The constraint condition due to the joint is that the points of the two bodies at the joint always coincide with each other, or the relative linear velocity between the two bodies at the point of the joint is always zero. This gives

$$\dot{\vec{P}}_d^i - \dot{\vec{P}}_d^j = 0 \quad (7.4)$$

Since vectors $\dot{\vec{R}}^i$, $\dot{\vec{q}}_d^i$ and $\vec{\Omega}^i$ are measured in their own local reference frames indicated by their superscripts, the matrix form of this equation should be

$$(\{\dot{R}^i\} + \{\dot{q}_d^i\} - [\tilde{q}_d^i] \{\Omega^i\}) - [A^{ij}] (\{\dot{R}^j\} + \{\dot{q}_d^j\} - [\tilde{q}_d^j] \{\Omega^j\}) = \{0\} \quad (7.5)$$

or simply

$$\{\dot{P}_d^i\} - [A^{ij}] \{\dot{P}_d^j\} = \{0\} \quad (7.6)$$

where $[A^{ij}]$ is the rotation transformation between the two body reference frames, which is

$$[A^{ij}] = [A^{i0}] [A^{0j}] \quad (7.7)$$

This velocity restriction can be represented by a '0' junction in multibond graphs. Using two blocks to represent the connected bodies, the multibond graph for the spherical joint can be represented in Figure 7-2. In the figure, \dot{P}_d^i and \dot{P}_d^j are the linear velocities of the points of the connected bodies at the joint and the transformer A^{ij}

indicates the rotation transformation between the two body reference frames.

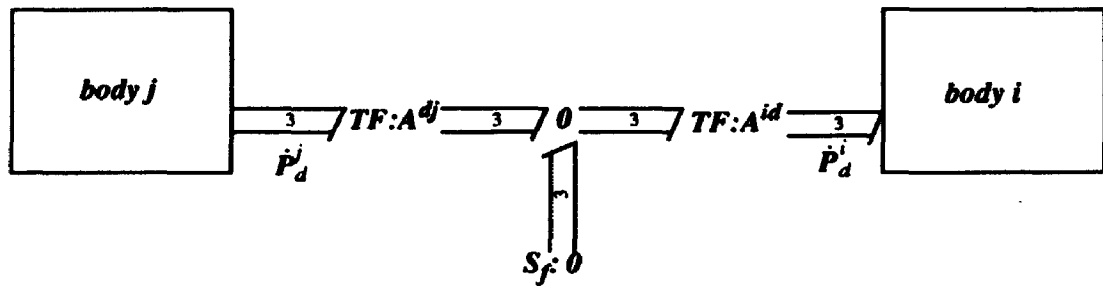


Figure 7-2 Multibond graph of a spherical joint

7.2.2 Pin Joints

Pin joints are widely used in mechanical systems. Figure 7-3 shows a sketch of a pin joint. A frame $\{e^d\}$ is attached on the pin with one base axis along the longitudinal axis of the pin and the other two base axes perpendicular to the longitudinal axis. The relative velocities of the two bodies at the joint are measured in this pin attached frame. It can be seen that a pin joint restricts the translational relative velocities in three directions and the rotational relative velocities in two directions between the connected bodies. It only allows relative rotation of the connected bodies along the longitudinal axis of the pin. Based on the analysis in the last section, the multibond graph for a pin joint can be set as in Figure 7-4. In the figure, \dot{P}_d^j , Ω_d^j and \dot{P}_d^i , Ω_d^i are the linear and angular velocities of the points of the connected bodies at the joint and the transformers A^{dj} and A^{id} indicate the rotation transformation between the two body reference frames and the pin attached frame, which include the rotation caused by the deformation of the flexible bodies. Note that the multibonds to the "0" junction of relative angular velocities consists of only two single bonds.

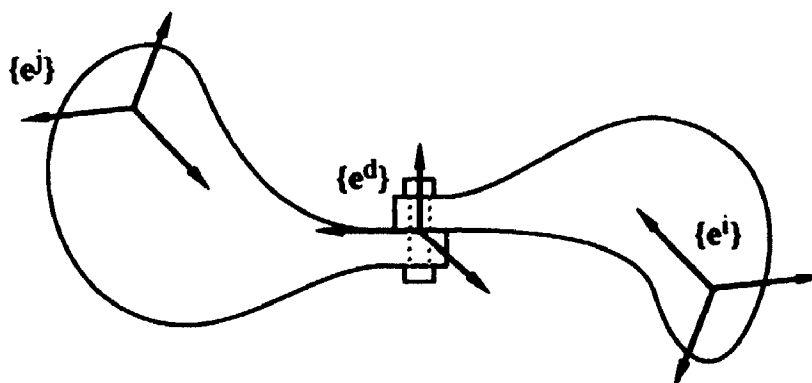


Figure 7-3 Sketch of a pin joint

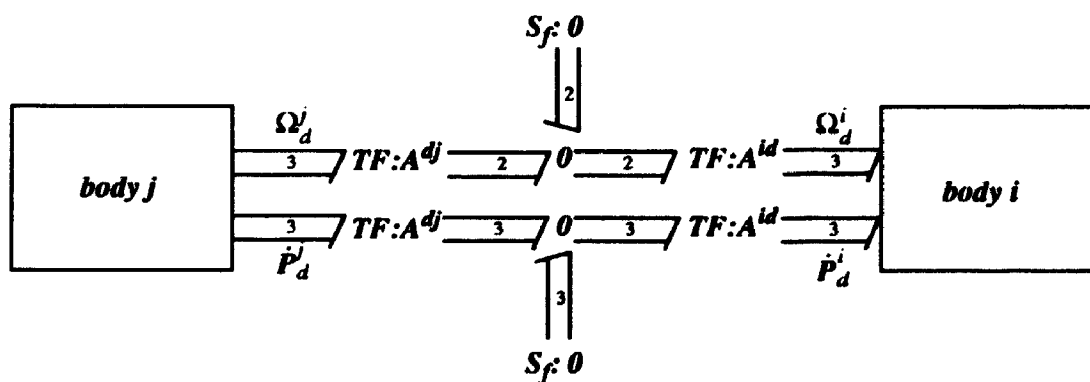


Figure 7-4 Multibond graph of a pin joint

7.2.3 Cylindrical Joints

A cylindrical joint is similar to a pin joint, in that it allows relative rotation about the longitudinal axis of the cylinder. However, it does not restrict all relative translations between the two connected bodies. The connected bodies can move relatively along the longitudinal axis of the cylinder, as shown in Figure 7-5.

Therefore, the constraint conditions of this kind of joint to the relative motion of the connected bodies are zero relative linear and angular velocities along the two base axes of the joint frame $\{e^d\}$ perpendicular to the longitudinal axis of the cylinder. These conditions can be represented by the multibond graph in Figure 7-6. In the figure, all flows have the same meaning as in Figure 7-4, except that the multibonds to the "0" junction, of relative linear velocities, decrease to two single bonds.

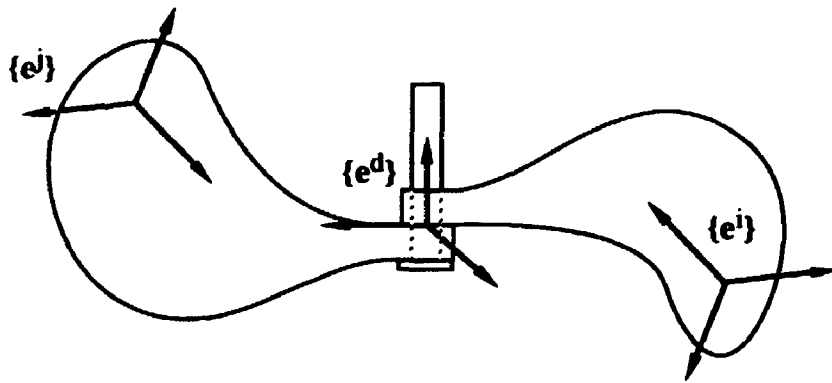


Figure 7-5 Sketch of a cylindrical joint

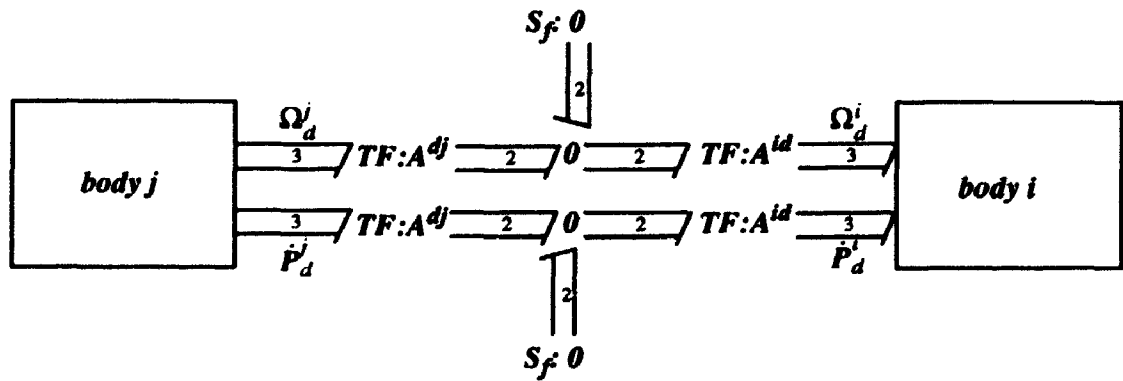


Figure 7-6 Multibond graph of a cylindrical joint

7.2.4 Translational Joints

Translational joints are the kinds of connections that only allow the relative translation of the connected bodies along one direction. This kind of joint can have a variety of forms, but it can be represented as in Figure 7-7. The joint attached frame is defined such that one base axis of it is aligned with the direction of allowed relative translation of the connected bodies and two others are in arbitrary directions. The constraint conditions of this kind of joint can be expressed as zero relative angular velocities along all base axes and zero relative linear velocities along the two base axes perpendicular to the direction of allowed relative translation. The multibond graph of this kind of joint is plotted in Figure 7-8. The meaning of all symbols is the same as in Figure 7-5, except that the multibonds to the "0" junction of relative angular velocities increase to three single bonds.

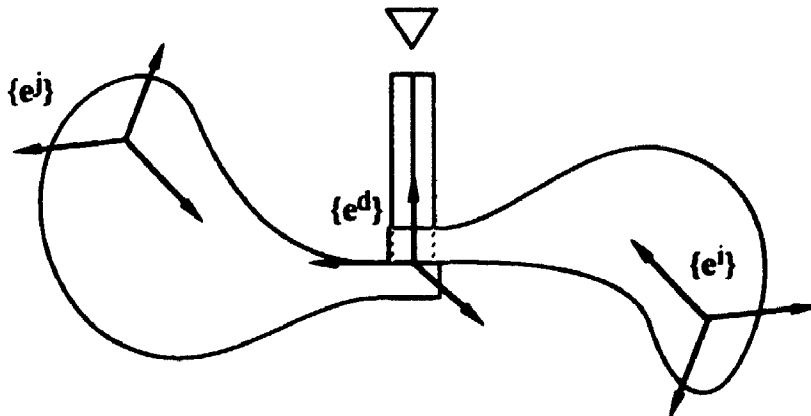


Figure 7-7 Sketch of a translational joint

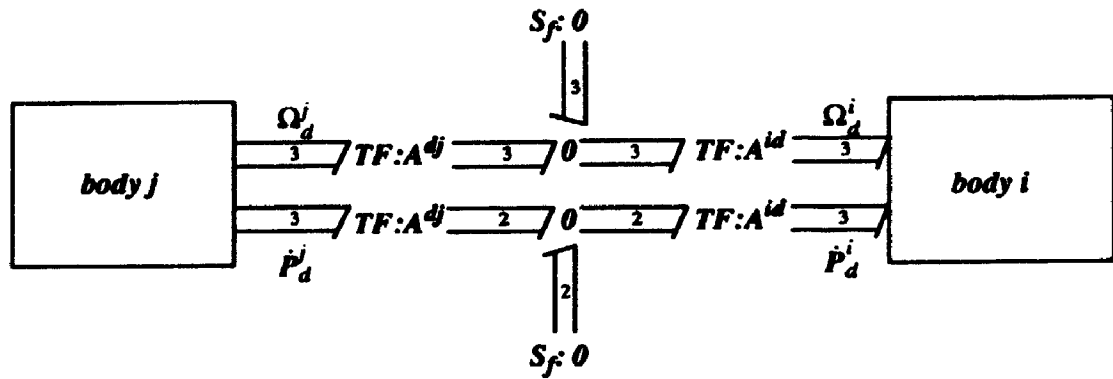


Figure 7-8 Multibond graph of a translational joint

7.2.5 Screw Joint

Screw joints are a type of joint in which the translational constraints are coupled with rotational constraints. The sketch of a screw joint is shown in Figure 7-9. A joint attached frame is so defined such that one base axis is along the longitudinal axis of the screw. Let the relative translation be s , relative rotation be θ , the slope of the screw be angle α , and the radius of the screw be ρ , the coupled condition between relative rotation and translation can be written as

$$\dot{s} = (\rho \tan \alpha) \dot{\theta} \quad (7.8)$$

Because the two relative velocities represented by the \dot{s} and $\dot{\theta}$ are coupled by the relation (7.8), there is only one degree of freedom of relative motion in the joint. Either of the two motions can be selected as the active motion and the other the passive one. Except for these two relative motions, there are no other relative motions allowed by the screw joint. Therefore, the constraint conditions for a screw joint can be described as two zero relative linear velocities and two zero relative angular velocities, along the two base axes of the joint attached frame which are not along the longitudinal axis of

the frame, and a coupled relation between the relative linear velocity and angular velocity along the third base axis along the longitudinal axis of the screw. These conditions can be represented by the multibond graph in Figure 7-10, in which the coupled relation between the relative rotation and translation is represented by a transform element.

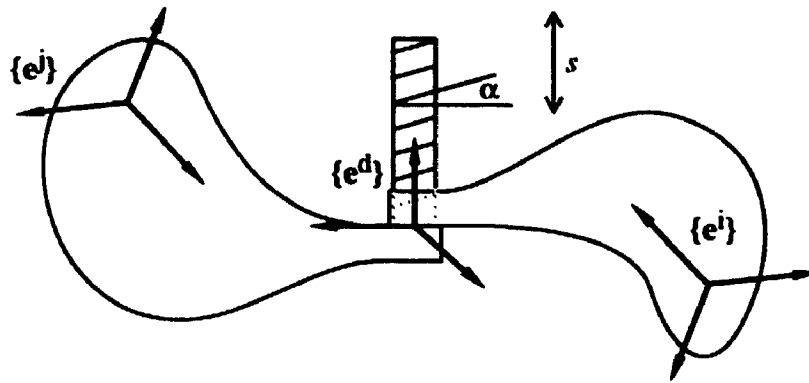


Figure 7-9 Sketch of a screw joint

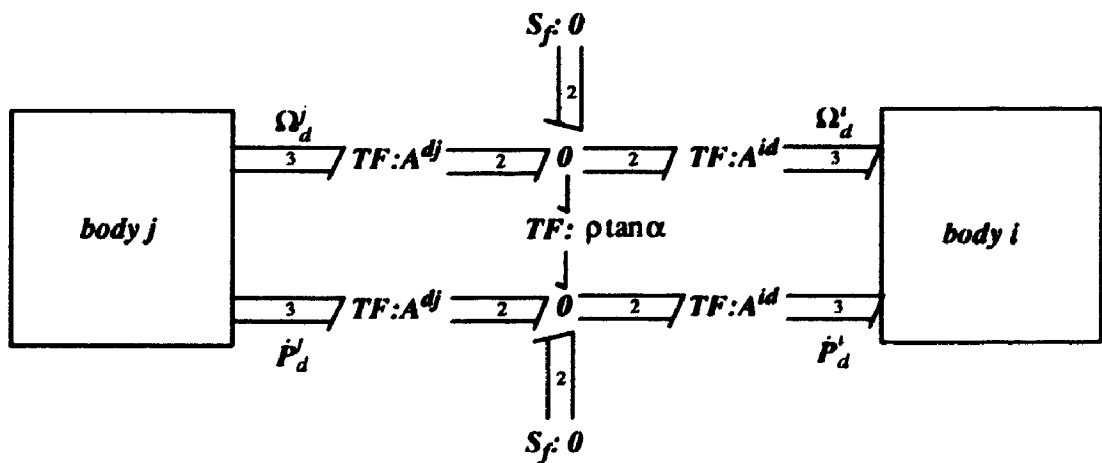


Figure 7-10 Multibond graph of a screw joint

7.2.6 Planar Joint

A sketch of a planar joint is shown in Figure 7-11. The joint attached frame is defined on the contact plane in a way that one of its three base axes is normal to the plane and the other two are in the plane. So the constraint conditions provided by this kind of joint are zero relative linear velocity along the normal base axis and zero relative angular velocities along the other two in-plane base axes. These constraint conditions can be represented by the multibond graph in Figure 7-12, where all letters have the same meaning as those in previous figures.

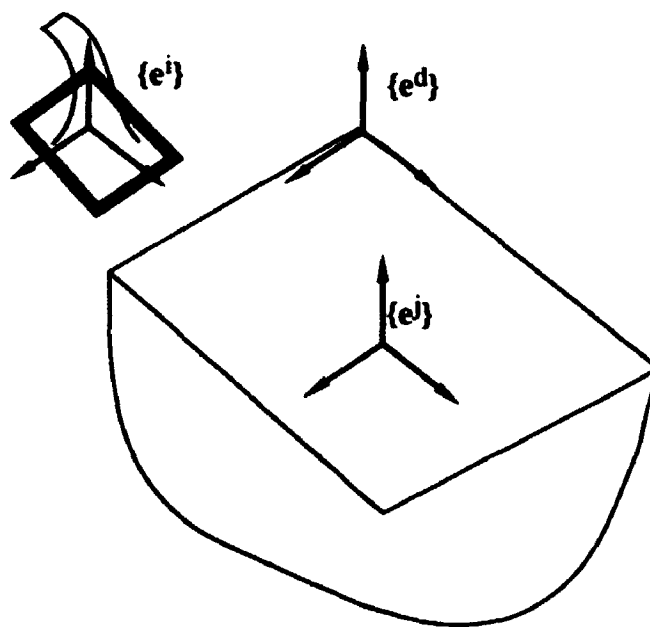


Figure 7-11 Sketch of a planar joint

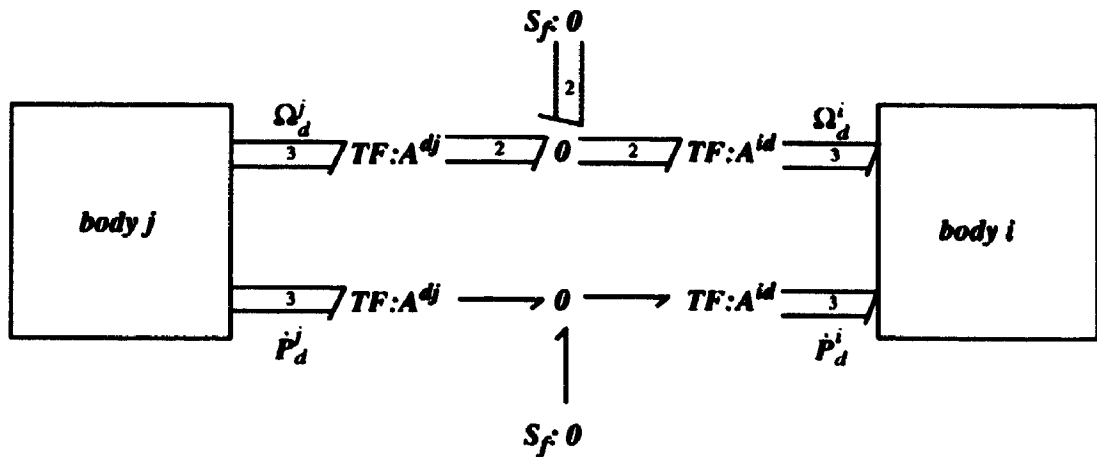


Figure 7-12 Multibond graph of a planar joint

7.2.7 Universal Joint

Figure 7-13 is a schematic representation of a universal joint. Two bodies i and j are connected through an intermediate body d known as the "spider". The joint attached frame is located on the intermediate body in the way shown in the figure, two base axes being along the cross and the third being normal to the plane of the cross. Each body has only one rotation degree of freedom, about different base axis of the intermediate body, and so the relative motions between these two connected bodies are the rotations along the two base axes on the cross. Therefore, the universal joint restricts all relative translations along three base axes of the joint frame and one relative rotation along the base axis normal to the cross of the intermediate body between the connected bodies. These constraint conditions can be represented in a multibond graph as shown in Figure 7-14.

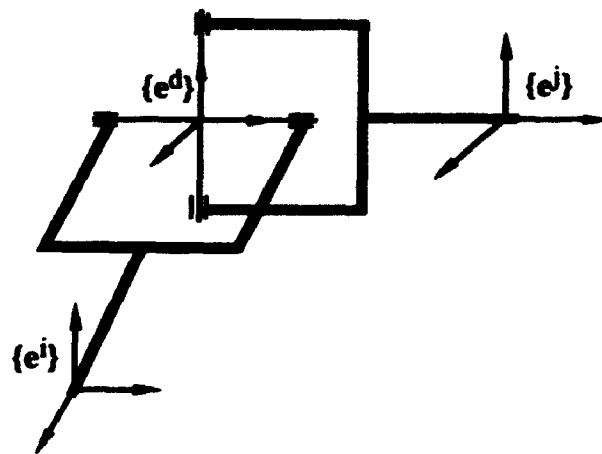


Figure 7-13 Sketch of a universal joint

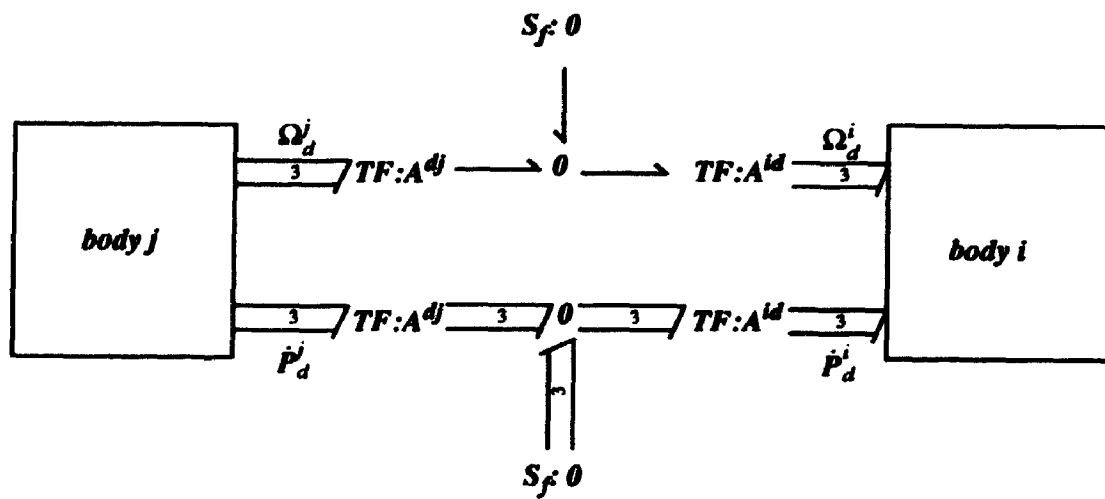


Figure 7-14 Multibond graph of a universal joint

7.3 Lagrange Multipliers and Artificial Constraint Element

From the discussion of section 7.2, it is clear that all constraint conditions represented by multibond graphs can be expressed in the form

$$[H_{ij}] \{h_{ij}\} = [H_i \ H_j] \begin{Bmatrix} h_i \\ h_j \end{Bmatrix} = \{0\} \quad (7.9)$$

where

$$\{h_i\} = \begin{Bmatrix} \{\dot{R}\} \\ \{\Omega\} \\ \{\dot{\eta}\} \end{Bmatrix}_i \quad (7.10)$$

$[H_{ij}]$ is a matrix consisting of position, orientation and vibrational displacement of the connected flexible bodies. This matrix is the well known Jacobian matrix for constraint conditions.

By Farkas Lemna [Haug 1989], for constraint equation (7.9), there exist unknown Lagrange multiplier vectors $\{\lambda_i\}$ and $\{\lambda_j\}$ such that the constraint forces acting on the connected bodies can be expressed as

$$\{F_{ic}\} = [H_i]^T \{\lambda_i\} \quad (7.11)$$

$$\{F_{jc}\} = [H_j]^T \{\lambda_j\} \quad (7.12)$$

Noting that matrices $[H_i]$ and $[H_j]$ are simply the transformation between velocities at the joint and the body reference frames, equations (7.11) and (7.12) mean that the constraint forces are the transformation of unknown forces $\{\lambda_i\}$ and $\{\lambda_j\}$ acting at the joint. Therefore, these Lagrange multipliers can be treated as effort inputs at the "0" junctions of the joint in all multibond graphs in section 7.2. Samanta [1990] used this idea in his work. The advantage of this concept is that all derivative causalities caused by the velocity constraint mentioned in the previous sections will be

eliminated. This will be discussed in Chapter 8.

Combined with the velocity conditions provided by the joints discussed in section 7.2, the bond graph of a joint using this idea can be represented by an element of zero compliance C_0 or infinite resistor R_∞ with causal stroke away from the elements, as shown in Figure 7-15.

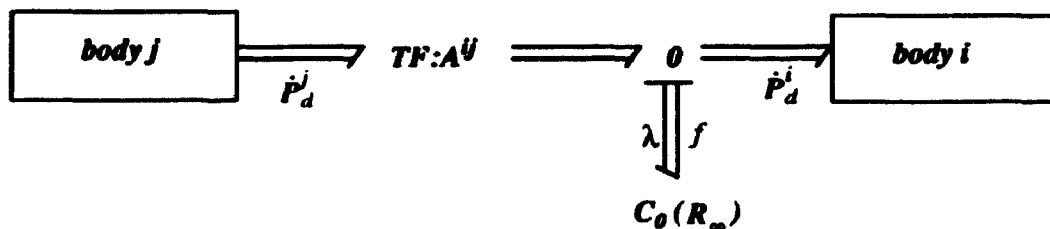


Figure 7-15 Multibond graph of a joint with Lagrange Multiplier

For zero compliance, the constitutive law is

$$[C_0] \{\dot{\lambda}\} = \{0\} = \{f\} \quad (7.13)$$

For infinite resistor, the constitutive law is

$$[R_\infty]^{-1} \{\lambda\} = \{0\} = \{f\} \quad (7.14)$$

Note that flow $\{f\}$ at the element is the sum of the flows of all other bonds, i.e. the relative velocities of the connected bodies. The equations above mean that the employment of elements C_0 and R_∞ satisfy the constraint conditions in velocity form.

Examining the functions of elements C_0 and R_∞ in bond graphs, it can be seen that they merely provide velocity constraints and unknown effort inputs. Their constitutive laws cannot be used to calculate the outputs from the inputs of the

elements. Therefore, they can be treated as a special kind of artificial element, which only provides velocity constraint and unknown effort. In this thesis, it is called Constraintor and represented by CN in multibond graphs. The bond graphs of different kinds of joints discussed above can be represented by element CN simply by replacing all zero S_f elements with CN elements and letting the causal stroke be away from them.

7.4 Multibond Graph of Flexible Multibody Systems

With the multibond graphs of single flexible bodies and mechanical constraints in hand, the multibond graph of a flexible multibody system can be obtained by assembling these individual bond graphs together. This assembly concept is somewhat similar to the finite element analysis methods. This procedure is illustrated in Figure 7-16, in which each block and each circle means the multibond graph representation of that body or joint. The issue in this step is the causal conflict, in which the integral causalities of each single body can not be kept unchanged in the multibond graph of the multibody system. Derivative causalities will appear: to some "I" and "C" elements. This is caused by the "0" junctions and velocity sources at the constraints. The physical meaning is that the constraints reduce the degree of freedom of the multibody system. The methods which are proposed to deal with this issue will be discussed in the next chapter.

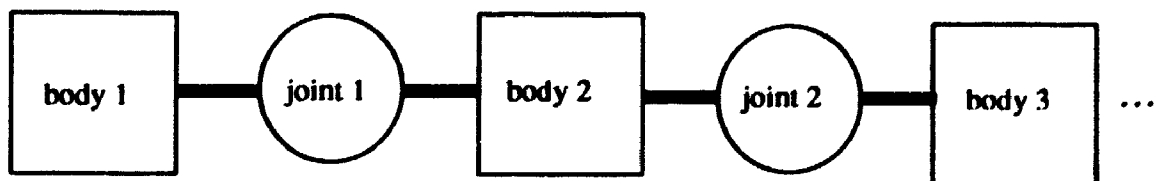


Figure 7-16 The structure of multibond graph of multibond systems

- Chapter 8 -

Derivation of Equations from Multibond Graphs and Numerical Algorithms for Simulation

8.1 Introduction

After the multibond graph of a flexible multibody system has been set up, the equations of motion can be derived in a systematic procedure. This procedure includes two steps, the first is causal assignment, and the other is the establishment of the equations from the caused multibond graph.

Numerical integration of the resulting equations will finally give the dynamic response of a flexible multibody system. The stability of numerical integration is the most important factor which needs to be considered.

This chapter will first discuss the causal assignment for multibond graphs of flexible multibody systems, then the procedure to derive the equations of motion will be explained. Finally, the chapter will compare existing numerical algorithms, for multibody system dynamics, and discuss their use.

8.2 Causality Consideration

From Table 2-2 (Chapter 2), it can be seen that each multiport element represents one or more mathematical relations between the effort and flow vectors, according to their causal signs. The direction of the causal sign has certain physical meanings. For example, an inertia element with integral causality means that the effort (force for mechanics) is given and the flow (velocity) can be determined from the constitutive

law of the element. This is the first type of dynamic problem, or forward dynamics. On the other hand, an inertia element with derivative causal sign means the flow (velocity) is given to the inertia and the unknown force can be found in terms of the constitutive law. This represents the second type of dynamic problem, or inverse dynamics.

In these multibond graph elements, some elements have an arbitrary choice for their causal signs, some have preferred choice, and some have only one choice. The systematic procedure for assigning causality in a multibond graph has been described in detail by Karnopp and Rosenberg [1975, 1983].

The multibond graph of a single flexible body without kinematic constraints has totally integral causality, which is shown in Figure 8-1. When a flexible body is interconnected to other bodies, it is subjected the constraint conditions described in Chapter 7; the total integral causality does not hold anymore. It can be seen that each constraint introduces a flow source which has causal stroke towards the flow source. Due to the causal property of the "0" junction that there must be one effort input to a "0" junction, one stroke at the bonds $\{\dot{P}_d\}$ and $\{\Omega_d\}$ must change direction and so some strokes in Figure 8-1 must change directions too. This will cause some inertia elements to have derivative causal signs.

This procedure can be indicated by an example of a two flexible link manipulator in Figure 8-2. Each link is a beam and they are connected to each other through a spherical joint. One link is also connected to the ground through a spherical joint. An inertial frame X-Y-Z is fixed on the ground. The body reference frames of these two flexible links are attached at the inboard ends of the links, as shown in the figure. The multibond graphs of these separated flexible links and spherical joints are shown in Figure 8-3. It is obvious that the multibond graphs of these two links have integral causal signs for all energy storage elements. To connect the multibond graphs of the links and joints together, the translation velocities of the two links at their joints which are restricted by the spherical joints must be represented in the multibond graph. For link 1, all translation velocities at the joint to the ground are $\{\dot{R}\}$, which is restrained to zero through the joint 1. The translation velocities of the other joint $\{\dot{R}_j\}$ can be

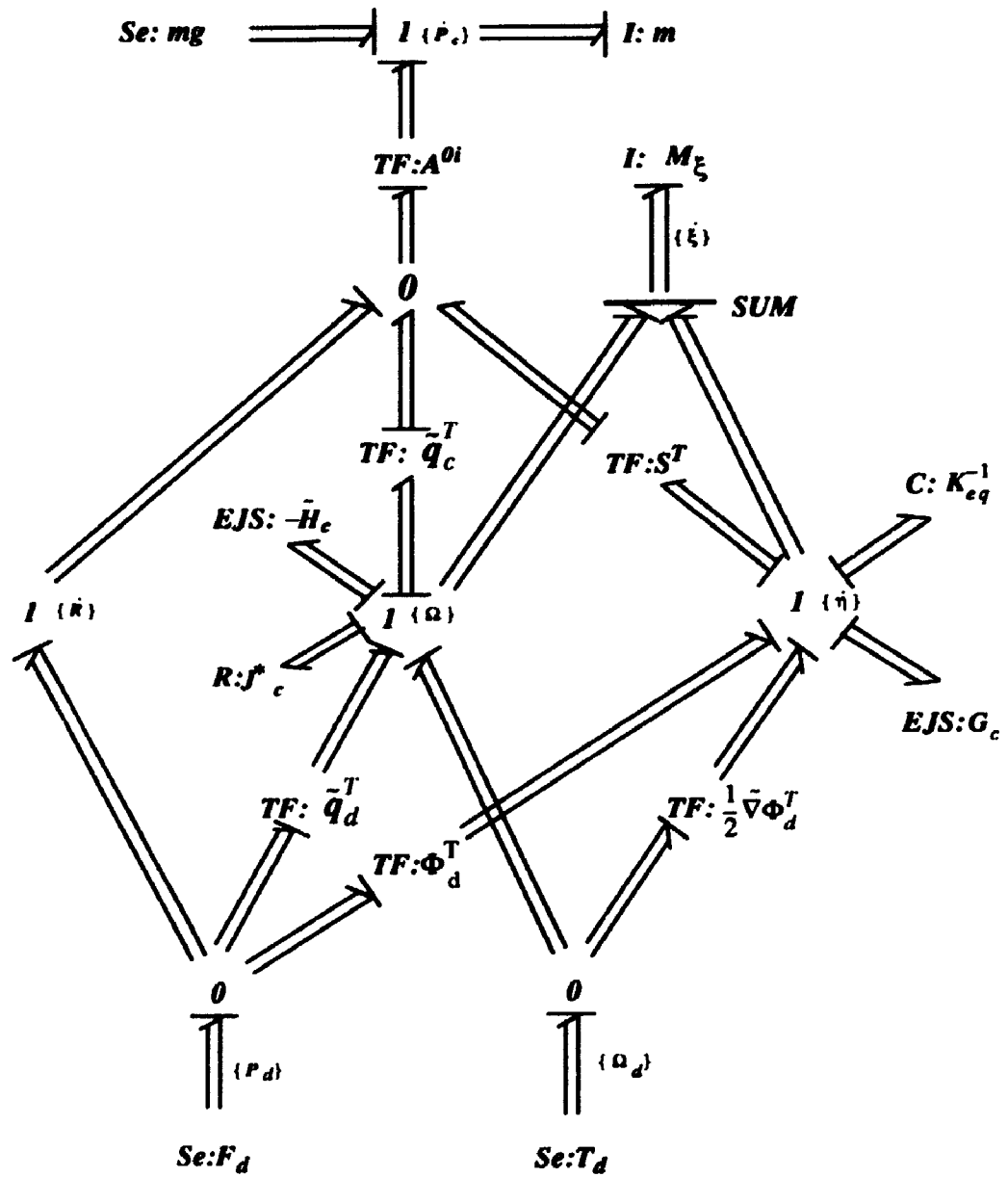


Figure 8-1 Multibond graph of a flexible body with integral causality

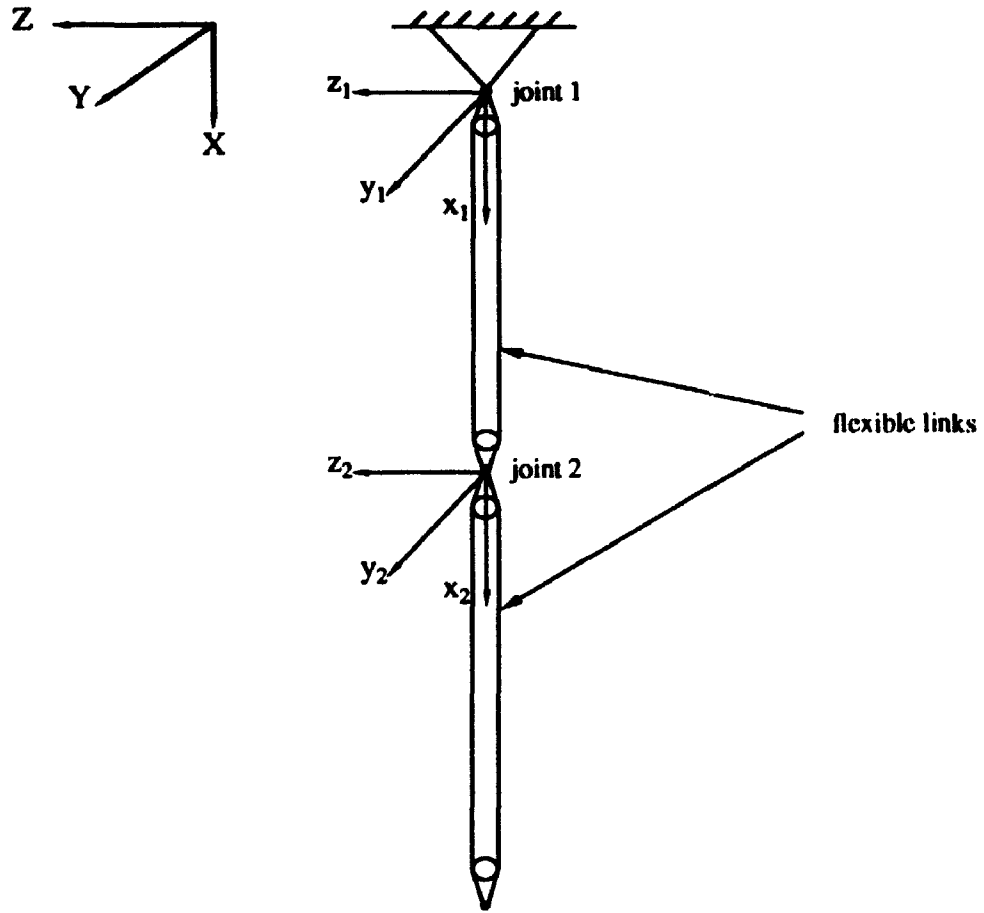


Figure 8-2 A flexible manipulator system

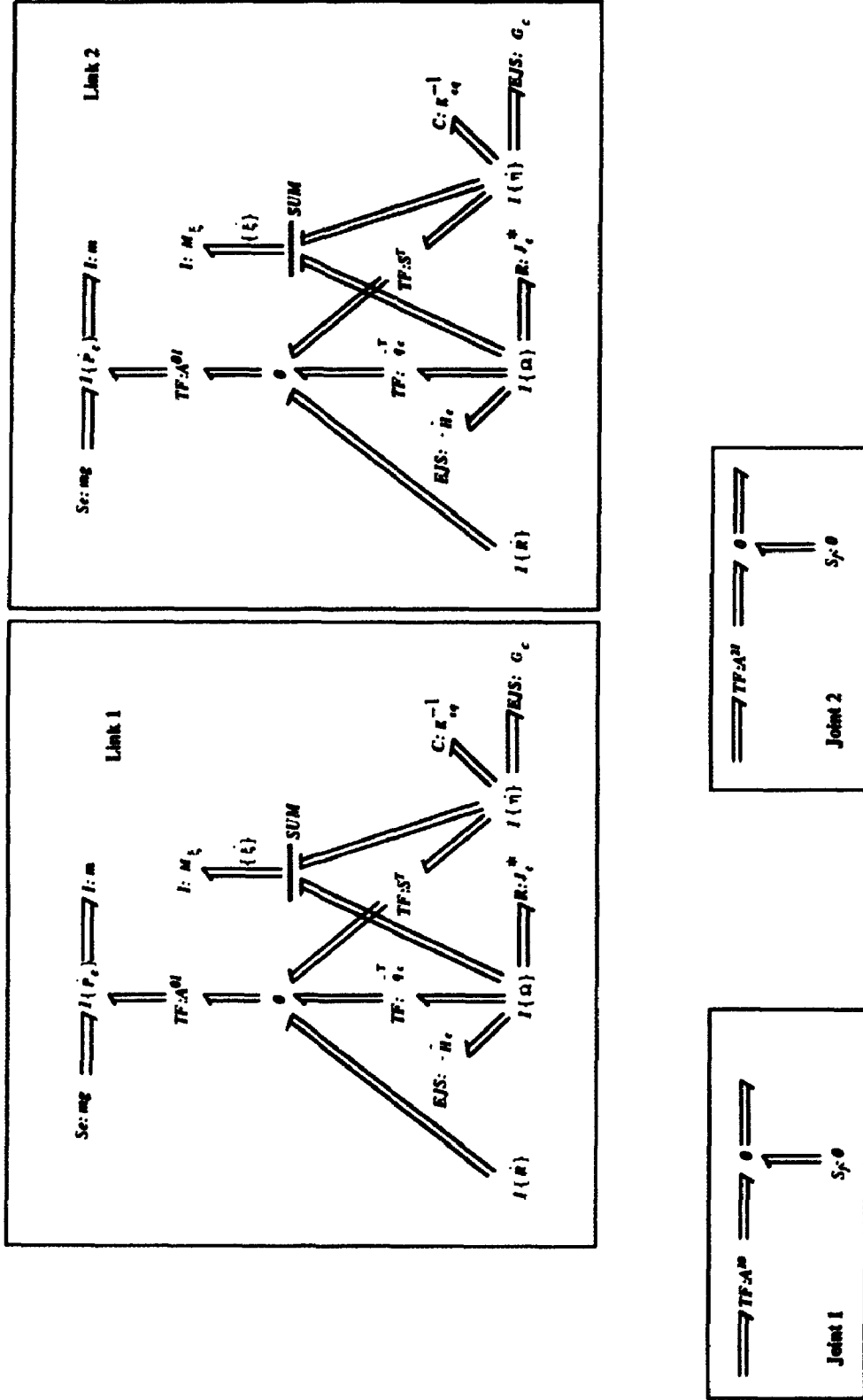


Figure 8-3 Multibond graphs of links and joints of a two flexible link system

expressed in the multibond graph as in Figure 8-4 according to the general multibond graph of a flexible body in Figure 6-2. For link 2, the translation velocities of the joint connected to link 1 are $\{\dot{R}\}$. So the connection can be fulfilled by connecting the right sides of two joints to two velocities $\{\dot{R}\}$ and connecting the left side of joint 1 to a zero flow source (ground) and the left side of joint 2 to the velocity $\{\dot{R}_l\}$. The multibond graph of joint 1 with the zero flow source (ground) can be simplified as a single zero flow source vector directed to the velocity $\{\dot{R}\}$ of the link 1, as is shown in Figure 8-4. The procedure of causal assignment of this multibond graph can be carried out according to the Systematic Causal Assignment Procedure (SCAP) [Karnopp and Rosenberg 1975]. The caused multibond graph of this system is shown in Figure 8-5. It can be seen that two derivative causal signs are at the inertia multiport element representing the translation of the two links. The physical meaning is obvious; since each spherical joint restricts three degrees of freedom for each link, the total degrees of freedom of the two link system are no longer 2×6 degrees of freedom.

The paragraphs above described the procedure of causal assignment of a constrained multibody system and the existence of derivative causality in energy storage elements. From Table 2-2, it can be seen that the derivative causalities in energy storage elements represent differentiation operations which may cause instability in numerical solution of the system if the numerical algorithm is not appropriately selected [Bos, 1986]. Several methods have been introduced to overcome this problem. They can be divided into two groups. One is to eliminate derivative causalities and use common numerical integrations and the other is to accept derivative causalities and adopt special numerical algorithms.

Among the first group is a method to add artificial stiff springs at constraints [Margolis and Karnopp 1979]. In this method, the ideal constraints are adjusted into real elastic constraints. Each body is connected through elastic joints. Therefore, each body has all degrees of freedom as a unconstrained single body and no derivative causality will appear. However, this method is only suitable for simple multibody systems because once the systems contain many bodies, this method increases the

number of degrees of freedom significantly.

The second method of the first group is to transfer the inertia elements with derivative causalities over some other elements to the inertia elements with integral causalities [Allen 1979, Bos 1986]. By this transfer, the derivative causalities are eliminated from the bond graph. From the point of view of establishing equations of motion, what this transfer does is to replace the dependent variables with independent ones according to the kinematic constraints. In general, however, this transfer is very complicated and needs tedious algebraic operations [Bos, 1986].

The third method of the first group is to employ Lagrange multipliers as the effort sources in the bond graph which represent the constraint forces at the constraints [Samento 1990]. This method retains the ideal constraints in the multibody system and also eliminates derivative causalities in the bond graph, in the sense that unknown constraint forces can appear in the bond graphs as the known effort sources. Since these unknown Lagrange multipliers need to be determined before they can be used as effort sources to the bond graphs, a pre-calculation for these Lagrange multipliers at each time step is needed. Therefore this method symbolically eliminates the derivative causal signs in the bond graphs which helps in the numerical algorithm as the second group does.

An alternative of this method is to employ the artificial constraint element *CN* introduced in the last chapter. This type of element provides velocity constraints and unknown effort sources at the joint. The velocity constraints represent the constraint conditions and the effort sources ensure total integral causality to the bond graph. These unknown effort sources (Lagrange multipliers) are left to the numerical algorithm to determine. This will be discussed in section 8.4.

The second group of methods dealing with the constraints is to accept the derivative causalities and adopt special numerical algorithms for simulation [Karnopp and Rosenberg 1983, Bos 1986, Felez 1990]. In Karnopp and Rosenberg's book [1983], the equations of system generated from a bond graph with derivatively caused storage elements are a set of differential and algebraic equations (DAE) with

independent and dependent variables. The solution can be found by replacing dependent variables with independent ones analytically according to the algebraic equations. Bos's method leaves derivative causalities in the bond graphs and sets up a group of equations according to the constitutive laws of each bond graph element. This set of equations represents a set of implicit differential equations and algebraic equations of the whole system. The difference between Bos' [1986] method and Karnopp and Rosenberg's [1983] is that instead of replacing the dependent variables with independent ones, a special numerical integration algorithm for simulation of the DAE systems [Petzold, 1982] has to be employed [Gear 1971, Orlandea 1977, Petzold 1982] in Bos' method.

8.3 The Equations of Motion of Multibody Systems and Numerical Algorithms in Other Computer-Aided Modelling Methods

There exist a number of computer programs in multibody system dynamics [Schiehlen, 1990]. Some of them possess the ability to consider flexible bodies. All these programs are based on analytical methods, e.g. Lagrange's equations, Newton-Euler equations, D'Alembert's principle, Kane's equations and so on. This section summarizes the forms of equations of motion generated from these methods and their numerical algorithms for simulation. This can give a better understanding of the equations of motion generated from multibond graphs.

The forms of equations of motion of a multibody system with holonomic constraints generated from analytical methods can be divided into two groups. One is a set of pure differential equations. The other is a set of differential and algebraic equations. The equations of motion generated from the Newton-Euler method, Lagrange's equation with Lagrange multipliers and D'Alembert's principle are in the second group. The equations of motion in this group can use Cartesian coordinates or relative coordinates directly as the generalized coordinates in the program. It is easier

for computer-aided modelling program to implement. The form of the equations of motion usually is

$$[M] \{\ddot{q}\} = \{Q(q, \dot{q})\} + [H]^T \{\lambda\} + \{F\} \quad (8.1)$$

$$\{g(q, \dot{q})\} = \{0\} \quad (8.2)$$

In the first equation, $\{q\}$ are the variables to describe the position, orientation and vibrational deformation of the each body in the system, $[M]$ is a time-variant mass matrix, $\{Q(q, \dot{q})\}$ are the generalized forces caused by displacement and velocities of the bodies, $\{F\}$ are the generalized external forces, $\{\lambda\}$ are the Lagrange multipliers, and $[H]$ is the Jacobian matrix of the constraint equation (8.2) which means

$$[H] = \left[\frac{\partial g}{\partial q} \right] \quad (8.3)$$

Since the equations of motion of this kind are Differential/Algebraic Equations (DAE), most well developed numerical algorithms for solving Ordinary Differential Equations (ODE) cannot be simply used for their numerical solution [Petzold, 1982]. Several algorithms have been developed to solve this kind of DAE. They can be summarized into two strategies. One is to change the DAE system to an ODE system by differentiating the algebraic constraint equation and employ any numerical methods for ODE systems. The other is to use a specially developed algorithm to solve the DAE directly.

In the first strategy, the constraint equation (8.2) is differentiated into

$$\{\dot{g}\} = [H] \{\dot{q}\} = \{0\} \quad (8.4)$$

$$\{\ddot{g}\} = [H] \{\ddot{q}\} + [\dot{H}] \{\dot{q}\} = \{0\} \quad (8.5)$$

Equation (8.5) is a second order differential equation. Together with equation (8.1), the

equations of motion become an ODE system which is

$$\begin{bmatrix} [M] & [H]^T \\ [H] & [0] \end{bmatrix} \begin{Bmatrix} \{\ddot{q}\} \\ \{\lambda\} \end{Bmatrix} = \begin{Bmatrix} \{Q\{q, \dot{q}\}\} \\ \Upsilon \end{Bmatrix} + \begin{Bmatrix} \{F\} \\ \{0\} \end{Bmatrix} \quad (8.6)$$

where

$$\{\Upsilon\} = -[H] \{\dot{q}\} \quad (8.7)$$

The most important drawback of this algorithm is the violation of the constraint equations resulting from the inaccuracy during the numerical integration process. This behavior is due to the fact that it integrates an undamped second order system (8.5) twice and the numerical integration of this system is unstable. Two methods have been proposed to overcome this problem. One is that instead of integrating equation (8.5), a new stable second order system is integrated which is

$$\{\ddot{g}\} + 2\alpha\{\dot{g}\} + \beta^2\{g\} = \{0\} \quad (8.8)$$

where α and β are positive constants, and usually chosen to be $\alpha = \beta$.

With this constraint equation, the equation of motion (8.6) becomes

$$\begin{bmatrix} [M] & [H]^T \\ [H] & [0] \end{bmatrix} \begin{Bmatrix} \{\ddot{q}\} \\ \{\lambda\} \end{Bmatrix} = \begin{Bmatrix} \{Q\{q, \dot{q}\}\} \\ \Upsilon^0 \end{Bmatrix} + \begin{Bmatrix} \{F\} \\ \{0\} \end{Bmatrix} \quad (8.9)$$

where

$$\{\Upsilon^0\} = -[H] \{\dot{q}\} - 2\alpha[H] \{q\} - \beta^2\{g\} \quad (8.10)$$

Note that in this form the variables q are not independent. The dependence of these variables is conducted by the constraint equation (8.8). The total unknown variables are $\{q\}$ and $\{\lambda\}$, which has the maximum variables of the system.

If the constraint forces are not of interest in the simulation, equation (8.9) can be reduced by eliminating the Lagrange's multipliers $\{\lambda\}$ for more economic numerical solution. There are two procedures to eliminate $\{\lambda\}$. One is proposed by Wittenburg

[1977] in which $\{\ddot{q}\}$, found from the constraint equation (8.8), is substituted into equation (8.1) for $\{\lambda\}$. This leads to

$$\{\lambda\} = -([H] [M]^{-1} [H]^T)^{-1} ([H] [M]^{-1} (\{Q\} + \{F\}) + Y^0) \quad (8.11)$$

$$[M] \{\ddot{q}\} = \{Q\} + \{F\} - [H]^T (([H] [M]^{-1} [H]^T)^{-1} ([H] [M]^{-1} (\{Q\} + \{F\}) + Y^0)) \quad (8.12)$$

The other is to use the orthogonal complement of the Jacobian matrix $[H]$ to eliminate $\{\lambda\}$ [Unda and others 1987]. Since the variables $\{\dot{q}\}$ are dependent, an independent subset $\{\dot{q}_i\}$ of them can be defined as

$$\{\dot{q}_i\} = [B] \{\dot{q}\} \quad (8.13)$$

where $[B]$ is a boolean matrix.

Together with the constraint equation (8.4), there is

$$\begin{bmatrix} [H] \\ [B] \end{bmatrix} \{\dot{q}\} = \begin{Bmatrix} \{0\} \\ \{\dot{q}_i\} \end{Bmatrix} \quad (8.14)$$

Thus

$$\{\dot{q}\} = \begin{bmatrix} [H] \\ [B] \end{bmatrix}^{-1} \begin{Bmatrix} \{0\} \\ \{\dot{q}_i\} \end{Bmatrix} = [S] [R] \begin{Bmatrix} \{0\} \\ \{\dot{q}_i\} \end{Bmatrix} \quad (8.15)$$

or

$$\{\dot{q}\} = [R] \{\dot{q}_i\} \quad (8.16)$$

Matrix $[R]$ is an orthogonal complement of Jacobian matrix of constraint condition, because

$$[H] \{\dot{q}\} = [H] [R] \{\dot{q}_i\} = \{0\} \quad (8.17)$$

Since components in $\{\dot{q}_i\}$ are independent, the following holds

$$[H] [R] = [0] \quad (8.18)$$

Using this property of matrix $[R]$, one can pre-multiply $[R]^T$ to equation (8.1) and gets

$$[R]^T [M] \{\ddot{q}\} = [R]^T \{Q\} + [R]^T \{F\} \quad (8.19)$$

where $\{\lambda\}$ has been eliminated. So the equations of motion in this form becomes

$$\begin{bmatrix} [R]^T [M] \\ [H] \end{bmatrix} \{\ddot{q}\} = \begin{bmatrix} [R]^T (Q + \{F\}) \\ \gamma^0 \end{bmatrix} \quad (8.20)$$

The numerical solution of equations (8.12) or (8.20) is more economical than equation (8.9). However, some preparation to eliminate Lagrange's multipliers has to be done first, which is the cost for a simpler numerical solution.

Another form of elimination of Lagrange multipliers should be mentioned here which will be used to verify the equations of motion generated from multibond graphs. It is the coordinate partitioning method [Wehage and Haug 1982]. In this method, variables $\{q\}$ are divided into independent subset $\{q_i\}$ and dependent one $\{q_d\}$

$$\{q\} = \begin{Bmatrix} \{q_d\} \\ \{q_i\} \end{Bmatrix} \quad (8.21)$$

and so

$$[H] = [H^d \ H^i] \quad (8.22)$$

Based on this partitioning, equation (8.1) can be divided into

$$[M^{dd}] \{\ddot{q}_d\} + [M^{di}] \{\ddot{q}_i\} = \{Q^d\} + [H^d]^T \{\lambda\} + \{F^d\} \quad (8.23)$$

$$[M^{ii}] \{\ddot{q}_i\} + [M^{id}] \{\ddot{q}_d\} = \{Q^i\} + [H^i]^T \{\lambda\} + \{F^i\} \quad (8.24)$$

Since $[H^d]$ is a nonsingular square matrix for independent constraints, $\{\lambda\}$ can be solved from equation (8.23) and substituted into equation (8.24). This yields

$$\begin{aligned} & ([M^{ii}] + [H^*]^T [M^{di}]) \{\ddot{q}_i\} + ([M^{id}] + [H^*]^T [M^{dd}]) \{\ddot{q}_d\} \\ &= \{Q^i\} + \{F^i\} + [H^*]^T (\{Q^d\} + \{F^d\}) \end{aligned} \quad (8.25)$$

where

$$[H^*] = -[H^d]^{-1} [H^i] \quad (8.26)$$

Instead of turning the DAE into ODE for numerical solution, the second strategy to find the numerical solution of equations (8.1) and (8.2) is to employ a special algorithm for the DAE system. Gear [1971] first proposed an algorithm for solving DAE for electrical circuits. Orlandea and others [1977] proposed an algorithm for solving equations (8.1) and (8.2) directly, which is used in the program ADAMS. Petzold and Gear [1982, 1984] studied the general DAE and the algorithm for its solution. The strategy in this algorithm is that the algebraic equations are treated as stiff differential equations and the differential equations are solved by implicit numerical integration for stiff ordinary differential equations.

This algorithm can be illustrated as follows. Suppose that mixed differential and algebraic equations result of the form

$$\{f(y, \dot{y}, t)\} = \{0\} \quad (8.27)$$

where some components of \dot{y} may not appear in some of the equations. When none of the components of \dot{y} appear in an equation, that equation is an algebraic equation; otherwise it is a differential equation.

An implicit numerical integration such as the k th-order Gear's algorithm has the

form

$$y^{i+1} - \Delta t b_{-1} y^{i+1} - \sum_{j=0}^{k-1} a_j y^{i-j} = \{0\} \quad (8.28)$$

where i is the time step, Δt the time increment and a_j 's and b_{-1} are constants.

The Newton-Raphson formula for solving \dot{y} and y from equation (8.27) can be found as

$$f_y^{(l)} \Delta y^{(l)} + f_{\dot{y}}^{(l)} \Delta \dot{y}^{(l)} = -f^{(l)} \quad (8.29)$$

where superscript l means the iteration step, and

$$y^{(l+1)} = \Delta y^{(l)} + y^{(l)} \quad (8.30)$$

$$\dot{y}^{(l+1)} = \Delta \dot{y}^{(l)} + \dot{y}^{(l)} \quad (8.31)$$

According to formula (8.28), the relation between $\Delta y^{(l)}$ and $\Delta \dot{y}^{(l)}$ at any time step can be found as

$$\Delta \dot{y}^{(l)} = \frac{1}{\Delta t b_{-1}} \Delta y^{(l)} \quad (8.32)$$

Substitution of this relation into equation (8.29) results in

$$\left(f_y^{(l)} + \frac{1}{\Delta t b_{-1}} f_{\dot{y}}^{(l)} \right) \Delta y^{(l)} = -f^{(l)} \quad (8.33)$$

At each time step, the iteration process of equations (8.30) to (8.33) is continued until all of the difference $\Delta y^{(l)}$ are smaller than a specified tolerance level and all y are found. Then the algorithm forwards to the next time step until the end of the simulation period.

Applying this algorithm to DAE system of equations (8.1) and (8.2), the function

$\{f(y, \dot{y}, t)\}$ and variable y can be

$$\{f(y, \dot{y}, t)\} = \begin{bmatrix} [M] & 0 & 0 \\ 0 & [I] & 0 \\ 0 & 0 & 0 \end{bmatrix} \{y\} + \begin{bmatrix} -\{Q\} - \{F\} - [H]^T \{\lambda\} \\ -\{\dot{q}\} \\ \{g\} \end{bmatrix} \quad (8.34)$$

$$y = \begin{bmatrix} \{\dot{q}\} \\ \{q\} \\ \{\lambda\} \end{bmatrix} \quad (8.35)$$

Since at each time step Newton-Raphson iteration is used, this algorithm is relatively slow.

8.4 The Equations of Motion Generated from Causal Multibond Graphs

As the multibond graphs of a flexible multibody system have been assigned causal signs according to the Systematic Causal Assignment Procedure [Karnopp and Rosenberg, 1975], the inputs and outputs of each bond graph element are determined by the causal strokes. The equations of all elements can be written in terms of the inputs, outputs and their constitutive laws. This full set of equations will form the equations of motion for the multibody system.

8.4.1 Procedures of Derivation of Equations of Motion

Based on the two kinds of multibond graph for constraints discussed in Chapter 7, the equations generated from the multibond graphs have also two forms.

For the first type of multibond graph representation of constraint discussed in Chapter 7, zero flow source elements will cause derivative causalities in the multibond graph.

Rosenberg [1971] first proposed a procedure to derive the general state space equations from bond graphs with mixed causality at storage elements. In his research, the equations generated from the bond graph have the form

$$\dot{X}_i = \Gamma_i(X_p, \dot{X}_d, U) \quad (8.36)$$

$$X_d = \Gamma_d(X_p, U) \quad (8.37)$$

where X_i , X_d are energy variables at the storage elements with integral and derivative causal signs, which represent the independent and dependent variables for the system. Note that this is a set of differential and algebraic equations.

This procedure to derive a set of differential and algebraic equations is also advanced to multibond graphs of rigid multibody systems by Bos [1986], which points out that this procedure needs the least analytical work by hand and so is superior for computer-aided modelling and simulation. For details of this procedure, the reader can refer to the reference [Bos 1986]. It verifies, with the aid of an example, that this set of differential and algebraic equations from a multibond graph of a multibody system has the same form as that of equations of motion derived by the coordinate partitioning method.

Karnopp [1977] proposed a procedure to derive differential equations from a mixed causal bond graph based on Lagrange's equation. This procedure introduces artificial flows into the bond graph which represent the independent generalized coordinates. The kinetic and potential energies of the system can be first written in terms of energy variables of all storage elements with integral or derivative causal signs. Then, the relations between these energy variables and the independent generalized coordinates are applied to rewrite the energies in terms of the generalized coordinates. Finally the Lagrange equation can be used to achieve the differential equations of the system.

Similar to this idea, Allen [1979] chose the energy variables at storage elements with integral causal signs as the independent coordinates and moved other storage elements with derivative causal signs over to these storage elements with integral causality. This results in a new bond graph which has all integral caused storage elements and the differential equations can be easily derived according to the Systematic Causal Assignment Procedure [Karnopp and Rosenberg, 1975].

Based on Karnopp and Allen, Bos [1986] proposed to use arbitrary independent coordinates as a "1" junction and move all storage elements to these junctions. This also results in a new bond graph with all integral caused storage elements. A set of differential equations can be derived from it. However, with the complex systems, this movement of elements needs complicated mathematical manipulation, and original physical meanings of each element are lost.

All these bond graph methods to derive pure differential equations from mixed causal bond graphs are equivalent to analytically eliminating dependent variables from differential/algebraic equations. The difference is that the former does so by modifying bond graphs, while the latter does so by manipulating differential/algebraic equations. Therefore, this thesis will not discuss this method.

For the second type of multibond graph representation of constraints, the artificial constraint element CN provides velocity constraint and unknown effort source at the joint. This ensures that the multibond graphs for each body have integral causalities. Recalling the equations of motion of a single flexible body, i.e. equation (4.74) in Chapter 4, the differential equations of motion of the whole system can be written as

$$\begin{bmatrix} [M_1^*] & & \\ & \dots & \\ & & [M_n^*] \end{bmatrix} \begin{bmatrix} \{\dot{h}_1\} \\ \dots \\ \{\dot{h}_n\} \end{bmatrix} = \begin{bmatrix} \{W_1\} \\ \dots \\ \{W_n\} \end{bmatrix} + \begin{bmatrix} \{F_1\} \\ \dots \\ \{F_n\} \end{bmatrix} + \begin{bmatrix} [H_{11}]^T & \dots & \dots \\ \dots & \dots & \dots \\ \dots & \dots & [H_{nm}]^T \end{bmatrix} \begin{bmatrix} \{\lambda_1\} \\ \dots \\ \{\lambda_m\} \end{bmatrix} \quad (8.38)$$

The independent constraints in velocity form at each joint form the algebraic equations which are

$$\begin{bmatrix} [H_{11}] & \dots & \dots \\ \dots & \dots & \dots \\ \dots & \dots & [H_{mn}] \end{bmatrix} \begin{bmatrix} \{h_1\} \\ \dots \\ \{h_n\} \end{bmatrix} = \{0\} \quad (8.39)$$

It will be verified by an example that the equations of motion generated from this type of multibond graph are differential/algebraic equations with maximum variables,

which have the form of equations (8.1) and (8.4).

8.4.2 An Example of a Two-Link Flexible Manipulator

This section is to demonstrate the procedure of the derivation of equations of motion, by an example for a two-flexible-links manipulator, and verify that they are the same as those derived from analytical methods.

The example two-flexible-links manipulator is shown in Figure 8-2. The multibond graphs of the system with two different types of multibond graph representations of spherical joints are shown in Figures 8-4 and 8-5. These multibond graphs have been marked with causal signs according to the Systematic Causal Assignment Procedure. In the zero flow source method, two multiport inertia elements corresponding to translation of two links get derivative causalities due to the constraints of two spherical joints. The multibond graphs using constraint element CN has total integral causal signs as discussed earlier.

The generation of equations of motion from Figure 8-4 is as follows:

Step 1: Using the constitutive law at inertia element $[M_{\xi}]$ in link 1, extending the effort sum to the end of each branch. This means

$$\begin{aligned}
 [M_{\xi_1}] \{\ddot{\xi}_1\} &= \begin{bmatrix} [J_1] & [D_1]^T \\ [D_1] & [M_1] \end{bmatrix} \begin{Bmatrix} \{\dot{\Omega}_1\} \\ \{\ddot{\eta}_1\} \end{Bmatrix} = \{e_{\xi_1}\} \\
 &= \left\{ \begin{array}{l} ([\bar{H}_1] - [J^*_{11}]) \{\Omega_1\} + [\bar{q}_{c_1}] [A^{10}] (m_1 \{\ddot{P}_{c_1}\} - m_1 \{g\}) \\ - [G_1] \{\dot{\eta}_1\} - [K_{eq1}] \{\eta_1\} - [S_1] [A^{10}] (m_1 \{\ddot{P}_{c_1}\} - m_1 \{g\}) \end{array} \right\} + \\
 &\quad + \left\{ \begin{array}{l} [\bar{q}_{d_1}] [A^{10}] (m_2 \{\ddot{P}_{c_2}\} - m_2 \{g\}) \\ - [\Phi_{d_1}] [A^{10}] (m_2 \{\ddot{P}_{c_2}\} - m_2 \{g\}) \end{array} \right\} \\
 &= \left\{ \begin{array}{l} ([\bar{H}_1] - [J^*_{11}]) \{\Omega_1\} \\ - [G_1] \{\dot{\eta}_1\} - [K_{eq1}] \{\eta_1\} \end{array} \right\} + \begin{bmatrix} m_1 [\bar{q}_{c_1}] & m_2 [\bar{q}_{d_1}] \\ -m_1 [S_1] & -m_2 [\Phi_{d_1}] \end{bmatrix} [A^{10}] \begin{Bmatrix} \{\ddot{P}_{c_1}\} - \{g\} \\ \{\ddot{P}_{c_2}\} - \{g\} \end{Bmatrix}
 \end{aligned} \tag{8.40}$$

Step 2: Using the constitutive law at inertia element $[M_{\xi}]$ in link 2, extending the effort sum to the end of each branch. This means

$$\begin{aligned}
 [M_{\xi_2}] \{\ddot{\xi}_2\} &= \begin{bmatrix} [J_2] & [D_2]^T \\ [D_2] & [M_2] \end{bmatrix} \begin{Bmatrix} \{\dot{\Omega}_2\} \\ \{\dot{\eta}_2\} \end{Bmatrix} = \{e_{\xi_2}\} \\
 &= \begin{Bmatrix} ([\bar{H}_2] - [J^*_{2}]) \{\Omega_2\} + [\bar{q}_{c_2}] [A^{20}] (m_2 \{\ddot{P}_{c_2}\} - m_2 \{g\}) \\ -[G_2] \{\eta_2\} - [K_{eq2}] \{\eta_2\} - [S_2] [A^{20}] (m_2 \{\ddot{P}_{c_2}\} - m_2 \{g\}) \end{Bmatrix} \\
 &= \begin{Bmatrix} ([\bar{H}_2] - [J^*_{2}]) \{\Omega_2\} \\ -[G_2] \{\eta_2\} - [K_{eq2}] \{\eta_2\} \end{Bmatrix} + \begin{bmatrix} [0] & m_1 [\bar{q}_{c_2}] \\ [0] & -m_2 [S_2] \end{bmatrix} [A^{20}] \begin{Bmatrix} \{\ddot{P}_{c_1}\} - \{g\} \\ \{\ddot{P}_{c_2}\} - \{g\} \end{Bmatrix}
 \end{aligned} \tag{8.41}$$

These two equations can be written into one compact form as

$$\begin{aligned}
 &\begin{bmatrix} [J_1] & [D_1]^T & [0] & [0] \\ [D_1] & [M_1] & [0] & [0] \\ [0] & [0] & [J_2] & [D_2]^T \\ [0] & [0] & [D_2] & [M_2] \end{bmatrix} \begin{Bmatrix} \{\dot{\Omega}_1\} \\ \{\dot{\eta}_1\} \\ \{\dot{\Omega}_2\} \\ \{\dot{\eta}_2\} \end{Bmatrix} + \begin{bmatrix} -m_1 [\bar{q}_{c_1}] [A^{10}] & -m_2 [\bar{q}_{d_1}] [A^{10}] \\ m_1 [S_1] [A^{10}] & m_2 [\Phi_{d_1}] [A^{10}] \\ [0] & -m_1 [\bar{q}_{c_2}] [A^{20}] \\ [0] & m_2 [S_2] [A^{20}] \end{bmatrix} \begin{Bmatrix} \{\ddot{P}_{c_1}\} \\ \{\ddot{P}_{c_2}\} \end{Bmatrix} = \\
 &= \begin{Bmatrix} ([\bar{H}_1] - [J^*_{1}]) \{\Omega_1\} \\ -[G_1] \{\eta_1\} - [K_{eq1}] \{\eta_1\} \\ ([\bar{H}_2] - [J^*_{2}]) \{\Omega_2\} \\ -[G_2] \{\eta_2\} - [K_{eq2}] \{\eta_2\} \end{Bmatrix} + \begin{bmatrix} -[\bar{q}_{c_1}] [A^{10}] & -[\bar{q}_{d_1}] [A^{10}] \\ [S_1] [A^{10}] & [\Phi_{d_1}] [A^{10}] \\ [0] & -[\bar{q}_{c_2}] [A^{20}] \\ [0] & [S_2] [A^{20}] \end{bmatrix} \begin{Bmatrix} m_1 \{g\} \\ m_2 \{g\} \end{Bmatrix}
 \end{aligned} \tag{8.42}$$

Step 3: Expressing velocities of the inertia elements with derivative causality in terms of velocities of the inertia elements with integral causality. This means that at inertia element m in link 1, there is

$$\begin{aligned}
\{\dot{P}_{c_1}\} &= [A^{01}] (\{\dot{R}_1\} + [\tilde{q}_{c_1}]^T \{\Omega_1\} + [S_1]^T \{\dot{\eta}_1\}) \\
&= [A^{01}] ([\tilde{q}_{c_1}]^T \{\Omega_1\} + [S_1]^T \{\dot{\eta}_1\})
\end{aligned} \tag{8.43}$$

and at inertia element m in link 2, there is

$$\begin{aligned}
\{\dot{P}_{c_2}\} &= [A^{02}] (\{\dot{R}_2\} + [\tilde{q}_{c_2}]^T \{\Omega_2\} + [S_2]^T \{\dot{\eta}_2\}) \\
&= [A^{02}] ([A^{21}] (\{\dot{R}_1\} + [\tilde{q}_{d_1}]^T \{\Omega_1\} + [\Phi_{d_1}]^T \{\dot{\eta}_1\}) + [\tilde{q}_{c_2}]^T \{\Omega_2\} + [S_2]^T \{\dot{\eta}_2\}) \\
&= [A^{01}] ([\tilde{q}_{d_1}]^T \{\Omega_1\} + [\Phi_{d_1}]^T \{\dot{\eta}_1\}) + [A^{02}] ([\tilde{q}_{c_2}]^T \{\Omega_2\} + [S_2]^T \{\dot{\eta}_2\})
\end{aligned} \tag{8.44}$$

These two equations can be written into a compact form as

$$\begin{Bmatrix} \{\dot{P}_{c_1}\} \\ \{\dot{P}_{c_2}\} \end{Bmatrix} = \begin{bmatrix} [A^{01}] [\tilde{q}_{c_1}]^T & [A^{01}] [S_1]^T & [0] & [0] \\ [A^{01}] [\tilde{q}_{d_1}]^T & [A^{01}] [\Phi_{d_1}]^T & [A^{02}] [\tilde{q}_{c_2}]^T & [A^{02}] [S_2]^T \end{bmatrix} \begin{Bmatrix} \{\Omega_1\} \\ \{\dot{\eta}_1\} \\ \{\Omega_2\} \\ \{\dot{\eta}_2\} \end{Bmatrix} \tag{8.45}$$

Equations (8.42) and (8.45) are equations of motion generated from multibond graphs in Figure 8-4. These are a set of differential/algebraic equations and have the form of equations (8.36) and (8.37).

The generation of equations of motion from Figure 8-5 is as follows

Step 1: Writing out the velocity constraints at two CN elements, respectively.

At CN_1

$$[A^{10}] \{\dot{P}_{c_1}\} - [\tilde{q}_{c_1}]^T \{\Omega_1\} - [S_1]^T \{\dot{\eta}_1\} = \left[[A^{10}] - [\tilde{q}_{c_1}]^T - [S_1]^T \right] \begin{Bmatrix} \{\dot{P}_{c_1}\} \\ \{\Omega_1\} \\ \{\dot{\eta}_1\} \end{Bmatrix} = \{0\} \tag{8.46}$$

At CN_2

$$\begin{aligned}
 & [A^{20}] \{\dot{P}_{c_2}\} - [\bar{q}_{c_2}]^T \{\Omega_2\} - [S_2]^T \{\dot{\eta}_2\} - [A^{21}] (\{\dot{R}_1\} + [\bar{q}_{d_1}]^T \{\Omega_1\} + [\Phi_{d_1}]^T \{\dot{\eta}_1\}) \\
 &= \left[[A^{20}] - [\bar{q}_{c_2}]^T - [S_2]^T \right] \begin{Bmatrix} \{\dot{P}_{c_2}\} \\ \{\Omega_2\} \\ \{\dot{\eta}_2\} \end{Bmatrix} - \\
 & \quad - [A^{21}] ([A^{10}] \{\dot{P}_{c_1}\} - ([\bar{q}_{c_1}]^T - [\bar{q}_{d_1}]^T) \{\Omega_1\} + ([S_1]^T - [\Phi_{d_1}]^T) \{\dot{\eta}_1\}) \quad (8.47) \\
 &= \left[-[A^{20}] \quad [A^{21}] ([\bar{q}_{c_1}]^T - [\bar{q}_{d_1}]^T) \quad [A^{21}] ([S_1]^T - [\Phi_{d_1}]^T) \quad [A^{20}] - [\bar{q}_{c_2}]^T - [S_2]^T \right] \{\dot{q}\}
 \end{aligned}$$

where

$$\{\dot{q}\} = \begin{Bmatrix} \{\dot{P}_{c_1}\} \\ \{\Omega_1\} \\ \{\dot{\eta}_1\} \\ \{\dot{P}_{c_2}\} \\ \{\Omega_2\} \\ \{\dot{\eta}_2\} \end{Bmatrix} \quad (8.48)$$

These two equations can be rearranged as

$$\begin{aligned}
 & \left[\begin{array}{ccc|ccc} [A^{10}] & [0] & & & & \\ -[A^{20}] & [A^{20}] & & & & \\ \hline & & -[\bar{q}_{c_1}]^T & & -[S_1]^T & [0] & [0] \\ & & [A^{21}] ([\bar{q}_{c_1}]^T - [\bar{q}_{d_1}]^T) & & [A^{21}] ([S_1]^T - [\Phi_{d_1}]^T) & -[\bar{q}_{c_2}]^T & -[S_2]^T \end{array} \right] \begin{Bmatrix} \{\dot{P}_{c_1}\} \\ \{\dot{P}_{c_2}\} \\ \{\Omega_1\} \\ \{\dot{\eta}_1\} \\ \{\Omega_2\} \\ \{\dot{\eta}_2\} \end{Bmatrix} \\
 &= \left[[L_d] \quad [L_i] \right] \begin{Bmatrix} \{\dot{q}_d\} \\ \{\dot{q}_i\} \end{Bmatrix} = \{0\} \quad (8.49)
 \end{aligned}$$

where

$$[L_d] = \begin{bmatrix} [A^{10}] & [0] \\ -[A^{20}] & [A^{20}] \end{bmatrix} \quad (8.50)$$

$$[L_i] = \begin{bmatrix} -[\tilde{q}_{c_1}]^T & -[S_1]^T & [0] & [0] \\ [A^{21}]([\tilde{q}_{c_1}]^T - [\tilde{q}_{d_1}]^T) & [A^{21}]([S_1]^T - [\Phi_{d_1}]^T) & -[\tilde{q}_{c_2}]^T & -[S_2]^T \end{bmatrix} \quad (8.51)$$

$$\{\dot{q}_d\} = \begin{Bmatrix} \{\dot{P}_{c_1}\} \\ \{\dot{P}_{c_2}\} \end{Bmatrix} \quad (8.52)$$

$$\{\dot{q}_i\} = \begin{Bmatrix} \{\Omega_1\} \\ \{\dot{\eta}_1\} \\ \{\Omega_2\} \\ \{\dot{\eta}_2\} \end{Bmatrix} \quad (8.53)$$

where $\{\dot{q}_d\}$ and $\{\dot{q}_i\}$ are dependant variables and independent variables.

Since the constraints are independent, matrix $[L_d]$ is nonsingular, equation (8.49) can be written as

$$\{\dot{q}_d\} = -[L_d]^{-1}[L_i]\{\dot{q}_i\} = [L]^* \{\dot{q}_i\} \quad (8.54)$$

where

$$\begin{aligned} [L]^* &= -[L_d]^{-1}[L_i] \\ &= -\begin{bmatrix} [A^{10}] & [0] \\ -[A^{20}] & [A^{20}] \end{bmatrix}^{-1} \begin{bmatrix} -[\tilde{q}_{c_1}]^T & -[S_1]^T & [0] & [0] \\ [A^{21}]([\tilde{q}_{c_1}]^T - [\tilde{q}_{d_1}]^T) & [A^{21}]([S_1]^T - [\Phi_{d_1}]^T) & -[\tilde{q}_{c_2}]^T & -[S_2]^T \end{bmatrix} \\ &= -\begin{bmatrix} [A^{01}] & [0] \\ [A^{01}] & [A^{02}] \end{bmatrix} \begin{bmatrix} -[\tilde{q}_{c_1}]^T & -[S_1]^T & [0] & [0] \\ [A^{21}]([\tilde{q}_{c_1}]^T - [\tilde{q}_{d_1}]^T) & [A^{21}]([S_1]^T - [\Phi_{d_1}]^T) & -[\tilde{q}_{c_2}]^T & -[S_2]^T \end{bmatrix} \end{aligned}$$

$$= \begin{bmatrix} [A^{01}] [\bar{q}_{c_1}]^T & [A^{01}] [S_1]^T & [0] & [0] \\ [A^{01}] [\bar{q}_{d_1}]^T & [A^{01}] [\Phi_{d_1}]^T & [A^{02}] [\bar{q}_{c_2}]^T & [A^{02}] [S_2]^T \end{bmatrix} \quad (8.55)$$

Step 2: Writing out constitutive laws at each inertia element.

At the inertia element $\{m\}$ of link 1

$$\begin{aligned} m_1 \{\ddot{P}_{c_1}\} &= m_1 \{g\} + [A^{01}] (\{\lambda_1\} - [A^{12}] \{\lambda_2\}) \\ &= m_1 \{g\} + [A^{01}] \{\lambda_1\} - [A^{02}] \{\lambda_2\} \end{aligned} \quad (8.56)$$

At the inertia element $\{M_{\xi}\}$ of link 1

$$\begin{aligned} [M_{\xi_1}] \{\ddot{\xi}_1\} &= \begin{bmatrix} [J_1] & [D_1]^T \\ [D_1] & [M_1] \end{bmatrix} \begin{Bmatrix} \{\Omega_1\} \\ \{\ddot{\eta}_1\} \end{Bmatrix} = \{e_{\xi_1}\} \\ &= \left\{ \begin{array}{l} ([\tilde{H}_1] - [J^*_{c_1}]) \{\Omega_1\} + [\bar{q}_{c_1}] (\{\lambda_1\} - [A^{12}] \{\lambda_2\}) + [\bar{q}_{d_1}] [A^{12}] \{\lambda_2\} \\ - [G_1] \{\ddot{\eta}_1\} - [K_{eq_1}] \{\eta_1\} - [S_1] (\{\lambda_1\} - [A^{12}] \{\lambda_2\}) - [\Phi_{d_1}] [A^{12}] \{\lambda_2\} \end{array} \right\} \\ &= \left\{ \begin{array}{l} ([\tilde{H}_1] - [J^*_{c_1}]) \{\Omega_1\} \\ - [G_1] \{\ddot{\eta}_1\} - [K_{eq_1}] \{\eta_1\} \end{array} \right\} + \begin{bmatrix} [\bar{q}_{c_1}] & ([\bar{q}_{d_1}] - [\bar{q}_{c_1}]) [A^{12}] \\ -[S_1] & ([S_1] - [\Phi_{d_1}]) [A^{12}] \end{bmatrix} \begin{Bmatrix} \{\lambda_1\} \\ \{\lambda_2\} \end{Bmatrix} \end{aligned} \quad (8.57)$$

At the inertia element $\{m\}$ of link 2

$$m_2 \{\ddot{P}_{c_2}\} = m_2 \{g\} + [A^{02}] \{\lambda_2\} \quad (8.58)$$

At the inertia element $\{M_{\xi}\}$ of link 2

$$\begin{aligned}
[M_{\xi_2}] \{\xi_2\} &= \begin{bmatrix} [J_2] & [D_2]^T \\ [D_2] & [M_2] \end{bmatrix} \begin{Bmatrix} \{\Omega_2\} \\ \{\ddot{\eta}_2\} \end{Bmatrix} = \{e_{\xi_2}\} \\
&= \begin{Bmatrix} ([\bar{H}_2] - [J^*_{2}]) \{\Omega_2\} + [\bar{q}_{c_2}] \{\lambda_2\} \\ -[G_2] \{\dot{\eta}_2\} - [K_{eq2}] \{\eta_2\} - [S_2] \{\lambda_2\} \end{Bmatrix} \\
&= \begin{Bmatrix} ([\bar{H}_2] - [J^*_{2}]) \{\Omega_2\} \\ -[G_2] \{\dot{\eta}_2\} - [K_{eq2}] \{\eta_2\} \end{Bmatrix} + \begin{bmatrix} [0] & [\bar{q}_{c_2}] \\ [0] & -[S_2] \end{bmatrix} \begin{Bmatrix} \{\lambda_1\} \\ \{\lambda_2\} \end{Bmatrix} \quad (8.59)
\end{aligned}$$

In the same arrangement of equations (8.50) to (8.53), equations (8.56) to (8.59) can be written into a compact form as

$$\begin{aligned}
&\begin{bmatrix} m_1 [I] & [0] & [0] & [0] & [0] & [0] \\ [0] & m_2 [I] & [0] & [0] & [0] & [0] \\ \hline [0] & [0] & [J_1] & [D_1]^T & [0] & [0] \\ [0] & [0] & [D_1] & [M_1] & [0] & [0] \\ [0] & [0] & [0] & [0] & [J_2] & [D_2]^T \\ [0] & [0] & [0] & [0] & [D_2] & [M_2] \end{bmatrix} \begin{Bmatrix} \{\ddot{P}_{c_1}\} \\ \{\ddot{P}_{c_2}\} \\ \{\Omega_1\} \\ \{\dot{\eta}_1\} \\ \{\Omega_2\} \\ \{\dot{\eta}_2\} \end{Bmatrix} = \begin{Bmatrix} \{0\} \\ \{0\} \\ ([\bar{H}_1] - [J^*_{1}]) \{\Omega_1\} \\ -[G_1] \{\dot{\eta}_1\} - [K_{eq1}] \{\eta_1\} \\ ([\bar{H}_2] - [J^*_{2}]) \{\Omega_2\} \\ -[G_2] \{\dot{\eta}_2\} - [K_{eq2}] \{\eta_2\} \end{Bmatrix} \\
&+ \begin{bmatrix} [A^{01}] & -[A^{02}] \\ [0] & [A^{02}] \\ \hline [\bar{q}_{c_1}] & ([\bar{q}_{d_1}] - [\bar{q}_{c_1}]) [A^{12}] \\ -[S_1] & ([S_1] - [\Phi_{d_1}]) [A^{12}] \\ [0] & [\bar{q}_{c_2}] \\ [0] & -[S_2] \end{bmatrix} \begin{Bmatrix} \{\lambda_1\} \\ \{\lambda_2\} \end{Bmatrix} + \begin{Bmatrix} m_1 \{g\} \\ m_2 \{g\} \\ \{0\} \\ \{0\} \\ \{0\} \\ \{0\} \end{Bmatrix} \quad (8.60)
\end{aligned}$$

or in a compact form with matrices corresponding to elements divided by dashed lines

$$\begin{bmatrix} [M^{dd}] & [0] \\ [0] & [M^{ii}] \end{bmatrix} \begin{Bmatrix} \{\ddot{q}_d\} \\ \{\ddot{q}_i\} \end{Bmatrix} = \begin{Bmatrix} \{0\} \\ \{Q^i\} \end{Bmatrix} + \begin{Bmatrix} [L_d]^T \{\lambda\} \\ [L_i]^T \{\lambda\} \end{Bmatrix} + \begin{Bmatrix} \{F^d\} \\ \{0\} \end{Bmatrix} \quad (8.61)$$

Both equations (8.49) and (8.60) or (8.61) are equations of motion of the system generated from the multibond graph in Figure 8-5. Equation (8.61) is the differential equation and equation (8.49) is the algebraic equation. These equations have the form of equations (8.1) and (8.4).

It has therefore been demonstrated that equations of motion generated from mixed causal multibond graphs, described earlier, are the same as the form of partitioned coordinates of equations of motion (8.49) and (8.60) or (8.61).

First, the equations of constraints (8.45) generated from mixed causal multibond graphs is the coordinate partitioned form of equations of constraints (8.49). This can be seen from the comparison of equations (8.45) and coordinate partitioned equations (8.54) and (8.55), which are same.

Secondly, Eliminating Lagrange multipliers $\{\lambda\}$ from equations (8.61) following the coordinate partitioning method, there is

$$[M^{ii}] \{\ddot{q}_i\} + [L]^*{}^T [M^{dd}] \{\ddot{q}_d\} = \{F^i\} + [L]^*{}^T \{Q^d\} \quad (8.62)$$

This equation is exactly the same as equation (8.44) that is generated from mixed causal multibond graph.

8.4.3 Numerical Algorithms

The equations of motion generated from two types of multibond graphs of flexible multibody systems have been verified to have the forms of maximum variables and minimum variables. They are all differential/algebraic equations in both types of multibond graphs. Both types of these DAE systems can be solved by implicit numerical integration for differential equations as discussed earlier. These equations can also be converted into differential equations, only, by differentiating the velocity constraint conditions equations (8.45) and (8.49) once. However, this method does not add value or provide benefits. Because vibration modes are included in the model, which contains high frequency components, the numerical stability must be ensured by

either taking very small time steps for an explicit integration or adopting an implicit integration procedure. Therefore, implicit integration methods for DAE systems discussed earlier are more suitable for solving equations of motion.

- Chapter 9 -

Applications

9.1 Introduction

The purpose of this chapter is to illustrate the validity of the multibond graph method developed in this thesis and the capability of a computer interface for generating multibond graphs. This will be done by the application of multibond graph method to examples. These examples are:

- (1) a flexible rotating beam,
 - (2) a crank-rocker mechanism with flexible coupler,
- and (3) a flexible robotic manipulator system.

The rotating beam included in this chapter is to show the vibration behavior of a flexible body undergoing high speed rotation. The example of crank-rocker mechanism is to demonstrate the procedure of multibond graph modelling for a practical engineering problem. It also illustrates the behavior for a flexible coupler in multibody systems. The dynamic simulation of the flexible robotic manipulator demonstrates another application area of the multibond graph technique.

9.2 Computer Program MULBOND

MULBOND is a computer program, designed in SUN workstation and SUNVIEW graphics user interface, which can also be run in X-Window interface. It was developed to implement the modelling and simulation methods discussed in the previous chapters. *MULBOND* is intended to assist engineers in modelling and analyzing the kinematic and dynamic behavior of planar and spatial mechanical systems using multibond graph techniques [He and ElMaraghy, 1992].

MULBOND uses multibond graphs to model physical systems, and generates equations of motion suitable for solution analysis by the standard simulation language software ACSL [Mitchell and Gauthier Associates, 1987]. An interactive, graphics-oriented editor is provided which permits convenient model construction and editing. This editor provides a standard set of multibond graph elements and other editing functions for the modelling. The output of this program is a source file written for ACSL which can be compiled and executed by ACSL for system simulation.

MULBOND uses one main window and several different panels. They are shown in the following figures (Figure 9-1 to Figure 9-10). In terms of functions, working areas are those areas in which models are constructed and results are displayed. Panels exist to support these working area operations by making available "point and click" function execution, and by displaying filenames and current directories. The details of this program can be found in its user manual [He and ElMaraghy, 1992].

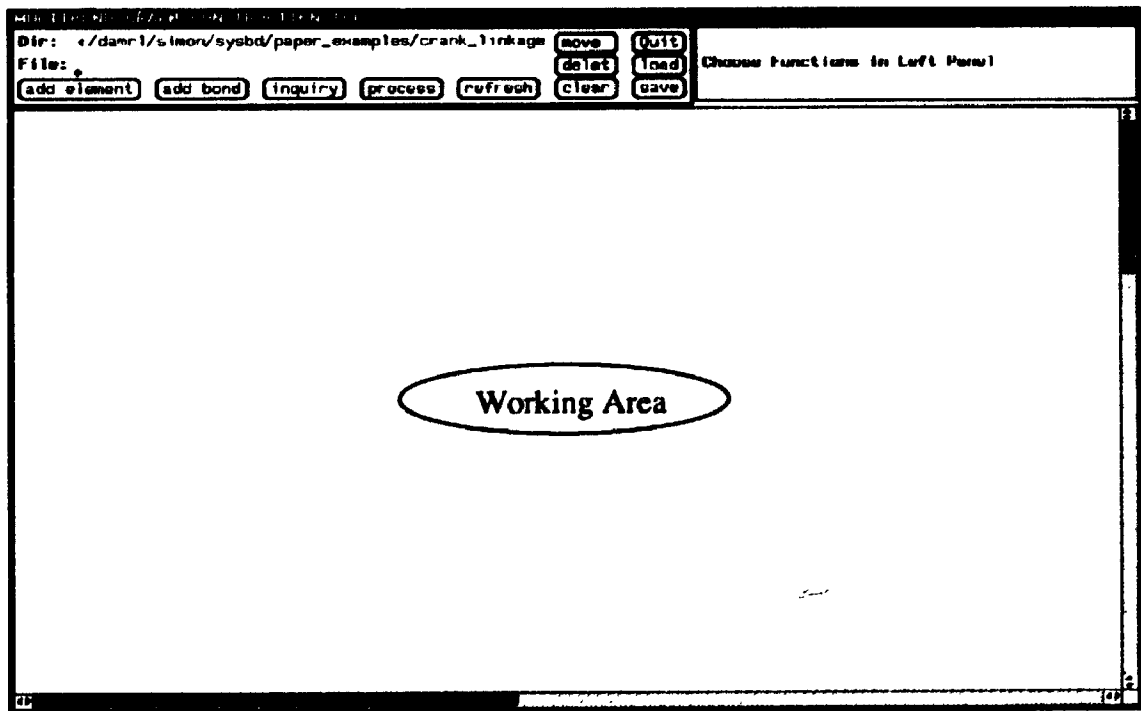


Figure 9-1 Environment of MULBOND for multibond graph construction

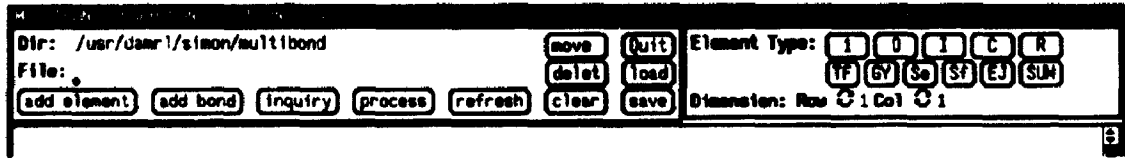


Figure 9-2 "add element" panel

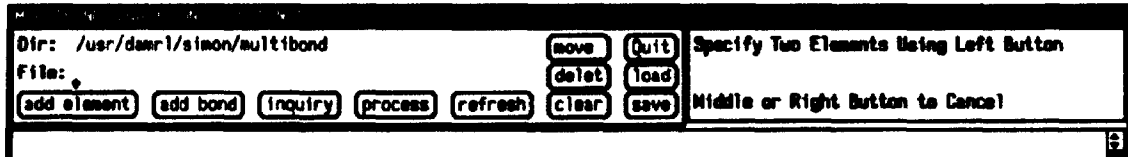


Figure 9-3 "add bond" panel

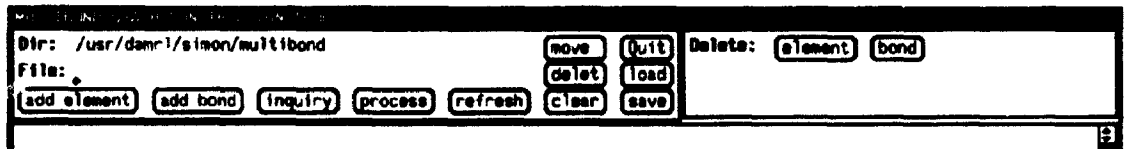


Figure 9-4 "delete" panel

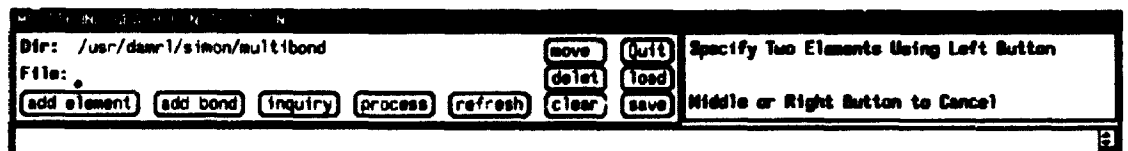


Figure 9-5 "move" panel

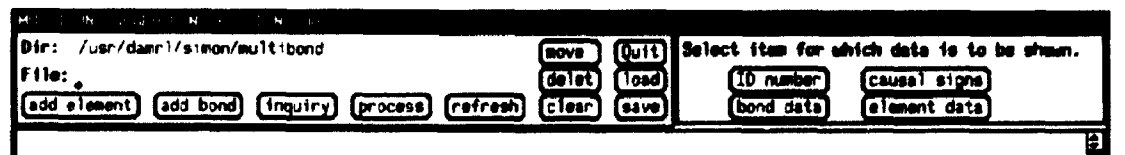


Figure 9-6 "inquiry" panel

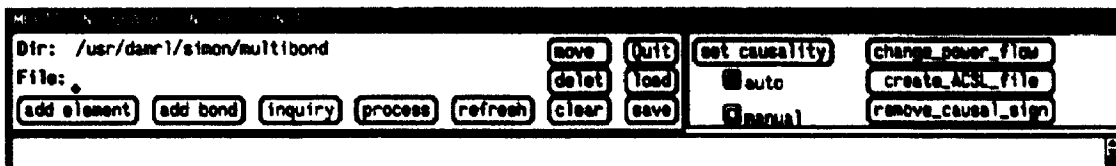


Figure 9-7 "process" panel

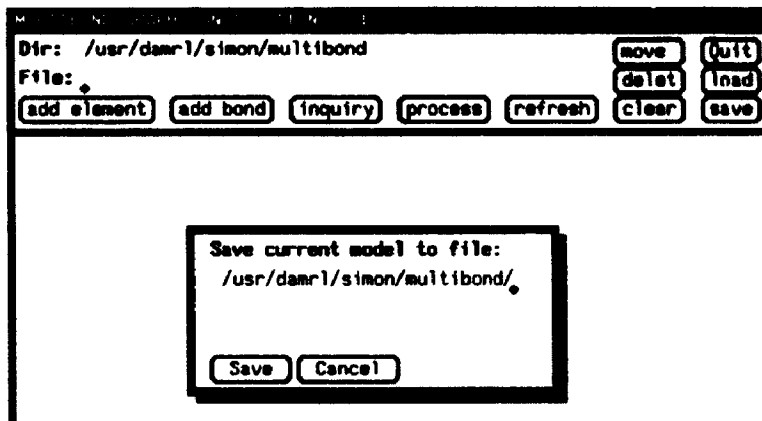


Figure 9-8 "Save" frame

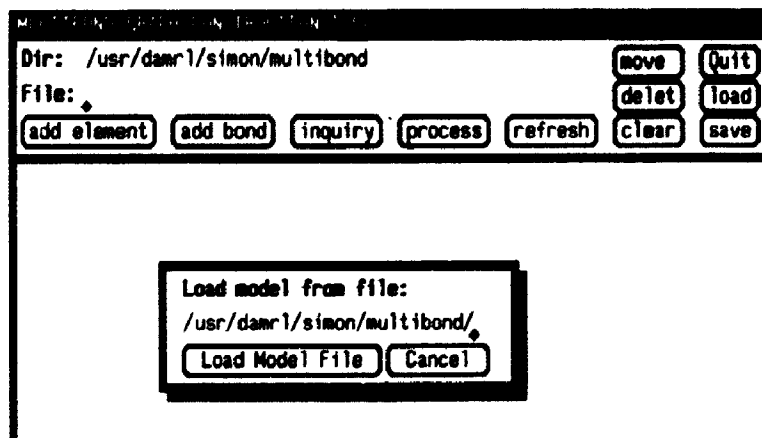


Figure 9-9 "load" frame

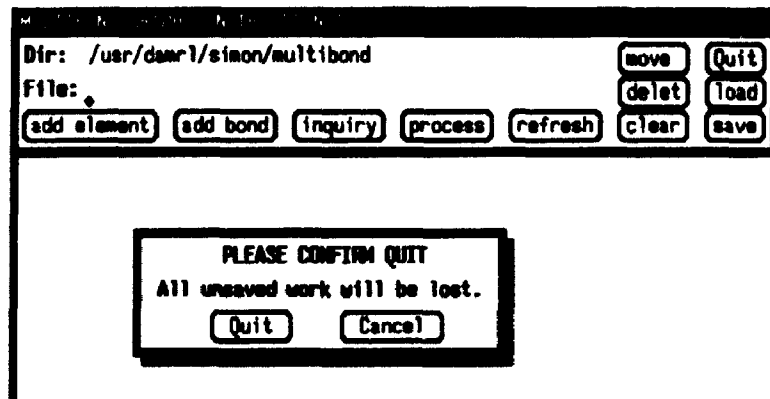


Figure 9-10 "Quit" frame

9.3 A Rotating beam

A long slender beam built into a rigid shaft is shown in Figure 9-11. The geometric data of this beam are also shown in the figure. The shaft is driven and rotates about the vertical z -axis and the beam vibrates in the horizontal x - y plane. This rotating beam model is applicable for helicopter blades, turbine blades, satellite antennae and flexible robot arms. In such applications, the dynamic stiffening effects due to the presence of axial centrifugal forces have significant influence on the prediction of transverse vibrations of the beam.

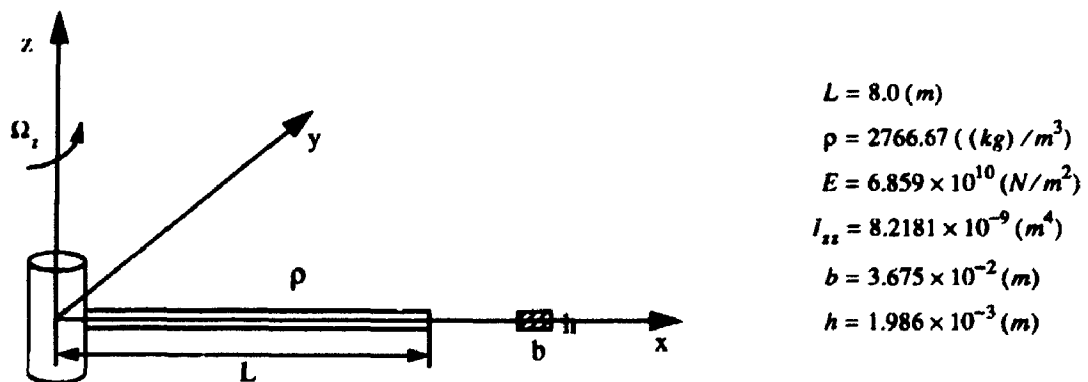


Figure 9-11 Rotating beam example

For a 2-D Euler beam shown in Figure 9-12, non-linear strain formula discussed in Chapter 4 can be simplified as follows.

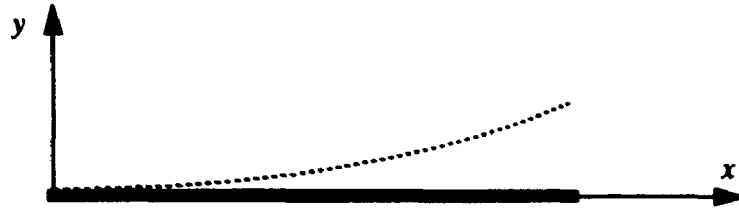


Figure 9-12 2-D Euler beam

Let \bar{u} , \bar{v} as the vibrational deformations of a point on the neutral axis of the beam along x and y axes, and using the assumed modes method

$$\bar{v} = \Phi_v^T(x) \{\eta\}_v \quad (9.1)$$

$$\bar{u} = \Phi_u^T(x) \{\eta\}_u \quad (9.2)$$

The deformations of any point in the 2-D beam are

$$u = \bar{u} - \frac{\partial \bar{v}}{\partial x} y \quad (9.3)$$

$$v = \bar{v} \quad (9.4)$$

Vector $\{\delta\}$ in equation (4.20) can be simplified accordingly

$$\{\delta\} = \{u_x \ u_y \ v_x \ v_y\}^T$$

$$= \begin{bmatrix} -\Phi_v^T y & \Phi_u^T \\ -\Phi_v^T & \mathbf{0} \\ \Phi_v^T & \mathbf{0} \\ \mathbf{0} & \mathbf{0} \end{bmatrix} \begin{bmatrix} \{\eta\}_v \\ \{\eta\}_u \end{bmatrix} = N_b \{\eta\} \quad (9.5)$$

where

$$N_b = \begin{bmatrix} -\Phi_{v,y}^T & \Phi_u^T \\ -\Phi_v^T & 0 \\ \Phi_v^T & 0 \\ 0 & 0 \end{bmatrix} \quad (9.6)$$

In terms of equations (4.17a) to (4.17f), only two elements in the strain vector are non-zero, which can also be simplified as

$$\{\epsilon\}_b = \begin{Bmatrix} \epsilon_x \\ \gamma_{xy} \end{Bmatrix} \quad (9.7)$$

By picking up corresponding elements in equation (4.23), the following are obtained

$$H_b^0 = \begin{bmatrix} 1 & 0 & 0 & 0 \\ 0 & 1 & 0 & 1 \end{bmatrix} \quad (9.8)$$

$$H_b^1 = \frac{1}{2} \begin{bmatrix} 1 & 0 & 0 & 0 \\ 0 & 0 & 0 & 0 \\ 0 & 0 & 1 & 0 \\ 0 & 0 & 0 & 0 \end{bmatrix} \quad (9.9)$$

$$H_b^A = \frac{1}{2} \begin{bmatrix} 0 & 1 & 0 & 0 \\ 1 & 0 & 0 & 0 \\ 0 & 0 & 0 & 1 \\ 0 & 0 & 1 & 0 \end{bmatrix} \quad (9.10)$$

Then the strain can be expressed as

$$\{\epsilon\}_b = B_b^0 \{\eta\} + \begin{Bmatrix} \{\eta\}^T B_b^1 \{\eta\} \\ \{\eta\}^T B_b^A \{\eta\} \end{Bmatrix} \quad (9.11)$$

where

$$B_b^0 = H_b^0 N_b \quad (9.12)$$

$$B_b^j = N_b^T H_b^j N_b \quad j = 1, 4 \quad (9.13)$$

These matrices are used to calculate stiffness matrices defined in equations (4.30) and (4.31) for 2-D beams.

Since this beam is connected to a rigid shaft, the bond graph for constraints introduced by Margolis and Karnopp [1979] is used, in which the constraints are modelled as artificial springs with high stiffness and extra compliance elements are added in the bond graph. This method is suitable for simple mechanical systems.

Figure 9-13 shows the multibond graph of the rotating beam in the window interactive environment. Since the beam is a slender beam, the shear deformation has been ignored. The first three normal modes of a cantilever beam are selected as the assumed modes to model the vibrational deformation of the beam.

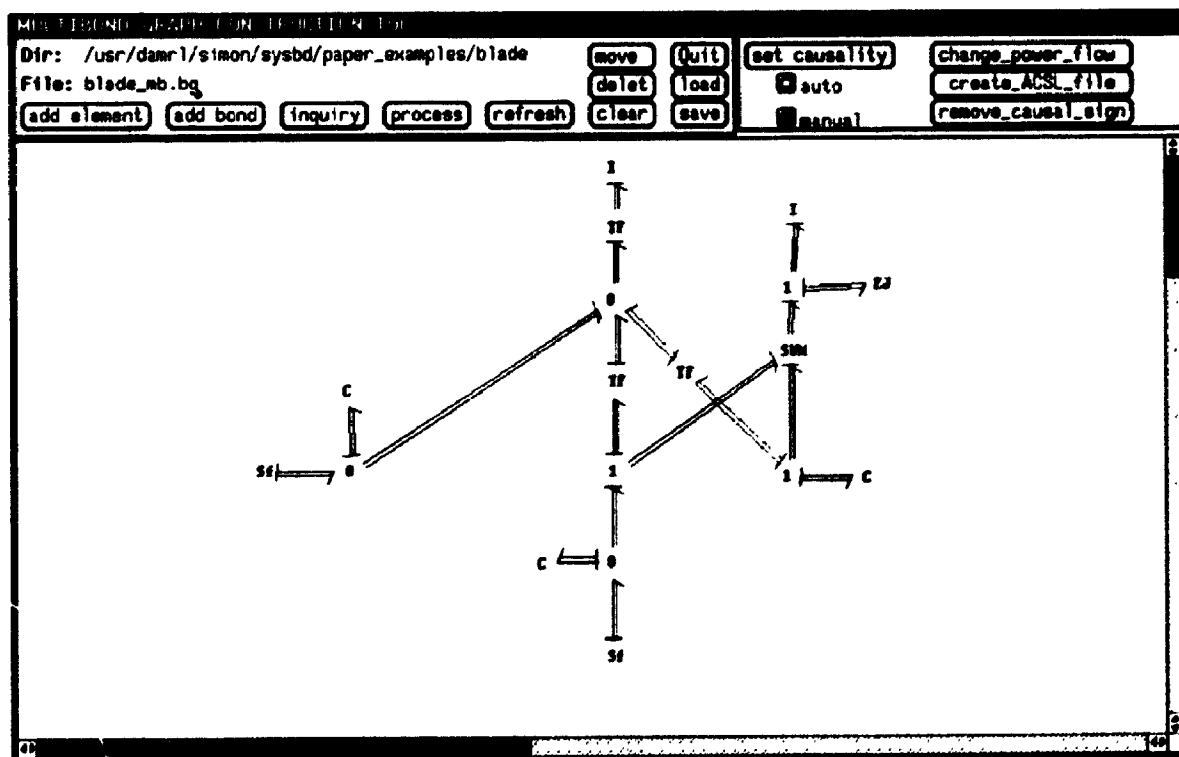


Figure 9-13 Multibond graph of the rotating beam in MULBOND environment

The natural frequencies of the rotating beam are calculated by assumed modes method with and without consideration of geometric stiffness as discussed in Chapter 2. The admissible functions for a uniform cantilever which has the same geometry as the rotating beam are employed as assumed modes [Craig, 1981]. They are

$$\phi_j = \cosh\left(\frac{\beta_j}{l}x\right) - \cos\left(\frac{\beta_j}{l}x\right) - \frac{(\cosh\left(\frac{\beta_j}{l}x\right) + \cos\left(\frac{\beta_j}{l}x\right))}{\sinh\left(\frac{\beta_j}{l}x\right) + \sin\left(\frac{\beta_j}{l}x\right)} \left[\sinh\left(\frac{\beta_j}{l}x\right) - \sin\left(\frac{\beta_j}{l}x\right) \right] \quad (9.14)$$

$$j = 1, \dots$$

where l is the length of the beam and β 's are roots of the characteristic equation

$$\cos\beta \cosh\beta + 1 = 0 \quad (9.15)$$

Based on equations (3.50), the eigen problems of this rotating beam, with and without consideration of geometric stiffness, are as follows

$$[[K] + \Omega^2 ([K_g] - [M])] \{a\} = \omega^2 [M] \{a\} \quad (9.16)$$

$$[[K] - \Omega^2 [M]] \{a\} = \omega^2 [M] \{a\} \quad (9.17)$$

where ω 's are the natural frequencies of the rotating beam and matrices $[K]$, $[K_g]$ and $[M]$ are calculated by equations (3.51) to (3.53)

The first two frequencies calculated from equations (9.16) and (9.17) are plotted in Figure 9-14. Solid lines show the eigenvalues of the rotating beam with consideration of geometric stiffness effects discussed earlier in Chapter 3. Dashed lines represent the eigenvalues of the rotating beam without the geometric stiffness terms. The eigenvalues at zero rotation speed represent the square of natural frequencies of a cantilever beam with same geometric data of this rotating beam. It can

be seen that the eigenvalues calculated with consideration of geometric stiffness increase as rotation speed goes up. This is the effect of geometric stiffness of a rotating beam. It can also be seen that the eigenvalues calculated without consideration of geometric stiffness decrease as rotation speed goes up. The first eigenvalue reaches zero when rotation speed is around the first natural frequency of the cantilever. This will cause the established model to become an unstable system. Of course, this is not valid. It indicates that the model without consideration of geometric stiffness of a rotating beam is incorrect.

The start up of this beam under a specified angular motion of the shaft is simulated. The angular velocity is assigned as

$$\Omega_s = \begin{cases} \frac{\bar{\Omega}_s}{T_s} \left[t - \frac{T_s}{2\pi} \sin\left(\frac{2\pi}{T_s} t\right) \right] & t < T_s \\ \bar{\Omega}_s & t \geq T_s \end{cases} \quad (9.18)$$

Simulations are carried out with $\bar{\Omega}_s = 2$ and $\bar{\Omega}_s = 4$ rad/s and $T_s = 15$ seconds. The simulation time is from 0 to 20 seconds. Tip deflections predicted by the multibond graph in Figure 9-13 with and without consideration of geometric stiffness are plotted in Figure 9-15.

These results show that with the increase of the rotating speed the geometric stiffness becomes more and more significant in prediction of transverse vibration behavior of a rotating beam. With $\bar{\Omega}_s = 4$ which is higher than the first natural frequency of the cantilever beam, the deflection predicted by the model without consideration of geometric stiffness diverges. This is because the model has become unstable.

This example indicates the importance of the consideration of nonlinear geometric stiffness for a flexible member undergoing relatively high speed rotation. Therefore, when the angular velocities of flexible bodies in a multibody system are not far lower than the first natural frequencies of these bodies, the geometric stiffness should be included.

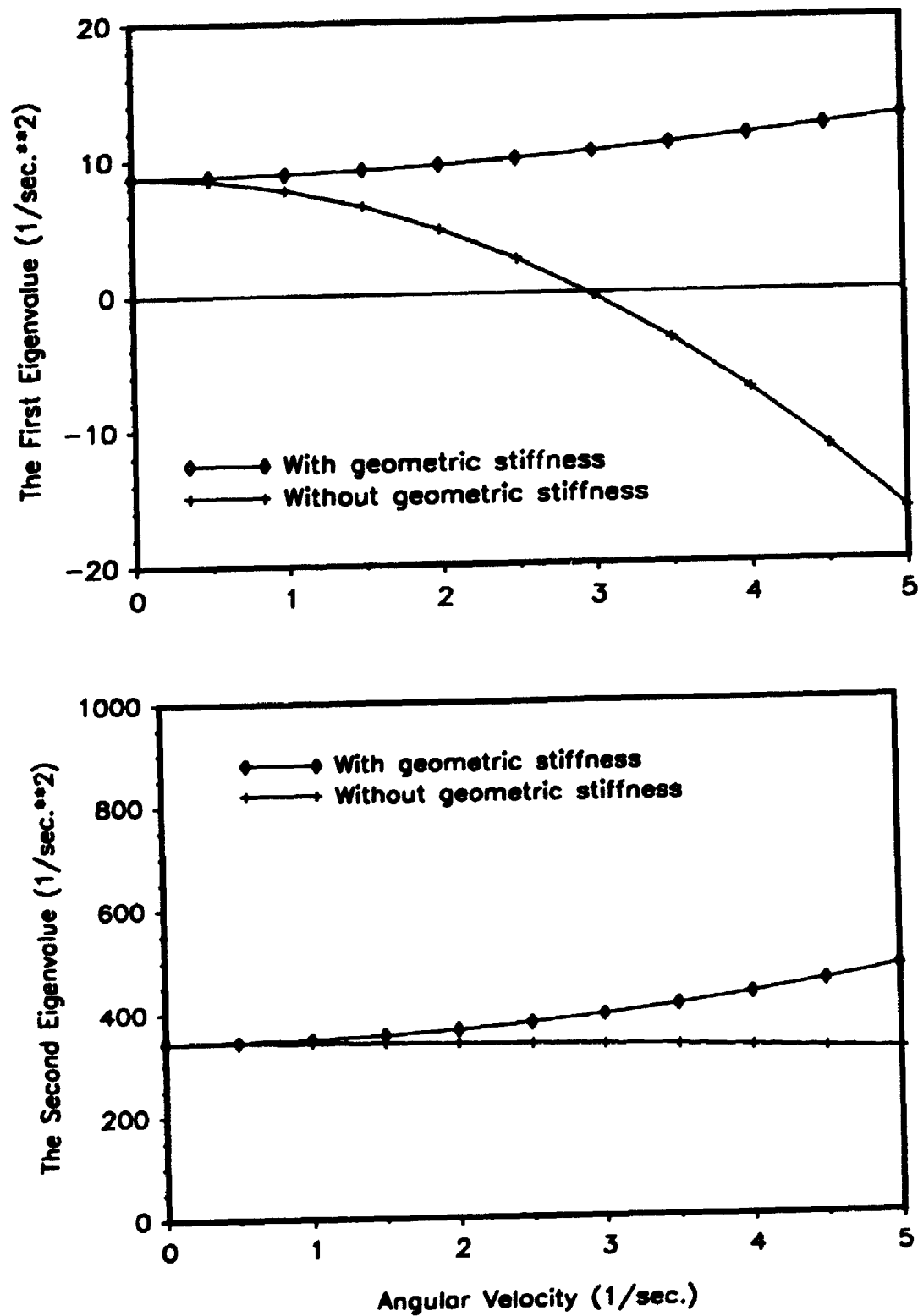


Figure 9-14 The first two eigenvalues of the rotating beam

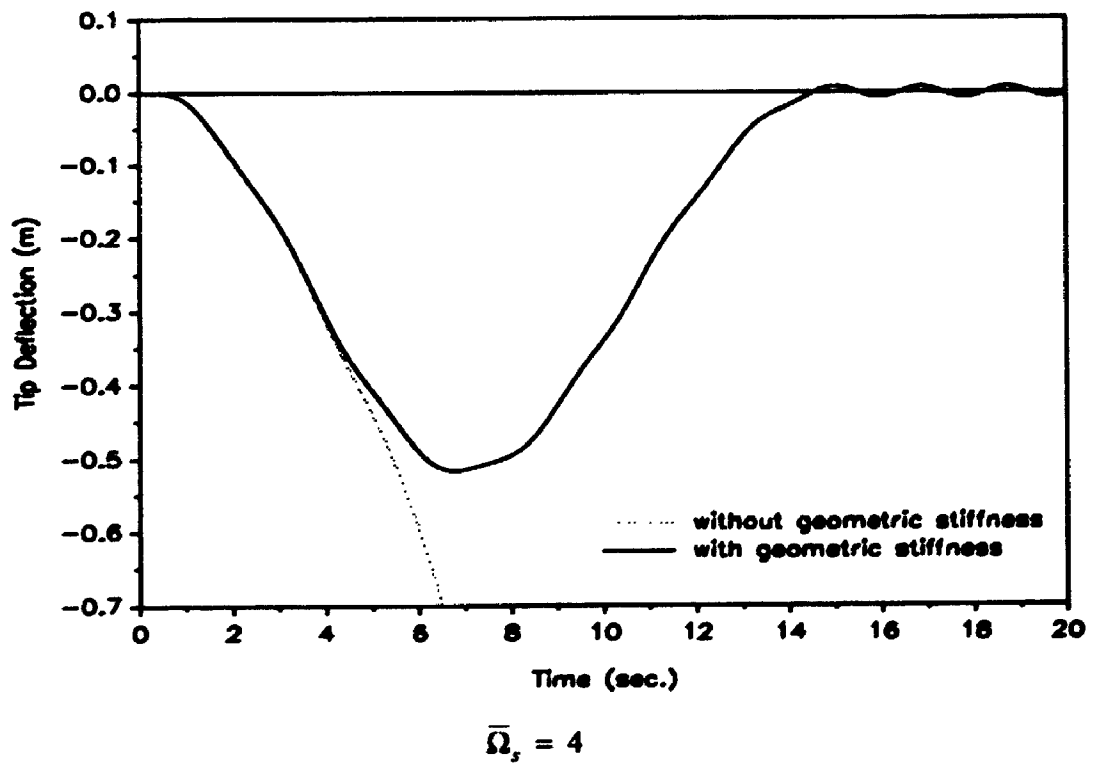
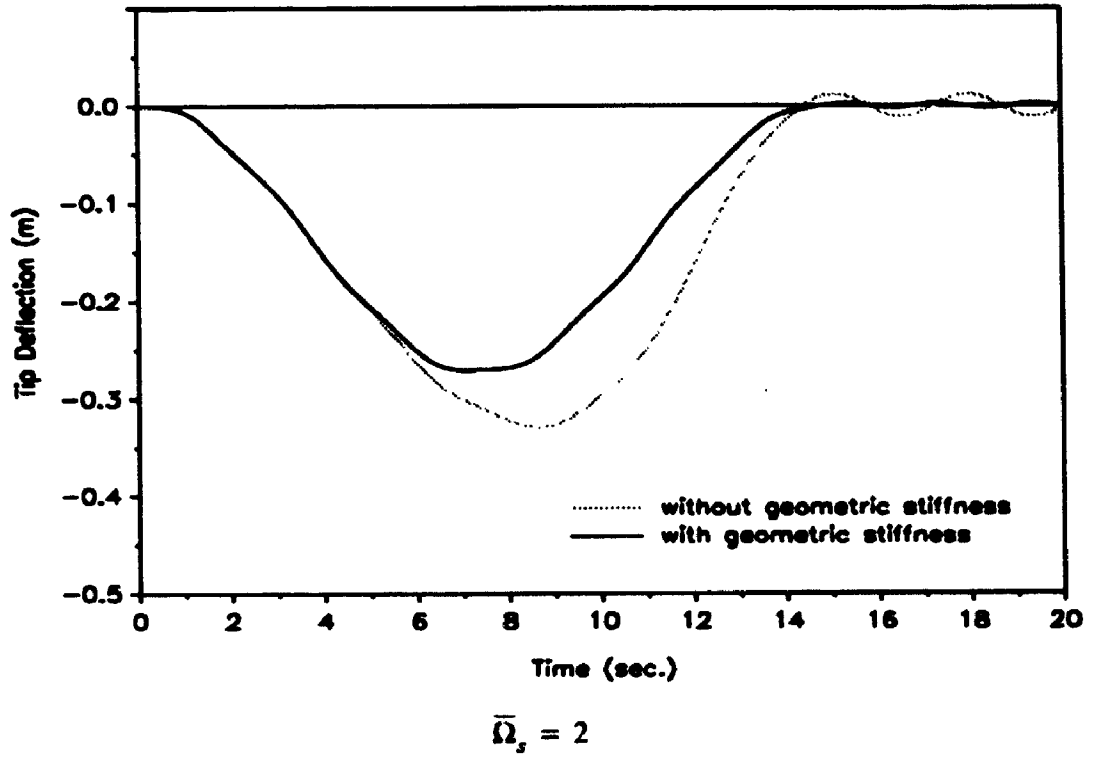


Figure 9-15 Tip deflections of the rotating beam in the rotation plane

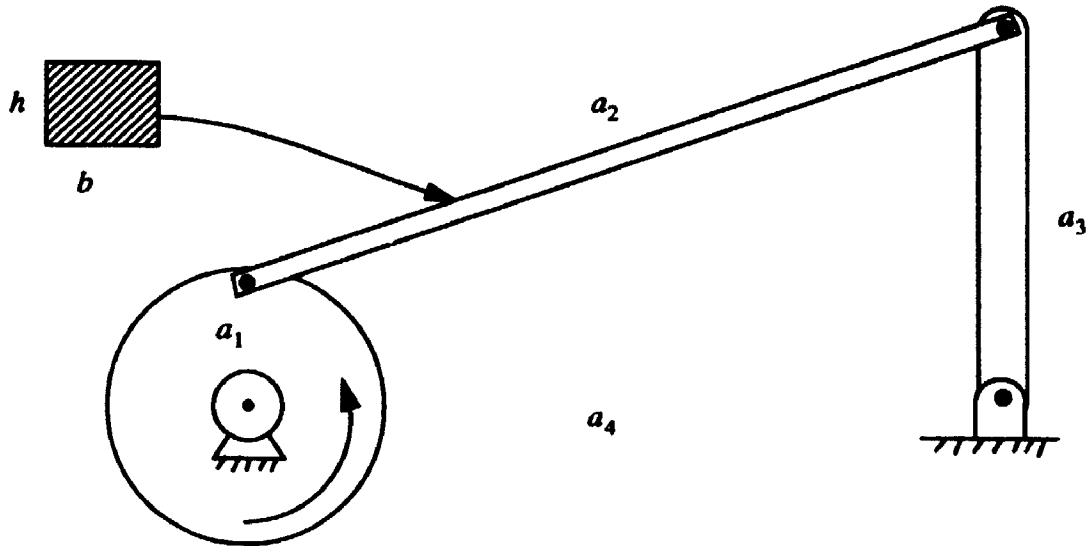
9.4 A Crank-Rocker Mechanism with Flexible Coupler

This example shows another aspect of the effects of nonlinear geometric stiffness on dynamic behavior of a flexible body in a multibody systems.

This crank-rocker mechanism is a planar four bar mechanism driven by a separately excited DC motor, which has been used by Samanta [1990] to illustrate his method for treating mechanical constraints in bond graphs. For comparison, all parameters are kept the same as in Samanta's paper.

Figure 9-16 shows the schematic diagram and physical parameters of the system. The crank and rocker are considered to be rigid bodies. The coupler is considered as a flexible beam. The multibond graph of this system is in Figure 9-17. Simulations of the actuator-mechanism dynamics during start-up are carried out using this multibond graph and the bond graph developed by Samanta [1990]. For the former, the first two normal modes of the coupler corresponding to hinged-hinged boundary condition and geometric stiffness due to the axial forces are considered. For the latter, as done by Samanta [1990], the first two normal modes of free-free beam are considered. Both bond graph models include 0.01 modal damping.

The simulations of the start-up of the system are implemented under the input voltage of 60V with these two bond graph models. The transient response is simulated in 1 second. The simulation results are plotted in Figure 9-18. In this case, most physical quantities of the system, e.g. the currents of the motor armature, the rotational speeds of the crank and the rocker, the resultant forces at joint 1 and along the longitudinal axis of the coupler, are almost the same. The predictions of the mid-point transverse deflections of the coupler by these two bond graphs have some differences. This is due to the effect of dynamic stiffening and softening on the transverse vibration caused by the dynamic axial forces in the coupler.



Mechanism Physical Properties:

$$a_1 = 0.102 \text{ (m)}, \quad a_2 = 0.610 \text{ (m)}, \quad a_3 = 0.406 \text{ (m)}, \quad a_4 = 0.559 \text{ (m)}$$

$$J_{1c} + J_{\text{motor}} = (0.00707 + 0.565) \text{ (Nm}\cdot\text{s}^2), \quad J_{3c} = 0.01245 \text{ (Nm}\cdot\text{s}^2)$$

$$J_{2c} = 0.042152 \text{ (Nm}\cdot\text{s}^2), \quad h = 0.010 \text{ (m)}, \quad b = 0.015 \text{ (m)}$$

Motor Physical Properties:

$$K_p = 0.678 \text{ (Nm/a)}, \quad r_a = 0.4 \text{ (ohms)}$$

$$L_a = 0.05 \text{ (henrys)}, \quad D = 0.226 \text{ (Nm/s)}$$

Figure 9-16 Crank-rocker mechanism example

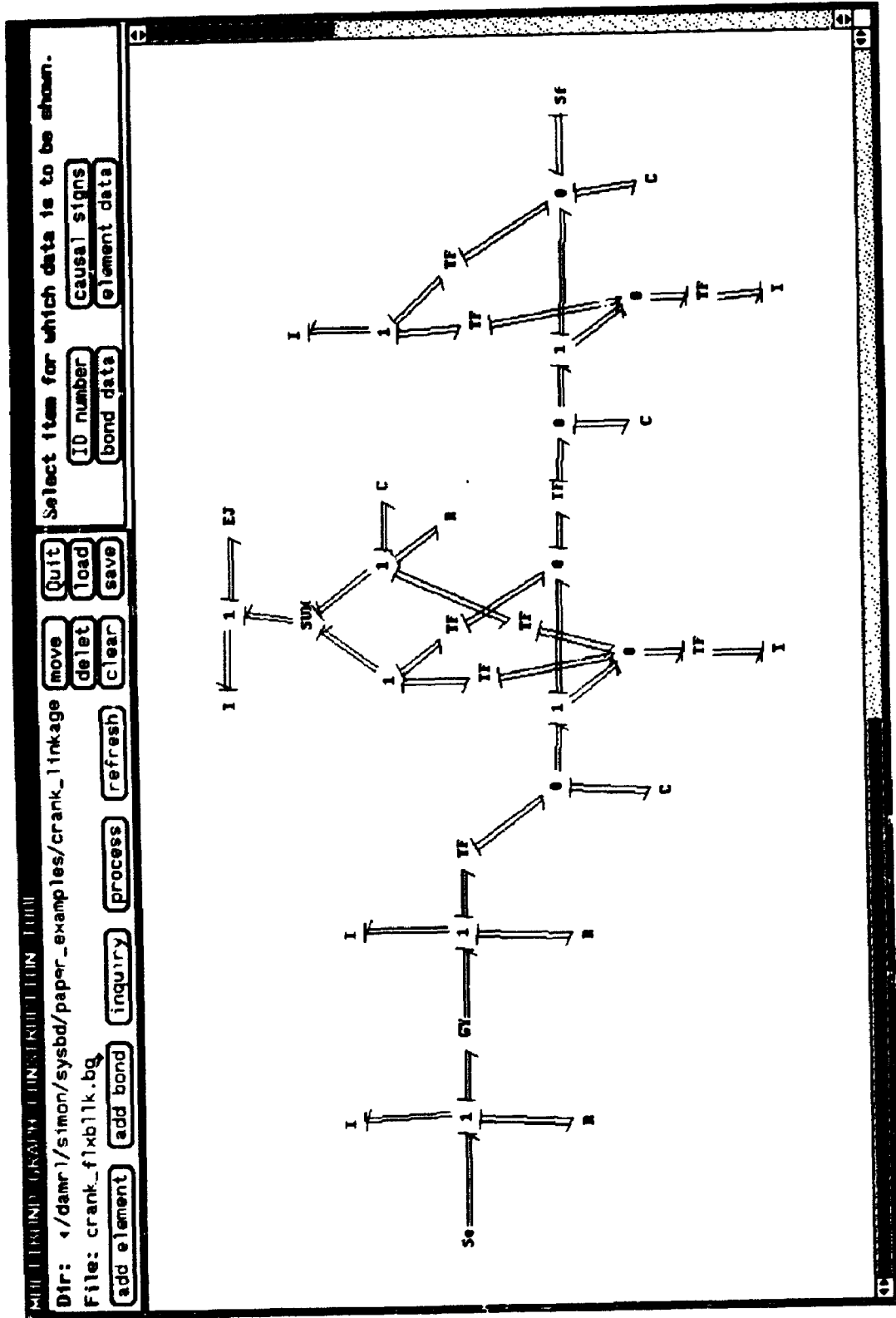


Figure 9-17 Multibond graph of the crank-rocker mechanism

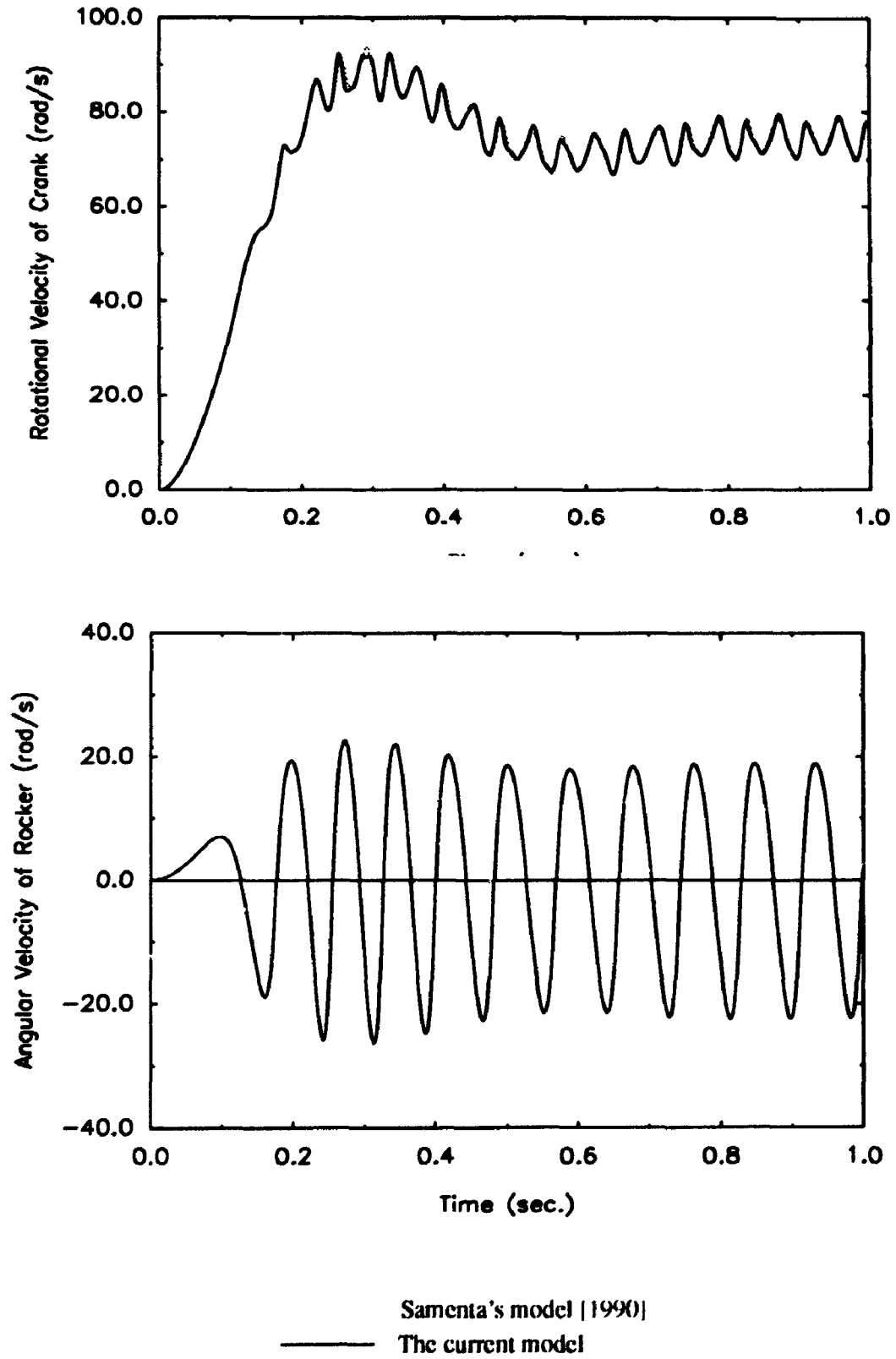


Figure 9-18 Transient response during start-up of a crank-rocker mechanism

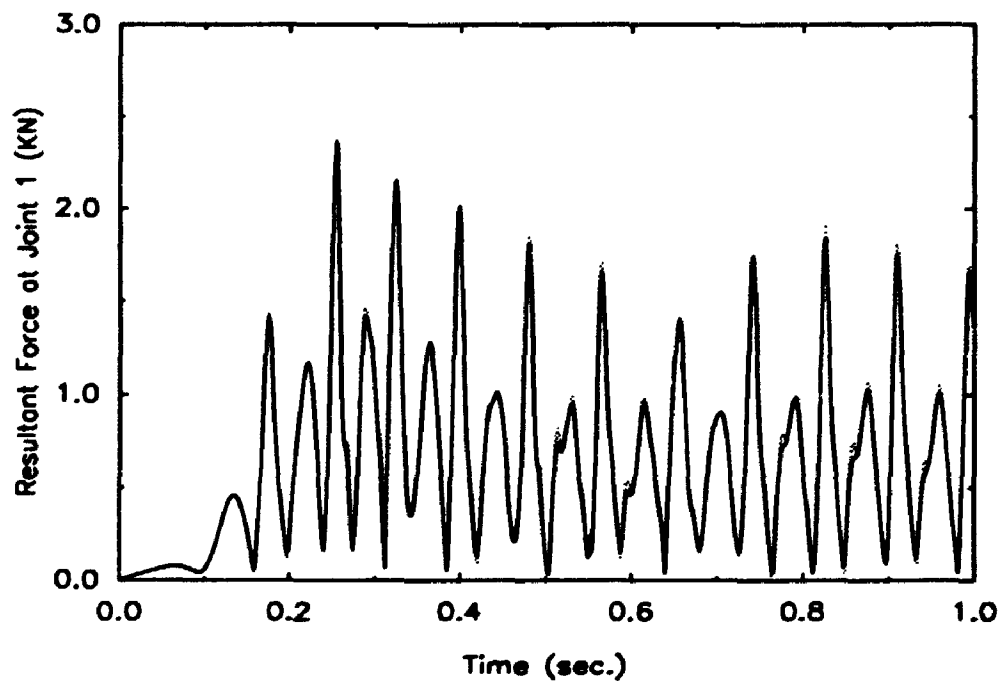
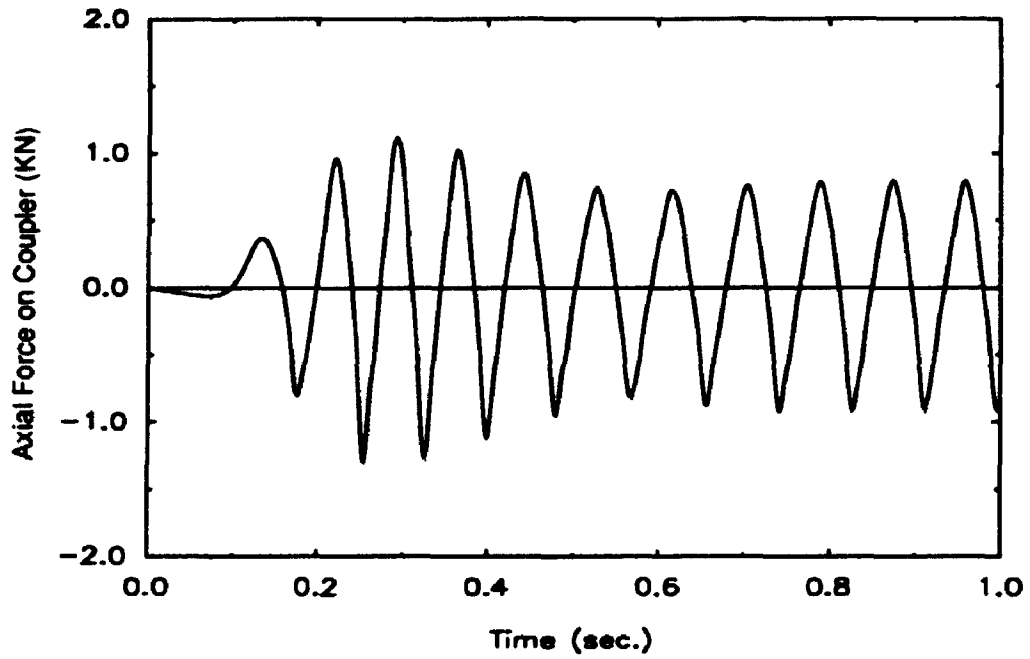


Figure 9-18 (Continued)

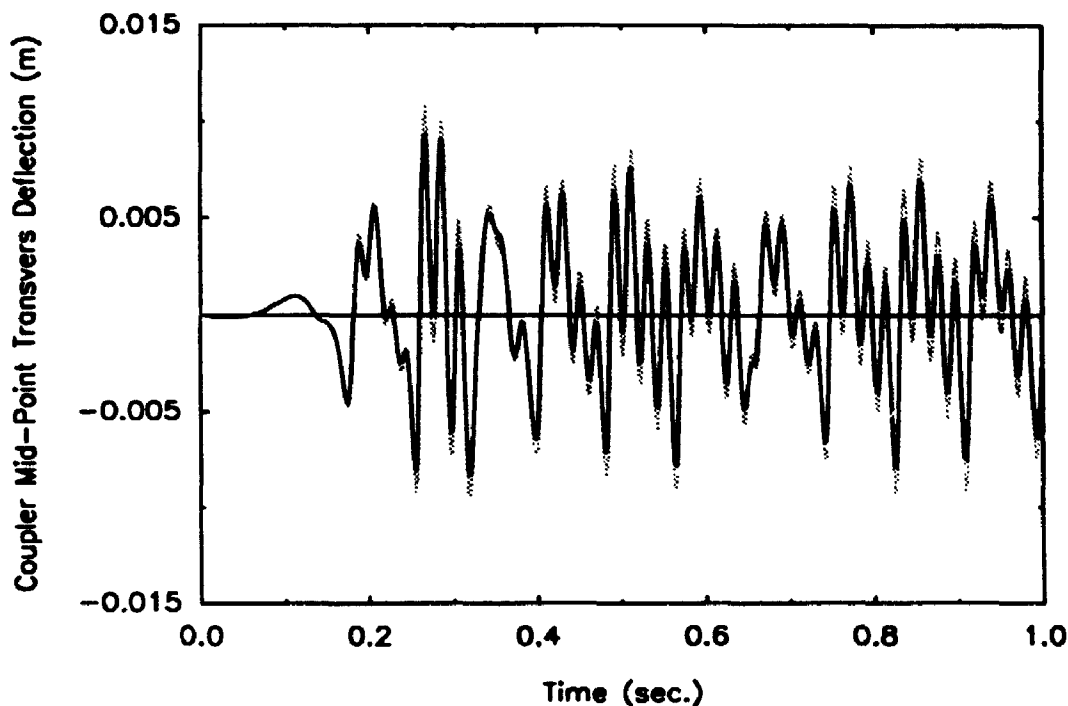
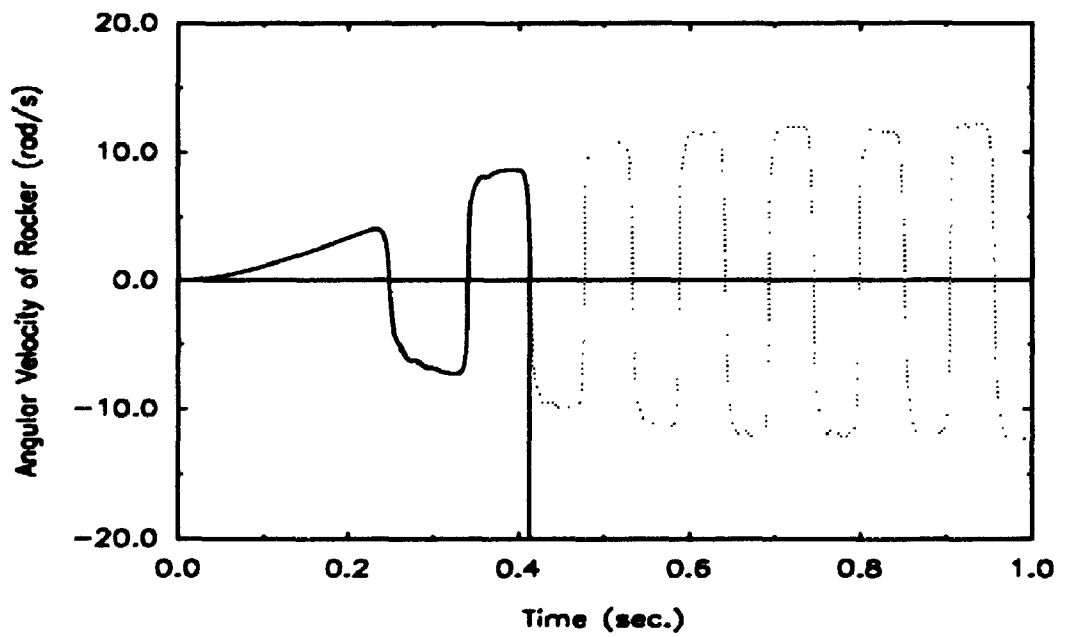
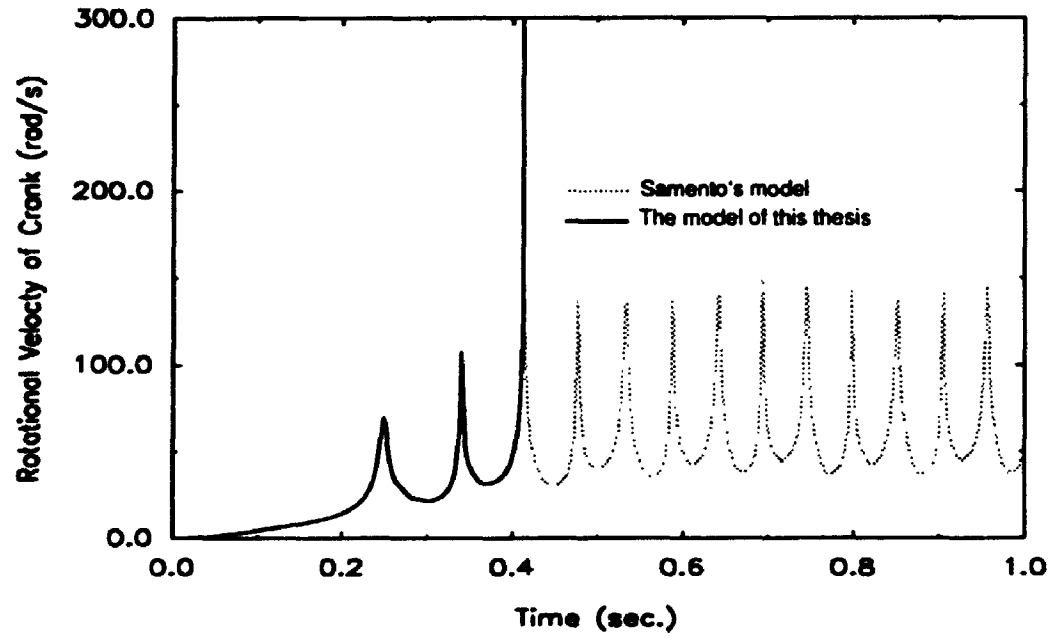


Figure 9-18 (Continued)

To further investigate the effect of dynamic stiffening and softening in this mechanism, the mass and the moment of inertia of the driven rocker are increased by 200 times the original one, and all other parameters are kept unchanged. This will increase the axial load to the coupler and so increase the effect of stiffening and softening. The simulation results are plotted in Figure 9-19. An interesting phenomenon happens in this case. At about 0.4 second from the start, the digital simulation overflows and all quantities diverge. Checking the plots, after the first rotation, a very large compressive axial load in the coupler is found which causes the buckling of the coupler because the coupler is a simple supported column in compression loading. Note that the model can identically predict buckling as the softening effect, due to compression, is included. This buckling caused the whole dynamic model of the system to become unstable and so the digital simulation overflowed. On the contrary, the bond graph model proposed by Samanta [1990] cannot predict this buckling and gives incorrect simulation results, which can be seen clearly in these figures.



..... Samento's model [1990]
 ——— The current model

Figure 9-19 Transient response during start-up of crank-rocker mechanism

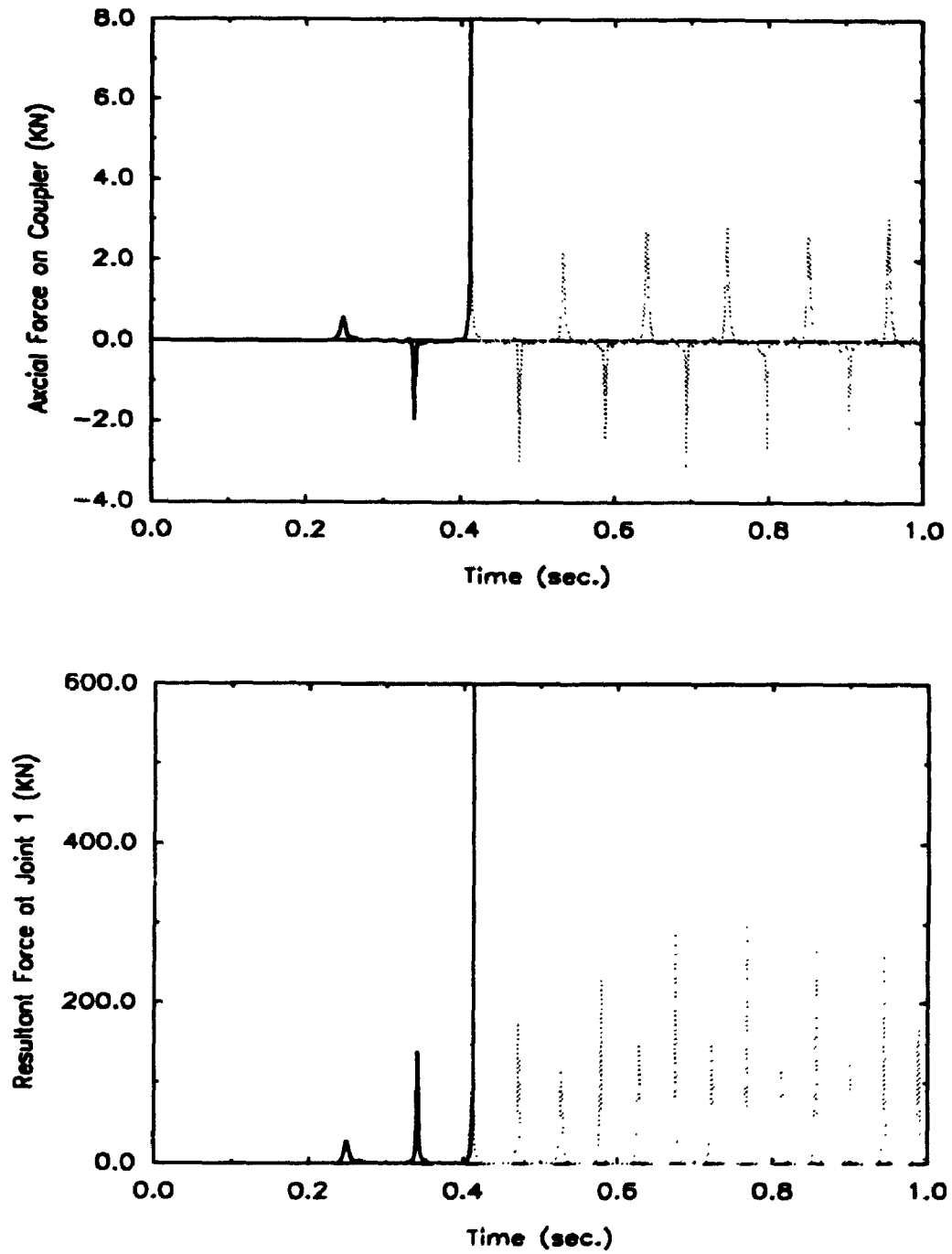


Figure 9-19 (Continued)

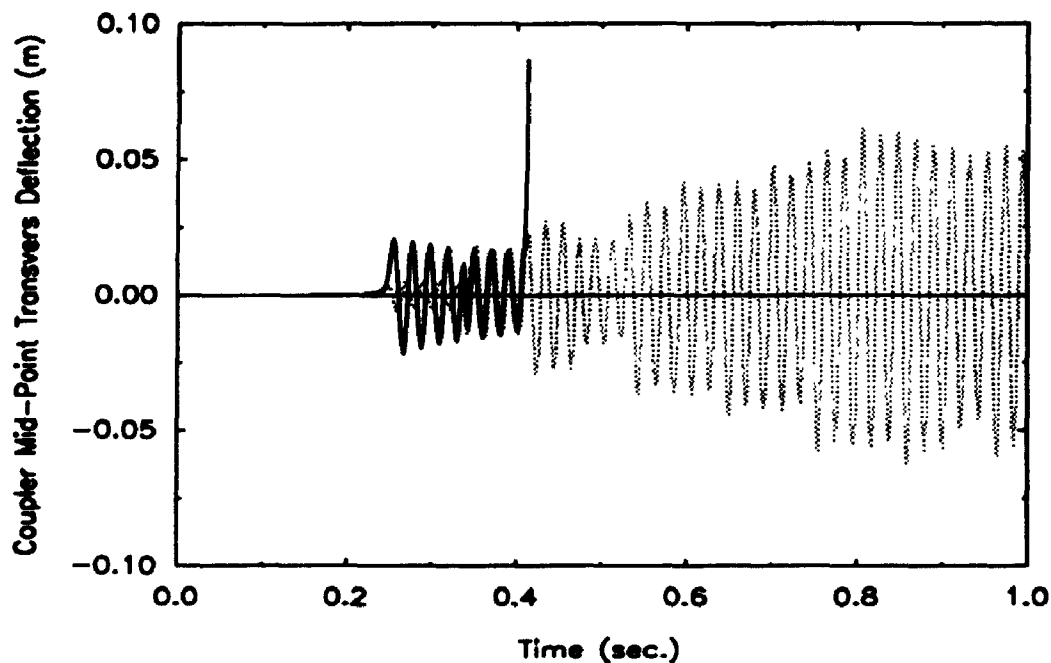


Figure 9-19 (Continued)

9.5 A Flexible Robotic Manipulator System

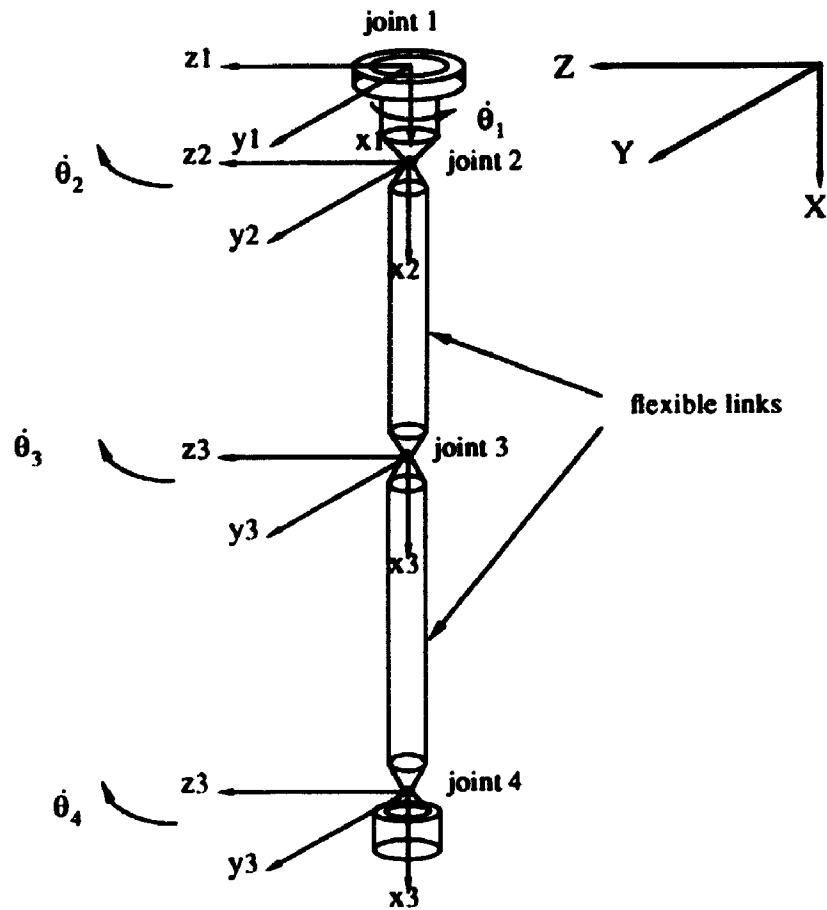
A flexible manipulator system that consists of two slender flexible links and two other links modelled as rigid bodies and which is used on a space shuttle or a space station is shown in Figure 9-20. Bodies 2 and 3 in the model are flexible tubular beams with circular cross-section. Each body is connected to its inboard body by a pin joint with rotation axes along z axes of their local reference frames. Body 1 is connected to the body of a space shuttle or a space station through a rotation base which can only rotate about the X axis. Body 4 is a payload of mass 200 kg. Inertia properties of components of the system, in their undeformed states, are presented in Table 9-1.

The initial configuration of the manipulator is shown in Figure 9-20; and gravity is considered negligible. Based on the discussion in previous chapters, the multibond

graph of this system can be created as in Figure 9-21. To avoid derivative causality, artificial compliant elements are introduced at each joint. The stiffness of these artificial compliant elements are chosen much higher than those of the flexible members so that the simulation results are not influenced by the artificial compliance.

Table 9-1 Geometric data of the flexible manipulator system

Body number	Mass (kg)	Principle moment of inertia (kg-m ²)		
		I _{xx}	I _{yy}	I _{zz}
1	50.0	0.00469	0.0195	0.0195
2	30.52	0.06250	40.7300	40.7300
3	38.16	0.07820	79.5300	79.5300
4	200.0	0.00782	0.0834	0.0834



Length of links:

$$L1 = 0.3 \text{ m} \quad L2 = 4.0 \text{ m}$$

$$L3 = 5.0 \text{ m} \quad L4 = 0.5 \text{ m}$$

Cross-section of link 2 & 3:

$$r_i = 0.04 \text{ m}$$

$$r_o = 0.05 \text{ m}$$



Young's modulus and mass density of link 2 & 3:

$$E = 6895 \cdot 10^7 \text{ N/m}^2$$

$$\rho = 2699 \text{ kg/m}^3$$

Figure 9-20 Flexible manipulator system example

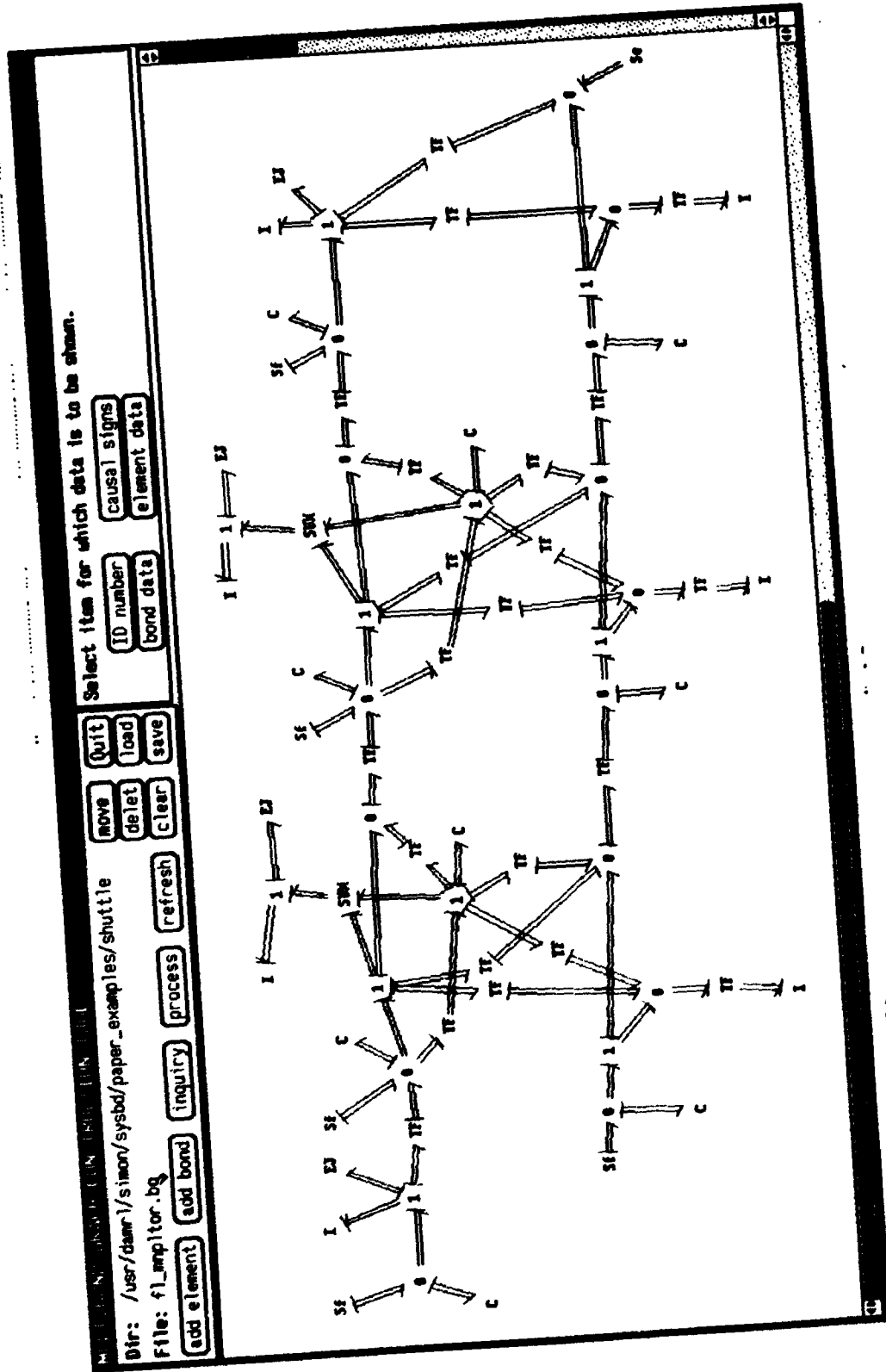


Figure 9-21 Multibond graph of the flexible manipulator system

To consider the vibrations of the flexible links according to the boundary conditions in this system, the first four normal modes of link 2 and link 3 are employed, two in the x-y plane and two in the x-z plane of the local reference frame. Due to the properties of pin joints at joint 2, joint 3, and joint 4, the normal modes of a cantilever are selected as the assumed modes in the x-z plane, and the normal modes of a simply supported beam are selected as the assumed modes in the x-y plane. They are

$$\Phi_{jxz} = \cosh\left(\frac{\beta_j}{l}x\right) - \cos\left(\frac{\beta_j}{l}x\right) - \frac{(\cosh\left(\frac{\beta_j}{l}x\right) + \cos\left(\frac{\beta_j}{l}x\right))}{\sinh\left(\frac{\beta_j}{l}x\right) + \sin\left(\frac{\beta_j}{l}x\right)} \left[\sinh\left(\frac{\beta_j}{l}x\right) - \sin\left(\frac{\beta_j}{l}x\right) \right] \quad (9.19)$$

$$\Phi_{jxy} = \sin\left(\frac{\beta_j}{l}x\right) \quad (9.20)$$

Two kinds of motion of this manipulator system are investigated. One is a planar maneuver, and the other is a 3-D maneuver. Torsional stiffness of the links are included in 3-D maneuver, but torsional vibrations of the links are ignored.

In the planar maneuver, joint 1 is fixed and the other three joints are subjected to the angular changes about z axes as follows

$$\theta_2 = \theta_3 = \frac{\pi}{4T_s} \left[t - \frac{T_s}{2\pi} \sin\left(\frac{2\pi}{T_s}t\right) \right] \quad t \leq T_s \quad (9.21)$$

$$\theta_2 = \theta_3 = \frac{\pi}{4} \quad t > T_s \quad (9.22)$$

$$\theta_4 = \frac{\pi}{T_s} \left[t - \frac{T_s}{2\pi} \sin\left(\frac{2\pi}{T_s}t\right) \right] \quad t \leq T_s \quad (9.23)$$

$$\theta_4 = \frac{\pi}{2} \quad t > T_s \quad (9.24)$$

where T_s is a time constant determined by the duration of the maneuver.

To investigate the influence of the flexibility of links on the maneuver of this

manipulator system, the ideal trajectory of this manipulator system with all links considered as rigid links is also calculated under the motion described by equations (9.21) to (9.24).

For this maneuver, the time constant T_r is chosen as 15 seconds. The duration of simulation for the transient response of the system is chosen as 20 seconds. The ideal payload tip trajectory and the joint angle movements are plotted in Figure 9-22. The joint torques required to achieve this movement are also calculated and plotted in Figure 9-23. The positions of this manipulator at different time points during the maneuver are shown in Figure 9-24.

Under the same maneuver, the motion of the flexible manipulator is simulated. The tip deviation and required joint driving torques are plotted in Figure 9-23 with comparison to the results from the rigid link manipulator system. From the comparison, the influence of the flexible links is very clear. It not only adds deviations to the tip position, which reduce the precision of the work, but it also changes the driving joint torques required to implement this maneuver. This change to the driving torque is a critical fact for the inverse dynamic control of the manipulator. This can be seen in the following simulation.

If the manipulator is a rigid link system and the joint torques obtained in the simulation plotted as solid lines in Figure 9-23 are input at the joints, the resultant motion should be as described by equations (9.21) to (9.24) and Figure 9-22. Now the real system has two flexible links. If these same torques are input to the system, the simulation results show that unacceptable errors of the position of the manipulator during the whole maneuver develop. The positions of the flexible manipulator are far from the positions expected. These results are plotted as dashed lines in Figure 9-24. Therefore, the consideration of the flexibility of real systems is very critical to position of dynamic simulation and control of the system.

In the spatial maneuver, the whole system is undergoing a 3-D motion with an angle driver in each joint. The relative angular displacements θ_i imposed at joint 2 to joint 4 are the same as the planar motion. The rotation of the base is imposed along x axis of body 1 as following

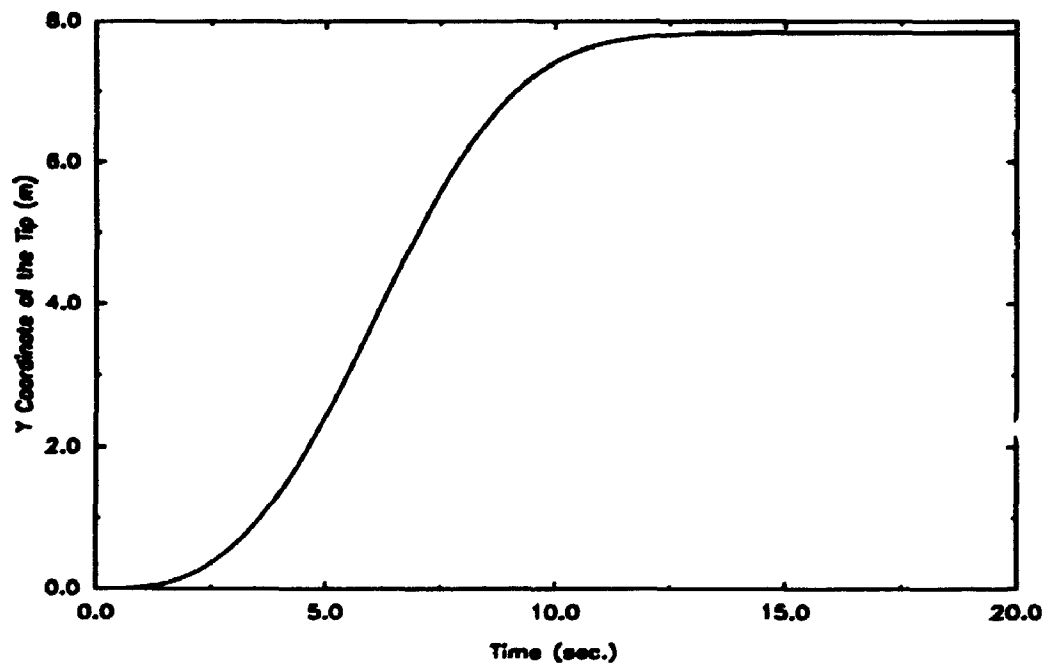
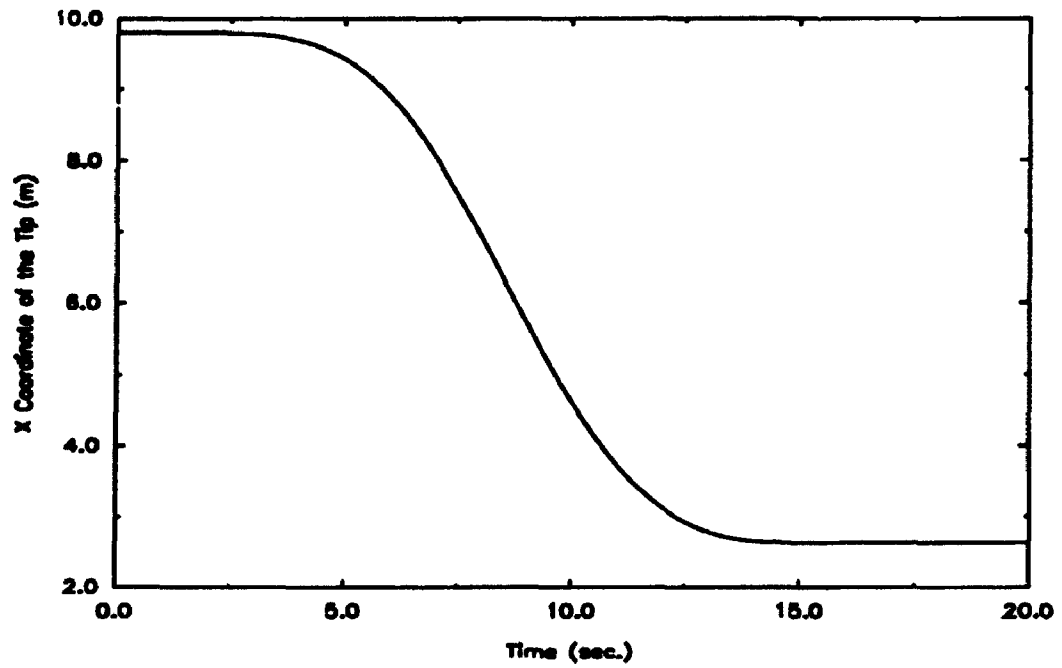
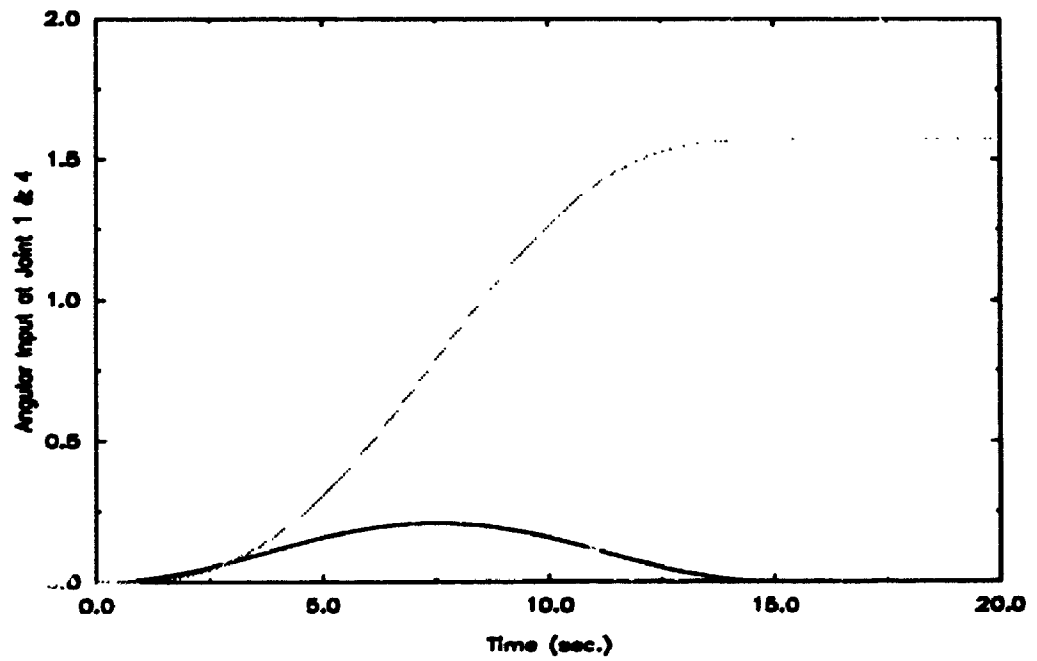
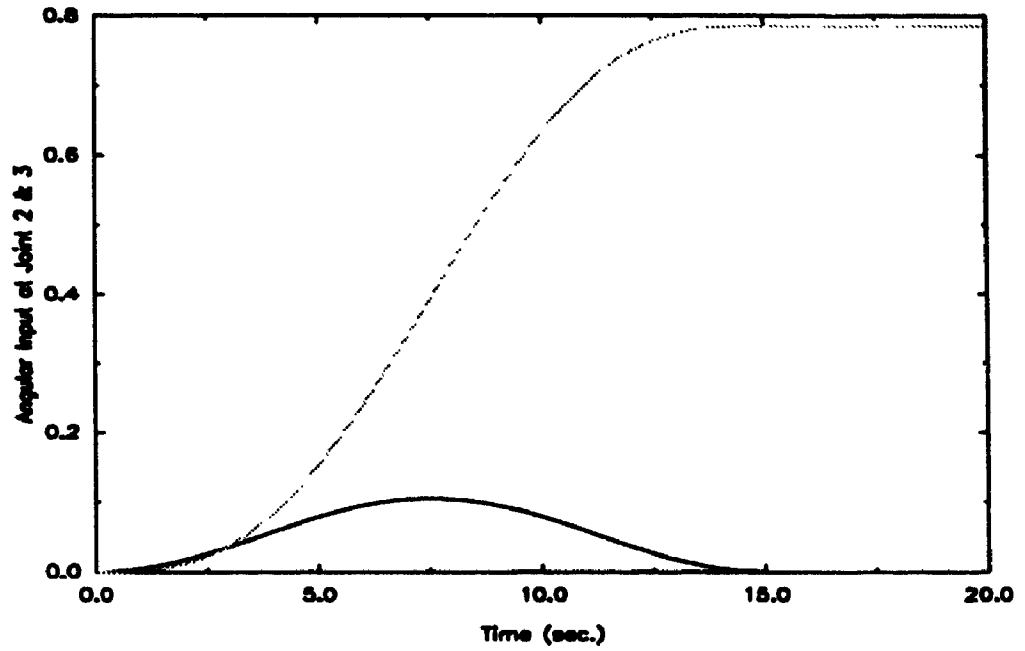


Figure 9-22 Ideal tip trajectory and joint angular velocity and displacement



— Velocity (rad/sec.)
..... Angle (rad)

(Figure 9-22 continued)

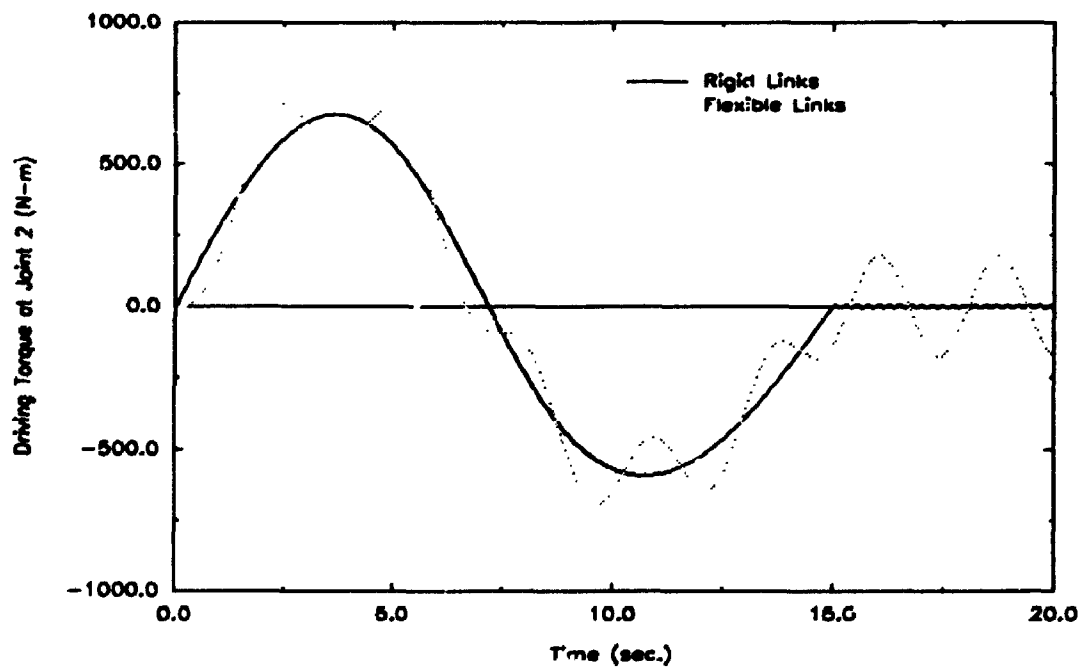
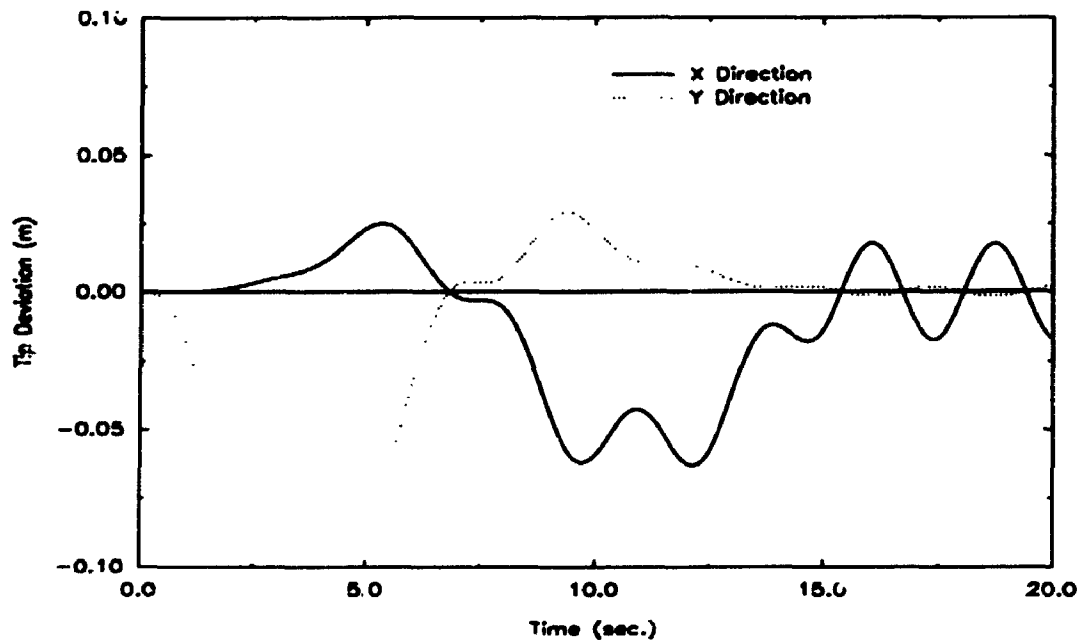
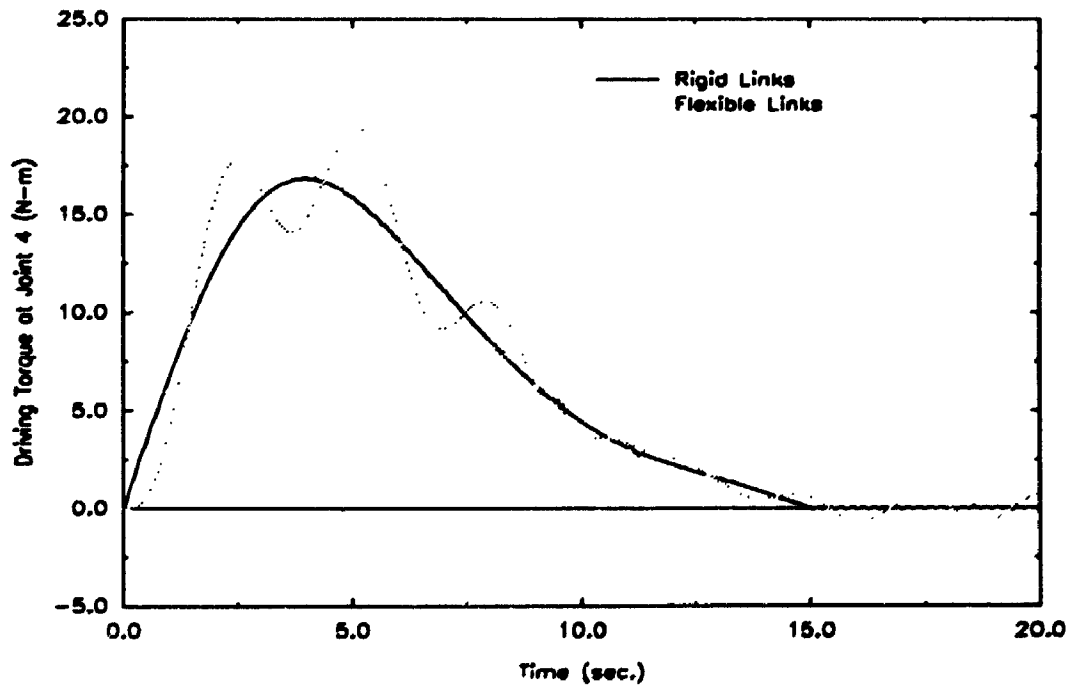
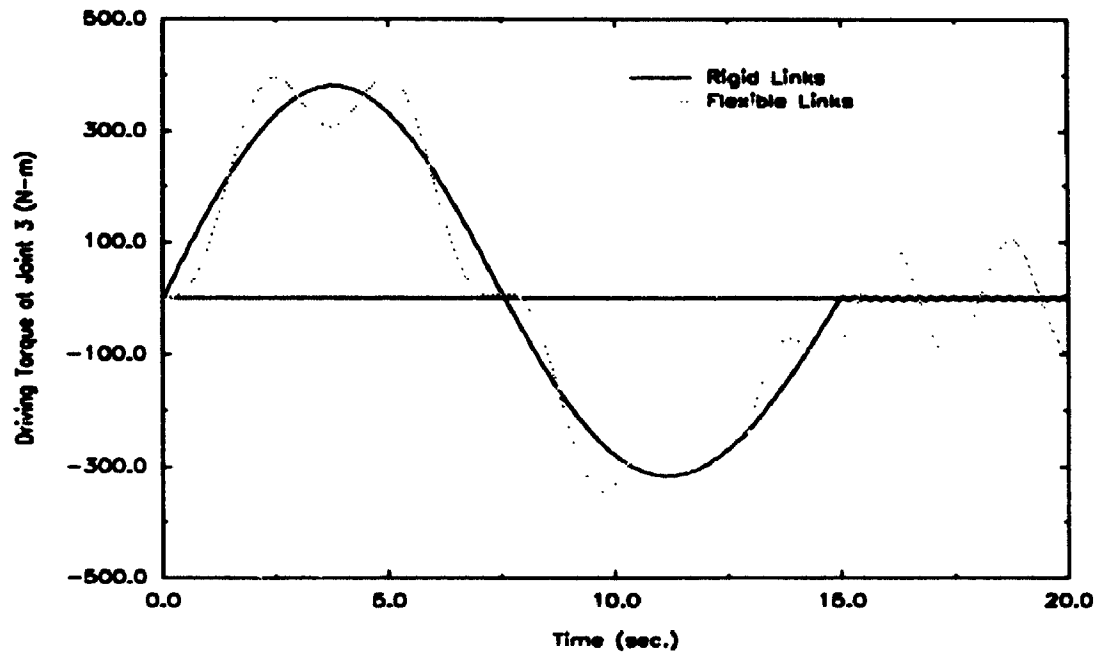


Figure 9-23 Payload tip deviation v.s. rigid body case and joint torques of the 2-D motion of the manipulator



(Figure 9-23 continued)

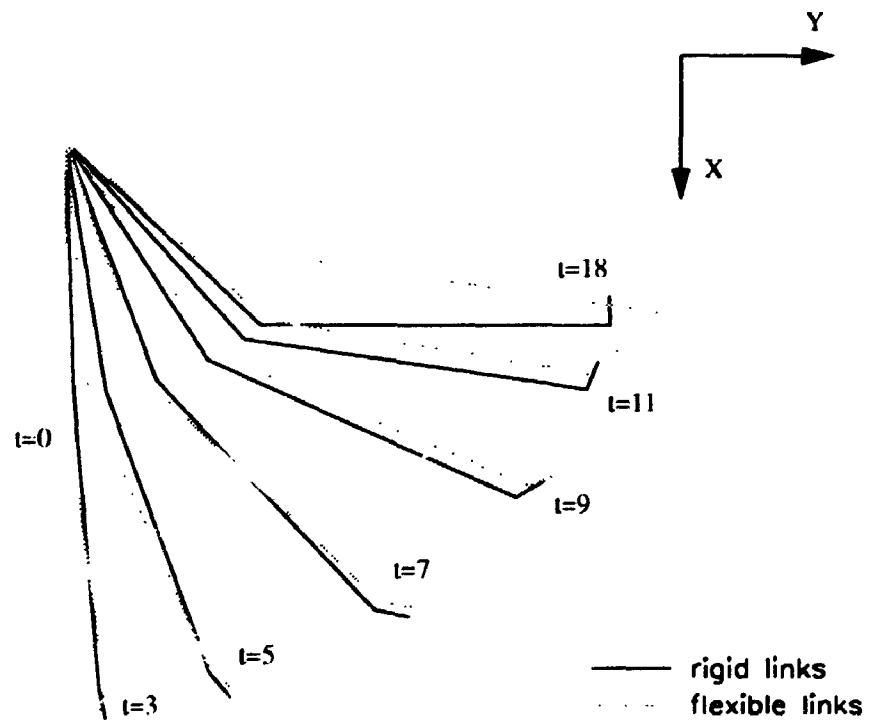


Figure 9-24 Positions of the manipulator during the maneuver

$$\theta_1 = \left(-\frac{\pi}{T_s}\right) \left[t - \frac{T_s}{2\pi} \sin\left(\frac{2\pi}{T_s}t\right) \right] \quad t \leq T_s \quad (9.25)$$

$$\theta_1 = \frac{\pi}{2} \quad t > T_s \quad (9.26)$$

The tip deviations and joint driving torques of the flexible manipulator are shown in Figure 9-25. In this figure, the joint torques required for this maneuver of the rigid link system are also shown for comparison. The influence of the flexible links on tip position and the driving torques can be seen very clearly in these plots. As in planar maneuver, these driving torques obtained from the rigid link system are imposed on the flexible manipulator. The positions of the flexible manipulator during the maneuver are simulated and plotted in Figure 9-26. The positions of the flexible manipulator are in error as compared to the positions to be expected. This example also shows how important the consideration of flexibility is in the simulation of the dynamics and control of the flexible manipulator systems.

In this chapter, three examples of flexible multibody systems have been investigated to demonstrate and validate the multibond graph method developed in this thesis. It can be seen that the development of multibond graphs of these multibody systems is quite straightforward based on the general multibond graph method developed in the previous chapters. The significant advantages are the ease of modelling, particularly evident in the case of mixed energy domains. It has been revealed, from the solution of these example problems, that the geometric stiffening and softening of flexible beams under large dynamic axial forces have significant effects on the prediction of dynamic behavior and digital simulation of the flexible systems. It has also shown that the inverse dynamic control to a flexible multibody system without consideration of the flexibility of the system would cause unaccepted errors in position control.

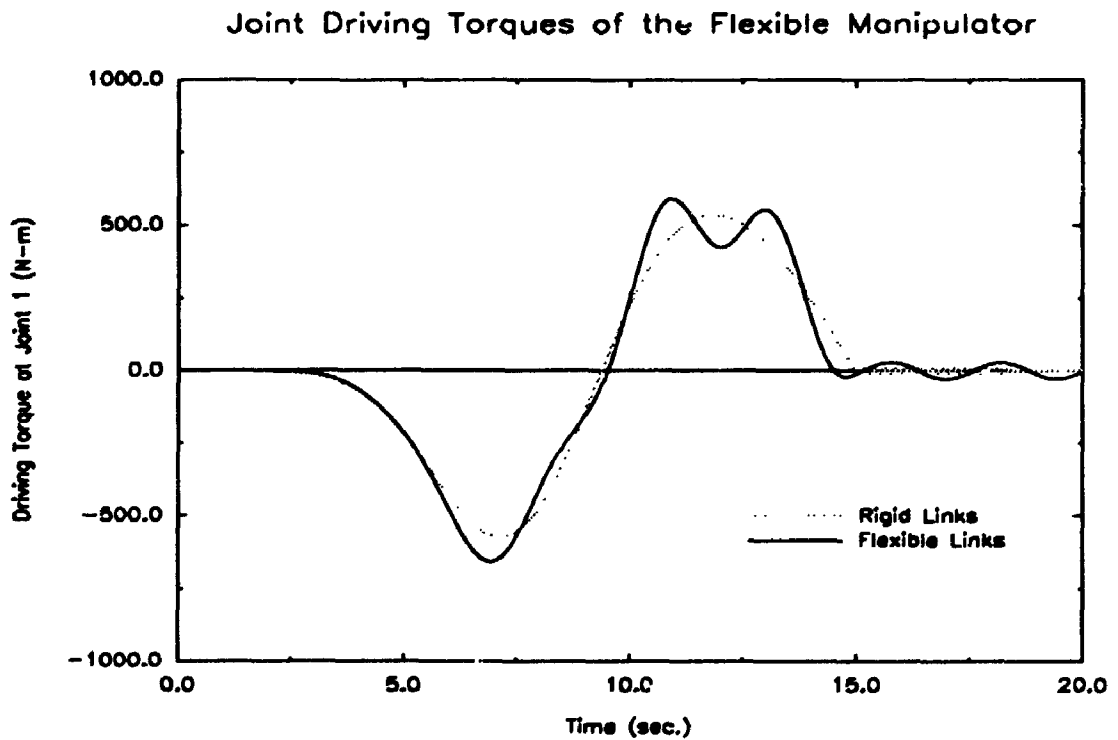
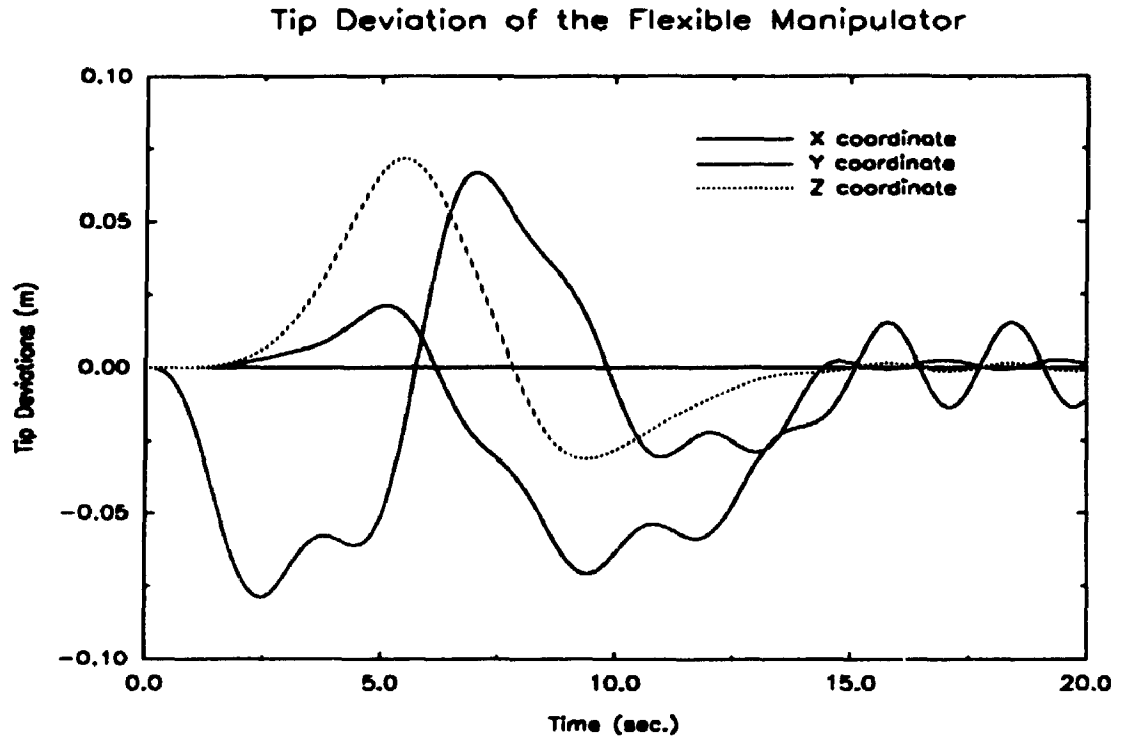
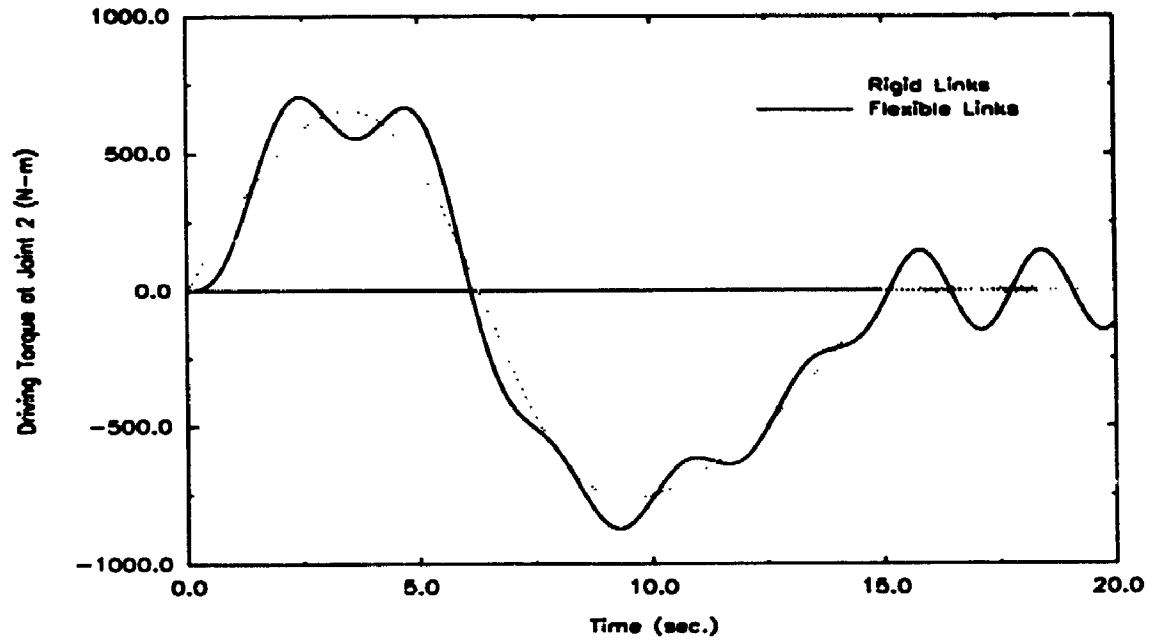
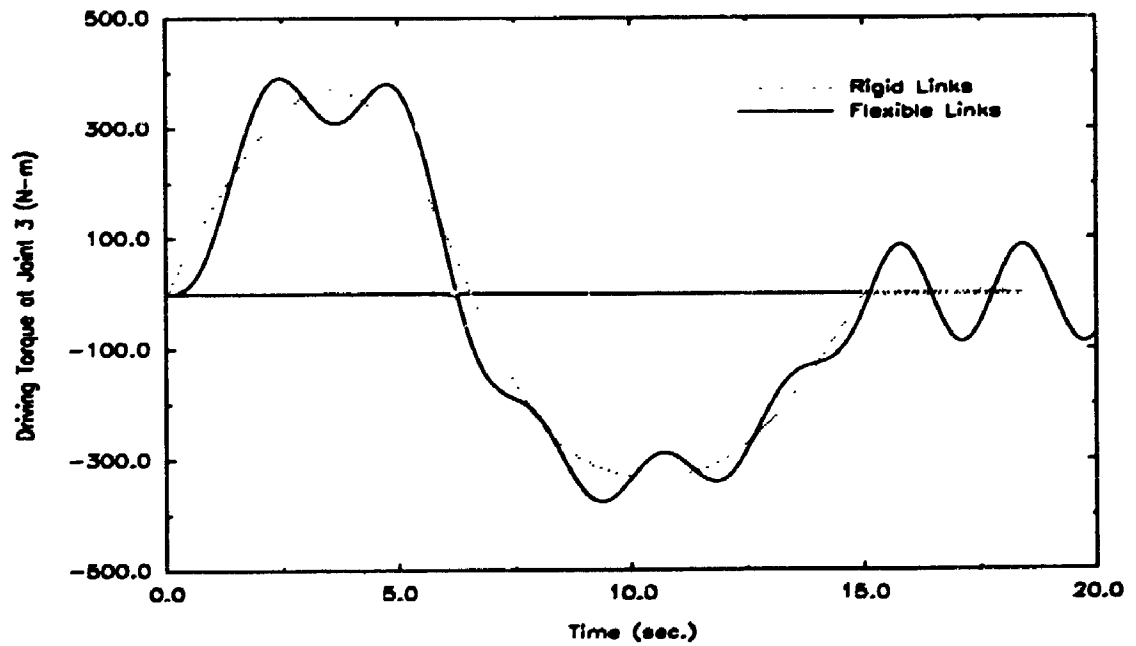


Figure 9-25 Tip deviations v.s. rigid body case and joint torques of the 3-D motion of the manipulator

Joint Driving Torques of the Flexible Manipulator

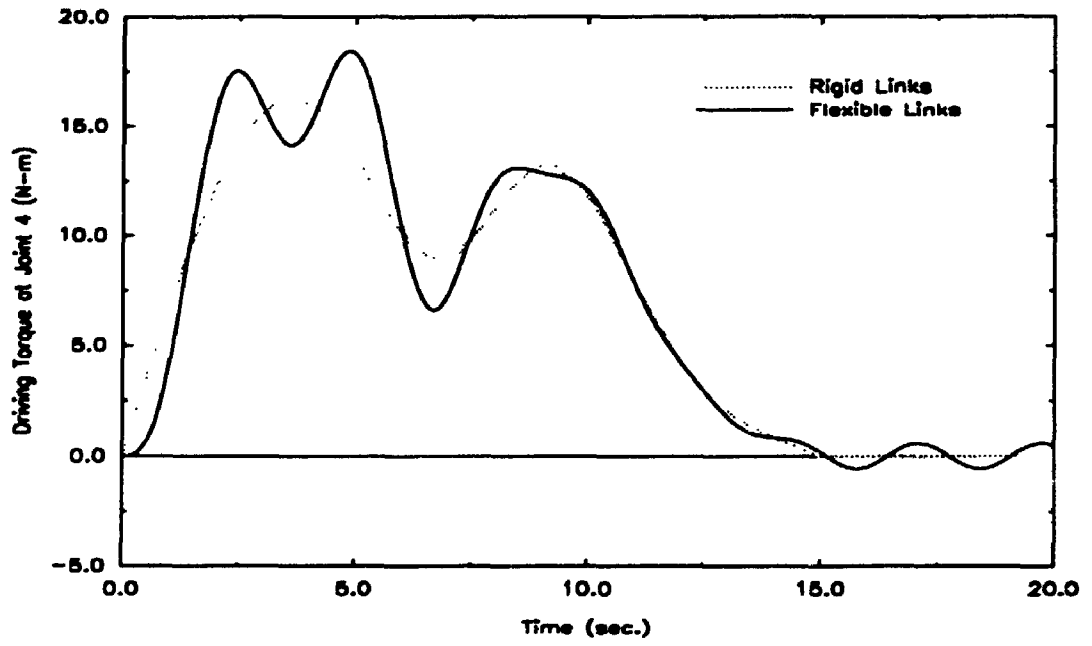


Joint Driving Torques of the Flexible Manipulator



(Figure 9-25 continued)

Joint Driving Torques of the Flexible Manipulator



(Figure 9-25 continued)

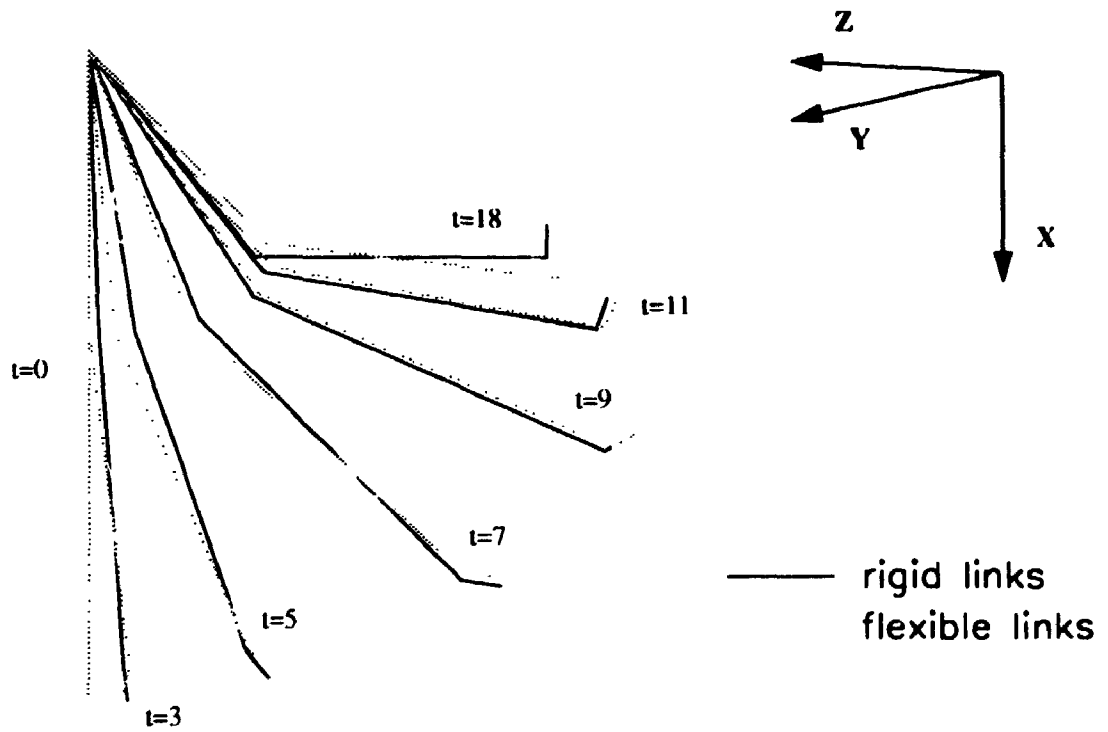


Figure 9-26 Positions of the flexible manipulator during the maneuver

- Chapter 10 -

Summary and Conclusions

Until now, bond graph was mostly used to model rigid multibody system dynamics and two dimensional flexible bodies. In this thesis, a multibond graph approach, for the computer-aided modelling and simulation of general flexible multibody system dynamics, has been developed. This approach provides an alternative to current computer-aided modelling and simulation of 3-D flexible multibody system dynamics with the added significant advantages of ease of modelling and including mixed energy domains.

The non-linear vibration behavior of a flexible body in a multibody system has been investigated using partial differential equations and is modelled by non-linear strain displacement relations for multibond graph modelling. The axial forces in a flexible body due to overall motion and constraints of connected bodies have significant influence on the numerical simulation of vibration behavior of the flexible body. It has been demonstrated that ignoring of the geometric stiffening/softening effect would lead to incorrect results, especially for high speed and heavily loaded flexible multibody systems.

The governing equations of motion of an arbitrary flexible body are derived in a form which can be represented by existing multibond graph terminology. The stiffening and softening effects are considered by non-linear strain displacement relations for multibond graph modelling. The application of floating frames as body reference frames is also discussed. The proper use of floating frames can simplify the governing equations to a certain degree. Based on these equations, general multibond graphs for a flexible body are developed. The acceleration coupling between rotation and vibrations is dealt with by a summation element. These multibond graphs have a compatible form with the multibond graphs of a rigid body and can be easily connected to multibond graphs of rigid bodies.

The multibond graphs of commonly used mechanical joints are also developed using restrictions on relative velocities between connected bodies provided by the joints (zero velocity sources). In this thesis, a new type of multiport element *Constraintor* is created for the constraints, which provides a means to get rid of the derivative causality and to generate governing equations in the form equivalent to the form generated by other analytical computer-aided modelling methods. With multibond graphs of individual bodies and joints, the multibond graph of the whole flexible multibody system can be obtained by assembling them together. The procedure is systematic.

The different forms of governing equations generated from other analytical computer-aided modelling methods and numerical algorithms are reviewed. The procedures to generate governing equations of motion from the multibond graph of the flexible multibody system are discussed. It is verified by an example that the governing equations generated from the multibond graph with zero velocity sources of constraints have the form of minimum variables, and the governing equations generated from the multibond graph with *Constraintor* of constraints have the form of maximum variables. Both forms are all differential/algebraic equations with index one and can be numerically solved by implicit integration methods.

A computer program for setting up multibond graphs and automatically generating simulation data files for the commercial simulation package ACSL has been developed on the Sun Workstation using the "C" language and SunView graphic user interface. It is an important tool for the "automatic" implementation of the method developed in the thesis.

Several applications in robotics and mechanisms have been implemented in the thesis. The rotating beam example shows the stiffening effect on transverse vibrations. The crank-rocker example illustrates the softening effect. And the flexible manipulator example demonstrates the importance of consideration of flexibility in inverse dynamic control. These examples prove the validity and capability of the multibond graph method and the computer program developed and implemented in the thesis.

References

- Allen, R.R., 1979, "Multiport Representation of Inertial Properties of Kinematic Mechanisms", *Journal of The Franklin Institute*, Vol. 308, No. 3, pp. 235 - 253.
- Allen, R.R., and Dubowsky, S., 1977, "Mechanisms as Components of Dynamic Systems: A Bond Graph Approach", *ASME Journal of Engineering for Industry*, pp. 104 - 111.
- Allen, R. R., 1981, "Dynamics of Mechanisms and Machine Systems in Accelerating Reference Frames," *ASME Journal of Dynamic Systems, Measurement, and Control*, Vol. 103, pp. 395 - 403.
- Amirouche, F. M. L., 1987, "Flexibility Effects - Estimation of the Stiffness Matrix in the Dynamics of a Large Structure," *Journal of Vibration, Acoustics, Stress, and Reliability in Design*, Vol. 109, July, pp. 283-288.
- Amirouche, F. M. L. and Huston, R. L., 1988, "Dynamics of Large Constrained Flexible Structures," *ASME Journal of Dynamic Systems, Measurement, and Control*, Vol. 110, pp. 78-83.
- Banerjee, K. and Dickens, J. M., 1990, "Dynamics of an Arbitrary Flexible Body in Large Rotation and Translation," *J. Guidance*, Vol. 13, No. 2, March-April.
- Banerjee, A. K., and Lemak, M. E., 1991, "Multi-Flexible Body Dynamics Capturing Motion-Induced Stiffness," *ASME Journal of Applied Mechanics*, Vol. 58, pp. 766-775.
- Banerjee, A. K. and Kane, T. R., 1989, "Dynamics of a Plate in Large Overall Motion," *ASME Journal of Applied Mechanics*, Vol. 56, pp. 887-892.
- Bisplinghoff, R. L., Ashley, H., and Halfman, R. L., 1955, *Aeroelasticity*, Addison-Wesley, pp. 95-97.
- Bonderson, L. S., 1975, "Vector Bond Graphs Applied to One-Dimensional Distributed

- Systems," *ASME Journal of Dynamic Systems, Measurement, and Control*, March, pp 75 -82.
- Book, W. J., 1982, "Recursive Lagrangian Dynamics of Flexible Manipulator Arms Via Transformation Matrices," *IFAC Computer Aided Design*, Session WA1 - Robotics, pp. 5-17.
- Book, W. J., 1984, "Recursive Lagrangian Dynamics of Flexible Manipulator Arms," *The International Journal of Robotics Research*, Vol. 3, No.3, Fall, pp. 87-101.
- Boresi, A. P. and Chong, K. P., 1987, *Elasticity in Engineering Mechanics*, Elsevier, New York.
- Bos, A.M., 1986, *Modelling Multibody Systems in Terms of Multibond Graphs with Application to a Motorcycle*, Ph.D. Thesis, The University of Twente, The Netherlands.
- Bos, A.M., 1985, "Formula Manipulation in the Simulation of Bond Graph Models of Mechanical Systems," *Proceedings of the European Conference at the University of Ghent, Belgium*, pp. 27 - 31.
- Bos, A.M., and Tiernego, M.J.L., 1985, "Formula Manipulation in the Bond Graph Modelling and Simulation of Large Mechanical Systems", *Journal of The Franklin Institute*, Vol. 319, No. 1/2, pp. 51-65.
- Breedveld, P. C., 1982, "Proposition for Unambiguous Vector Bond Graph Notation," *ASME Journal of Dynamic Systems, Measurement, and Control*, Vol. 104, 267-270.
- Breedveld, P. C., 1984, "Decomposition of Multiport Elements in a Revised Multibond Graph Notation," *Journal of the Franklin Institute*. Vol. 318, No.4, 253-273.
- Breedveld, P.C., 1985, "Multibond Graph Elements in Physical Systems Theory," *Journal of The Franklin Institute*, Vol. 319, No. 1/2, pp. 1 - 36.
- Broenink, J. F., 1990, *Computer-Aided Physical-Systems Modeling and Simulation: a bond graph approach*, Ph. D. Thesis, University of Twente, Netherlands.
- Brown, F.T., 1972, "Lagrangian Bond Graphs", *ASME Journal of Dynamic Systems,*

Measurement, and Control, Vol. 94, No. 3, pp. 213 - 221.

Cavin, R. K. and Dusto, A. R., 1977, "Hamilton's Principle: Finite Element Methods and Flexible Body Dynamics," *AIAA J.* 15 (12) 1684-1690.

Craig, R.R., 1981, *Structural Dynamics*, John Wiley & Sons, New York, pp. 214~216.

Dubowsky, S., Gardner, T. N., 1977, "Design and Analysis of Multilink Flexible Mechanisms with Multiple/Clearance Connections," *Journal of Engineering for Industry*, Vol. 99, No. 1, Feb.

Erdman, A. G., Sandor, G. N., Bakberg, R. G. 1971, "A General Method for Kineto-Elastodynamic Analysis and Synthesis of Mechanism," *Journal of Engineering for Industry*, ASME 71-WA/DE-6, New York.

Gear, C. W., 1971, "Simultaneous Numerical Solution of Differential-Algebraic Equations," *IEEE Transactions on Circuit Theory*, Vol. CT-18, No. 1, pp. 89 - 95.

Gear, C. W. and Petzold, L.R., 1984, "ODE methods for the Solution of Differential/Algebraic Systems," *SIAM J. Numer. Anal.*, Vol. 21, No. 4, pp. 716-728.

Granda, J.J., 1982, "Computer Aided Modeling Program (CAMP): A Bond Graph Preprocessor for Computer Aided Design and Simulation of Physical Systems Using Digital Simulation Languages", Ph.D. Thesis, Department of Mechanical Engineering, University of California, Davis, CA.

Felcz, J., et al, 1990, "BONDYN: A Bond Graph Based Simulation Program for Multibody Systems," *ASME Journal of Dynamic Systems, Measurement, and Control*, Vol. 112, pp. 717-727.

Gupta, V. K., 1974, "Dynamic Analysis of Multi-Rigid-Body Systems," *Journal of Engineering for Industry*, August, pp. 886-892.

He, S. X. N. and ElMaraghy, W. H., 1991, "Corrected Partial Differential Equations for

Transverse Vibration of Rotating Bars," *DAMRL Report 1991-06-03*, The University of Western Ontario.

He, S. X. N. and ElMaraghy, W. H., 1992, "User's Manual for MULBOND," *DAMRL Report 1992-06-01*, The University of Western Ontario.

Ho, J.Y.L. and Herber, D.R., 1985, "Development of Dynamics and Control Simulation of Large Flexible Space System," *J. of Guidance and Control*, Vol. 8, No. 3, pp. 347-383.

Ho, J. Y. L., 1977, "Direct Path Method for Flexible Multibody Spacecraft Dynamics," *J. Spacecraft and Rockets* 14(2), 102-110.

Huang, Y. and Lee, C. S. G., 1988, "Generalization of Newton-Euler Formulation of Dynamic Equations to Nonrigid Manipulators," *Journal of Dynamic System, Measurement, and Control*, Vol. 110, 308-315.

Huston, R. L., 1981, "Multi-Body Dynamics Including the Effects of Flexibility and Compliance," *Computers & Structures*, Vol. 14, No. 5-6, pp. 443-451.

Ider, S. K. and Amirouche, F. M. L., 1989, "Influence of Geometric Nonlinearities in the Dynamics of Flexible Treelike Structures," *J. of Guidance and Control*, Vol.12, No.6, pp. 830-837.

Karnopp, D., and Rosenberg, R.C., 1968, *Analysis and Simulation of Multiport Systems - The Bond Graph Approach to Physical System Dynamics*, The M.I.T. Press.

Karnopp, D., 1977, "Lagrange's Equations for Complex Bond Graph Systems", *ASME Journal of Dynamic Systems, Measurement, and Control*, Vol. 99, pp. 300 - 306.

Kane, T. R., 1968, *Dynamics*, Holt, Rinehan and Winston.

Kane, T. R., Ryan, R. R. and Banerjee, A. K., 1987, "Dynamics of a Cantilever Beam Attached to a Moving Base," *J. Guidance*, Vol. 10, No. 2, 139-151.

Karnopp, D and Rosenberg, R., 1975. *System Dynamics: A United Approach*. John Wiley & Sons, Inc.

Likins, P. W., 1972, "Finite Element Appendage equations for Hybrid Coordinate Dynamic Analysis," *International Journal of Solids and Structures*, Vol. 8, 709-731.

Likins, P. W., 1974, "Geometric Stiffness Characteristics of a Rotating Elastic Appendage," *Int. J. Solids Structures*, 10, pp. 161-167.

Low, K. H., 1987, "A Systematic Formulation of Dynamic Equations for Robot Manipulators with Elastic Links," *J. Robotic Systems*, Vol.4, No.3, 435-456.

Margolis, D.L., 1978, "Bond Graphs, Normal Modes, and Vehicular Structures", *Vehicle Systems Dynamics*, Vol. 7, pp. 49 - 63.

Margolis, D.L., and Karnopp, D., 1979, "Bond Graphs for Flexible Multibody Systems", *ASME Journal of Dynamic Systems, Measurement, and Control*, Vol. 101, pp. 50 - 57.

Margolis, D.L., 1980, "An Algorithm for Incorporating Subsystem Modes into Overall Dynamic System Models," *Journal of The Franklin Institute*, Vol. 310, No. 2, pp. 107-117.

Margolis, D.L., 1980, "Bond Graphs for Distributed System Models Admitting Mixed Causal Inputs," *ASME Journal of Dynamic Systems, Measurement, and Control*, Vol. 102, pp. 94-100.

Margolis, D.L., 1980, "Dynamical Models for Multidimensional Structures using Bond Graphs," *ASME Journal of Dynamic Systems, Measurement, and Control*, Vol. 102, pp. 180-187.

Mecrman, J. W., 1981, "Bond Graph Modelling and Simulation Techniques," *Int. J. Modelling and Simulation*, Vol. 1, No. 1, pp. 52-56.

McInnis, J. B. and ElMaraghy, W. H., 1989, "Automated Bond Graph Construction and Analysis for MBSD," *ASME Computer in Engineering (CIE'89)*, San Francisco, July.

- Meirovitch, L., 1967, *Analytical Methods in Vibrations*, MacMillan, New York.
- Mitchell and Gauthier Associates, 1987, *Advanced Continuous Simulation Language Reference Manual*, Mitchell and Gauthier Associates, Concord, Mass.
- Modi, V. J. and Ibrahim, A. M., 1988, "On the Transient Dynamics of Flexible Orbiting Structures," *Large space Structure: Dynamics and Control*, edited by S. N. Atluti and A. K. Amos, Springer-Verlag, New York, pp. 93 -114.
- Nikravesh, P. E., 1984, "Some Methods for Dynamic Analysis of Constrained Mechanical Systems: A survey," *Computer Aided Analysis and Optimization of Mechanical System Dynamics*, Springer, Berlin, pp. 351-368.
- Paul, B., 1975, "Analytical Dynamics of Mechanisms-A Computer Oriented Overview," *Mechanism and Machine Theory*, Vol. 10, pp. 481-507.
- Paynter, H.M., 1961, *Analysis and Design of Engineering Systems*, The M.I.T. Press.
- Petzold, L. R., 1982, "Differential/algebraic equations are not ODE's," *SIAM Journal of Science and Statistics Computing*, Vol. 3, No. 3, pp.367-384.
- Roberson, R. R. and Schwertassek, R., 1988, *Dynamics of Multibody Systems*, Springer-Verlag Berlin.
- Rosenberg, R.C., 1971, "State-Space Formulation for Bond Graph Models of Multiport Systems", *ASME Journal of Dynamic Systems, Measurement, and Control*, Vol. 93, No. 1, pp. 35 - 40.
- Rosenberg, R.C., 1972, "Multiport Models in Mechanics", *ASME Journal of Dynamic Systems, Measurement, and Control*, Vol. 94, No. 3, pp. 206 - 212.
- Rosenberg, R.C., 1974, *A users guide to ENPORT-4*, Wiley, New York.
- Rosenberg, R.C., and Karnopp, D., 1983, *Introduction to Physical System Dynamics*, McGraw-

Hill.

Winfrey, R. C., 1971, "Elastic Link Mechanism Dynamics," *Journal of Engineering for Industry*, Vol. 93, No. 1, pp. 268-272.

Samanta, B., 1990, "Dynamics of Flexible Multibody Systems Using Bond Graphs and Lagrange Multipliers," *ASME Journal of Mechanical Design*, Vol. 112, pp. 30-35.

Schiehlen, Werner (Editor), 1990, *Multibody Systems Handbook*, Springer-Verlag, Berlin Heidelberg.

Shabana, A. A. and Wehage, R. A., 1983, "A Coordinate Reduction Technique for Dynamic Analysis of Spatial Substructures with Large Angular Rotations," *Journal of Structure Mechanics*, 11(3), 401-431.

Shames, I. H. and Dym, C. L., 1985, *Energy and Finite Element Methods in Structural Mechanics*, McGraw-Hill, New York.

Singh, R. P. and VanderVoort, R. J., 1985, "Dynamics of Flexible Bodies in Tree Topology - A Computer-Oriented Approach," *J. Guidance*, Vol. 8, No. 5, pp.584-590.

Thoma, J. U., 1975, *Introduction to Bond Graphs and Their Application*, Permagon Press.

Thoma, J. U., 1985, "Block Bond Graphs for Simulation of Nonlinear Systems: A Technical Note," *Transactions of The Society for Computer Simulation*, Vol. 2, No. 3, pp. 249-255.

Tiernego, M. J. L. and Bos, A. M., 1985, "Modelling the Dynamics and Kinematics of Mechanical Systems with Multibond Graphs," *Journal of the Franklin Institute*, Vol. 319, 37-50.

Turcic, D. A. and Midha, Ashok, 1984, "Generalized Equations of Motion for the Dynamic Analysis of Elastic Mechanical Systems," *ASME Journal of Dynamic Systems, Measurement, and Control*, Vol. 106, pp. 243-248.

Unda, J., de Jalon, J., Losantos, F. and Eparantza, R., 1987, "A Comparative Study on Some Different Formulations of the Dynamic Equations of Constrained Mechanical Systems," *ASME Journal of Mechanisms, Transmissions, and Automation in Design*, Vol. 109, pp. 466 - 474.

Wehage, R. A. and Haug, E. J., 1982, "Generalized Coordinate Partitioning for Dimension Reduction in Analysis of Constrained Dynamic Systems," *ASME Journal of Mechanical Design*, Vol. 104, pp. 247 - 255.

Wielenga, T. J., 1984, *Simplification in the Simulation of Mechanisms Containing Flexible Members*, Ph.D. Thesis, Mechanical Engineering, University of Michigan.

Winfrey, R. C., 1972, "Dynamic Analysis of Elastic Link Mechanisms by Reduction of Coordinates," *Journal of Engineering for Industry*, Vol. 94, pp. 557-582.

Wittenburg, I. J., 1977, *Dynamics of Systems of Rigid Bodies*, B. G. Teubner Stuttgart.

Wu, S. C. and Haug, E. J., 1988, "Geometric Non-linear Substructures for Dynamics of Flexible Mechanical Systems," *International Journal for Numerical Methods in Engineering*, Vol. 26, 2211-2226.

Wu, S. C., Haug, E. J. and Kim, S. S., 1989, "A Variational Approach to Dynamics of Flexible Multibody Systems," *Mech. Struct. & Mach.*, 17(1), 3-32.

Yazman, M. A., Servettaz, G., Maschke, B., 1989, "Bond-Graph Modelling of Flexible Manipulators," *IFAC/IMACS/IFORS International Symposium AIPAC'89*, July, Nancy-France.